Activity and substrate specificity of bacterial and human ribosomal oxygenases

DISSERTATION
der Fakultät für Biologie der
Ludwig-Maximilians-Universität
München zur Erlangung des
Doktorgrades der Naturwissenschaften

Vorgelegt von
Katharina Elisabeth Marianne Bräuer,
geb. Schubhart

Angefertigt am Helmholtz Zentrum München,
Institut für Molekulare Toxikologie und Pharmakologie,
Nachwuchsgruppe Epigenetik

Erstgutachter:
Prof. Dr. Dirk Eick
Zweitgutachter:
Prof. Dr. Angelika Böttger

Eingereicht am: 24.08.2017
Tag der mündlichen Prüfung: 08.02.2018

Summary

Recently, several iron and 2-oxoglutarate (2OG) dependent oxygenases were subclassified as ribosomal oxygenases (ROXs). ROXs have emerged as enzymes that affect translation by hydroxylation of translation factors like the eukaryotic release factor eRF1[1], tRNA[2,3], or ribosomal proteins. Bacterial ancestor ycfD, mammalian OGFOD1, Myc-induced nuclear antigen (MINA53), and NO66 target the ribosome directly and modify different ribosomal proteins[4-6].

In my thesis, ribosomal oxygenases ycfD, OGFOD1, MINA53, and NO66 were investigated by generating knockout strains and CRISPR/Cas9 knockout cell lines, respectively, and examining those in growth behaviour and with regard to ribosome composition. Hereby, MINA53 and NO66 catalyzed hydroxylation of their ribosomal targets were confirmed. Further, novel modifications on ribosomal proteins can be identified by the LC-MS/MS data sets. Knockout of ycfD did not affect growth behaviour of bacteria or ribosome profiles.

Identification and characterization of the interaction with cell cycle regulator CCNA2 connects OGFOD1 to the cell cycle. OGFOD1 knockout was not viable in cells, further indicating a cell cycle related function of OGFOD1. Also interaction of OGFOD1 with eukaryotic elongation factor 2 kinase (eEF2K) might further strengthen OGFOD1 function in translation regulation.

MINA53 and NO66 share several similarities in substrate specificity, domain architecture, and subcellular localization. As homo-oligomerization seemed to emerge as a common feature of 2OG oxygenases, the function of the oligomerization of both proteins was analyzed in more detail with regard to substrate binding. Indeed, disruption of dimerization caused a loss of interaction of NO66 with its substrate RPL8. Phylogenetic studies were conducted to follow evolution of both proteins, revealing the conservation of the protein domain structures. However, analyses on genomic level identified NO66 as single exon gene in different organisms.

Zusammenfassung

Ribosomale Oxygenasen (ROXs) wurden kürzlich als Unterfamilie der Eisen(II)-2-Oxoglutarat abhängigen Oxygenasen (2OG Oxygenasen) definiert. Diese beeinflussen die Translation durch Hydroxylierung von ribosomalen Proteinen, dem eukaryotischen „release factor“ eRF1[1] und tRNA[2,3]. Bakterielles ycfD, humane Proteine OGFOD1, „Myc-induced nuclear antigen“ (MINA53) und NO66 haben ribosomale Proteine als Substrat[4-6].

In dieser Arbeit wurden ycfD und die humanen Homologe OGFOD1, MINA53 und NO66 charakterisiert. Hierfür wurde ein bakterieller Knockout-Stamm für ycfD und für die humanen Proteine CRISPR/Cas9 Knockout Zelllinien hergestellt und im Hinblick auf Wachstum und ihre Ribosomen untersucht. Anhand von LC-MS/MS konnten die publizierten ribosomalen Substrate von MINA53 und NO66 bestätigt werden. Zusätzlich können mit den produzierten massenspektrometrischen Daten neue Modifikationen an ribosomalen Proteinen identifiziert werden. Knockout von ycfD hingegen hatte keinen Effekt auf Wachstum oder ribosomales Profil.

Zellzyklusregulator CCNA2 wurde als neuer Interaktionspartner von OGFOD1 identifiziert und charakterisiert. Eine Verbindung der ribosomalen Oxygenase OGFOD1 mit dem Zellzyklus kann auch hergestellt werden, da Knockout-Zellen von OGFOD1 nicht überlebensfähig waren. Die Interaktion mit der „eukaryotic elongation factor 2 kinase“ (eEF2K) weist auf eine Rolle von OGFOD1 in der Translationsregulation hin.

MINA53 und NO66 teilen viele Gemeinsamkeiten. Beide modifizieren ribosomale Proteine, haben dieselbe Domänen-Architektur und befinden sich im Nukleolus. In den letzten Jahren kristallisierte sich Oligomerisierung als eine verbreitete Eigenschaft von 2OG Oxygenasen heraus. Deshalb wurde die Funktion der Oligomerisierung von MINA53 and NO66 im Hinblick auf Substratbindung näher analysiert. Mutations- und Deletionsmutanten in der Dimerisierungsdomäne führten auch zu verhinderter Substratbindung bei NO66. Zudem wurde anhand von phylogenetischen Untersuchungen die Evolution beider Proteine verfolgt. Auf Proteinebene sind die Domänenstrukturen konserviert, auf Genomebene hingegen wurde NO66 als „Single Exon Gene“ in verschiedenen Organismen indentifiziert.

Table of content

List of figures

List of tables

1 Introduction

2-oxoglutarate (2OG) and iron (FeII) dependent oxygenases (2OG oxygenases) were studied quite extensively over the last decades. Their roles in collagen biosynthesis and in regulation of the hypoxic response assigned them important roles in the cell. More recently, investigations in the epigenetic field defined a subgroup of 2OG oxygenases as histone, DNA, and RNA modifying proteins. With ongoing research to elucidated the roles of the many not yet characterized 2OG oxygenases, the subfamiliy of ribosomal oxygenases (ROXs) was discovered. These enzymes seem to regulate gene expression at the level of translation. In this thesis, bacterial ancestor ycfD and its human homologues OGFOD1, Myc-induced nuclear antigen (MINA53) and NO66 were studied in more detail.

1.1 Translation and its regulation by post-translational modifications

1.1.1 The ribosome and translation

The ribosome is a huge protein-RNA complex responsible for the translation of genes encoded on messenger RNA (mRNA) into polypeptide chains.
Deciphering the mRNA code is carried out by the codon:anticodon helix formed by mRNA and transfer RNA (tRNA) in the decoding site of the ribosome.
Translation always follows a certain succession of events. It starts with the small ribosomal subunit binding to the 5' untranslated region (UTR) of the mRNA and scanning for a translation start side on the mRNA. Once the start codon AUG is found, three initiation factor proteins bind to the small subunit as well as the initiator tRNA methionine responsible for decoding AUG. Thereby the initiation complex is formed. Now the large ribosomal subunit can bind, which results in the release of the initiation factors.
The large subunit provides three tRNA binding sites. First, the tRNA binds in the A (amino acid) site where the codon:anticodon formation of mRNA and tRNA ensures the binding of the cognate tRNA and thereby addition of the correct amino acid to the growing polypeptide chain. Following, the ribosome translocates this tRNA to the P (polypeptide) position. Here the delivered amino acid gets transferred from tRNA to the polypeptide chain. Through the peptide release channel, the nascent protein chain gets elongated out of the ribosome. From the E (exit) position, the tRNA gets released back into the cytoplasm where it is recycled. Delivery of amino acids by tRNAs drives the elongation of the protein. The stop codon on the mRNA signals for translation termination, termination factors help to complete protein translation and to release the newly synthesized protein. Small and large subunit dissociate from the mRNA[7,8].

The aforementioned basic translation concept gets expanded more and more. Not only the core-ribosome protein composition seems to be distinct in different tissues and cell types, also the ribo-actome or different translation factors with manifold modifications contribute to a new field of gene expression on the post-transcriptional level.
Dependent on cell type, developmental stage or as reactions to changing environmental conditions, the core-ribosome stays the same whereas none-essential ribosomal proteins can be interchanged, resulting in specialized ribosomes[9-11]. Also modifications of ribosomal

RNA (rRNA), tRNA, mRNA, ribosomal proteins, or translation factor come more into focus as they contribute in specializing the ribosomes[9,11,12].

1.1.2 Translation regulation by modifications

In addition to the already highly complex formation of the functional ribosome, modifications of ribosomal proteins were detected from bacteria to yeast to humans[4,13-16]. The conservation indicates a universal function of post-translational modifications (PTMs) of ribosomal proteins.
Many of the discovered and studied modifications are involved in different steps of ribosome maturation and assembly. For instance, the loss of the methylation of L3 (uL3[17]) made bacteria cold sensitive due to less efficient ribosome assembly[13,18]. Interestingly, the modification of L7/L12 (bL12) itself is temperature depended and increases with decreasing temperatures. In yeast the loss of the histidine methylation of Rpl3p was shown to result in a deficiency of early rRNA processing. This affected the 60S subunit assembly and translation initiation[14]. Aditionally, methylations, acetylation, and methylthiolation were identified in bacterial ribosomal proteins[13].

However, not only the assembly of ribosomes is regulated by PTMs of ribosomal proteins or rRNA, there are also reports of PTMs on the ribosome affecting translation directly. One example is the hydroxylated Pro62 in human RPS23 (uS12). This residue is located in the PNSA loop which is part of the platform for the codon:anticodon minihelix[19]. Proline 62 gets hydroxylated by the ribosomal oxygenase (ROX) OGFOD1 and this modification leads to changes in translation accuracy[20].

1.2 Ribosomal oxygenases might regulate translation

Hydroxylation of ribosomal proteins is carried out by ribosomal oxygenases (ROXs) of the superfamily of 2-oxoglutarate (2OG) and iron (FeII) dependent oxygenases (2OG oxygenases) and is conserved throughout evolution from bacteria to mammals[4].

1.2.1 Superfamily of 2OG oxygenases

2OG oxygenases form an enzyme superfamily that is conserved from bacteria to mammals. So far there are six 2OG oxygenases found in bacteria[4], in humans more than 60 proteins were identified[21-24].
Substrates are manifold including proteins, RNA, and DNA[17,19]. Therefore the functional range of 2OG oxygenases in mammalians covers various different processes in the cell. Additional domains like zink finger domains for DNA binding or protein-protein interaction domains contribute to their substrate specificity[23].
The family classifying feature is the double-stranded β-helix (DSBH) domain (Jumonji-C (JmjC), cupin, or jelly-roll domain). It consists of two sheets of four β-helices opposing each other to form a barrel like structure. Inside the barrel, three amino acids build the catalytic center binding the co-factor iron and coordinating the co-substrate 2-oxoglutarate (Figure 1). The iron-coordinating motif is highly conserved through all 2OG oxygenases and consists of HxD/E ... H[21,24].

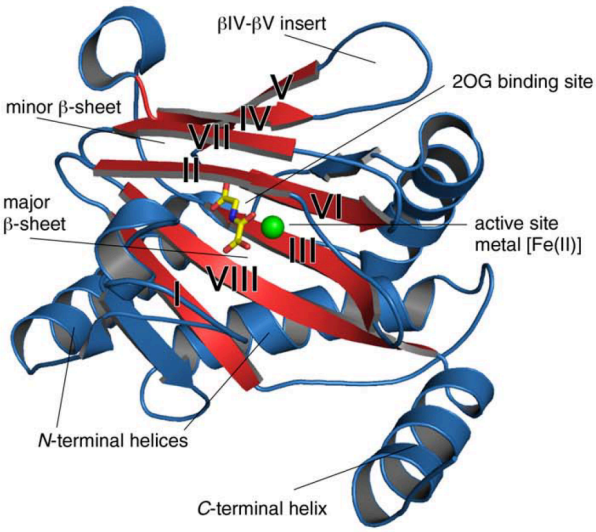

Figure 1: Representation of a typical JmjC domain with the iron (FeII) in green, N-oxalylglycine (NOG) as co-substrate analogue depicted in yellow sticks, the eight core β-helices are in red. From McDonough et al[21].

The reaction mechanism catalyzed by 2OG oxygenases comprises sequential binding of 2OG to the active side followed by the substrate and then oxygen. This results in a two-electron oxidation of the substrate and generation of succinate and carbon dioxide (CO_2) (Figure 2)[21,24,25].

In addition to the oxidation of proteins or tRNA leading to stably hydroxylated residues, demethylation is another product of some of the 2OG oxygenases. Demethylation occurs as a two step reaction, starting with hydroxylation of a N^{ε}-methyl group followed by fragmentation, which results in the demethylated product and formaldehyde (Figure 2 in gray)[24,26].

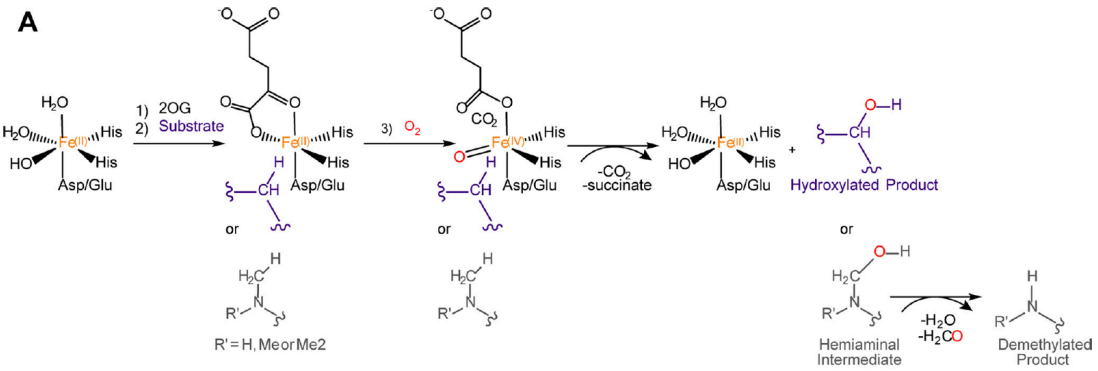

Figure 2: General enzymatic reaction carried out by 2OG oxygenases; in the active side, FeII (orange) is bound by the HxD/E...H motif, after 2OG binding and iron binding, oxidative decarboxylation of 2OG generates CO_2 and succinate; in gray N-methyl demethylation via hydroxylation of the methyl group and subsequent formaldehyd release. From Markolovic et al [24].

An example of 2OG oxygenases are PLOD1-3 which give collagen its stable but still flexible structure through lysine-hydroxylation[27,28]. Also the hypoxia response pathway is regulated by oxygenases sensing the oxygen levels. Hydroxylation of HIF1α (hypoxia inducible factor) by asparaginyl hydroxylase FIH (factor inhibiting HIF-1) targets HIF1α for proteasomal degradation. Low oxygen levels inhibit the asparaginyl hydroxylase FIH as it needs atmospheric oxygen as cofactor. The resulting loss of hydroxylation of HIF1-α leads to

stabilization of this transcription factor and subsequent translocation to the nucleus. Here it can dimerize with HIF1-β and activate hypoxia response genes[29].

2OG oxygenases emerged as major players in epigenetic regulation. More than 20 2OG oxygenases act as histone lysine demethylases (KDMs), like the JARID family or JMJD2 a-d[30]. Additionally, the Tet subfamily (Tet1, Tet2, and Tet3) catalyses the oxidation of 5-methylcytosine to 5-hydroxymethylcytosine in DNA[31-33]. FTO, member of the AlkB homologue (AlkBH) subfamily demethylates the N6-methyladenosine in mRNA[34]. TYW5 and AlkBH8 are other examples for RNA modification[2,35-37] , as they hydroxylate tRNAs. Known functions of 2OG oxygenases are summarized in Figure 3[24].

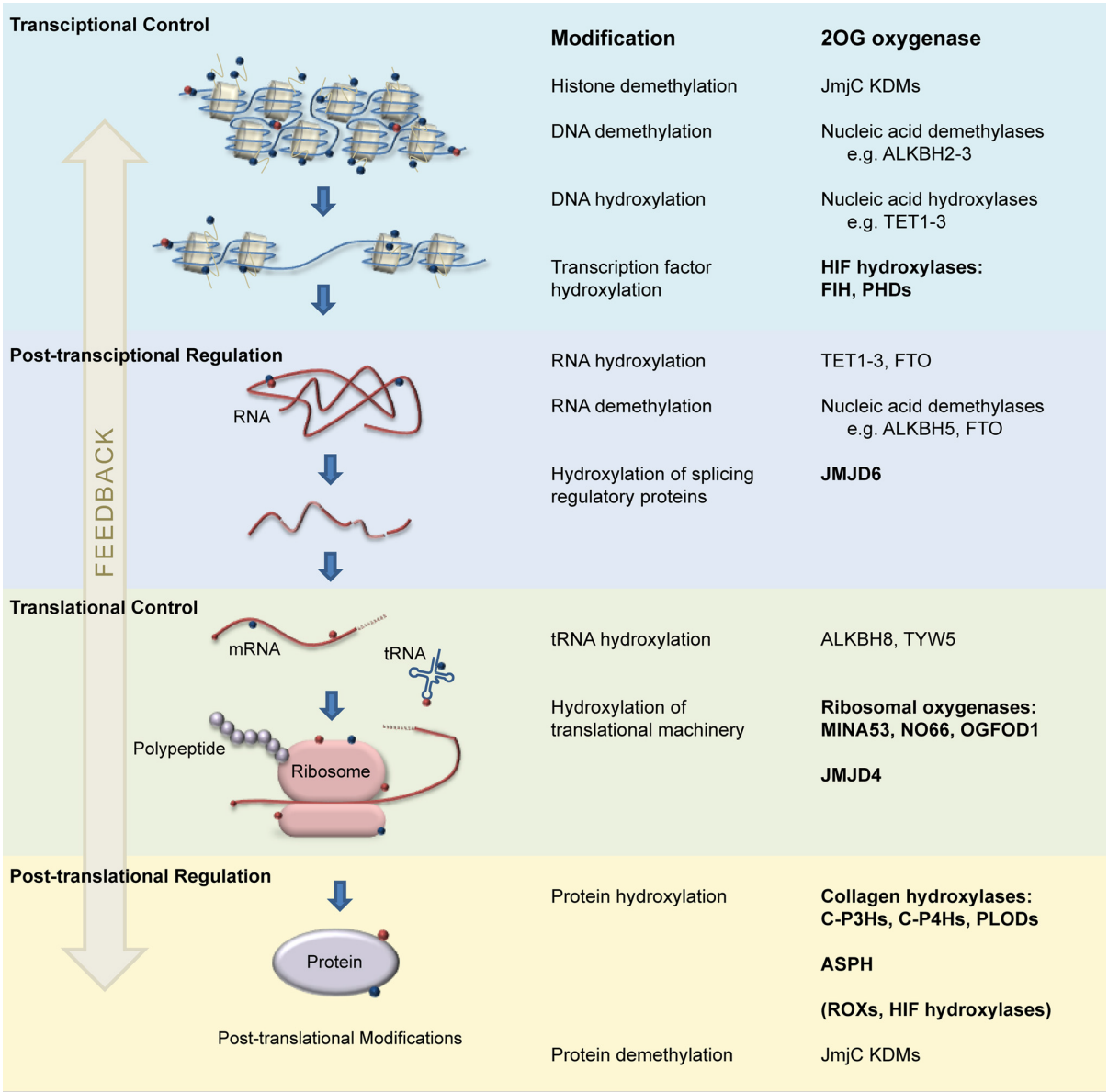

Figure 3: By hydroxylation and demethylation reactions, 2OG oxygenases are involed in transcriptional, post-transcriptional, translational, and post-translational processes; (ALKBH stands for alkylated DNA repair protein alkB homolog; TET1–3, ten-eleven translocation 1–3; FTO, fat mass- and obesity-associated protein; TYW5, tRNA wybutosine-synthesizing protein 5; C-P4Hs, collagen prolyl 4-hydroxylases; C-P3Hs, collagen prolyl 3-hydroxylases; PLODs, pro-collagen lysine 2-oxoglutarate 5-dioxygenase enzymes; P4HTM, transmembrane prolyl 4-hydroxylase). From Markolovic et al[24].

1.2.2 Ribosomal oxygenases

The identification of 2OG oxygenases hydroxylating ribosomal proteins directly or translation related proteins indicates a novel type of translation regulation[4,6]. These ribosomal oxygenases (ROXs) are conserved from bacteria to eukaryotes. In bacteria ycfD is the only ribosomal oxygenase, in human six enzymes, ALKBH8, TYW5, JMJD4, MINA53, NO66, and OGFOD1 (Figure 4) were subclassified as ROXs[38,39].

ALKBH8 is one homologue of the bacterial AlkB enzyme. AlkB is responsible for repair of alkylation damages of nucleobases[36,40]. The AlkB domain and the methyltransferase domain of ALKBH8 modify the uridine at position 34 of the anticodon tRNA[41,42].

TYW5 hydroxylates wybutosine in position 37 of phenylalanine tRNA[34,48], adjacent to the 3' position of the anticodon.

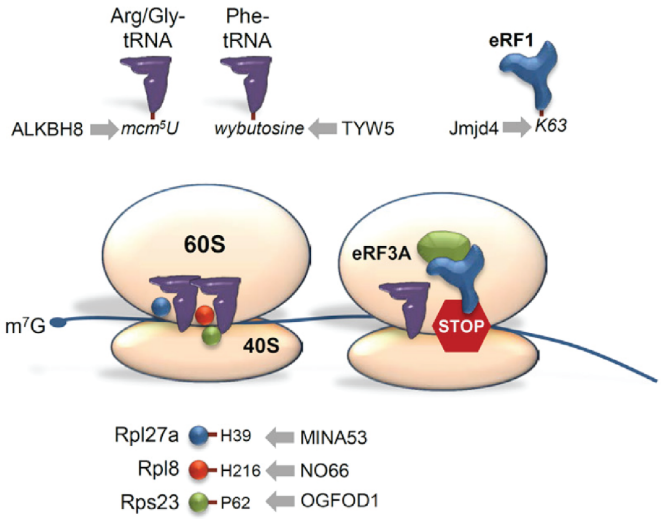

Figure 4: Human 2-Oxoglutarate oxygenases targeting translation by hydroxylating ribosomal protein, translation factors or tRNA. Adapted from Ploumakis et al[43].

Recently, Jmjd4 was identified to hydroxylate a lysine in the NIKS motif of the translation release factor eRF1[1]. This motif is responsible for optimal translation termination.

ROXs directly targeting the ribosome are bacterial ycfD[11] and its eukaryotic homologues OGFOD1[5,20,44], MINA53, and NO66[11,42]. These four enzymes will be discussed in detail in the following subchapters.

1.2.2.1 Bacterial ancestor ycfD

In 1999, *E.coli* ribosomal proteins were analyzed for post-translational modifications by mass spectrometry[45]. In addition to several methylated and acetylated proteins, the authors mentioned an „unknown“ modification in ribosomal protein L16 (RPL16, uL16[17]) at arginine 81 (R81)[45]. Some years later, interaction of ycfD with RPL16 was identified using overexpressed GFP-tagged ycfD in bacteria and also the RPL16-R81 modification as hydroxylation catalyzed by ycfD could be found[4]. This interaction was corroborated and was

suggested that ycfD-binding occurs with RPL16, which is not incoorporated into the ribosome[46].
R81 of RPL16 is located in closest proximity to the peptidyl transferase center (PTC) in the large ribosomal subunit (Figure 5). RPL16 is essential for the association of the large and small subunit to form the 70S initiation complex[47]. In addition, it is important for the peptidyl transferase activity[48] and seems to stabilize the binding of A-site tRNA[49]. Hereby, arginine 56 in RPL16 together with others coordinate tRNA binding. Distinct mutations in RPL16 lead to antibiotic resistance[50].

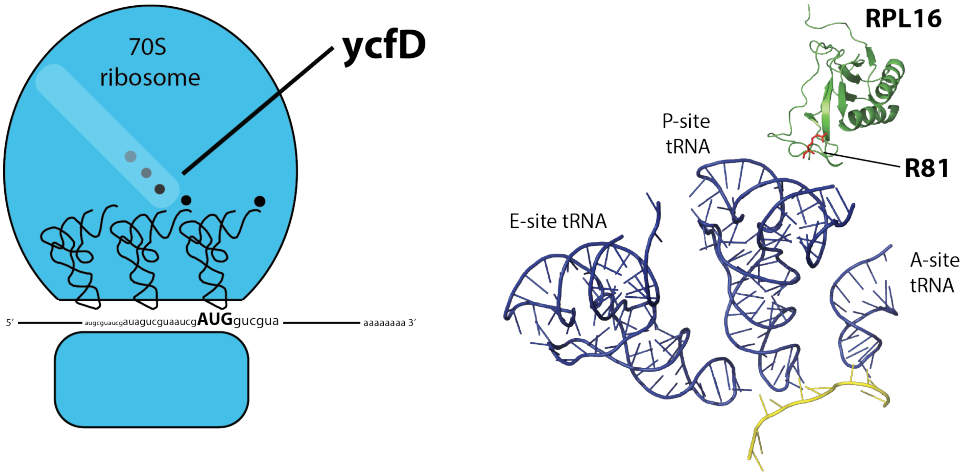

Figure 5: *Thermus thermophilus* 70S ribosome (PDB accession number 2J02 and 2J03); crystal structure on the right reduced to E-, P- and A-site tRNA in blue, mRNA in yellow and RPL16 in green, by ycfD hydroxylated arginine 81 in red (R81).

The molecular function of R81 hydroxylation is still unclear. However, overexpression of His-tagged ycfD led to tremendous growth defects whereas the knockout was viable[4,46]. Under stress conditions like growth in minimal medium, growth defects for the knockout were observed[4].

1.2.2.2 Mammalian homologues Myc-induced nuclear antigen (MINA53) and NO66

Human homologues of ycfD, Myc-induced nuclear antigen (MINA53) and NO66 are two ROXs sharing some striking similarities. Both proteins are localized in the nucleoli, even in the same nucleolar subcompartment[51,52]. Crystal structures revealed a JmjC domain, a proposed dimerisation domain[38,58,59] and a winged helix (WH) domain are highly conserved between the two human proteins and are also shared with bacterial ycfD[6] (Figure 6).

MINA53 and NO66 also modify ribosomal proteins. Both proteins catalyze hydroxylation of histidine residues (H); MINA53 hydroxylates H39 of the ribosomal proteins RPL27a (uL15), NO66 H216 in RPL8 (uL2)[6,17]. Those modified histidine residues are located in the peptide release tunnel close to the peptidyl transferase center (Figure 7)[4].

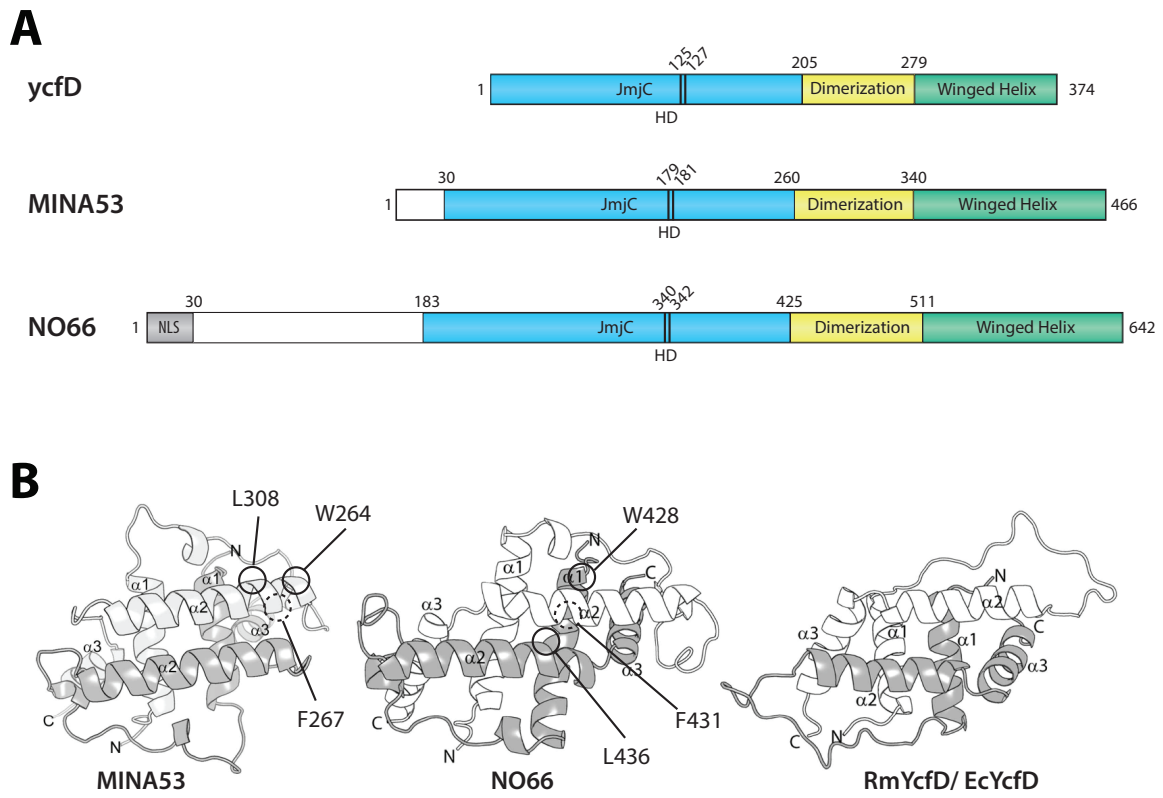

Figure 6: Schematic drawing of ycfD, MINA53, and NO66 domain structure; B) Comparison of dimerization domains, residues essential for interaction in MINA53 and NO66[53] are indicated by circles; figure B is adapted from Chowdhury et al[6].

MINA53 was inititally identified as myc target gene being involved in proliferation[54]. MINA53 mRNA expression was upregulated in alveolar macrophages from coal miners exposed to mineral dust[55]. Following this initial finding, higher MINA53 expression was detected in various cancer types[55-70], similar to the upregulation of oncogene c-MYC[71].

MINA53 is also assigned a role in the cell fate decision from naive CD4+ T cells. T helper type 2 (T_H2) bias correlates with interleukin 4 (IL-4) levels. IL-4 levels feed back positively to drive T_H2 development. MINA53 was found to act as genetic determinant of the T_H2 bias by binding the interleukin 4 (IL-4) promoter and regulating IL4 levels[72]. In mice, MINA53 ablation led to a reduced allergic reaction potentially by reduced IL-4 expression[73]. Others identified MINA53 as regulator of the reciprocal regulatory T cell (Treg) to T_H17 balance[74,75].

The earlier reported histone H3K9me3 demethylase activity[76] could not be confirmed in an *in vitro* assay[77]. A proteomic approach reported the interaction of MINA53 with DNA repair and chromatin binding proteins[78].

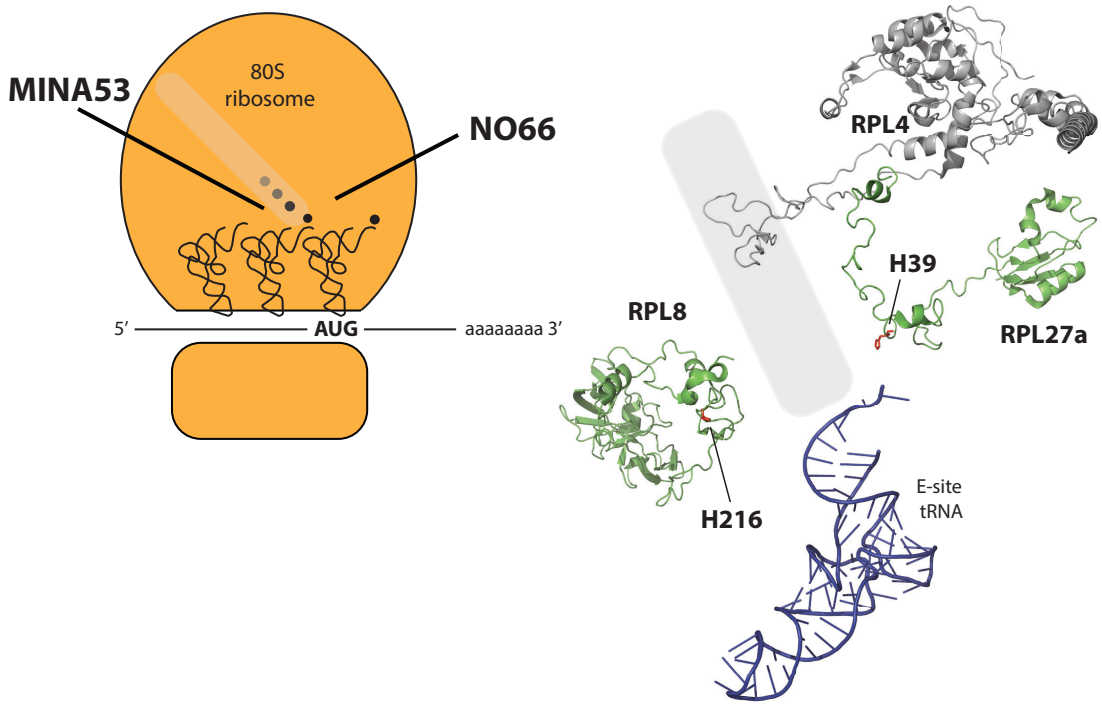

Figure 7: *Homo sapiens* 80S ribosome (PDB accession number 3J3A, 3J3AB and 3J3D). Crystal structure on the right reduced to E-site tRNA in blue, RPL27a with histidine 39 (H39) marked in red as substrate of MINA53, RPL8 with histidine 216 (H216) marked in red as substrate of NO66. Gray bar indicates probable location of the peptide exit tunnel supported by RPL4 (in gray) localization.

First reports described NO66 as a nucleolar protein which cofractionated with pre-ribosomal particles[51]. However, another field of intensive research about NO66 focuses on the regulation of the osteoblast-specific transcription factor Osterix. Osterix is essential for osteoblast differentiation and bone formation and was shown to interact directly with NO66. Additionally NO66 seemed to inhibit Osterix promoter activity[79-82]. In this context, NO66 was shown to demethylate H3K4me3 and H3K36me3 and thereby modify the activity of osteoblast specific promoters[79,83]. Interaction of NO66 with the Polycomb repressive chromatin modifier pointed also towards a role in epigenetic regulation[84]. This finding was later challenged by the identification of JARID1B/KDM5B as the histone demethylase regulating osteoblast specific promoters during differentiation[85]. Like for MINA53, catalytic activity of NO66 towards histones could not be confirmed[77].

1.2.2.3 Proline hydroxylase OGFOD1

OGFOD1 is conserved from yeast to human[86-88]. Structure-wise, OGFOD1 is a special 2OG oxygenase as it consists of two barrel like DSBH domains. However, enzymatic activity is only carried out by the N-terminal domain as it harbours the essential HxD...H triad to coordinate iron (Figure 8). The two DSBHs are seperated by a domain linker. An N-terminal nuclear localization sequence (NLS) is responsible for its nuclear distribution.

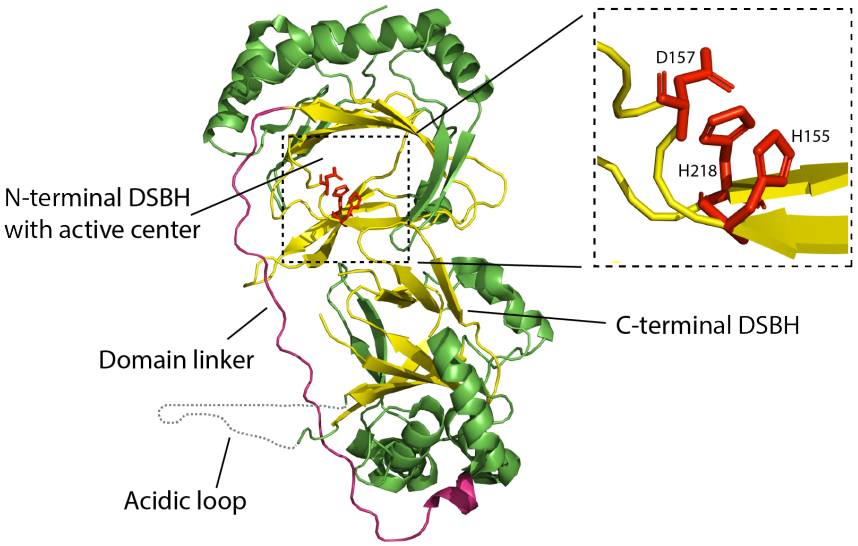

Figure 8: Crystal structure of human OGFOD1 (PDB accession number 4NHX); barrel-like DSBHs are shown in yellow, residues in red show the catalytic center with the HxD...H motif, the domain linker is depicted in magenta, the acidic loop is indicated as dashed line.

2010, OGFOD1 was identified as stress granule component. Interaction proteins comprised some stress granule proteins, the eIF2alpha kinase heme-regulated inhibitor (HRI), and eIF2alpha itself. Overexpression of OGFOD1 resulted in decreased polysome levels and increased amounts of phosphorylated eIF2alpha during recovery from stress. Knockdown on the other hand led to enhanced recovery of translation by enhanced polysome formation during the recovery from stress[89].
Under ischemic conditions, OGFOD1 gene silencing seemed to mediate a resistance to cell death[90].
In a screen of B cells and chronic lymphocytic leukemia (CLL), OGFOD1 was found to have higher transcript and protein levels[91]. Also an involvement in cancer was shown in breast cancer cells, OGFOD1 displayed a high expression[92]. Consistent with this, knockdown in breast cancer cells led to an inhibiton of proliferation probably resulted by an observed G2/M arrest. Another suggestion of OGFOD1 being involved in proliferation regulation or cell cycle control was given recently. Using a whole cell proteomics approach quantitative values of probability for proteins to function in chromatin biology were assessed. Hereby, si-RNA induced OGFOD1 knockdown led to a strong reduction of cells in S-phase[93].

Three accompanying publications in 2014 found that OGFOD1 in *Homo sapiens* (*H.sapiens*), Sud1 in *Drosophila melanogaster* (*D.melanogaster*) and Tpa1 in *Saccharomyces cerevisiae* (*S.cerevisiae*) hydroxylate Pro62 (Pro64 in *D.melanogaster* and *S.cerevisiae*) of RPS23 (uS12)[5,17,20,44].
The human homolog OGFOD1 was shown to hydroxylate RPS23 at proline 62[5] (Figure 9, right picture). RPS23 in bacteria (S12) is localized in the small ribosomal subunit and builds the platform for the codon:anticodon minihelix by interaction of the PNSA loop with the 16S rRNA[19]. The PNSA loop is essential for mRNA decoding (Figure 9)[5], mutations in this region affect the accuracy of decoding and revealed P44 (P62 in humans) as absolutely essential[19].

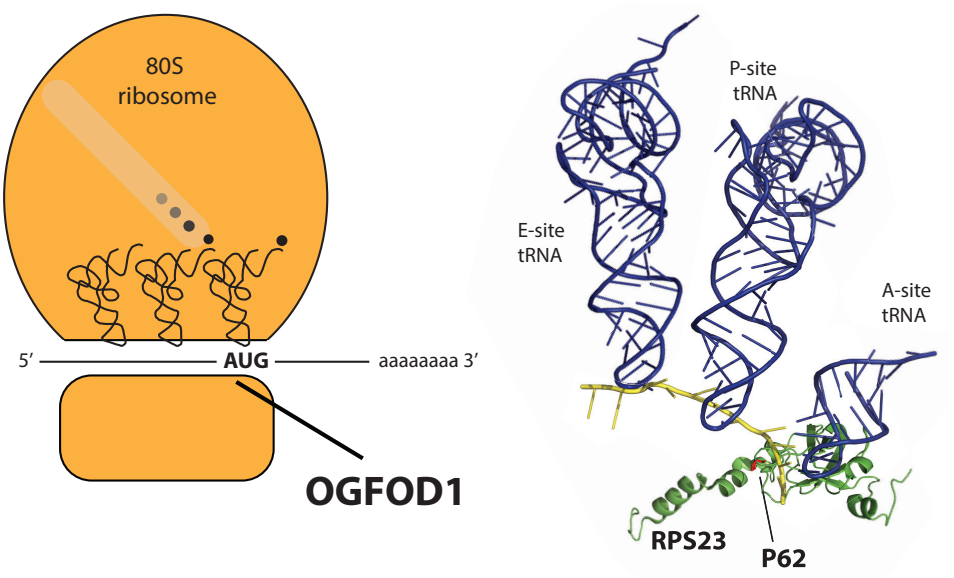

Figure 9: *H.sapiens* 80S ribosome (3J3A, 3J3AB and 3J3D), A- and P-site tRNA from *T.thermophilis* 70S ribosome (PDB: 2J02 and 2J03); crystal structures on the right reduced to E-, P- and A-site tRNA in blue, mRNA in yellow and RPS23 in green, by OGFOD1 hydroxylated proline 62 (P62) in red.

In human, only one hydroxylation occurs (trans-3-hydroxyproline) whereas in yeast the RPS23 seems to be hydroxylated twice. Translational accuracy was tenfold reduced in yeast tpa1 knockout strains[20].
In Drosophila, ubiquitous RNAi knockdown of OGFOD1 homologue Sudestada1 (Sud1) was lethal in the second larval stage. Restricted knockdown to different Drosophila tissues led to reduced cell size and reduced cell number. Next to a decrease in protein synthesis, stress granule formation and activation of the unfolded protein response was observed upon Sud1 knockdown[44,94].
In a case studie of two patients suffering of microcephaly, hearing loss, and overlapping dysmorphic features, mutations in RPS23 were identified. The severeness of ribosomopathies in human highlights the importance of intact and correctly modified ribosomal proteins in general and RPS23 specifically[95].

S.cerevisiae homolog Tpa1 was analyzed by different groups. Related to the function of OGFOD1 in hydroxylating RPS23 (uS12), Tpa1 function in yeast seems to be related to translation. Increased readthrough of stop codons was observed upon deletion of Tpa1[96] as well as decreased translation termination efficacy probably caused by increased stop codon readthrough[87]. Aditionally interaction with the translation termination factors eRF1 and eRF3 as well as with poly(A) binding protein Pab1 indicates a role of Tpa1 in correct translation termination[96]. More recently, another function of Tpa1 was reported. Related to bacterial homolog AlkB, deletion of Tpa1 causes a methylmethane sulfonate sensitivity in *S.cerevisiae*. Tpa1 was shown to repair both single and double-stranded methylated DNA[97].
Function of *Schizosaccharomyces pombe* Ofd1 seems to be related to the FIH role in hypoxia response in humans[98-102].

1.3 Aim of the thesis

This thesis aimed to investigate the ribosomal oxygenases (ROXs) including the prokaryotic ycfD and human OGFOD1, MINA53, and NO66 proteins.

Substrate specificities, mode of interaction with substrates, and characterization of the different protein domains of these proteins should be analyzed. Hereby cell biological and biochemical approaches should be used, like localization and immunoprecipitation assays of different protein variants with their respective substrates, or interaction changes caused by overexpression or knockout. Generation of knockout strains/cell lines should further allow characterization of the cell lines with regards to their ribosome composition and changed PTMs on ribosomal proteins. Knockout cell lines reconstituted with different protein variants could help to characterize those variants in more detail.
Cell cycle regulator CCNA2 should be examined as novel interactor of OGFOD1 by characterizing it as substrate and defining protein sequences or domains necessary for interaction.
MINA53 and NO66 form homo-oligomers *in vivo* and *in vitro*. The homo-oligomerization of both proteins should be investigated with protein-protein interaction studies using deletion and point mutants affecting the dimerization domain. Substrate binding in those mutants should be further analyzed by immunoprecipitation assays and with knockout cell lines reconstituted with different MINA53/NO66 constructs. In a long-term perspective, homo-oligomerization should be evaluated as potential inhibitor target.

2 Results

2.1 Characterization of bacterial ycfD

To find out more about the function of RPL16 arginine 81 (R81) hydroxylation catalyzed by ycfD, the generation of different bacterial knockout strains was planned.
The comercially available ycfD knockout strain JW1114-2[103] showed growth defects in minimal media[4]. By generating genomic modified strains like a ycfD knockout strain, a strain carrying a catalytically inactive ycfD and a strain with RPL16 mutated in the hydroxylated R81 we planned to further pinpoint the mechanisms causing this growth phenotype.

2.1.1 Generation of ycfD knockout and mutant strains

BW25113 (*rpsL150*) was used as initial strain to generate BW25113 (*rpsL150*, ycfD-neo/kan-cassette) and BW25113 (*rpsL150*, ycfD-H125A,D127A) (Figure 10). The ycfD knockout (BW25113 (*rpsL150*, ycfD-neo/kan-cassette)) was generated by inserting a counter selection cassette. This resulted in the deletion of nucleotides 51-1071 of the ycfD gene (Figure 10 B).
BW25113 (*rpsL150*, ycfD-H125A,D127A) encodes the iron-binding defective ycfD (Figure 10 C). The strains generated were confirmed by genomic PCRs and subsequent sequencing.

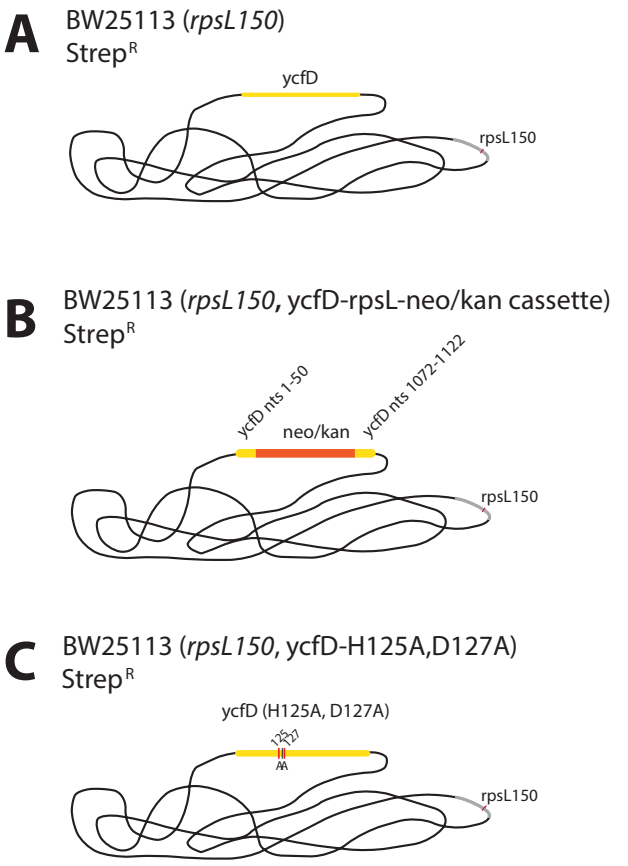

Figure 10: Strains generated using "Counter Selection BAC Modification Kit" from Gene Bridges

YcfD hydroxylates arginine 81 (R81) in RPL16[4]. Thus we also tried to generated a strain with mutated RPL16 R81 to alanine (A). However, using the counter selection kit it was not possible to exchange RPL16 with the counter selection cassette, most likely because RPL16 is

an essential gene and deletion would be lethal. Generated ycfD defective strains were viable under all conditions tested.

2.1.2 Growth assays of different ycfD mutated strains

Earlier studies showed that overexpression of His-tagged ycfD led to tremendous growth defects, whereas the knockout is viable[4,46]. However, under stress conditions like minimal medium, growth defects of the knockout strain were observed[4].

To examine the effects of ycfD, growth assays were performed. BW25113 (*rpsL150*) as wild type strain was investigated under different growth conditions like rich medium (LB medium), minimal medium (M9) or with chloramphenicol (CAP) (Figure 11 A). The same experimental setup was applied for BW25113 (*rpsL150*, ycfD-H125A, D127A) (ycfD AxA mutant strain) and BW25113 (*rpsL150*, ycfD-neo/kan-cassette) (ycfD KO strain) (Figure 11 B and C).

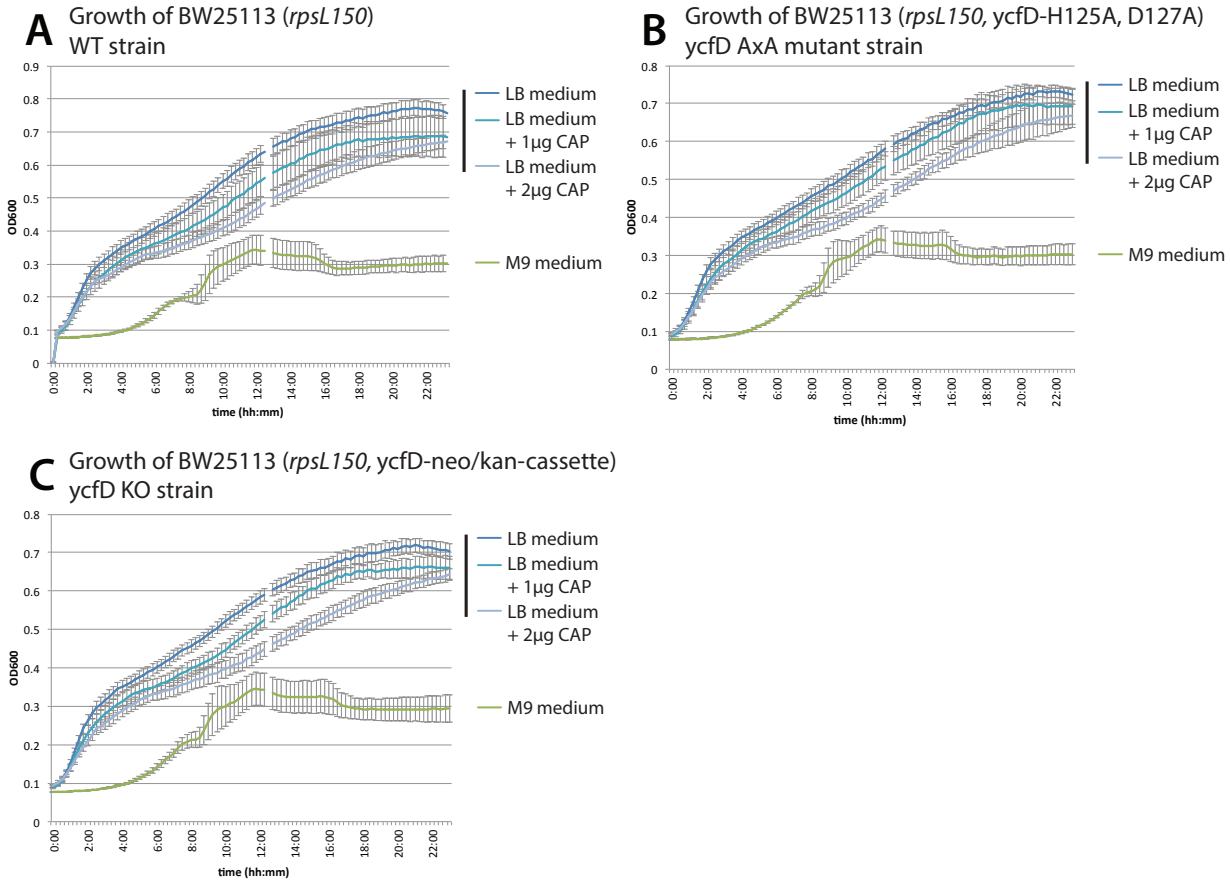

Figure 11: Bacterial growth of different strains at 37°C in different medium for 23h; A) BW25113 (*rpsL150*) as wild type control, B) BW25113 originated strain BW25113 (*rpsL150*, ycfD-H125A, D127A), and C) BW25113 (*rpsL150*, ycfD-neo/kan-cassette) were grown under in LB or M9 medium or with LB medium supplemented with chloramphenicol (CAP).

With increasing CAP concentrations in the LB medium, bacterial growth of all three tested strains was generally reduced (Figure 11). However, minimal media diminished growth significantly independent of genomic ycfD background (Figure 12).

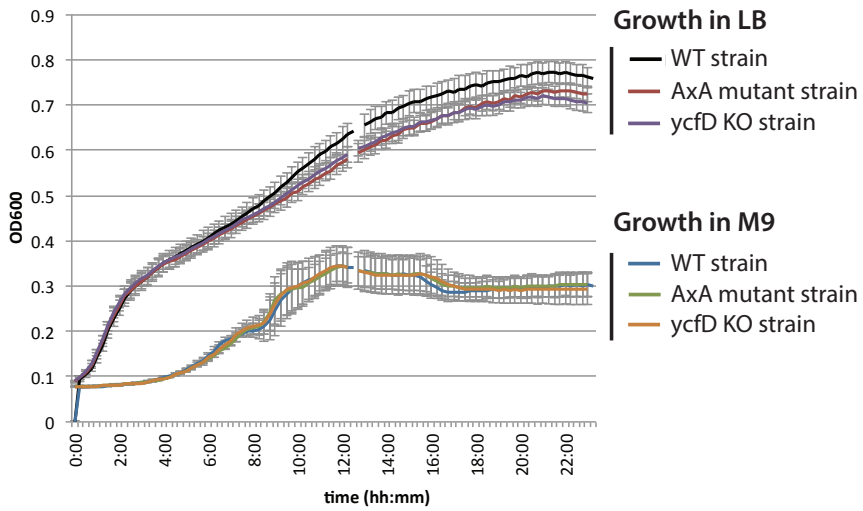

Figure 12: Bacterial growth of different strains at 37°C in LB medium for 23h; BW25113 (*rpsL150*) as wild type control and other BW25113 originated strains were grown in LB or M9 medium.

As this result is contradictory to the observed growth defects of the ycfD knockout strain JW1114[4], this strain was also included in the growth assay. Contrary to the published data, no growth phenotyp of ycfD defective strains could be observed as neither BW25113, nor BW25113 (*rpsL150*), or JW1114 showed distinguishably different growth in LB medium or M9 minimal medium (Figure 13). The reported recovery of the wild type strain (BW25113) in minimal medium[4] could not be reproduced (Figure 13).

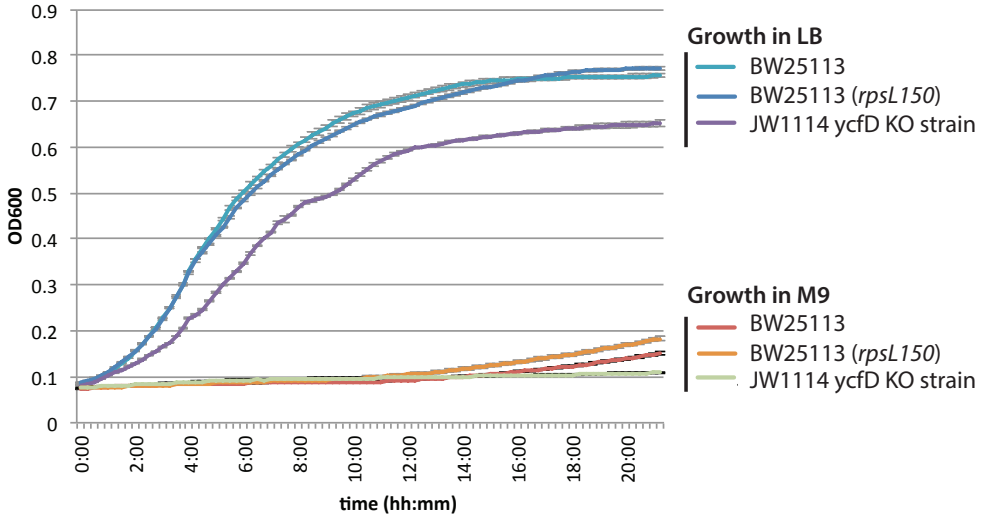

Figure 13: Bacterial growth of different strains at 25°C in LB medium for 22h; BW25113 and BW25113 (*rpsL150*) as wild type control and JW1114 were grown in either LB medium or M9 minimal medium.

Therefore, no growth deficiency of bacteria lacking ycfD (JW1114), lacking ycfD in nts 51-1071 (BW25113 (*rpsL150*, ycfD-neo/kan-cassette), or BW25113 (*rpsL150*, ycfD-H125A,D127A) harboring the active side mutation, could be observed in the used experimental setup.

2.1.3 Ribosome profiles of different ycfD mutated strains

Ribosomes of the different aforementioned bacterial strains have also been analyzed (in collaboration with Daniel Wilson's Lab, Gene Center Munich with the help of Dr. Agata Starosta). Ribosomes were isolated, loaded onto a sucrose gradient (10-40%) and the fractions analyzed.

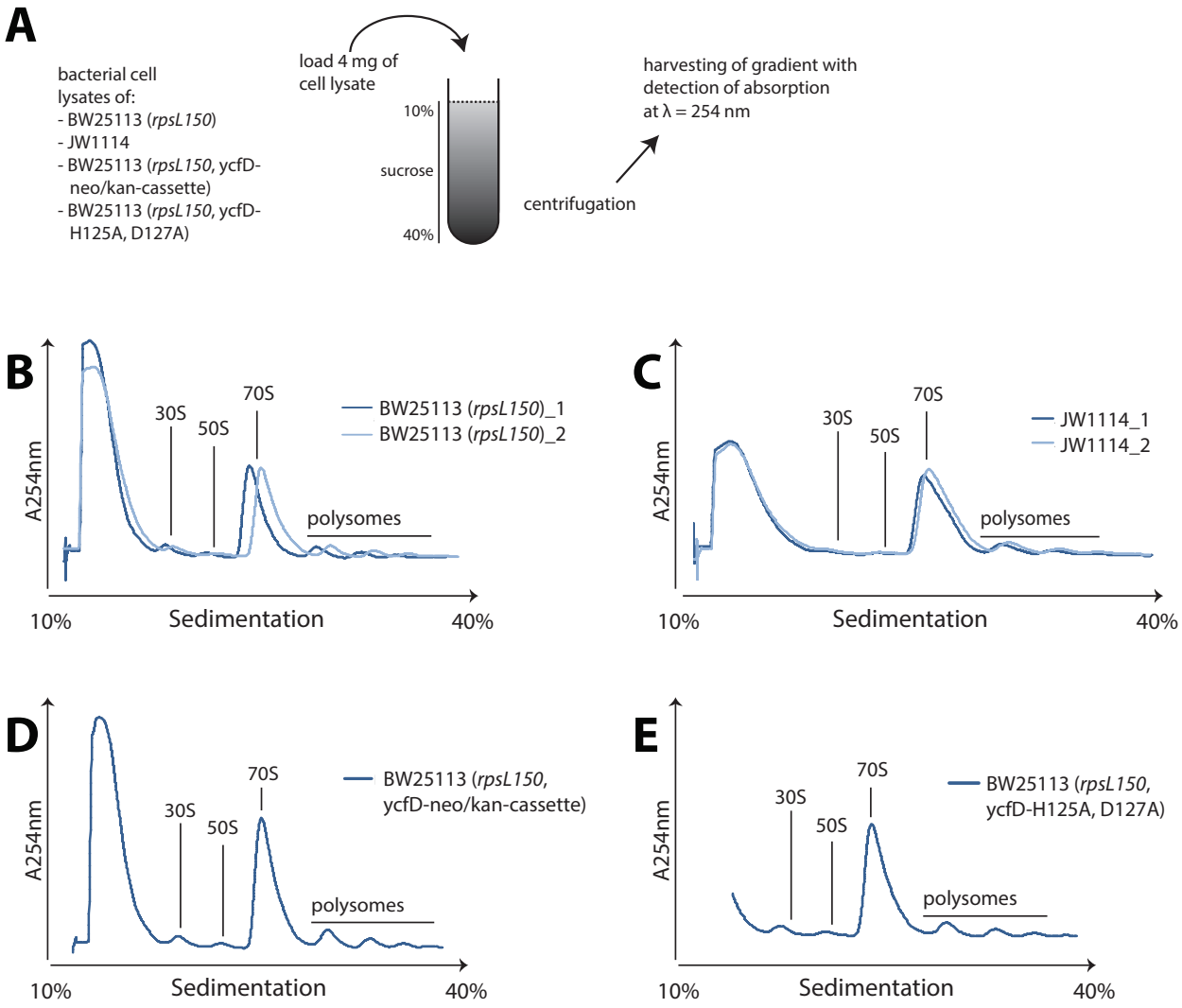

Figure 14: Sucrose gradient A_{260} absorbance ribosome profiles; A) Bacterial lysates were loaded onto a 10-40% sucrose gradient. Following ultracentrifugation, the gradients were fractionated from top to bottom while continuously recording the absorption profile at λ = 254 nm; B-E) Ribosome profiles of B) BW25113 (rpsL150), C) JW1114, D) BW25113 (rpsL150, ycfD-neo/kan-cassette), and E) BW25113 (rpsL150, ycfD-H125A, D127A), the positions of different ribosomal species are indicated

The wild type ribosome profiles displayed a typical bacterial polysome profile (Figure 14 B). The first peak is A_{260} absorbing material, containing no ribosomes. The second and third peaks correspond to the small (30S) and the large ribosomal subunits (50S). The largest amount of ribosomes appears as monosomes (70S peak). Ribosomes associated with mRNA appear in several peaks (polysome peaks). Differences in peak size or complete loss of one ribosomal fraction in the gradient indicate assembly defects or variations in translation activity[104]. Here, ribosome profiles of all tested strains did not show obvious differences (Figure 14).

No differences were detected in growth phenotypes of the different ycfD mutant strains and wild type. Also ribosome profiles of the corresponding strains resulted in no detectable differences. As aditionally generation of a strain mutated in RPL16 was not possible, no further experiments were conducted for ycfD.

2.2 Investigations of human ribosomal oxygenase OGFOD1

2.2.1 Characterization of Cyclin-A2 (CCNA2) as novel interaction partner for OGFOD1

Inital experiments based on immunoprecipitation of GFP-tagged OGFOD1 performed by Dr. Alexander Wolf (HelmholtzZentrum München, experiments performed in C. Schofield lab in Organic Chemistry Department, Oxford) indicated cell cycle protein CCNA2 as novel interaction partner of OGFOD1.
To validate CCNA2 as interaction partner of OGFOD1 and to identify potential hydroxylated prolines in CCNA2, several assays were performed in this thesis.

2.2.1.1 Mode of interaction of OGFOD1 with CCNA2 *in vivo* and *in vitro*

To confirm interaction of OGFOD1 with CCNA2, co-immunoprecipitation (co-IP) assays on endogenous protein level and in different overexpression systems were performed.

First, two CCNA2 antibodies were tested for their capability to immunoprecipitate CCNA2 in Hek293T cells (Figure 15). Sc-751 antibody bound to Protein G Sepharose 4 Fast Flow beads could precipitate CCNA2, as the signal from the eluted protein in the „Beads“ fraction (B) was detectable (Figure 15 B). This antibody binds CCNA2 quite efficiently, as not much protein is detected in the flow through fraction (F), whereas C4710 antibody could not sufficiently precipitate CCNA2, as major protein fractions are lost in the flowthrough (Figure 15 C). Therefore, sc-751 was used for all further endogenous IP experiments.

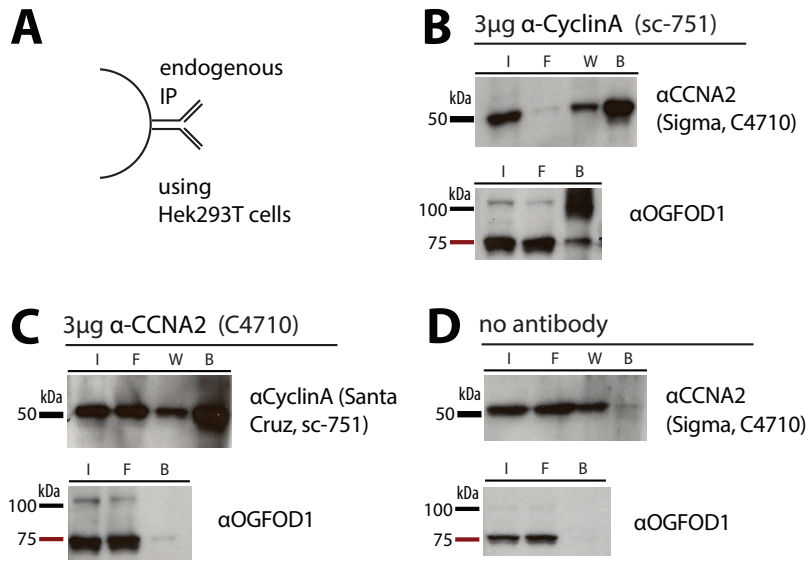

Figure 15: Test of two different CCNA2 antibodies for their capability to immunoprecipitate endogenous CCNA2 from Hek293T cells; A) Protein G Sepharose beads are pre-incubated with B) anti-CyclinA, Santa Cruz sc-751 antibody, C) anti-CCNA2, Sigma C4710 antibody, D) no antibody before adding Hek293T cell lysates. Cyclin-A2/CCNA2 and OGFOD1 were detected with indicated antibodies in subsequent Western blotting. I= Input, F= Flow Through, W= Wash fraction, B= Beads Fraction

OGFOD1 interaction with CCNA2 can be shown on endogenous level, as OGFOD1 with 75 kDa is detected in the CCNA2 IP samples and therefore got co-precipitated with CCNA2 (Figure 15 B, anti-OGFOD1 staining). Notably, with anti-OGFOD1 staining, there is a second

band appearing at around 100 kDa, which can be observed in all IPs using sc-751 (Figure 15A, anti-OGFOD1 staining, B). The 100 kDa band was already reported before as high-affinity complex of OGFOD1 with RPS23 that is stable under SDS/PAGE conditions[5]. Control experiment with no antibody coupled to the sepharose beads did exclude unspecific binding of CCNA2 and OGFOD1 to the beads (Figure 15 D).

To analyze direct interaction of CCNA2 and OGFOD1, I used recombinant proteins. Bacteria expressing either GFP, GFP-CCNA2, or His-OGFOD1 were lysed. GFP or GFP-CCNA2 lysates were mixed with His-OGFOD1 lysates and subsequently, GFP-IP was performed.
GFP-CCNA2 co-immunoprecipitated OGFOD1 (Figure 16 B), whereas control experiment with GFP and His-OGFOD1 did not show interaction (Figure 16 C).

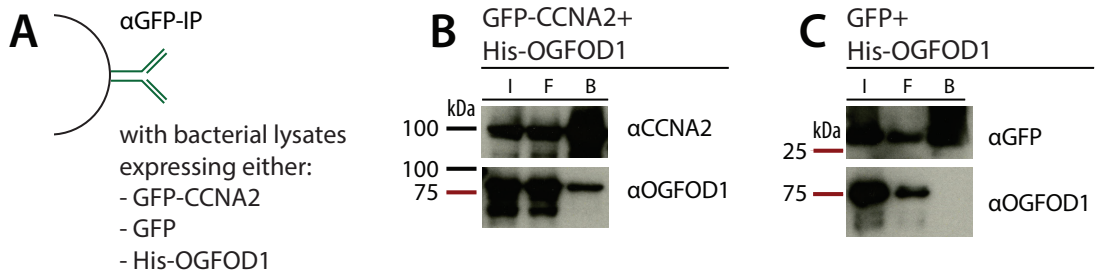

Figure 16: Direct interaction of CCNA2 and OGFOD1 using bacterial expressed proteins; A) BL21 were transformed with GFP-CCNA2, GFP and His-OGFOD1. Lysates of GFP-tagged proteins were preincubated with GFP-Trap_A beads, second lysate was added afterwards to the reaction, following GFP-IP was performed; B) GFP-CCNA2 expressing bacteria were lysed and mixed with His-OGFOD1 lysates; C) GFP expressing bacteria were lysed and mixed with lysates with His-OGFOD1; CCNA2, OGFOD1, and GFP were detected with indicated antibodies in subsequent Western blotting. I=Input, F= Flowthrough, B= Beads fraction

To determine, if CCNA2 in complex with CDK1 or CDK2 is bound by OGFOD1, co-immunoprecipitation of CDK1 and CDK2 with CCNA2 and OGFOD1 was tested. Therefore, IP of CCNA2, OGFOD1, CDK1, and CDK2, was performed with subsequent Western blotting. First, interaction of CCNA2 with OGFOD1 and vice versa could be confirmed (Figure 17, A and B). Binding of CCNA2 to OGFOD1 is specific, as cell cycle protein Cyclin B1 (CCNB1) can not be detected in OGFOD1 IP samples (Figure 17 B). CCNA2 IP results in co-precipitation of OGFOD1, CDK1 and CDK2 (Figure 17 A).
However, the interaction of OGFOD1 with CCNA2 seems to be direct and not in complex with either CDK2 or CDK1, as both do not co-precipitate with OGFOD1 (Figure 17 B). Additionally, neither CDK1 nor CDK2 bind OGFOD1 (Figure 17 C and D). IgG control antibody IP proves specificity of OGFOD1 interaction with CCNA2 as well as CCNA2-CDK1/2.

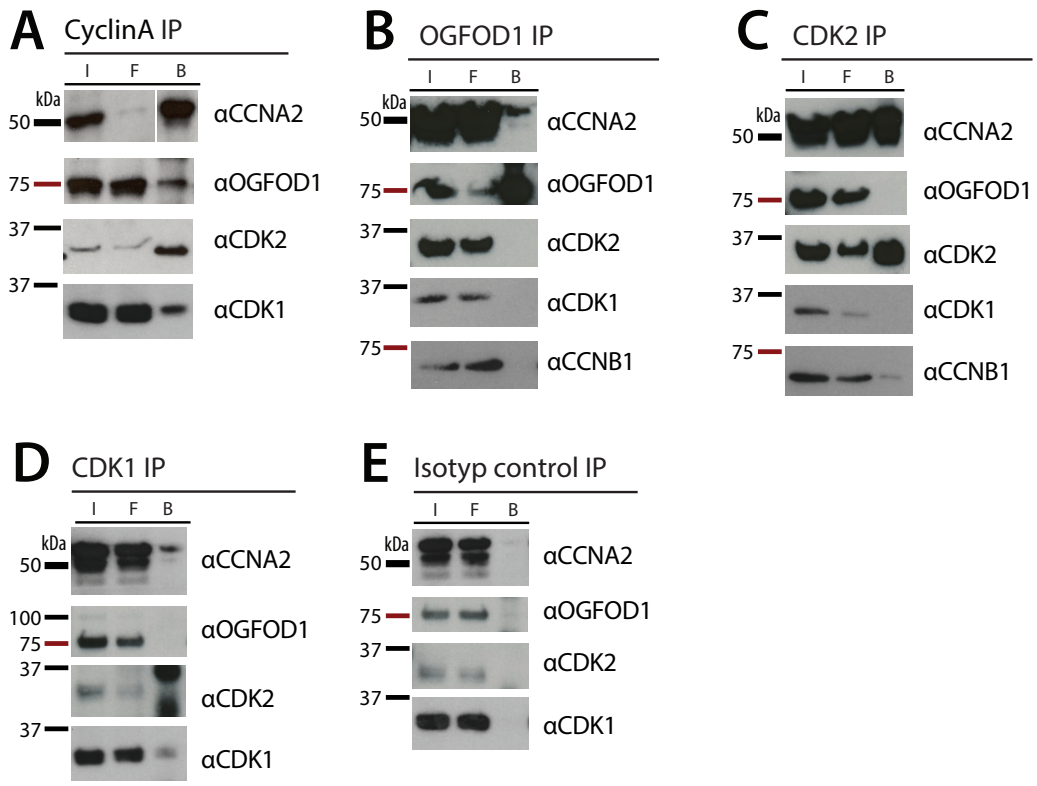

Figure 17: Interaction of CCNA2 and OGFOD1 does not occur in complex with CDK2 or CDK1; Protein G Sepharose beads are pre-incubated with A) anti-CyclinA, B) anti-OGFOD1, C) anti-CDK2, D) anti-CDK1, and E) Isotype control for anti-CyclinA before adding Hek293T cell lysates. CCNA2, OGFOD1, CCNB1, CDK2, and CDK1 were detected with indicated antibodies in subsequent Western blotting. I= Input, F= Flow Through, B= Beads Fraction

Further *in vitro* studies even suggested a competition of CCNA2 binding between OGFOD1 and CDK2. For these experiments, bacterial lysates expressing GFP-CCNA2 was first incubated with untagged OGFOD1 and subsequently with His-tagged CDK2 or vice versa. Direct CCNA2-binding could again be deteceted (Figure 18 B and C). Established CDK2-CCNA2 inhibited additional OGFOD1-CCNA2 interaction (Figure 18 E). OGFOD1-CCNA2 complex formation allowed additional binding of CCNA2 and CDK2 (Figure 18 D). In the negative control neither OGFOD1 nor His-CDK2 can be detected in the IP lane (Figure 18 F).

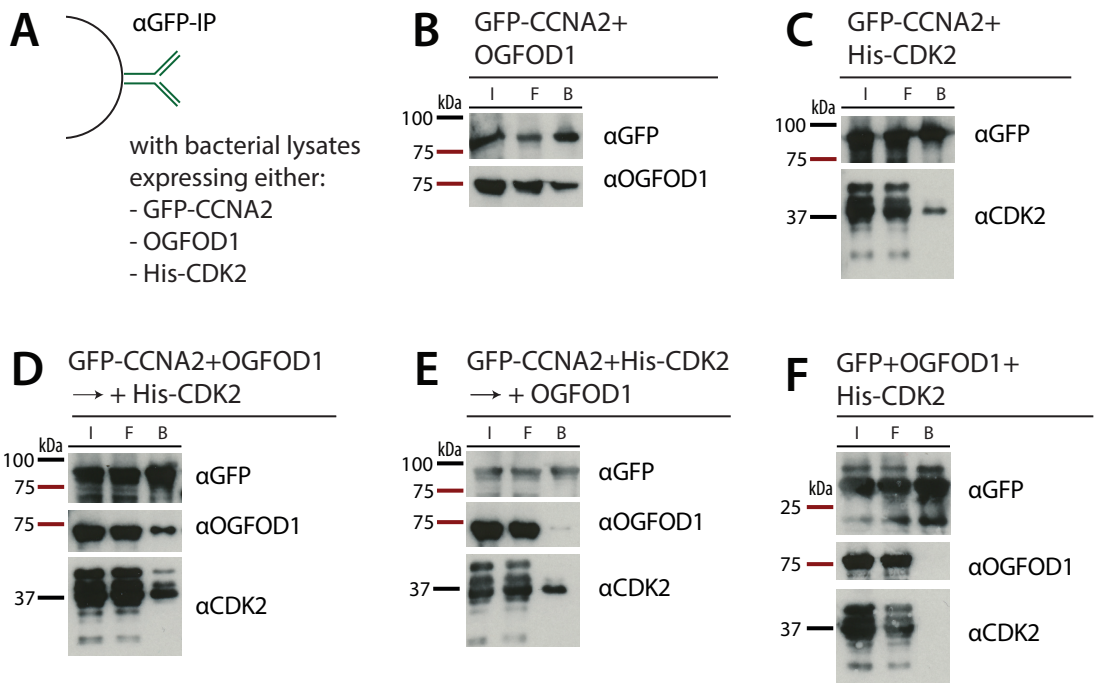

Figure 18: OGFOD1 and CDK2 might compete in binding of CCNA2; A) BL21 were transformed with GFP-CCNA2, untagged OGFOD1 and His-CDK2. Bacteria lysates were mixed and diluted in wash buffer, GFP-IP was performed; B), C) GFP-CCNA2 expressing bacteria were mixed with OGFOD1 lysates or His-CDK2 lysates; D) GFP-CCNA2 lysates expressing bacteria mixed with lysates first with OGFOD1 lysates and following with His-CDK2 lysates or in E) vice versa; F) shows the control experiment with GFP mixed with OGFOD1 and His-CDK2 lysates; GFP-CCNA2, OGFOD1, His-CDK2, and GFP were detected with indicated antibodies in subsequent Western blotting. I=Input, F= Flowthrough, B= Beads fraction

Interaction of CCNA2 and OGFOD1 could be shown by another independent interaction assay, the fluorescent-2-hybrid (F2H) assay. In this assay, genetically modified baby hamster kidney (BHK) cells carry a GFP-anchoring platform in the nucleus[105]. Overexpressed GFP-tagged proteins get localized to the nuclear platform and concentrate thereby in a distinct spot. Co-expression of a mCherry-tagged protein of interest leads in case of interaction to a colocalization in this spot, visible as yellow dot in the overlay of both channels.
Known interaction partner of OGFOD1, ribosomal protein RPS23[5], was used as positive control for this assay. OGFOD1-RPS23 binding was detectable (Figure 19 B-B'''), whereas GFP-NLS was not able to recruit RPS23-mCherry (Figure 19 A-A'''). The same is true for GFP-NLS and CCNA2-mCherry (Figure 19 C-C'''). GFP-OGFOD1 and CCNA2-mCherry accumulated in the same distinct spot in the nucleus (Figure 19 D-E'''), which confirmed OGFOD1-CCNA2 binding.

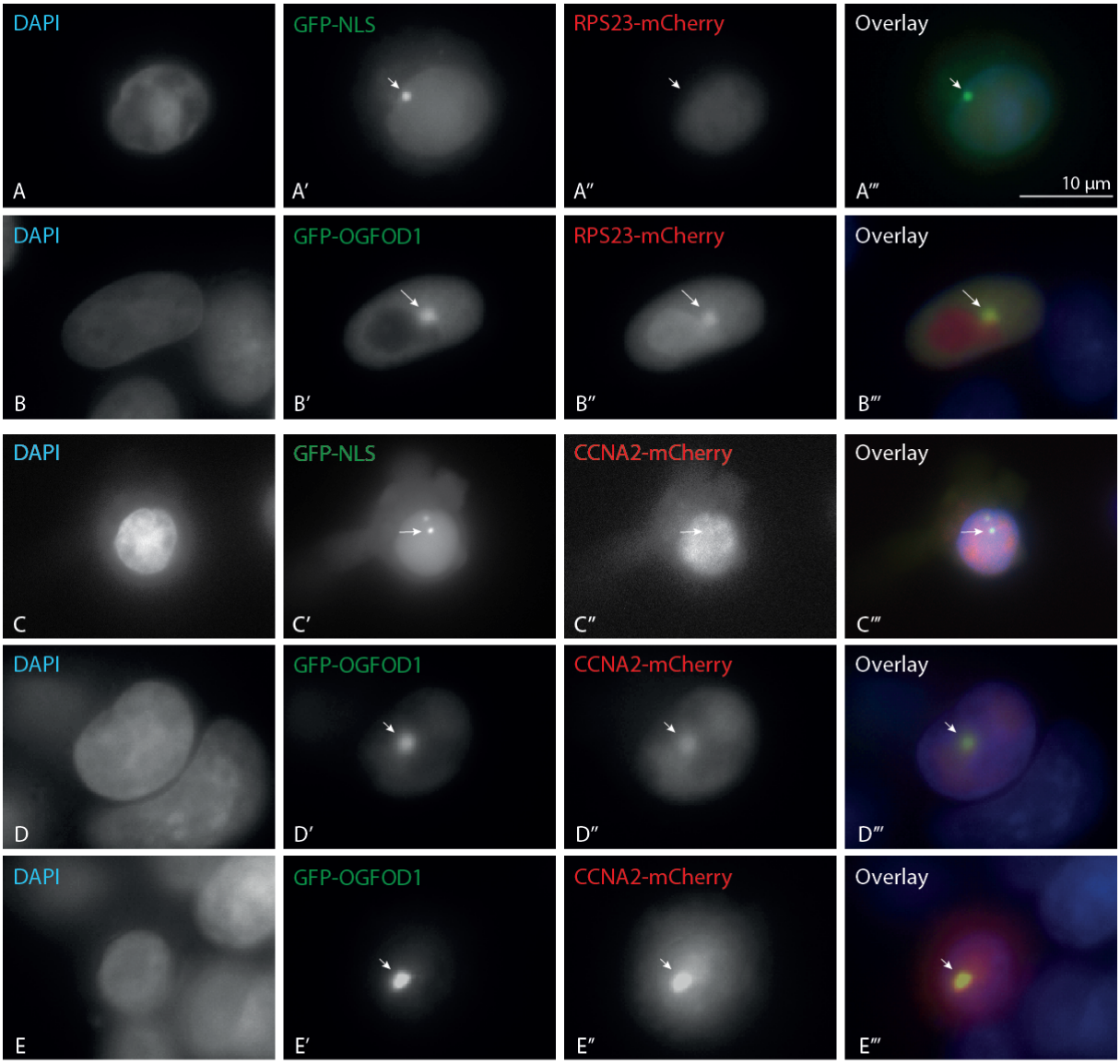

Figure 19: Fluorescent two-hybrid (F2H) assay to study interaction of OGFOD1 and CCNA2; Engineered baby hamster kidney cells (BHK) were transfected with the platform reagent to translocate the GFP tagged protein to the GFP-anchoring platform in the genome resulting in a distinct spot in the nucleus indicated here by arrows; different combinations of GFP-tagged and mCherry-tagged proteins were co-transfected: A-A''' GFP-NLS and RPS23-mCherry, B-B''' GFP-OGFOD1 and RPS23-mCherry, C-C''' GFP-NLS and CCNA2-mCherry, D-D''' GFP-OGFOD1 and CCNA2-mCherry, E-E''' GFP-OGFOD1 and CCNA2-mCherry. Nuclei were counterstained with DAPI, scale is the same for all images

2.2.1.2 *In vivo* and *in vitro* studies to identify OGFOD1 and CCNA2 interaction domains

To further characterize the binding of CCNA2 and OGFOD1, interaction domains in both proteins were analyzed in more detail. Therefore, several deletion and point mutants were generated and tested for binding.

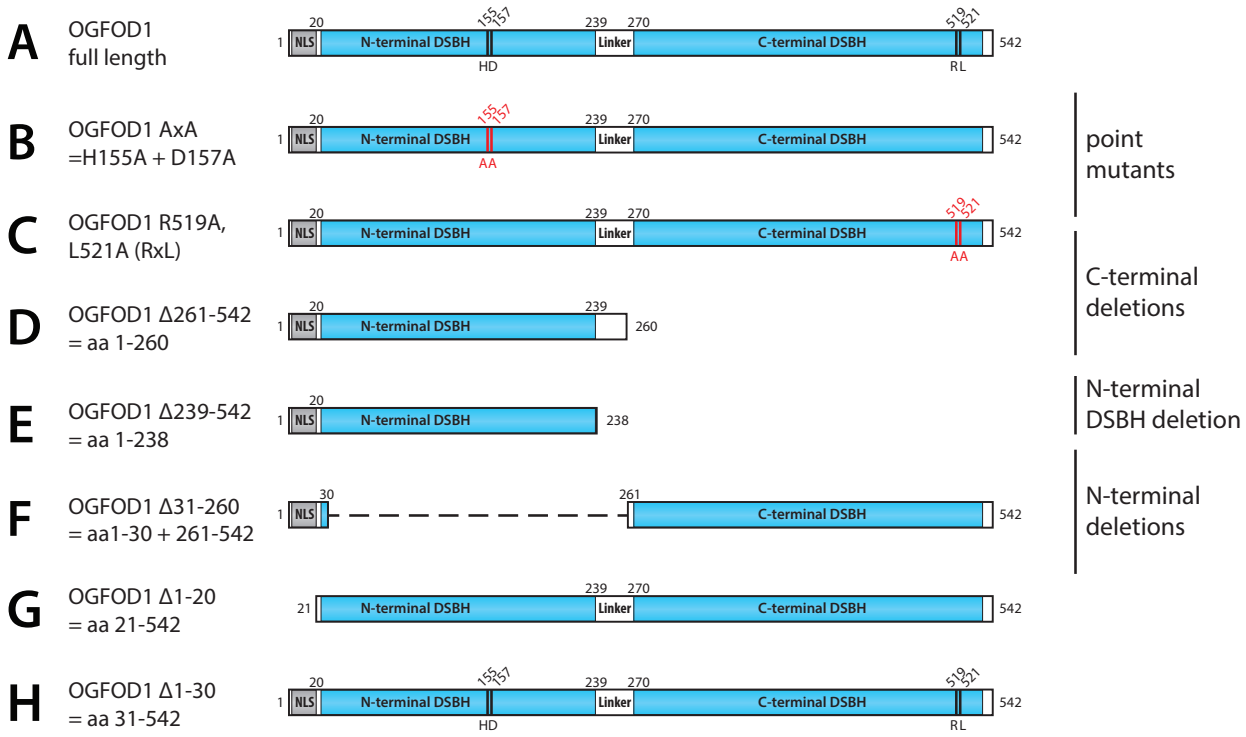

Figure 20: Schematic drawing of OGFOD1 domain structure and generated mutants; nuclear localization signal (NLS) is colored in gray, DSBH domains in blue, mutated amino acids are indicated in red.

Wild type OGFOD1 exhibits the catalytically active N-terminal DSBH domain containing the iron coordinating HxD...H motif and a C-terminal DSBH lacking the iron-binding motif. N-terminal and C-terminal DSBH domains are separated by a linker sequence. The very N-terminal nuclear localization signal (NLS) causes the nuclear localization of the protein (Figure 20 A). The OGFOD1 AxA variant has a mutated iron binding motif, histidine 155 (H155) and aspartic acid (D157) are changed to alanine (A) (Figure 20 B) and is thereby catalytically inactive[5]. RxL motifs were identified to be responsible for CCNA2 binding to substrates like cyclin-dependent kinase inhibitor 1B or CDK-Inhibitor 1[106,107]. One RxL motif was identified in OGFOD1 and mutated (arginine 519 (R519) and leucine 521 (L521) to A) (Figure 20 C).
Several deletion mutants were generated. OGFOD1 1-260 (Δ261-543) lacks the C-terminal DSBH (Figure 20 D), in „aa 1-238“ (Δ239-543) additionally the linker region is deleted (Figure 20 E). OGFOD1 1-30+261-542 (Δ31-260) is depleted of the N-terminal DSBH (Figure 20 F), „aa 21-542“ (Δ1-20) (Figure 20 G) and „aa 31-542“ (Δ1-30) (Figure 20 H) lack the NLS sequence.

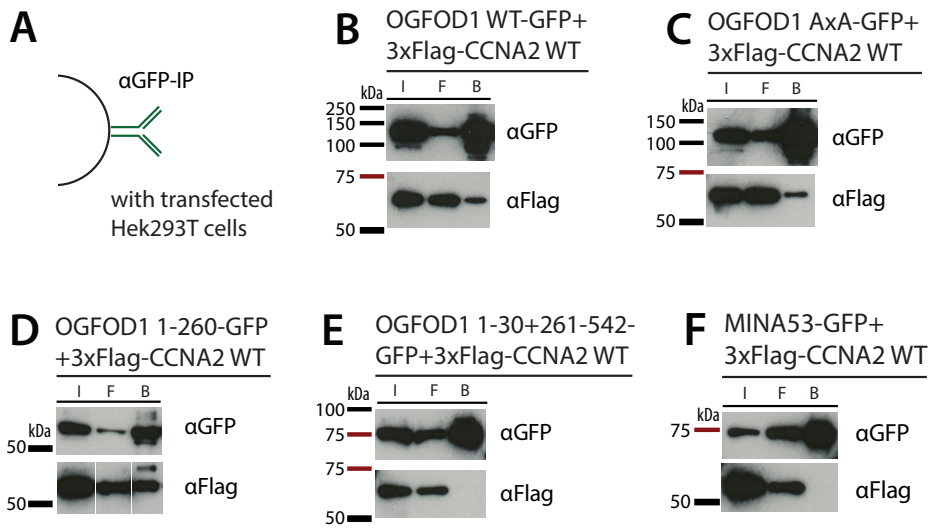

Figure 21: Interaction studies with GFP-tagged OGFOD1 wild type and mutants and Flag-tagged CCNA2 ; A) Hek293T cells were co-transfected and used for GFP-IP; B)-E) GFP-IP was performed with cells overexpressing proteins as indicated; F) MINA53-GFP was used as control; OGFOD1-GFP and mutants, MINA53-GFP, Flag-tagged CCNA2, and endogenous CCNA2 were detected with indicated antibodies in subsequent Western blotting. I=Input, F= Flowthrough, B= Beads fraction

Anti-GFP-IP of OGFOD1-GFP co-precipitated Flag-tagged CCNA2, as confirmed with Flag antibody staining in Western blot (Figure 21 B). Also OGFOD1 iron binding mutant AxA showed interaction with Flag-tagged CCNA2 (Figure 21 C). The OGFOD1 mutant 1-260 did bind to CCNA2 (Figure 21 D) whereas the mutant lacking those amino acids (OGFOD1 aa 1-43 and 261-542 Figure 21 E) did not. Control experiment (Figure F) with another ribosomal oxygenase, MINA53-GFP, and Flag-CCNA2 did not show interaction and confirmed a specific interaction of CCNA2 and OGFOD1.

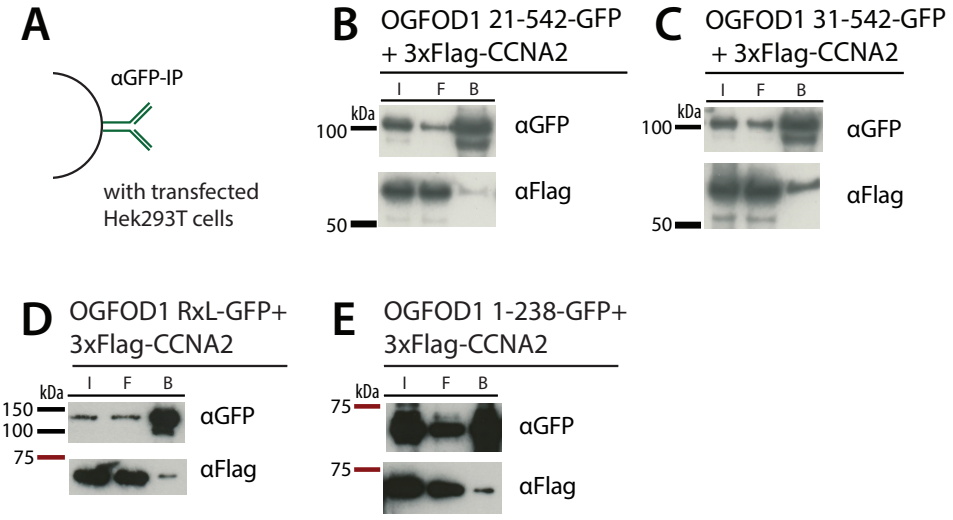

Figure 22: Interaction studies with GFP-tagged OGFOD1 wild type and mutants and Flag-tagged CCNA2 ; A) Hek293T cells were co-transfected and used for GFP-IP; B)-E) GFP-IP was performed with cells overexpressing proteins as indicated; OGFOD1-GFP and mutants and Flag-tagged CCNA2 were detected with indicated antibodies in subsequent Western blotting. I=Input, F= Flowthrough, B= Beads fraction

Both mutants lacking the NLS sequence still interacted with OGFOD1. OGFOD1 lacking the first 20 amino acids (Figure 22 Blot B) might show a reduced ability to interact, whereas OGFOD1 lacking amino acids 1-30 interacted comparable to wild type (Figure 22 Blot C).

Mutation of a putative CCNA2 interaction motif (OGFOD1 RxL) also showed no reduced binding capacity (Figure 22 Blot D). Also, the linker connecting both DSBHs of OGFOD1 did not seem to be important for interaction, OGFOD1 1-238 is potent of binding to CCNA2 (Figure 22 E).

The interaction of CCNA2 and OGFOD1 was also characterized in more detail by using different CCNA2 mutants.

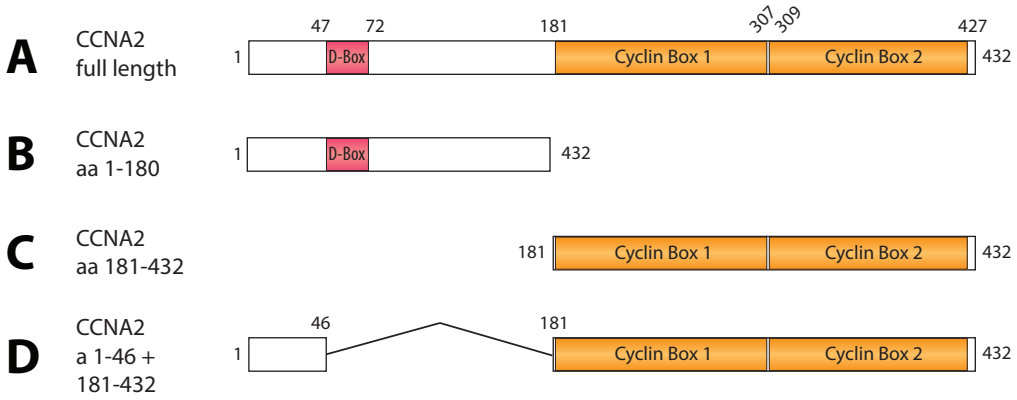

Figure 23: Schematic drawing of CCNA2 domain structure and generated mutants; destruction box (D-Box) is colored in red, the two cyclin boxes in orange

The CCNA2 protein harbours the so-called destruction box (D-Box) and two cyclin boxes.
The D-Box is necessary for cell cycle dependent degradation of CCNA2 by the APC complex, the cyclin boxes are needed for binding to cyclin dependent kinases (CDKs)[108-111].
Three different deletion mutants were generated, CCNA2 1-180 lacks the two cyclin boxes (Figure 23 B), CCNA2 181-432 lacks the entire N-terminus including the D-box (Figure 23 C), and CCNA2 1-46+181-432 is missing the destruction box (Figure 23 D).

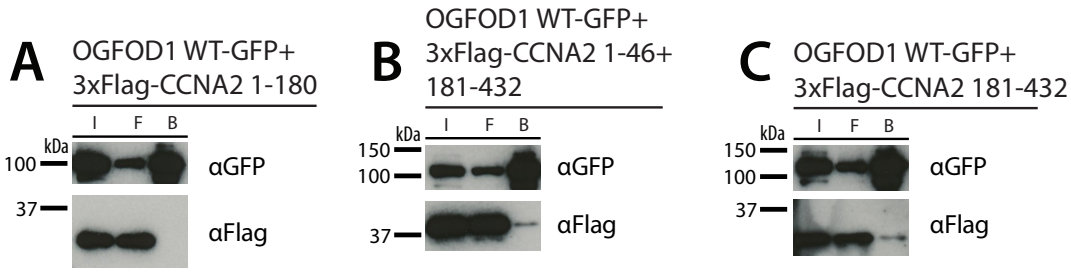

Figure 24: Interaction studies with Flag-tagged CCNA2 wild type and mutants and GFP-tagged OGFOD1; A) Hek293T cells were co-transfected and used for GFP-IP; B)-F) GFP-IP was performed with cells overexpressing proteins as indicated; Flag-tagged CCNA2 and mutants and OGFOD1-GFP were detected with indicated antibodies in subsequent Western blotting. I=Input, F= Flowthrough, B= Beads fraction

CCNA2 1-46+181-432 and CCNA2 181-432 showed OGFOD1 binding (see Figure 24 B and C), whereas CCNA2 1-180 did not co-precipitate OGFOD1 in anti-GFP-IP experiments in Hek293T cells. This pointed towards a binding domain within the cyclin boxes.

In an *in vitro* approach with recombinant protein, I was not able to confirm this binding domain. In this assay, recombinant GFP-tagged CCNA2 or variants expressed in bacteria were tested for binding of recombinant untagged OGFOD1 in anti-GFP-IP experiments. Here,

contrary to the aforementioned cell-based assays, the CCNA2 mutant 1-180 exhibited a stronger OGFOD1 binding (Figure 25 D), compared to CCNA2 181-432 and 1-46+181-432 (Figure 25 E and F). Control experiment confirmed specific binding of OGFOD1 to CCNA2.

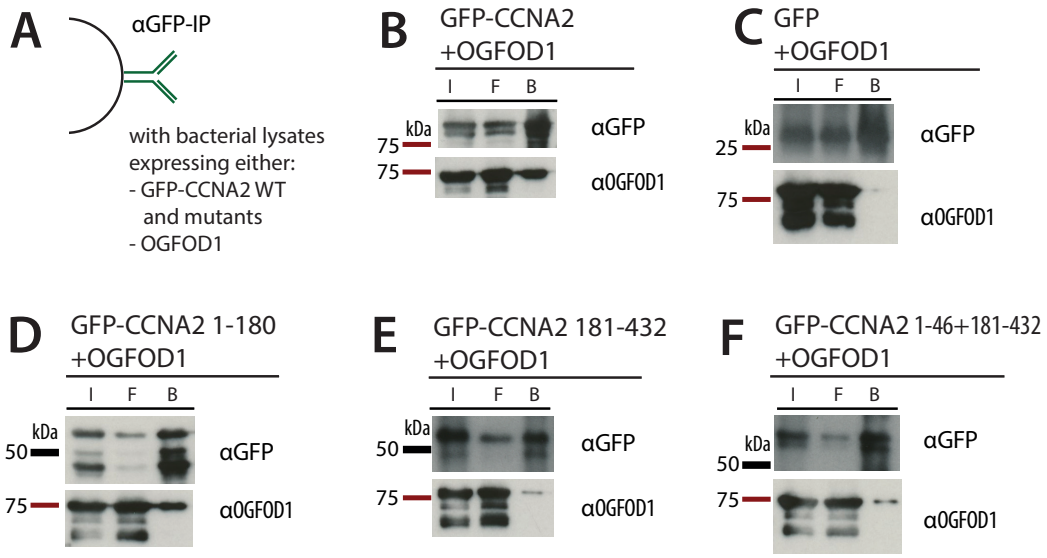

Figure 25: Binding of CCNA2 and mutants to OGFOD1; A) BL21 were transformed with GFP-CCNA2 wild type or mutants and untagged OGFOD1. Lysates of GFP-tagged proteins were preincubated with GFP-Trap_A beads, second lysate was added afterwards to the reaction, following GFP-IP was performed; B)-F) GFP-IP was performed with bacterial lysates expressing proteins as indicated; GFP-tagged CCNA2 and mutants and OGFOD1 were detected with indicated antibodies in subsequent Western blotting, I=Input, F= Flowthrough, B= Beads fraction

These experiments indicated, that the N-terminal DSBH in OGFOD1 is crucial for CCNA2 binding independently of catalytic activity. For CCNA2, no OGFOD1 biding domain was identified with certainty.

2.2.1.3 Investigations to identify hydroxylated prolines in CCNA2 modified by OGFOD1

After having confirmed OGFOD1-CCNA2 binding with different assays, CCNA2 was examined in regard to being an OGFOD1 substrate. Online prediction programs suggested different prolines of CCNA2 to be hydroxylated (see Table 1). iHyd-PseAAC offered P155 and P402 as hydroxyproline sites[112]. PredHydroxy proposed P402-OH with a probability of 0.61[113]. Predictor RF-Hydroxysite[114] predicted P135 with high significance (0.78), P89, P195 and P273 with lower significance (0.5-0.6).

Program	**Prolines in CCNA2**					
iHyd-PseAAC			P155			P402
PredHydroxy						P402
RF-Hydroxysite	P89	P135		P195	P273	

Table 1: Online proline hydroxylation programs used for prediction of CCNA2 proline hydroxylations; in gray identified potenial proline hydroxylation sites with low probability and significance, in black with higher significance; searches were performed 25.08.2016.

To identify hydroxylation sites in CCNA2, liquid chromatography tandem mass spectrometry (LC-MS/MS) was used. Different experimental set-ups were exhibited to circumvent low protein coverages. Endogenous protein, overexpressed 3xFlag-CCNA2, and recombinant GST-CCNA2 were immunoprecipitated (Table 2) and analyzed by label-free LC–MS/MS (Juliane Merl-Pham, Stefanie Hauck, HelmholtzZentrum München). Hydroxylated prolines could be detected in different conditions like co-expression of OGFOD1 or the inactive OGFOD1 AxA mutant before immunoprecipitation (Table 2).

Typ of IP	sample name	CCNA2 coverage [%]	Identified proline hydroxylation
Flag-CCNA2 IP	Flag-CCNA2+ OGFOD1	41	1x P89
			1x P135
			1x P137
	Flag-CCNA2+ OGFOD1 AxA	46	
	Flag-CCNA2+ OGFOD2i1	44	1x P88
			1x P89
endogenous IP	anti-CCNA2 (sc-751)	45	
	no AB	--	
recombinant GST-CCNA2 IP	GST-CCNA2+ His-OGFOD1	60	1x P402
	GST-CCNA2+ His-OGFOD1 AxA	58	
	GST-CCNA2	60	1x P35
			1x P89
	1:10 diluted GST-CCNA2+ His-OGFOD1	56	1x P89
	1:10 diluted GST-CCNA2+ His-OGFOD1 AxA	47	1x P88
	1:10 diluted GST-CCNA2		1x P89
		54	

Table 2: Overview of performed LC-MS/MS experiments, CCNA2 coverage in each experiment and sample, and by LC-MS/MS identified hydroxylated prolines on CCNA2

In the different IP experiments with Flag-tagged CCNA2, endogenous CCNA2, or in an in vitro assay, different proline hydroxylations were suggested. In the recombinant approach CCNA2 hydroxylated prolines were also suggested in samples containing only GST-CCNA2. Depending on experiment, different hydroxylated prolines were identified or even none (endogenous IP, Table 2), therefore no reliable hydroxylation could be detected with LC-MS/MS.
Protein coverage of CCNA2 in the three experiments ranged from 41-60%. Therefore, several peptides with potential hydroxylation sites were not detected (Figure 26 A). However, attempts to increase CCNA2 coverage by combined digest with Chymotrypsin/Trypsin did not result in higher protein coverages (data not shown).

In order to specify OGFOD1-catalyzed proline hydroxylation in CCNA2, we used matrix-assisted laser desorption/ionization - time of flight mass spectrometry (MALDI-TOF-MS).

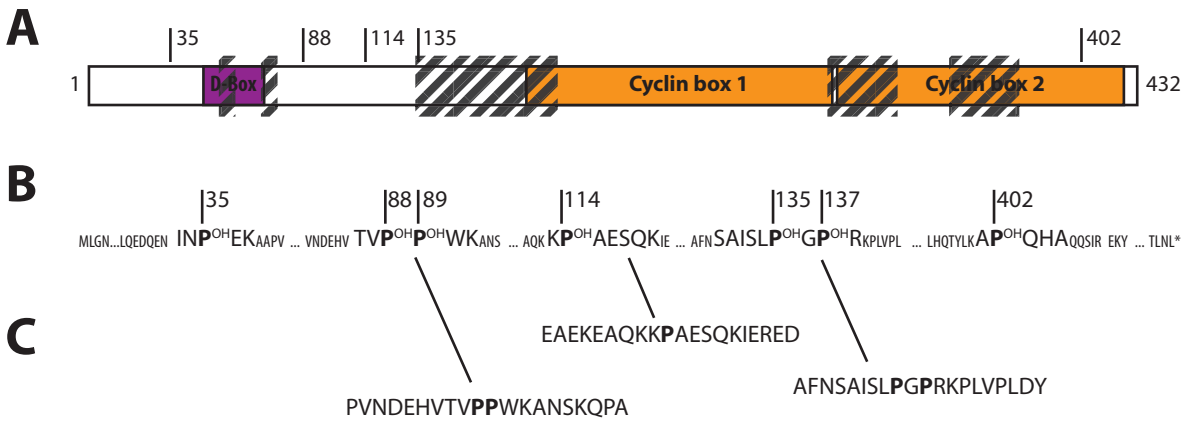

Figure 26: Schematic overview of domains of CCNA2; A) coverage of CCNA2, dashed boxes indicate not covered sequences; B) identified potential hydroxyprolines by LC-MS/MS; C) selected peptides tested using peptide hydroxylation assay with MALDI-TOF.

Here we generated peptides spanning prolines, which were suggested by preceding LC-MS/MS analysis to be hydroxylated (Figure 26 C). These peptides were incubated with recombinant OGFOD1 and co-factors and subsequently analyzed for hydroxylation by MALDI (in cooperation with Cyrille Thinnes in the C. Schofield laboratory in the Chemistry Research Laboratory, Oxford).

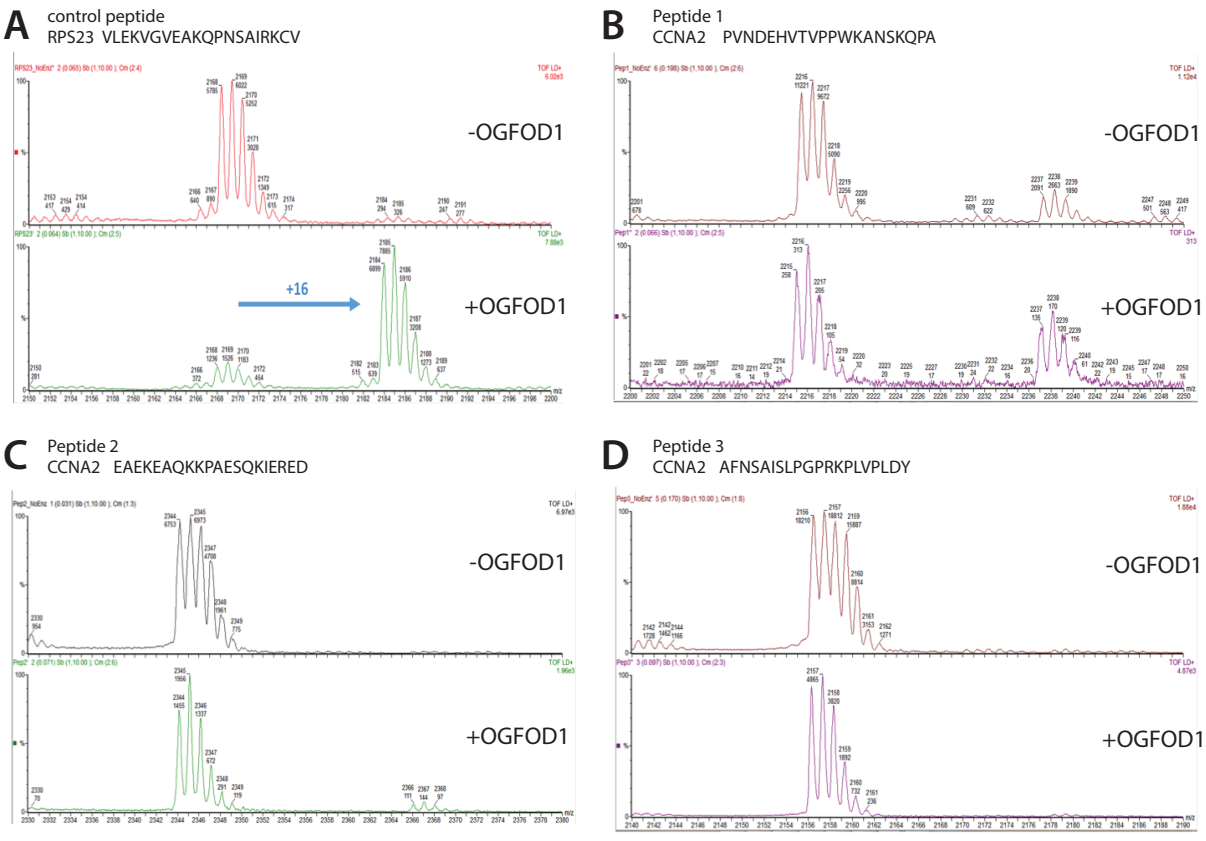

Figure 27: CCNA2 peptide hydroxylation assay by MALDI-TOF; A) control 20-mer peptide of RPS23[5] shows a 16 Da shift after addition of OGFOD1 in vitro, B)-D) tested CCNA2 20-mer peptides masses without OGFOD1 and with OGFOD1 addition; Reaction Conditions: 7.7 µM recombinant OGFOD1, 50 µM peptide, 300 µM 2oxoglutarate, 100 µM Fe(II), and 1mM Ascorbate; reaction was incubated for 3h at RT and quenched with formic acid.

Recombinant OGFOD1 was catalytically active as addition of the protein causes a 16 Da shift in the known substrate peptide of RPS23[5] (Figure 27 A). The three tested CCNA2 peptides covering P88 and P89 (peptide 1), P114 (peptide 2), and P135 and P137 (peptide 3) did not show a mass shift after addition of OGFOD1. Therefore, in this assay no OGFOD1-catalyzed hydroxylation of the selected peptides could be observed (Figure 27 B-D).

2.2.1.4 Effects of OGFOD1-CCNA2 interaction onto the cell cycle

OGFOD1 binding of one of the major cell cycle regulating cyclins raised the question, if OGFOD1 expression is also regulated in a cell cycle dependent way. To address this, the HeLa cell line stably expressing Cell Cycle Chromobody® fused to the red fluorescent protein Tag RFP® (Chromotek) were used in immunofluorescence (IF) to monitor the OGFOD1 expression pattern. Additionally, Hek293T cells were synchronized and expression levels of OGFOD1 through the cell cycle were checked using western blot. Also interaction of CCNA2 and OGFOD1 throughout the cell cycle was monitored. Furthermore, cell cycle progression of synchronized cells overexpressing GFP-tagged OGFOD1 and the OGFOD1 AxA mutant was analyzed.

Studies to characterize OGFOD1 and CCNA2 localization and expression throughout the cell cycle

To determine the subcellular distributions of proteins throughout the cell cycle, the HeLa cell line stably expressing a RFP-tagged nano-antibody against endogenous PCNA[115] was used. Proliferating cell nuclear antigen (PCNA) localization provides a precise marker for S phases as it is a helping factor for DNA synthesis during replication. With starting S phase, PCNA protein gets associated with DNA polymerase δ and localizes to small distinct dots in the nuclei corresponding to active sites of replication. With ongoing replication, PCNA coupled to polymerase shifts to nucleolar DNA resulting in bigger dots during mid-S phase. In late S-phase, DNA at the periphery of the nucleus gets replicated[116]. Mitotic cells (Pro-, Meta-, Ana- and Telophase) were distinguished by characteristic DNA patterns[117].

Immunofluorescent analyses confirmed increasing CCNA2 levels in early S phase and the sudden degradation in prometaphase[109] (Figure 28).

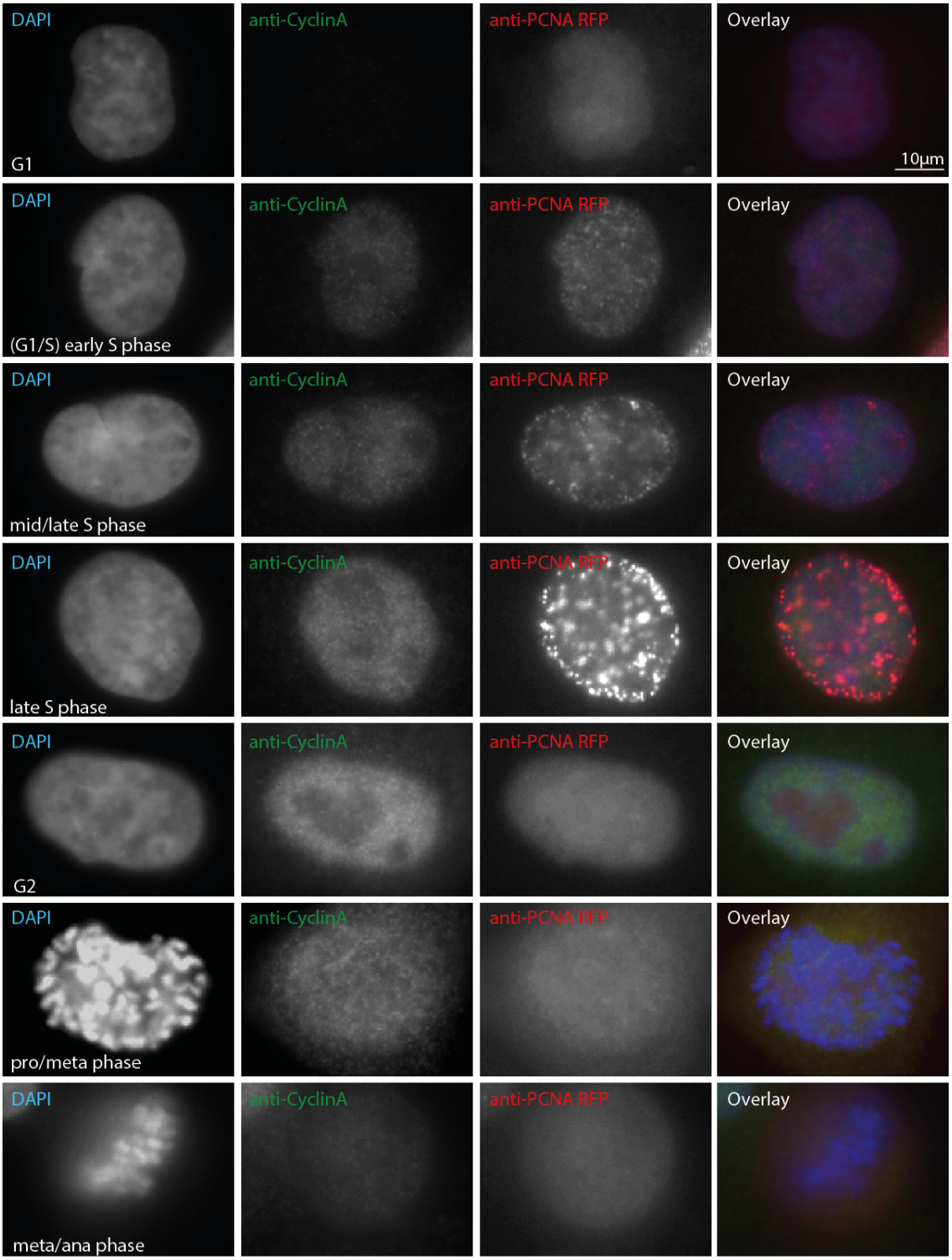

Figure 28: Distribution of CCNA2 during the cell cycle in HeLa chromobody (Chromotek) cells; fixed cells were stained with anti-Cyclin A antibody and Alexa-488 coupled secondary antibody, DNA was counterstained with DAPI.

In contrast to CCNA2, OGFOD1 localization or expression did not show any dependency on the cell cycle. OGFOD1 protein was detectable in all cell cycle phases and there seemed to be no difference in protein amount (Figure 29).

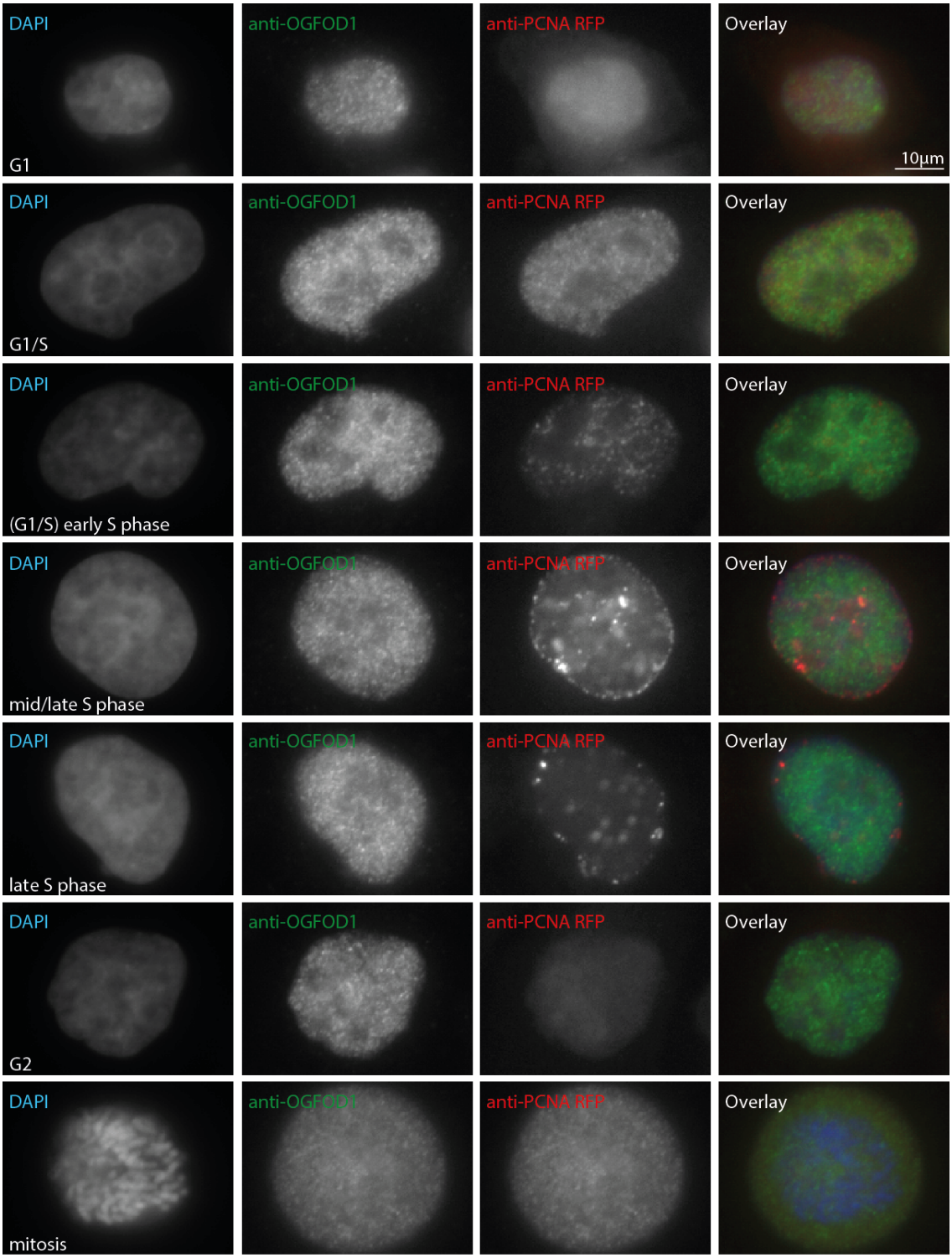

Figure 29: Distribution of OGFOD1 during the cell cycle in HeLa chromobody (Chromotek) cells; fixed cells were stained with anti-OGFOD1 antibody and Alexa-488 coupled secondary antibody, DNA was counterstained with DAPI.

To investigate OGFOD1 protein amounts in the different cell cycle phases in more detail, Hek293T and HeLa cells were synchronized with a double thymidine block which leads to an early S phase block (Figure 30 A). After release from the second thymidine block, cells were monitored for their progression through the cell cycle by flow cytometric analysis of DNA content (Figure 30 D) and by western blot (Figure 30 C). In an asynchronized cell population,

most cells were in G0/G1 phase with two chromosome sets (2N), some cells are replicating their DNA in S phase, whereas the next peak displays cells in G2 or M phase with 4N DNA content (Figure 30 B). The profiles displayed here show the early S phase block, as cells from 0 h after release nearly completly were concentrated in a peak corresponding to S phase (Figure 30 D). Hek293T cells progress from early S phase to G1 in around 9 h, HeLa cells are slower and reached G1 after 12h (for HeLa, see Figure 31).

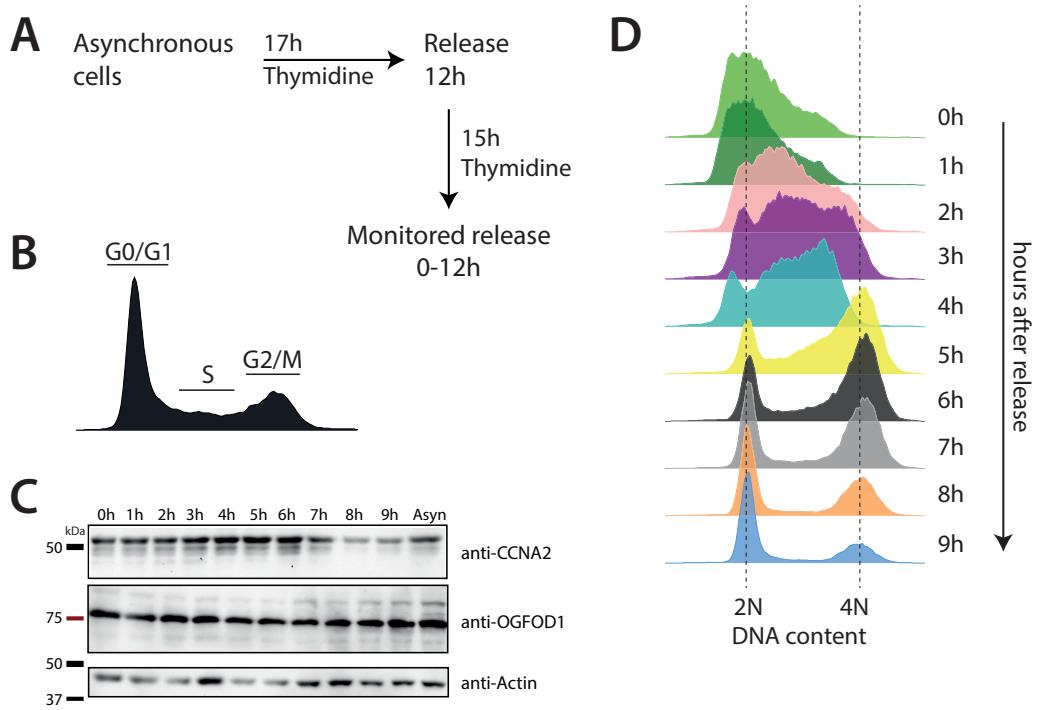

Figure 30: A) Experimental scheme for Hek293T/HeLa cell synchronization. Cells were synchronized by a double thymidine block resulting in early S phase block; B) Cell cycle profile of a asynchronized cell population, cellular DNA content allows classification of cells into the different cell cycle phases as indicated, relative DNA content is plotted against cell number; C) Protein levels corresponding to each time point OGFOD1, Cyclin A2, and Actin as loading control obtained from Hek293T cells at different time points during synchronization; D) Flow cytometry achieved DNA profiles after Hoechst33342 staining of synchronized Hek293T cells (0-9h)

In accordance with the immunofluorescence analysis, CCNA2 protein levels were regulated by the cell cycle (Figure 30 C). Protein levels changed with the progession of the cells from early S phase to mitosis. Highest levels of CCNA2 were detectable from hour 4 to hour 6 after release, which corresponds to late S-phase to mid/end of mitosis. OGFOD1 levels were unchanged throughout the progression of the cell cycle (Figure 30 C).

Studies to analyze interaction of CCNA2 and OGFOD1 throughout the cell cycle

Due to the cell cycle independency of OGFOD1 protein levels, we asked if interaction with CCNA2 happens only in distinct phases of the cell cycle. For this purpose, synchronized Hek293T/HeLa cells were collected for 9 hours/12 hours after release and endogenous anti-OGFOD1 and anti-CCNA2 IP were performed.

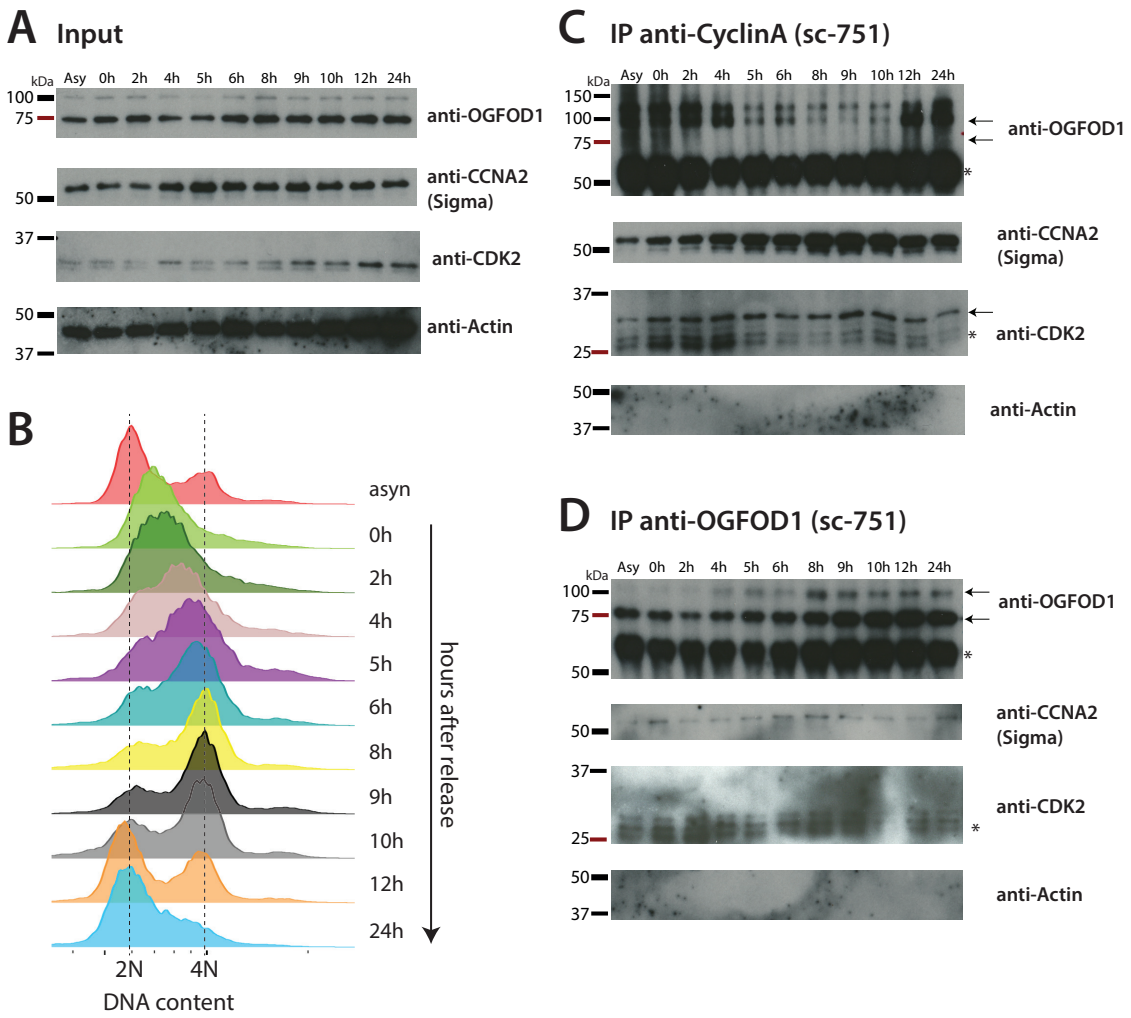

Figure 31: Interaction studies of OGFOD1 with CCNA2 in HeLa cells during the cell cycle; HeLa cells were synchronized with a double thymidine block. Samples were taken after indicated hours after release. Cell cycle profiles were obtained by flow cytometry after NUCLEAR-ID® Red DNA stain (ENZO life sicence, ENZ-52406) staining of DNA. In A) western blot analysis of input fractions, in B) DNA content of cells harvested to indicated time points determinded by flow cytometry; C) western blot analysis of IP of endogenous CCNA2, in D) of IP of endogenous OGFOD1; blots were stained with anti-OGFOD1, anti-CCNA2, anti-CDK2 and anti-Actin as loading control; asterisks indicates heavy or light chain of IP antibody.

IP of CCNA2 and OGFOD1 in HeLa cells revealed cell cycle independent interaction.

Western blot analysis of synchronized cells showed cell-cycle regulated expression of CCNA2, but not of OGFOD1. CKD2 levels were unaltered compared to the loading control Actin (Figure 31 A). Most cells were synchronized with the double thymidine block (Figure 31 B).

CCNA2 co-precipitated CDK2, but not actin (Figure 31 C). OGFOD1 monomer band at 75kDa could not be co-precipitated by CCNA2, however two higher bands above 100 kDa appeared (Figure 31 C). A steric hinderance of the OGFOD1 binding site by the CCNA2 IP antibody can not be excluded in this assay. With OGOFD1 being precipitated, weak CCNA2 interaction bands appeared cell cycle independent, even though levels of precipitated OGFOD1 were different. CKD2 and Actin were not interacting with OGOFD1 (Figure 31 D).

Identification of the impact of OGFOD1 overexpression onto CCNA2 and the cell cycle

To analyze a potential impact of OGFOD1 overexpression onto the cell cycle, synchronized Hek293T cells were transfected and analyzed for their cell cycle progression (Figure 32).

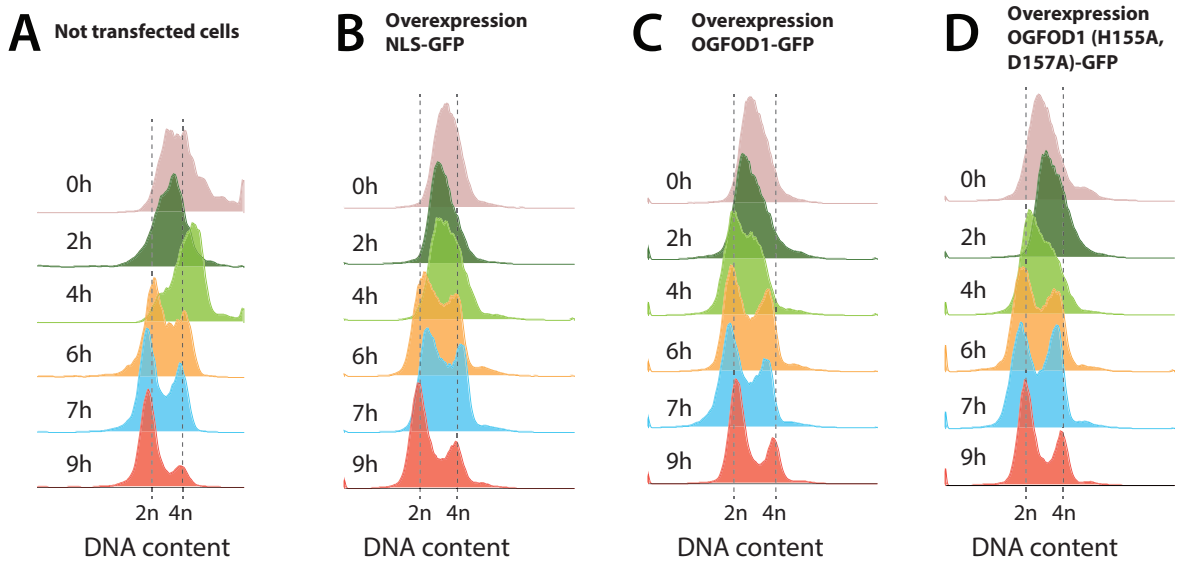

Figure 32: Influence of GFP-tagged OGFOD1 on cell cycle progression; Hek293T cells were synchronized with a double thymidine block. Between the first and second block, cells were transfected with indicated GFP-tagged proteins. Samples were harvested after indicated hours after release. Cell cycle profiles were obtained by flow cytometry after NUCLEAR-ID® Red DNA stain (ENZO life science, ENZ-52406) staining of DNA. In A) untransfected cells B)-D) overexpression of GFP-tagged proteins as indicated

In initial experiments, Hek293T cells were transfected between first and second thymidine treatment with NLS-GFP, OGFOD1-GFP, or OGFOD1 (H155A, D157A)-GFP. After the final release, progression through the cell cycle under the different conditions was monitored by flow cytometry of GFP-positive cells. At least 10.000 cells per sample were recorded, but due to technical problems, for time points 0 h and 2 h of untransfected cells (Figure 32 A) around 3000 cells were recorded (exact cell numbers in Appendix 6.1.1, Figure 69). Staining of the fixed cells with same amount of DNA dye, despite different cell numbers might lead to the slightly shifted DNA profiles (Figure 32 A).

Overexpression of NLS-GFP (Figure 32 B) seemed to have only minor effects on cell cycle progression, as the DNA profiles showed the block in early S-phase and cell cycle progression comparable to not transfected cells (Figure 32 A). Upon overexpression of GFP-OGFOD1, the cells seemed to remain longer in the S phase block, a major subset of cells seems not to be able to proceed further (Figure 32 C). In comparison to cells overexpressing NLS-GFP (Figure 32 B), already at 4 h post-release the main peak of OGFOD1-GFP overexpressing cells is oriented more to the 2N content (Figure 32 C). Also the cells at 6 and 7 h seemed not to proceed to 4N and mitosis, but might remain in the intermediate state of S phase. However, profiles at 9 h were similar in all samples. Therefore, a block of cells overexpressing OGFOD1-GFP might not be permanent.

Overexpression of iron-binding defective OGFOD1 (OGFOD1-H155A, D157A) displays similar profiles than NLS-GFP cells (Figure 32 D).

Overexpression of OGFOD1 and AxA mutant was also tested in another setting. Hek293T cells were co-transfected with Flag-CCNA2 and either OGFOD1, or OGFOD1 AxA (H155A, D157A), or OGFOD2I1 (Figure 33 A and more detailed list in Appendix 6.1.1 Figure 71). An anti-Flag IP of CCNA2 was performed and the CCNA2 interaction partners were analyzed by LC-MS/MS.

A

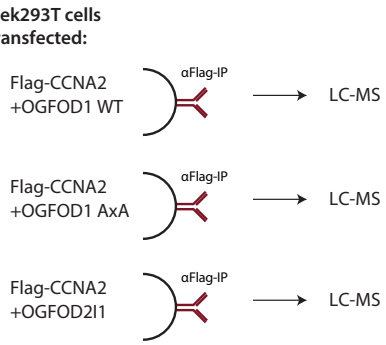

B

Accession	Unique peptides	Confidence score	Name	Description	Ogfod1 WT/ control	Ogfod1 MUT/ control
P55795	2	353	HNRNPH2	Heterogeneous nuclear ribonucleoprotein H2	77.98	88.12
Q7L014	6	189	DDX46	Probable ATP-dependent RNA helicase DDX46	68.95	2.76
Q9BYN8	2	64	MRPS26	28S ribosomal protein S26, mitochondrial	47.59	63.52
O00299	2	49	CLIC1	Chloride intracellular channel protein 1	46.40	67.65
P49591	2	55	SARS	Serine--tRNA ligase, cytoplasmic	31.58	38.92
Q15637	2	41	SF1	Splicing factor 1	30.96	57.78
P20674	2	59	COX5A	Cytochrome c oxidase subunit 5A, mitochondrial	30.67	42.04
Q86VP6	3	61	CAND1	Cullin-associated NEDD8-dissociated protein 1	22.18	18.08
P30520	2	58	ADSS	Adenylosuccinate synthetase isozyme 2	18.87	25.95
Q8N543	9	224	OGFOD1	Prolyl 3-hydroxylase OGFOD1	18.10	16.01
P49755	2	72	TMED10	Transmembrane emp24 domain-containing protein 10	16.82	20.95
Q15181	3	86	PPA1	Inorganic pyrophosphatase	14.69	19.46
Q99497	3	75	PARK7	Protein deglycase DJ-1	12.45	15.62
P30048	2	68	PRDX3	Thioredoxin-dependent peroxide reductase, mitochondrial	11.73	10.62
P62937	3	90	PPIA	Peptidyl-prolyl cis-trans isomerase A	11.18	12.62
P62273	2	56	RPS29	40S ribosomal protein S29	11.02	12.37
P35080	2	60	PFN2	Profilin-2	10.35	18.36
P15927	2	46	RPA2	Replication protein A 32 kDa subunit	10.05	9.10
P27797	8	222	CALR	Calreticulin	10.00	11.56

Figure 33: Selection of proteins with highest enrichment identified in Flag-CCNA2 IP with additional overexpression of OGFOD1 wild type (WT), OGOFD1 H155A, D157A (MUT), and OGFOD2 Isoform 1 (OGFOD2I1, „control“) using LC-MS/MS; A) Anti Flag-IP was performed with ANTI-FLAG® M1 Agarose Affinity Gel with Hek293T cell lysates overexpressing indicated proteins and analyzed by LC-MS/MS; B) Proteins identified to be highly enriched in the Flag-CCNA2-IP versus the control sample.

Comparison of CCNA2 binding proteins revealed several proteins like HNRNPH2 or DDX46 which were enriched in Flag-CCNA2 IP samples when OGFOD1 wild type (WT) or OGFOD1 MUT (OGOFD1 AxA) were overexpressed (Figure 33 B).

We also performed anti-CCNA2 IP of endogenous CCNA2 and characterized the binding proteins with LC-MS/MS. Many known interactors of CCNA2 were identified like cyclin dependent kinases (CDKs) 1 and 2 or SKP2, also SCAPER[121,122] was highly enriched in CCNA2 IP versus the control (see Appendix 6.1.1, Figure 70). LC-MS/MS results of the Flag-CCNA2 IP (Figure 33) were filtered for specific interaction partners of CCNA2, that were identified before in mass spectrometry results from endogenous immunoprecipitated CCNA2.
Using these parameters, RPA2 and RPA1 were identified as proteins which showed most increased binding to CCNA2, when OGFOD1 or OGFOD1 AxA mutant were overexpressed (Figure 34 B, more detailed list in Appendix 6.1.1 Figure 73). DExD/H-box protein DDX46

binding to CCNA2 was increased with OGFOD1 WT overexpression, but not with the OGFOD1 AxA mutant. CDK2 or SCAPER binding to CCNA2 on the other hand seemed to be weakend.

A

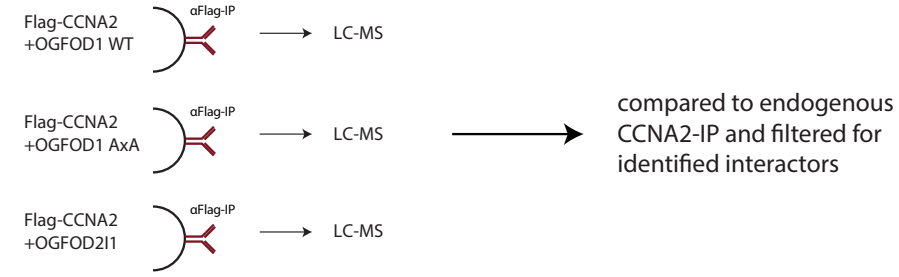

B

Accession	Unique peptides	Confidence score	Name	Description	Ogfod1 WT/ control	Ogfod1 MUT/ control
P15927	2	46	RPA2	Replication protein A 32 kDa subunit	10.05	9.10
P60174	8	273	TPI1	Triosephosphate isomerase	8.71	10.28
P27694	3	95	RPA1	Replication protein A 70 kDa DNA-binding subunit	4.74	3.72
P55209	6	227	NAP1L1	Nucleosome assembly protein 1-like 1	4.26	4.32
Q9H0U4	2	57	RAB1B	Ras-related protein Rab-1B	3.65	3.34
Q14974	7	184	KPNB1	Importin subunit beta-1	2.79	3.15
P31930	2	68	UQCRC1	Cytochrome b-c1 complex subunit 1, mitochondrial	2.78	2.95
Q04837	2	70	SSBP1	Single-stranded DNA-binding protein, mitochondrial	2.68	2.66
P78527	23	628	PRKDC	DNA-dependent protein kinase catalytic subunit	2.20	2.15
				...		
P20248	**21**	**784**	**CCNA2**	**Cyclin-A2**	**0.82**	**0.60**
				...		
Q9BY12	15	475	SCAPER	S phase cyclin A-associated protein in the endoplasmic reticulum	0.64	0.59
Q7Z2Z1	10	340	TICRR	Treslin	0.62	0.60
P28749	16	477	RBL1	Retinoblastoma-like protein 1	0.56	0.55
Q12834	16	599	CDC20	Cell division cycle protein 20 homolog	0.55	0.48
Q92793	4	107	CREBBP	CREB-binding protein	0.54	0.55
O75496	5	104	GMNN	Geminin	0.52	0.44
P63208	4	121	SKP1	S-phase kinase-associated protein 1	0.50	0.42
Q9Y3Z3	24	778	SAMHD1	Deoxynucleoside triphosphate triphosphohydrolase SAMHD1	0.45	0.38
Q9H211	5	149	CDT1	DNA replication factor Cdt1	0.43	0.43
P24941	7	291	CDK2	Cyclin-dependent kinase 2	0.42	0.34

Figure 34: Selection of proteins filtered for specific CCNA2 interaction with highest (more than 2 fold) and lowest (less than 0.6) enrichment identified in Flag-CCNA2 IP with additional overexpression of OGFOD1 wild type (WT), OGOFD1 H155A, D157A (MUT), and OGFOD2 Isoform 1 (OGFOD2I1, „control“) using LC-MS/MS; A) Samples from Flag-IP were analyzed by LC-MS/MS, the results were selected by specific interaction partners of CCNA2 identified by endogenous CCNA2-IP before; B) Proteins identified to be highly enriched or decreased in the Flag-CCNA2-IP versus the control sample

To exclude, that changes in CCNA2 binding where due to OGFOD1 induced changes of the subcellular localization of CCNA2, immunofluorescent stainings with overexpressed OGFOD1 were performed (Figure 35). Overexpression of OGFOD1-GFP and NLS-GFP did not alter endogenous CCNA2 localization (Figure 35 B'' and C''), as it is distributed like CCNA2 in cells with no transfection (Figure 35 A'').

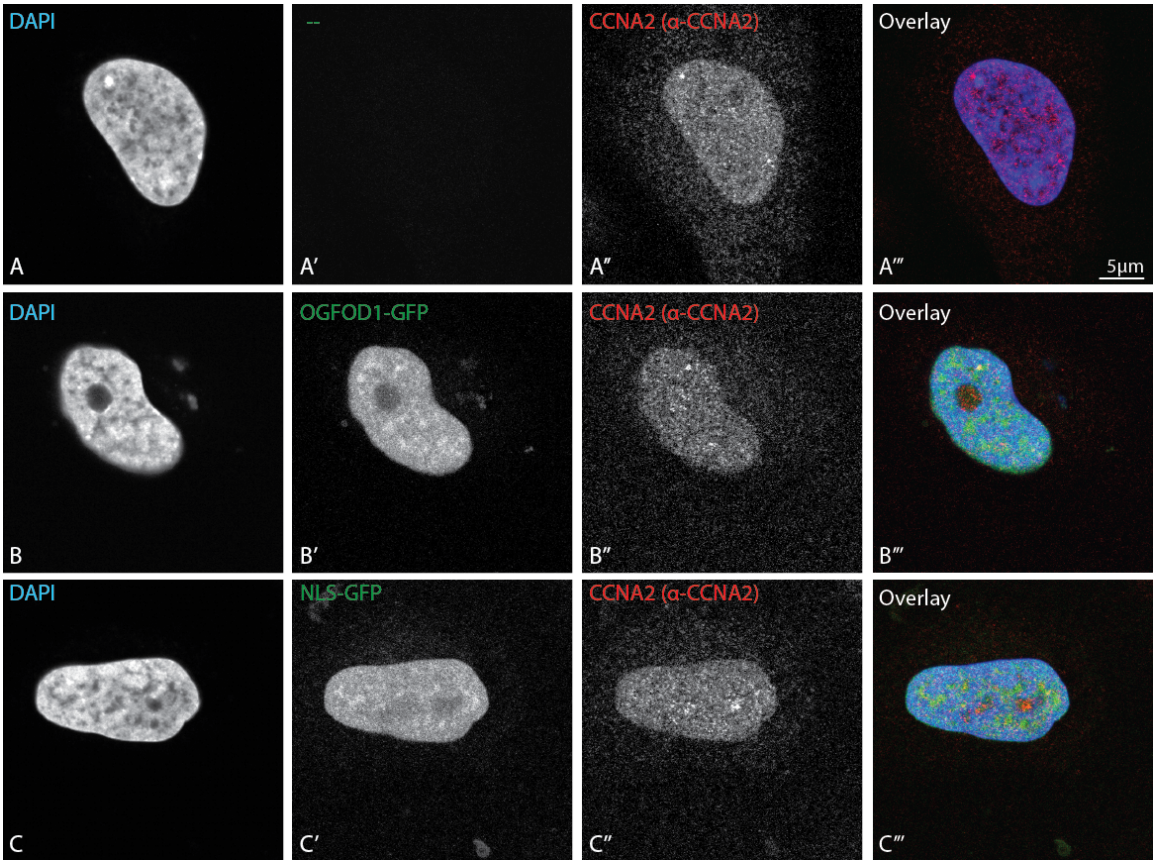

Figure 35: OGFOD1 overexpression and endogenous CCNA2 localization; with indicated construct transfected HeLa cells were fixed and stained with anti-CCNA2 antibody and Alexa-594 coupled secondary antibody, DNA was counterstained with DAPI.

2.2.2 Identification of eEF2K as potential novel interaction partner for OGFOD1

Recently, eukaryotic elongation factor-2 kinase (eEF2K) was reported to be hydroxylated on a proline residue[118]. eEF2K phosphorylates eukaryotic elongation factor 2 (eEF2), this modification inhibits eEF2s ability to interact with the ribosome and thereby impairs translation elongation. Proline 98 hydroxylation of eEF2K restrained its activity and might regulate translation via eEF2[118].

As OGFOD1 is a prolyl hydroxylase, we were interested if OGFOD1 is the so far unknown enzyme modifying eEF2K. For this, GFP-IPs and the F2H assay were performed.

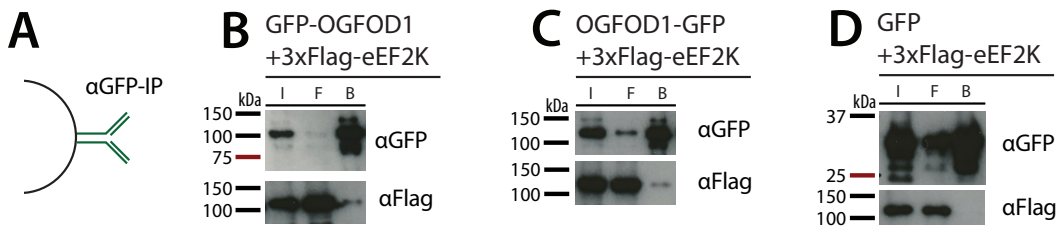

Figure 36: Interaction studies with GFP-tagged OGFOD1 wild type and Flag-tagged eEF2K ; A) Hek293T cells were co-transfected and used for GFP-IP; B)-D) GFP-IP was performed with cells overexpressing proteins as indicated; OGFOD1-GFP and Flag-tagged eEF2K were detected with indicated antibodies in subsequent Western blotting. I=Input, F= Flowthrough, B= Beads fraction.

N-/ or C-terminal GFP-tagged OGFOD1 was coexpressed with Flag-tagged eEF2K in Hek293T cells and subjected to GFP-IP (Figure 36). As control, NLS-GFP was coexpressed with Flag-eEF2K. Interaction of Flag-eEF2K with GFP-tagged OGFOD1 can be observed upon GFP-IP (Figure 36 B and C), whereas the GFP control did not co-precipitate the Flag-tagged eEF2K (Figure 36 D).

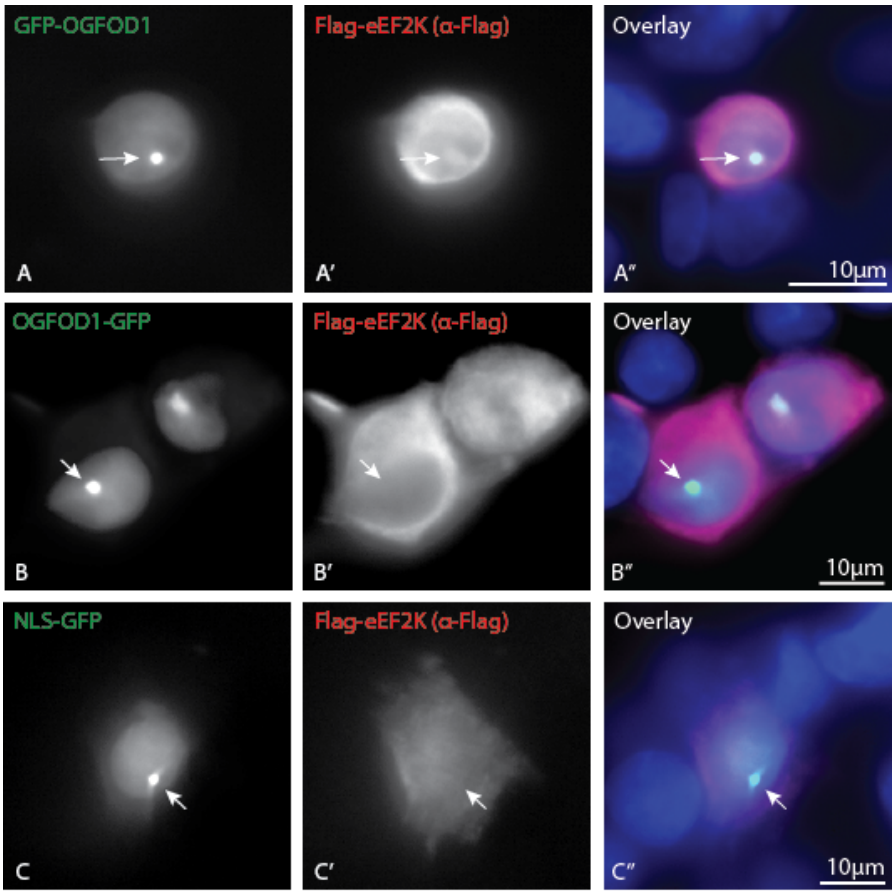

Figure 37: Fluorescent two-hybrid (F2H) assay to study interactions of OGFOD1 and eEF2K; different combinations of GFP-tagged and Flag-tagged eEF2K were co-transfected: A-A'' GFP-OGFOD1 and Flag-eEF2K, B-B'' OGFOD1-GFP and Flag-eEF2K, C-C'' GFP-NLS and Flag-eEF2K, Nuclei were counterstained with DAPI, Flag-tagged eEF2K was stained with anti-Flag antibody and corresponding Alexa594 coupled secondary antibody, arrows indicate location of the GFP spot also in the other channels.

The F2H assay did not confirm results from IP experiments. Coexpression of GFP-tagged OGFOD1 and Flag-eEF2K did not result in a recruitment of Flag-tagged eEF2K by OGFOD1 to the distinct nuclear spot of GFP-tagged OGFOD1 (Figure 37 A-B''). The control experiment with NLS-GFP and Flag-eEF2K showed the same results (Figure 37 C-C'').

2.2.3 OGFOD1 and stress granules

OGFOD1 was initially described as component of stress granules (SGs). Cellular stress response often inhibits translation, the ribosomes dissociate and the small subunits with the still bound mRNA get accumulated. These cytoplasmic and dynamic RNA-protein complexes are called stress granules[119,120].
Upon arsenite treatment, a small fraction of OGFOD1 accumulates in the cytoplasm in RNA-binding protein TIA1 positive stress granules[5,89].

To get more insights about OGFOD1 function in stress granules, first translocation and timing of OGFOD1 translocation in response to stress was tested.

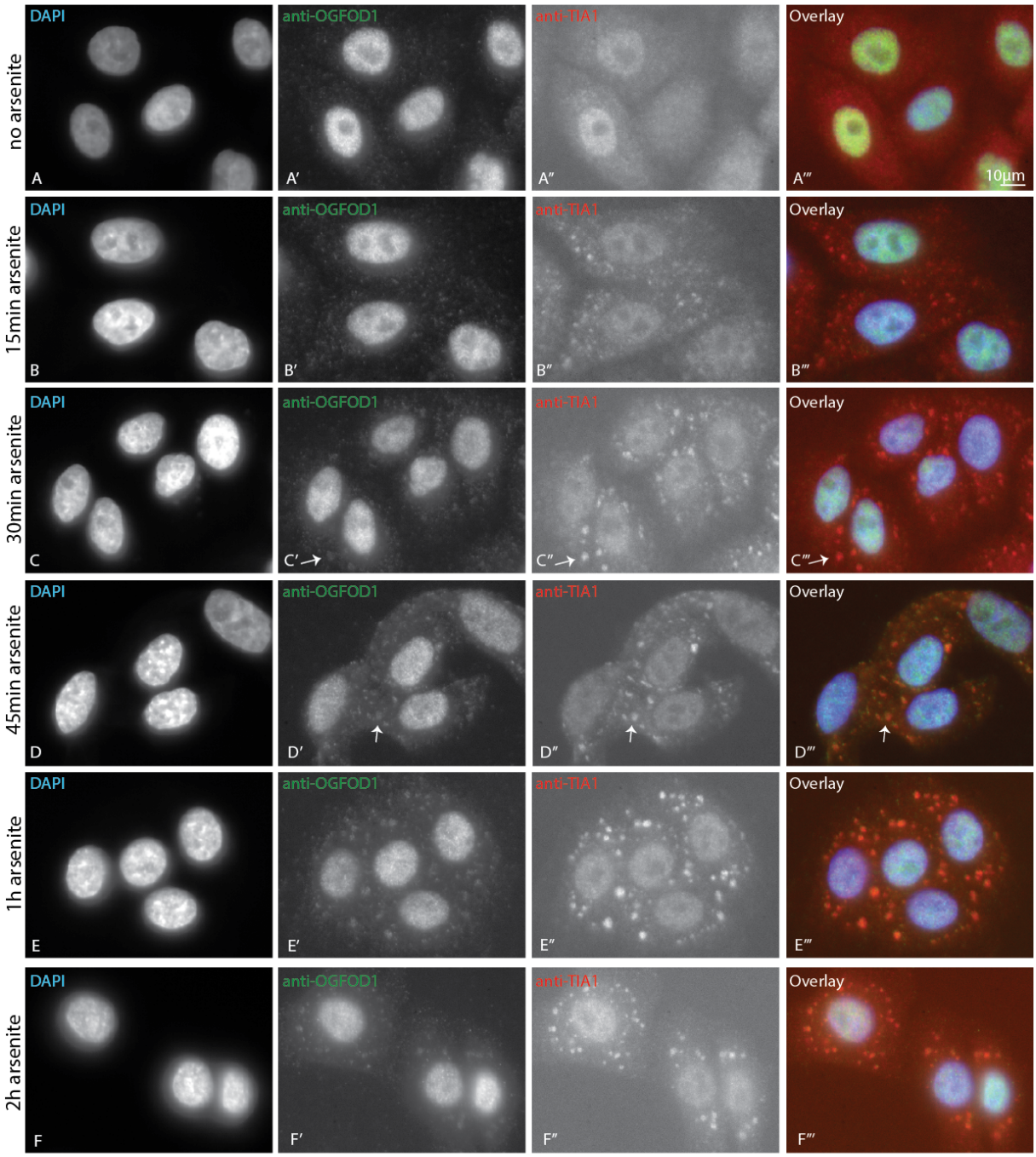

Figure 38: OGFOD1 and TIA-1 reorganization in arsenite treated HeLa cells over time; A-F''' HeLa cells were treated with 1 mM arsenite for indicated times, then fixed and co-stained with anti-OGFOD1 and anti-TIA-1 antibodies and Alexa-488 and Alexa-594 coupled secondary antibodies; DNA was counterstained with DAPI, asterisks indicate colocalized stress granules in OGFOD1 and TIA-1 antibody staining.

To monitor recruitment of OGFOD1 to the stress granules, cells were incubated with 1mM arsenite for various time periods (0, 15, 30, 45 min, 1 h, 1 h 30 min and 2 h). Assembly of stress granules was observed over time by anti-TIA1 antibody staining and costaining with anti-OGFOD1. TIA-1 positive stress granules appeared already 15 minutes after arsenite treatment (Figure 38 B''). First spots of OGFOD1 in the cytoplasm colocalized with TIA-1 can

be detected at the same incubation time (Figure 38 B'), however they get more distinct with longer arsenite incubation (Figure 38 E').

In order to identify a domain in OGFOD1 responsible for SG recruitment, GFP tagged full length OGFOD1 and variants were expressed in HeLa cells. The ability of GFP-tagged OGFOD1 to translocate to SGs should have been monitored after arsenite treatment.
Full length OGFOD1 with N- and C-terminal GFP-tag and NLS-GFP as control were expressed in HeLa cells, 48 h after transfection cells were stressed for 1 h with 1 mM sodium arsenite. However, cells expressing GFP-tagged OGFOD1 showed TIA-1 stress granules, but no translocation of GFP-tagged OGFOD1 (data not shown). A large GFP-tag (25 kDa) might hinder SG recruitment, therefore the smaller hemagglutinin tag (HA-tag, around 5 kDa) was tested.

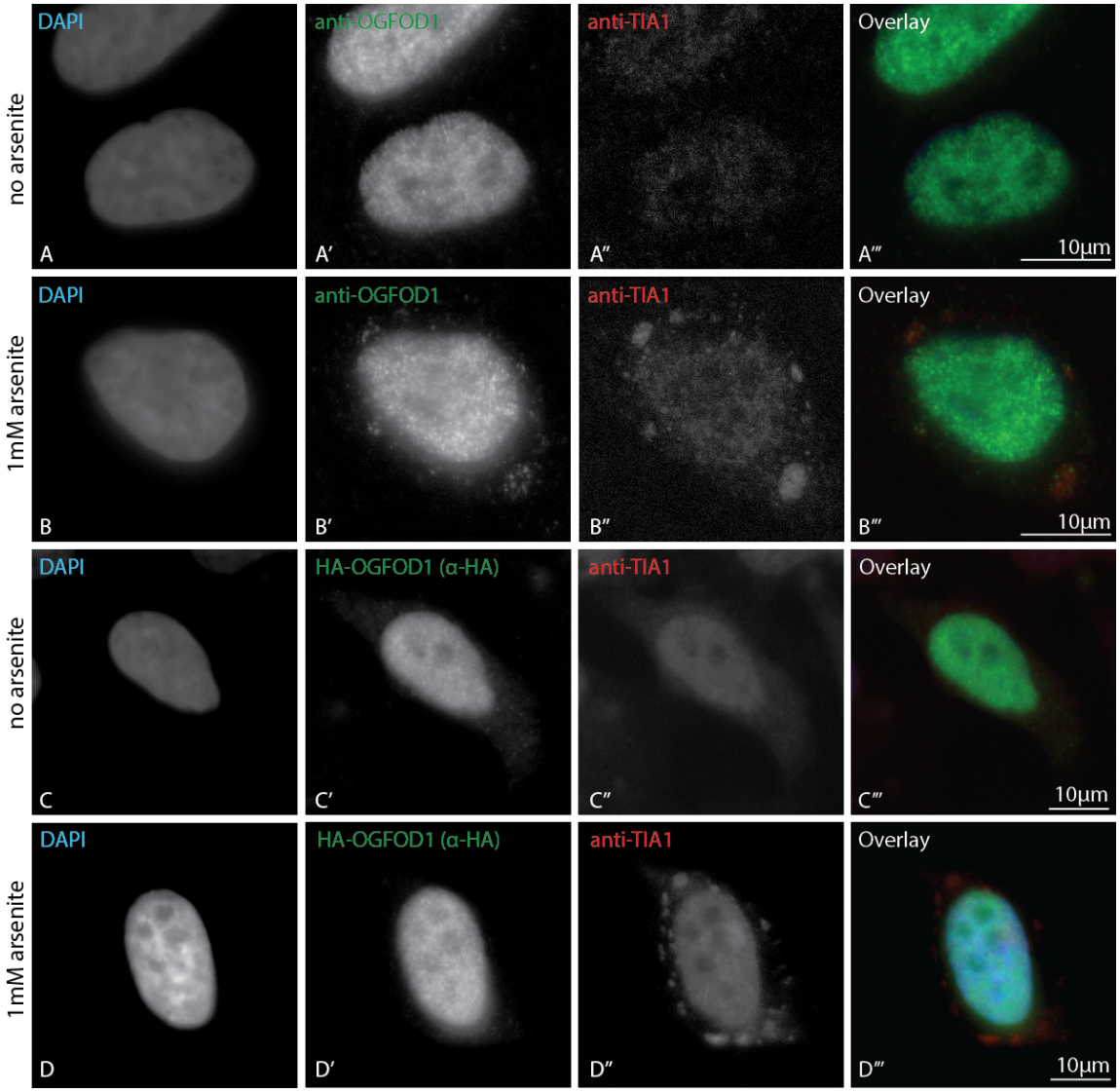

Figure 39: OGFOD1, HA-OGFOD1, and TIA-1 reorganization in arsenite treated HeLa cells over time, A-B''' HeLa cella were treated with 1 mM arsenite for 1 h, then fixed and co-stained with anti-OGFOD1 and anti-TIA-1 antibodies and Alexa-488 and Alexa-594 coupled secondary antibodies; C-D''' HeLa cells were transfected with HA-OGFOD1, allowed to recover from transfection for 48 h and treated with 1 mM arsenite for 1 h, then fixed and co-stained with anti-HA and anti-TIA-1 antibodies and Alexa-488 and Alexa-594 coupled secondary antibodies; DNA was counterstained with DAPI.

However, also HA-OGFOD1 did not change localization after stress (Figure 39 D') in contrast to the stress granule marker TIA-1 (Figure 39 D''). Endogenous OGFOD1 translocates after arsenite stress to TIA-1 positive stress granules (Figure 39 B'), whereas the localization in unstressed cells is restricted to the nucleus (Figure 39 A').

The next attempt to circumvent the tag-dependent inhibition of SG translocation, OGFOD1 with an internal HA-tag was generated. In the linker sequence connecting the two DSBHs, the amino acids 248-256 were exchanged by the HA-tag sequence.

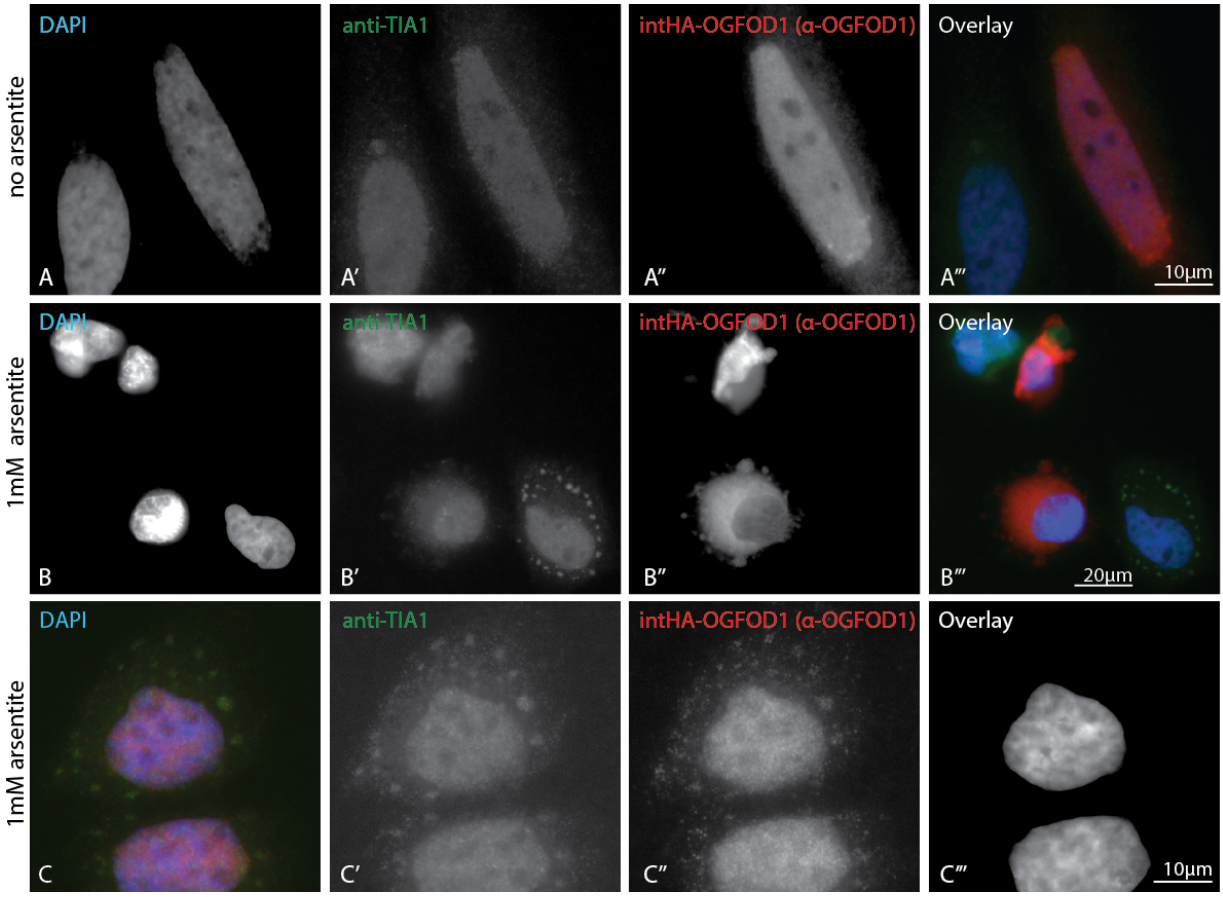

Figure 40: OGFOD1, internal HA-OGFOD1, and TIA-1 reorganization in arsenite treated HeLa cells over time; A-C''' HeLa cells were transfected with internally HA-tagged OGFOD1 (intHA-OGFOD1), allowed to recover from transfection for 48 h and in B-C''' additinally treated with 1 mM arsenite for 1 h, then fixed and co-stained with anti-OGFOD1 and anti-TIA-1 antibodies and Alexa-488 and Alexa-594 coupled secondary antibodies; DNA was counterstained with DAPI.

However, the internal HA-tag was not recognized by anti-HA antibody in IF experiments upon overexpression of the intHA-OGFOD1 variant (data not shown). Therefore, anti-OGFOD1 staining was used, cells expressing higher OGFOD1-levels were assumed to express internal-HA tagged OGFOD1. However, expression of internally HA-tagged OGFOD1 should be confirmed by western blot.
Cells with higher level of OGFOD1 staining were mostly in apoptosis, as the nuclei were brighter and deformed (Figure 40 B). Endogenous OGFOD1 identified by lower protein expression levels compared to overexpressing cells, localized upon arsenite treatment to TIA-1 positive stress granules (Figure 40 C''). The internal HA tagged OGFOD1 could not be observed in stress granules, but also no cells with normal nuclear morphology and higher

OGFOD1 levels could be detected. Therefore, the tag or already OGFOD1 overexpression seemed to cause induction of apoptosis or necrosis.

2.2.4 Characterization of OGFOD1 by knockout cell lines

Knockout cell lines in Hek293 cells were generated with the CRISPR (Clustered Regularly Interspaced Short Palindromic Repeats)/Cas9 system[121]. With this method, sequence specific double stranded DNA breaks (dsDNA) can be introduced by guideRNAs (gRNAs) coupled to the RNA guided DNA endonuclease Cas9. For editing, the DNA target sequence has to be associated with a protospacer adjacent motif (PAM).

2.2.4.1 Generation of OGFOD1, MINA53 and NO66 knockout constructs

Using the online CRISPR Design tool (http://crispr.mit.edu/), guide RNAs were designed and cloned for OGFOD1 and two other ROXs, NO66 and MINA53, according to the protocol of Ran and colleagues[121] (Figure 41).

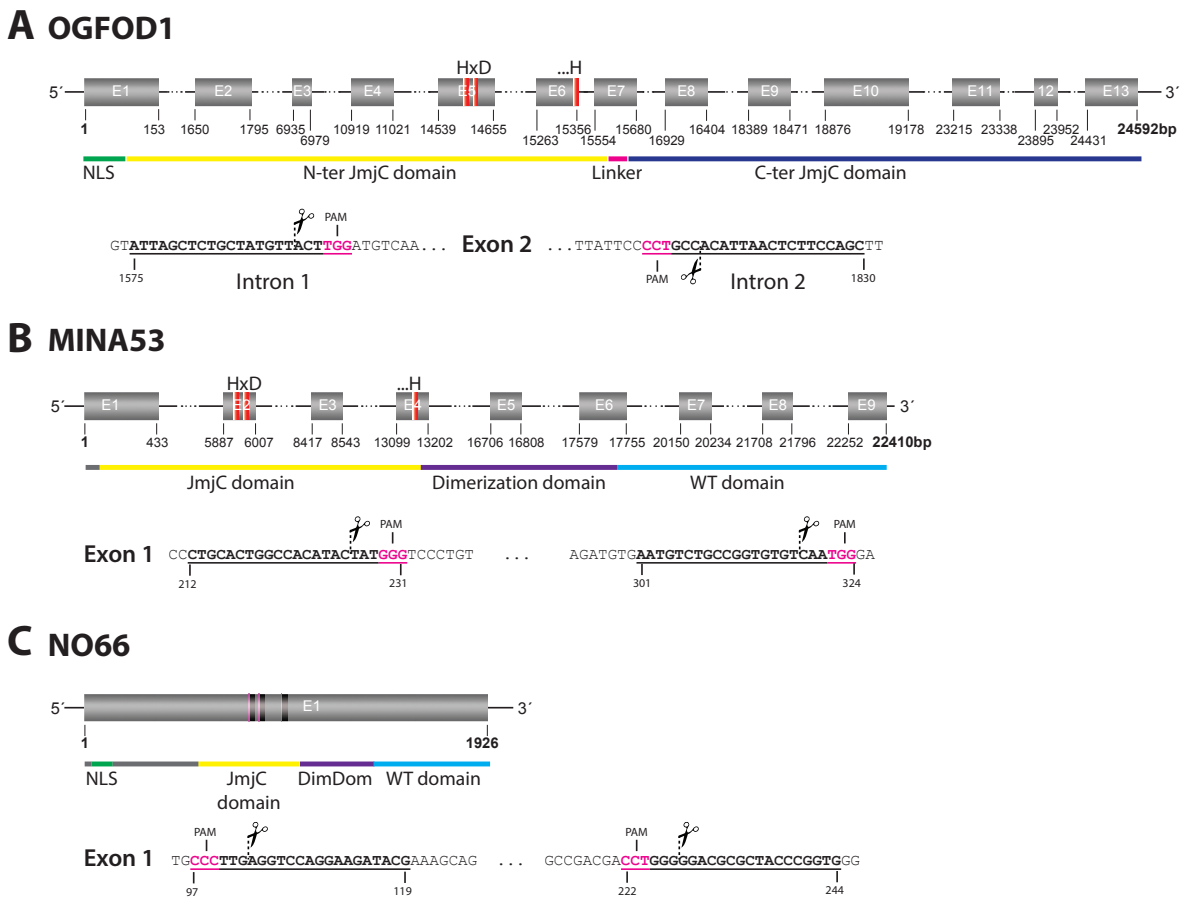

Figure 41: Schematical gene structure with intron and exon structures of OGFOD1, MINA53, and NO66 and selected DNA sequences targeted by designed gRNAs; scissors indicate planned cutting site for Cas9, underlined sequences are targeted sequence by the gRNAs, PAM sequence is in magenta.

The chosen RNA guides target the locus of OGFOD1 and bind 5' and 3' of the second exon in the intronic sequences. CRISPR/Cas9 mediated dsDNA break should lead to excision of exon

2. The exclusion of exon 2 results in an premature stop codon in the protein sequence, producing a shortened 51 amino acid peptide (Figure 41 A).
MINA53 gene was targeted in Exon 1, genomic modification leads to a frame shift producing a stop codon in exon 1 (Figure 41 B).
NO66 is a one exon gene (single exon gen, SEG) containing no introns. Therefore, the guideRNAs were chosen 97 and 222 bp after the start codon. As for the other contructs, loss of the nucleotides leads to frame shift and premature stop (Figure 41 C).

2.2.4.2 Identification of modified cell lines for OGFOD1

To validate knockouts, first clones were screened on the genomic level by PCR amplification of genomic loci of the targeted genes. Those knockout strains were further validated by western blot. NO66 and MINA53 knockouts are described in a following chapter (2.3.2).

For OGFOD1, out of 15 tested clones no homozygous clones were detected, but one clone seemed to be heterozygous for OGFOD1 gene modification. PCR analysis of clone D2 for OGFOD1 knockout showed this heterozygous genomic situation, as we can see wildtype and knockout band in PCR analysis (Figure 42 A). The amplified sequence revealed for the deletion allele (Figure 42 B, O1D2_DEL) a sucessful editing at the upstream cutting site. For the downstream cutting site, the sequence was not available. The wild type allele (Figure 42 B, O1D2_WT) showed the unmodified genomic situation. Even though one allele of OGFOD1 gene was edited resulting in a premature stop codon at amino acid 52 (Figure 42 D), the general protein level of OGFOD1 seemed to be unchanged compared to wild type cells (Figure 42 C).

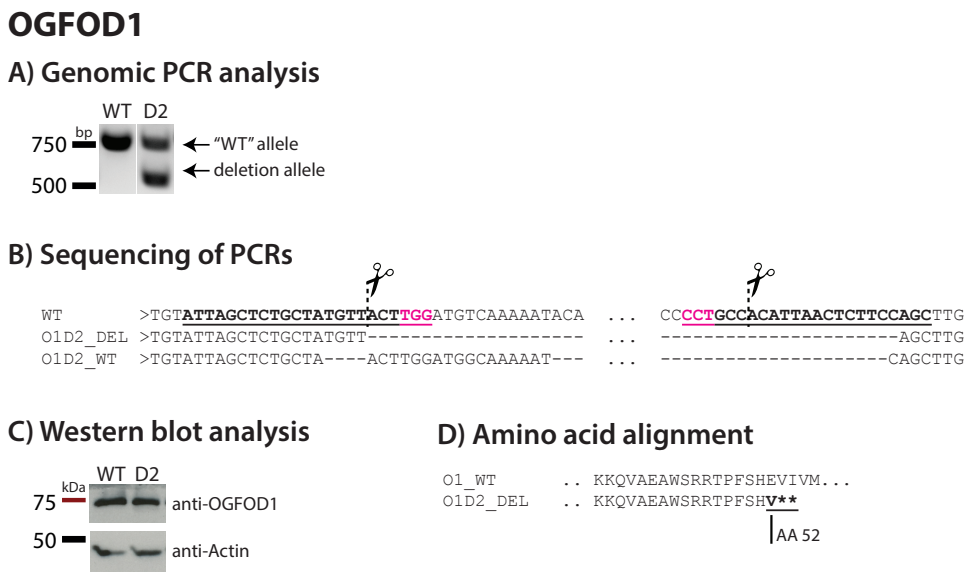

Figure 42: Validation of OGFOD1 heterozygous knockout strain D2; A) Screening of genotypes by amplification of the genomic locus of OGFOD1 for clone D2 and Hek293 untreated cells as control (WT); B) Sequencing of PCR amplified targeted genomic DNA locus, underlined gRNA targeting site, scissors indicate cutting site, in magenta the PAM sequence; C) Western blot analysis of protein amount, endogenous OGFOD1 and Actin as loading control were detected with indicated antibodies; D) Amino acid alignment of protein sequence after genome editing and wild type sequence.

The heterozygous knockout cell line for OGFOD1 (Hek293 O1D2) was further analyzed in immunofluorescence stainings. Also IF experiments using antibodies directed against

OGFOD1 showed that same protein levels can be detected in the wild type cells like in the heterozygous knockout cell line (Figure 43).

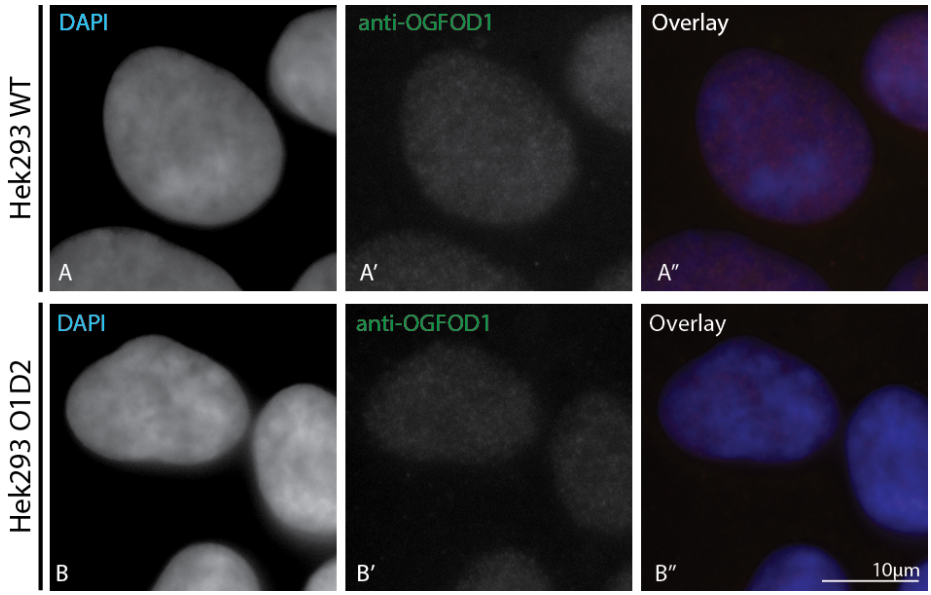

Figure 43: OGFOD1 protein levels in Hek293 and Hek293 OGFOD1 D2 cells; fixed cells were stained with anti-OGFOD1 antibody and Alexa-488 coupled secondary antibody, DNA was counterstained with DAPI.

A second attempt to generate homozygous knockout cells for OGFOD1 starting with the heterozygous clone D2 did not succeed. The second round of transfection with CRISPR plasmids and following selection with puromycin resulted in no surviving cells.
In contrast, generation of knockout cell lines for NO66 and MINA53 was successful and several knockout cell lines have been established (described in 2.3.2). These results imply that homozygous OGFOD1 knockout in Hek293 cells could be lethal.

2.2.4.3 Characterization of Hek293 OGFOD1 heterozygous knockout cell line

Growth assay of heterozygous knockout strain Hek293 OGFOD1 D2

First, growth assays were performed to examine potential roles of OGFOD1 in the cell.

OGFOD1 D2 +/- and wild type Hek293 cell growth was assayed under normoxia (Figure 44 A) and hypoxia (Figure 44 B). OGFOD1 heterozygous cells (O1D2) showed a slight decrease in cell number, but not significant (Figure 44 A and B).

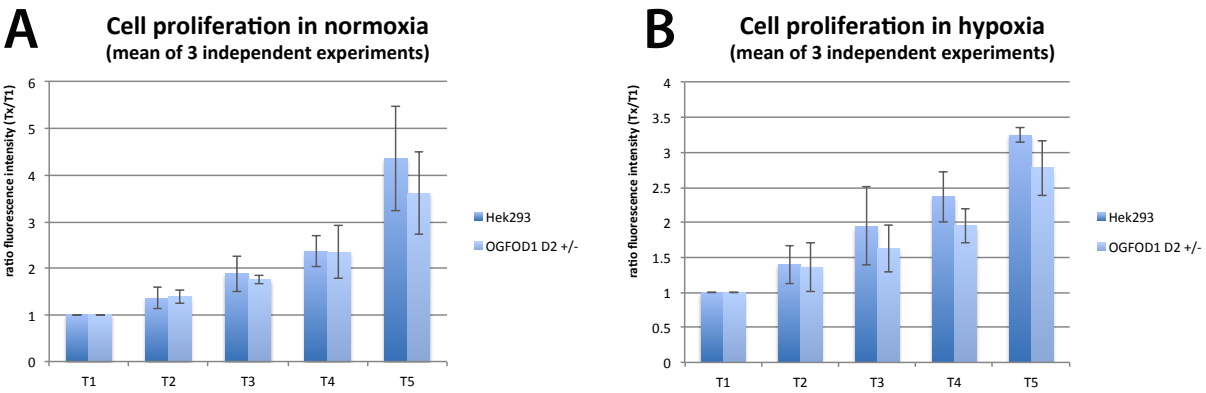

Figure 44: Growth assay for OGFOD1 heterozygous knockout cell line OGFOD1 D2; 1.1*10^3 cells of Hek293 O1D2 and wild type Hek293 were seeded in six biological replicates and for 5 days measured for cell viability using AquaBluer (alamar blue); mean values of three technical replicates are shown, error bars represent the standard deviations A) cells were kept under normal oxygen conditions (approx. 21 %); B) cells were kept under hypoxic conditions (0.1 %)

Results are similar for the growth under hypoxic conditions (Figure 44 B), although overall cell numbers were lower.

Ribosome analysis of heterozygous knockout strain Hek293 OGFOD1 D2

To adress OGFOD1's function as ribosomal oxygenase, ribosomes of the cell line Hek293 OGFOD1 D2 were isolated and analyzed with two methods. First, ribosome profiles after sucrose gradients were determined. Secondly, isolated ribosomes of wild type and heterozygous knockout cells were subjected to LC-MS/MS and analyzed for protein content and for changed PTMs on ribosomal proteins.

The ribosome profiles of OGFOD1-D2 ribosomes displayed no obvious changes compared to the wild type profiles (see in Appendix 6.1.2, Figure 74 A and B).

2 pmol of crude ribosomes were additionally analyzed by label-free LC MS/MS (in collaboration with Ignasi Forné, Axel Imhof Lab, Biomedical Center Munich, LMU). Results are summarized in the section 2.3.2.2.

2.3 Human ribosomal oxygenases MINA53 and NO66

2.3.1 Interaction studies of MINA53/NO66 mutants with the respective substrates

The human ribosomal oxygenases MINA53 and NO66 hydroxylate histidine residues in the ribosomal proteins RPL27a and RPL8, respectively. Both proteins are localized in the nucleoli, even in the same nucleolar subcompartment[51,52]. Crystal structures also reveal a remarkable analogy. The Fe(II) and 2OG oxygenases characterizing JmjC domain, a dimerization domain[38,58,59] and a winged helix (WH) domain have been proposed for the two human proteins and are also conserved in bacterial ycfD[6] (see Figure 45 and Figure 6 A).

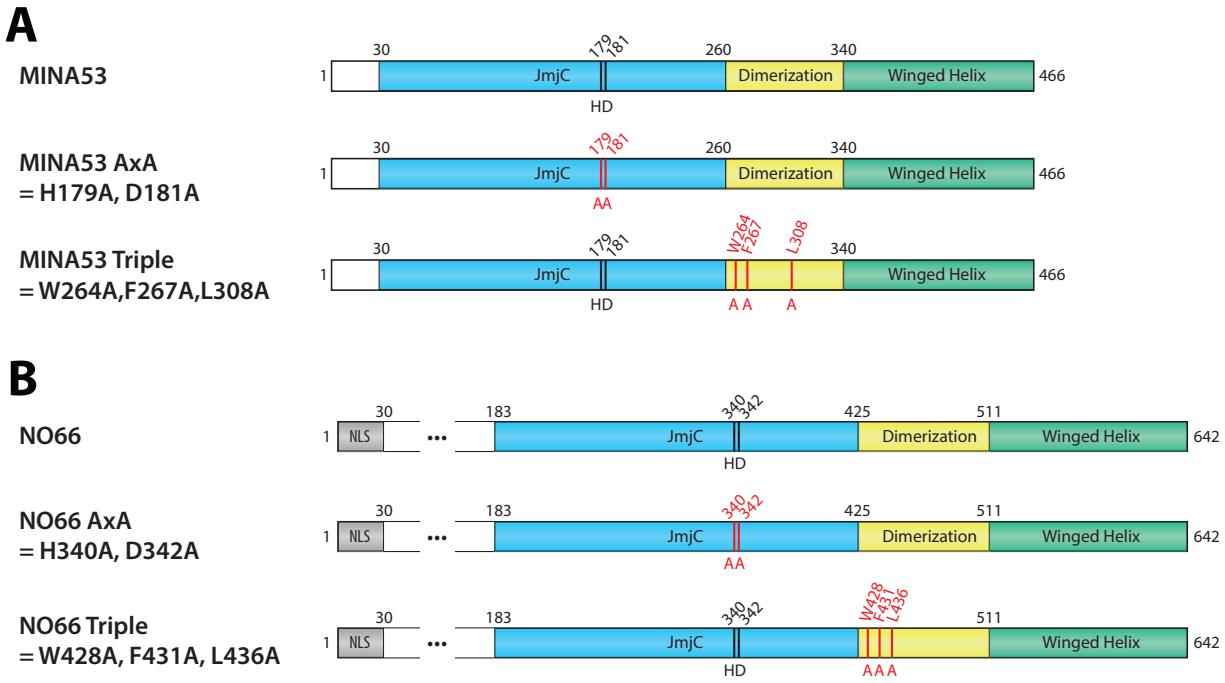

Figure 45: Schematic drawing of MINA53 and NO66 domain structure and generated mutants; A) MINA53 sequence consists of the JmjC domain (blue) with the iron coordinating motif H179, D181 (mutated in red), the dimerization domain (yellow), and the winged helix domain (green); the triple mutant is mutated in the dimerization domain in W264, F267, and L308 to A; B) NO66 consists of the same domains as MINA53, the iron coordinating motif is H340, D342 (mutated in red), the NLS sequence is colored in gray; the triple mutant is mutated in the dimerization domain in W428, F431, and L436 to A.

Both MINA53 and NO66 form dimers or even oligomers in crystal structures[6,122,123], this homo-oligomerization was linked to the enzymatic activity in *in vitro* assays[6,122].
In order to corobate those results *in vivo*, dimerization in cells was tested and confirmed in the course of a bachelor thesis by Kevin Brockers[53]. MINA53 and NO66 showed homo-oligomerization in cells and also the proposed dimerization domain in crystal structure has been confirmed in cells. Variants of MINA53 and NO66 lacking the dimerization domain (amino acids 271-339 for MINA53, amino acids 439-511 for NO66) showed no homo-oligomerization. Based on crystal structure data, Kevin Brockers also generated MINA53 Triple (W264A, F267A, L308A) and NO66 Triple (W428A, F431A, L436A) mutants. Those mutants have been shown to form no oligomers in cells[53].

Within this thesis, experiments have been performed to gain further insights into the importance of homo-oligomerization in cells. Therefore GFP-tagged wild type, AxA, and

Triple mutant of MINA53/NO66 have been co-expressed with Flag-tagged RPL27a/RPL8, and subsequently GFP-IP was performed.

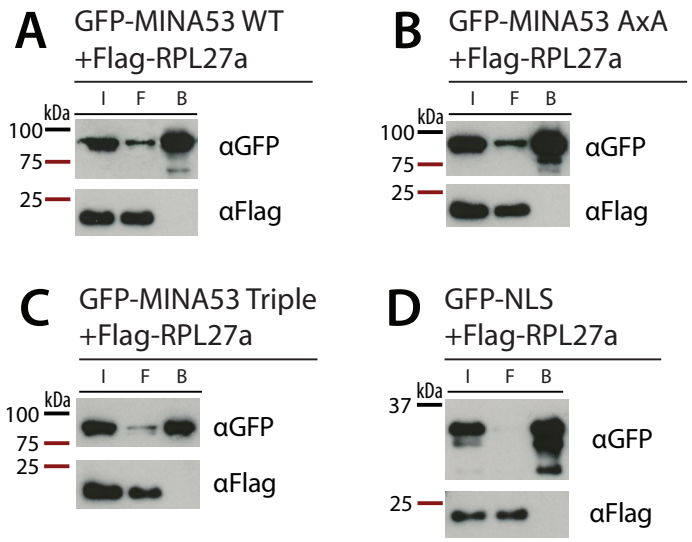

Figure 46: Interaction studies of MINA53 with substrate RPL27a; Hek293T cells were co-transfected and used for GFP-IP; A)-D) GFP-IP was performed with cells overexpressing proteins as indicated; GFP-tagged MINA53 and mutants, and Flag-tagged RPL27a were detected with indicated antibodies in subsequent Western blotting; I = input, F = flow-through, B = beads.

Using MINA53 wild type, the iron binding AxA mutant (MINA53 H179A, D181A), and the triple mutant for MINA53, no interaction of any GFP-MINA53 variant with Flag-RPL27a could be detected (Figure 46 A-C), although RPL27a is an established substrate of MinA53[4].

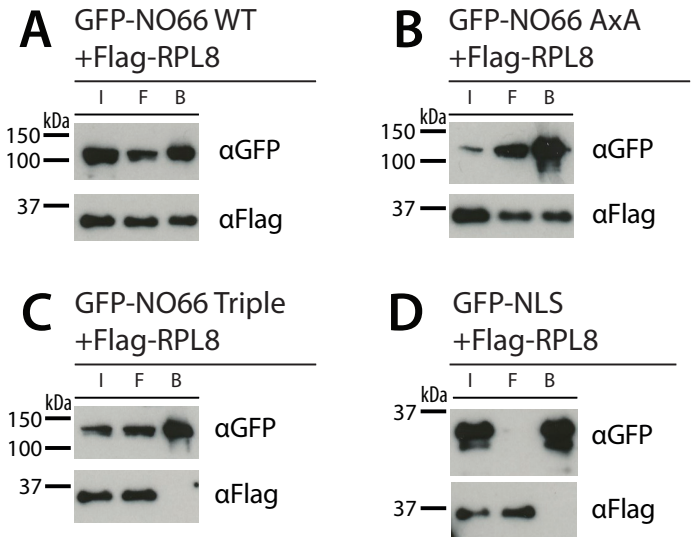

Figure 47: Interaction studies of NO66 with substrate RPL8; Hek293T cells were co-transfected and used for GFP-IP; A)-D) GFP-IP was performed with cells overexpressing proteins as indicated; GFP-tagged NO66 and mutants, and Flag-tagged RPL8 were detected with indicated antibodies in subsequent Western blotting; I = input, F = flow-through, B = beads.

The same experimental set-up was used for NO66 with its substrate RPL8. For GFP-NO66 and Flag-RPL8, interaction could be observed upon GFP-IP of GFP-NO66 (Figure 47 A). Also

for the AxA mutant, the interaction still took place (Figure 47 B). The triple mutant, that is not capable of oligomerization, did not interact with RPL8 (Figure 47 C). The control experiment with NLS-GFP also displayed no interaction (Figure 47 D).

Therefore, the triple mutation in the dimerization domain of MINA53 and NO66 altered the dimerization behaviour of both proteins and for NO66 also changed the binding behavior towards the substrate RPL8.

2.3.2 Characterization of MINA53 and NO66 by knockout cell lines

2.3.2.1 Identification of modified cell lines for MINA53 and NO66

Before described for OGFOD1 (2.2.4), also MINA53 and NO66 CRISPR/Cas9 knockout cells were generated and clones first screened by PCR amplification of genomic loci of targeted genes. Later western blot analysis of protein levels were performed.

In contrast to OGFOD1 where knockout seemed to be lethal in Hek293 cells (see Chapter 2.2.4), MINA53 and NO66 were positive for successful genome editing. Four out of five MINA53 clones were analyzed and could be verified to be MINA53 knockouts also on protein level (Figure 48 A-C). In clone 3, genome editing was precisely carried out as planned, Cas9 induced the double strand break exactly 3 bp upstream of the PAM sequence (Figure 48 B).

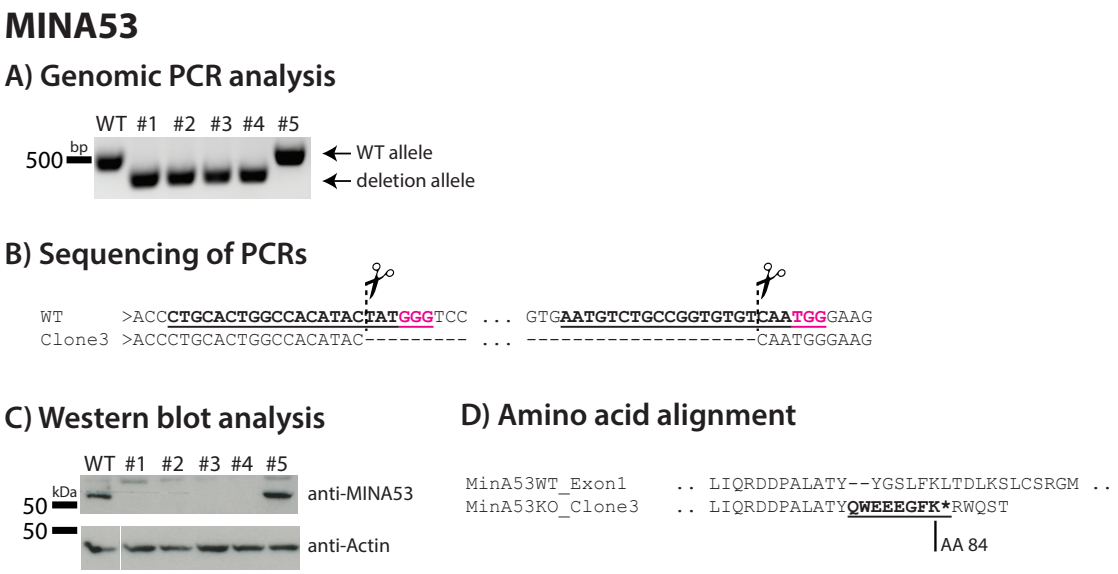

Figure 48: Validation of MINA53 knockouts; A) Screening of genotypes by amplification of the genomic locus of MINA53 for knockout clones 1-4, wild type clone #5, and Hek293 untreated cells as control (WT); B) Sequencing of PCR amplified targeted genomic DNA locus, underlined gRNA targeting site, scissors indicate cutting site, in magenta the PAM sequence; C) Western blot analysis of protein amount, endogenous MINA53 and Actin as loading control were detected with indicated antibodies; D) Amino acid alignment of protein sequence after genome editing and wild type sequence.

Four tested clones for NO66 genome editing were knockouts not only on the genomic level but also on protein level (Figure 49 A). Sequencing revealed for clone 3 that Cas9 did cut in the upstream region not precisely but leaving one more basepair before the double strand break (Figure 49 B, framed in blue). This mistake resulted in a premature stop codon already

at amino acid 114 instead of a planed premature stop codon at amino acid 131 (Figure 49 D). Western blot analysis confirmed the knockout in all tested clones (Figure 49 C).

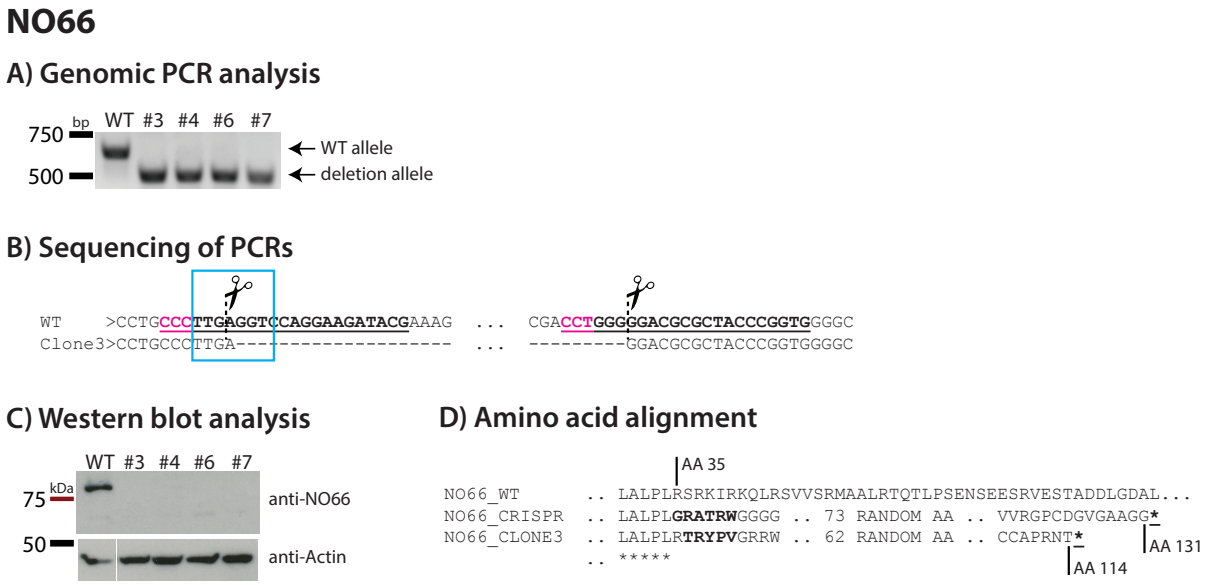

Figure 49: Validation of NO66 knockouts; A) Screening of genotypes by amplification of the genomic locus of NO66 for knockout clones 3, 4, 6, 7 and Hek293 untreated cells as control (WT); B) Sequencing of PCR amplified targeted genomic DNA locus, in magenta the PAM sequence; C) Western blot analysis of protein amount, endogenous NO66 and Actin as loading control were detected with indicated antibodies; D) Amino acid alignment of protein sequence after genome editing, sequence of planned editing, and wild type sequence.

2.3.2.2 Characterization of knockout strains for MINA53 and NO66

To characterize the roles of the respective ribosomal oxygenases, knockout cell lines for MINA53 and NO66 were further analyzed. The knockout was confirmed by immunofluorescence staining of endogenous protein levels, additionally growth assays were performed. Also, ribosomes were isolated and analyzed by analytical sucrose gradients and LC-MS/MS.

Analysis of MINA53 and NO66 knockout strains by immunofluorescence

MINA53 knockout strains #3 and #4 were analyzed by immunofluorescence. Staining of MINA53 in wild type Hek293 showed the nucleolar distribution (Figure 50 A'). Consistent with western blot protein levels (Figure 48 C), knockout cells showed no signal of remaining MINA53 (Figure 50 B' and C').

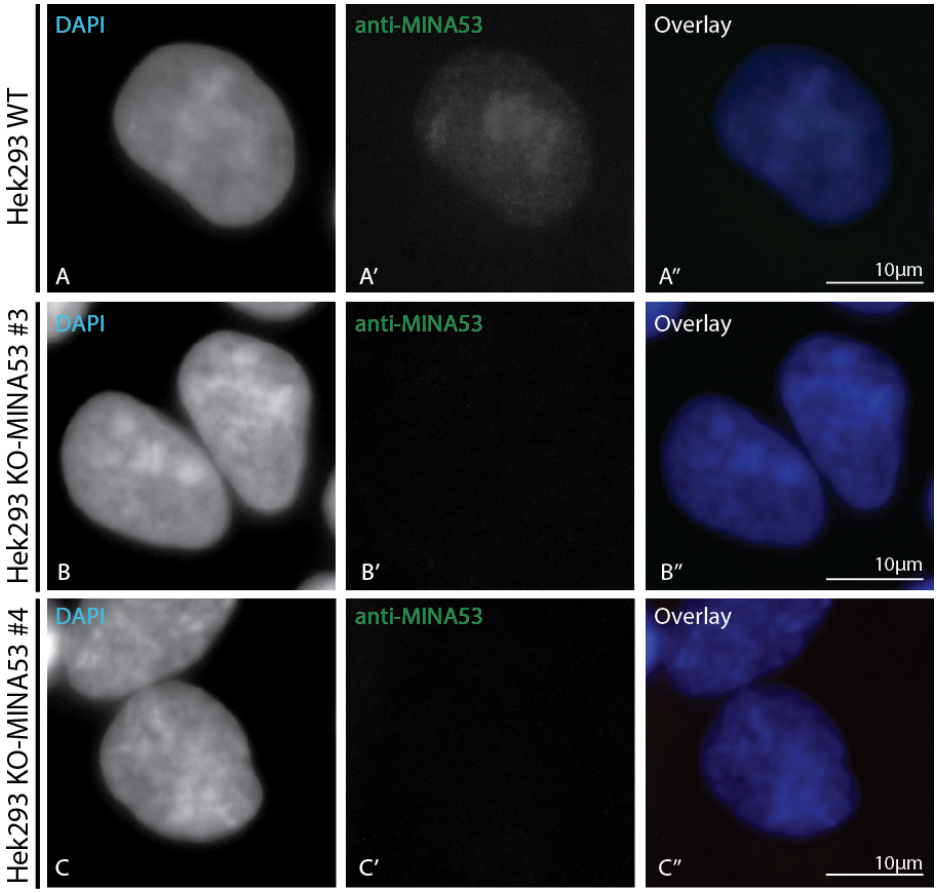

Figure 50: MINA53 protein levels in Hek293 and Hek293 KO-MINA53 #3 and #4; fixed cells were stained with anti-MINA53 antibody and Alexa-488 coupled secondary antibody, DNA was counterstained with DAPI.

To test, if nucleoli are affected by loss of MINA53 protein, MINA53 knockout #4 cells were counterstained with upstream binding transcription factor (UBF) and NO66. UBF plays a critical role in mediating the recruitment of RNA polymerase I to rDNA promoter regions and is a nuleolar protein[124].

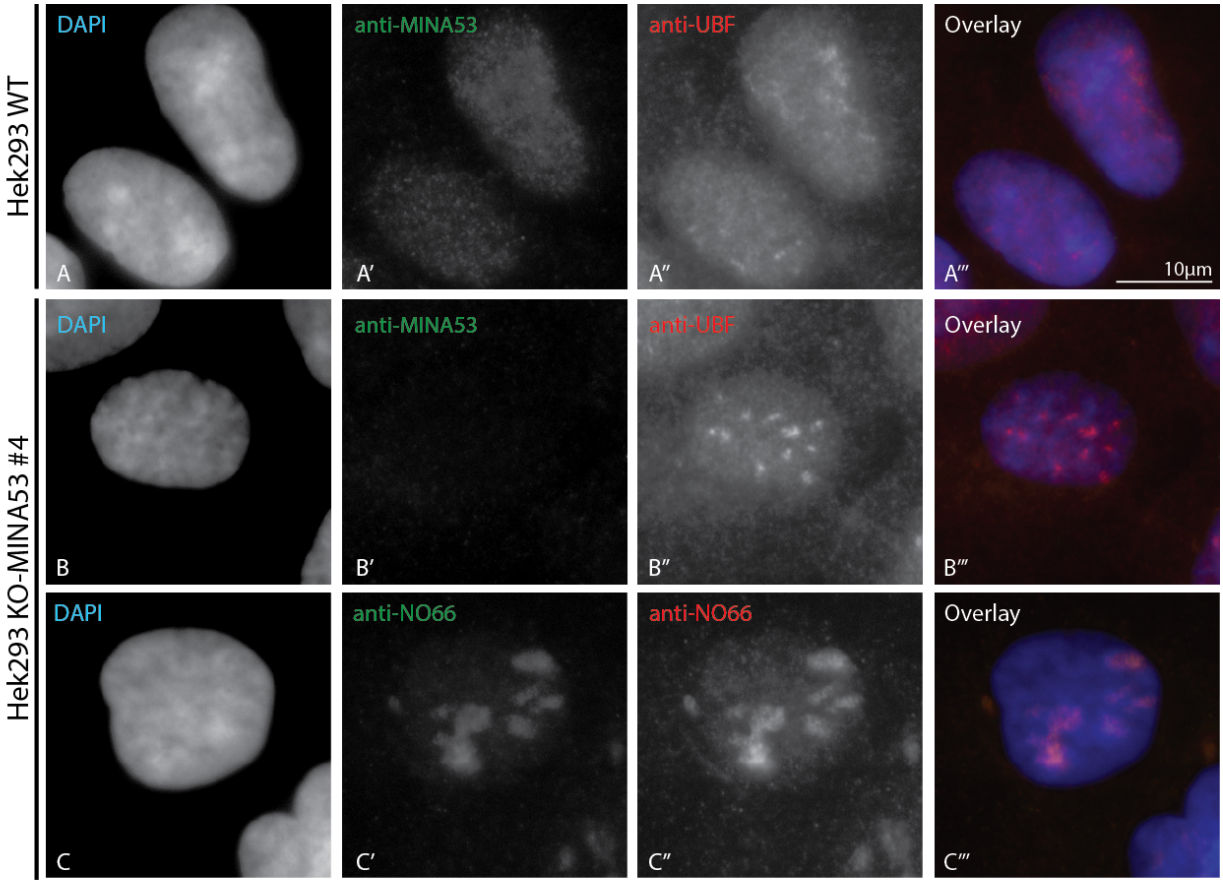

Figure 51: MINA53 and UBF protein levels in Hek293 and Hek293 KO-MINA53 #4; fixed cells were stained with anti-MINA53, anti-UBF, and anti-NO66 antibodies and Alexa-488 or Alexa-594 coupled secondary antibody, DNA was counterstained with DAPI.

Knockout of MINA53 did not change NO66 or UBF localization in nucleoli. Compared to wild type cells, stainings of UBF (Figure 51 A'') and NO66 (Figure 51 C' and C'') were also comparable in KO-MINA53#4 (Figure 51 B'', C', and C'').

Initial NO66-stainings in the knockout cell lines Hek293 KO-NO66 #3 and #4 (Figure 52) revealed a different picture. Knockout strain #3 was a complete NO66 knockout, as no NO66 was detected in IF (Figure 52, B-B''). However, in Hek293 KO-NO66 #4 IF staining revealed that around 30-40% of cells still express NO66 (Figure 52 C-C''), even though protein levels detected by western blot suggested a complete loss of NO66 protein (Figure 49 C). For further experiments NO66 knockout cell line #3 was used.

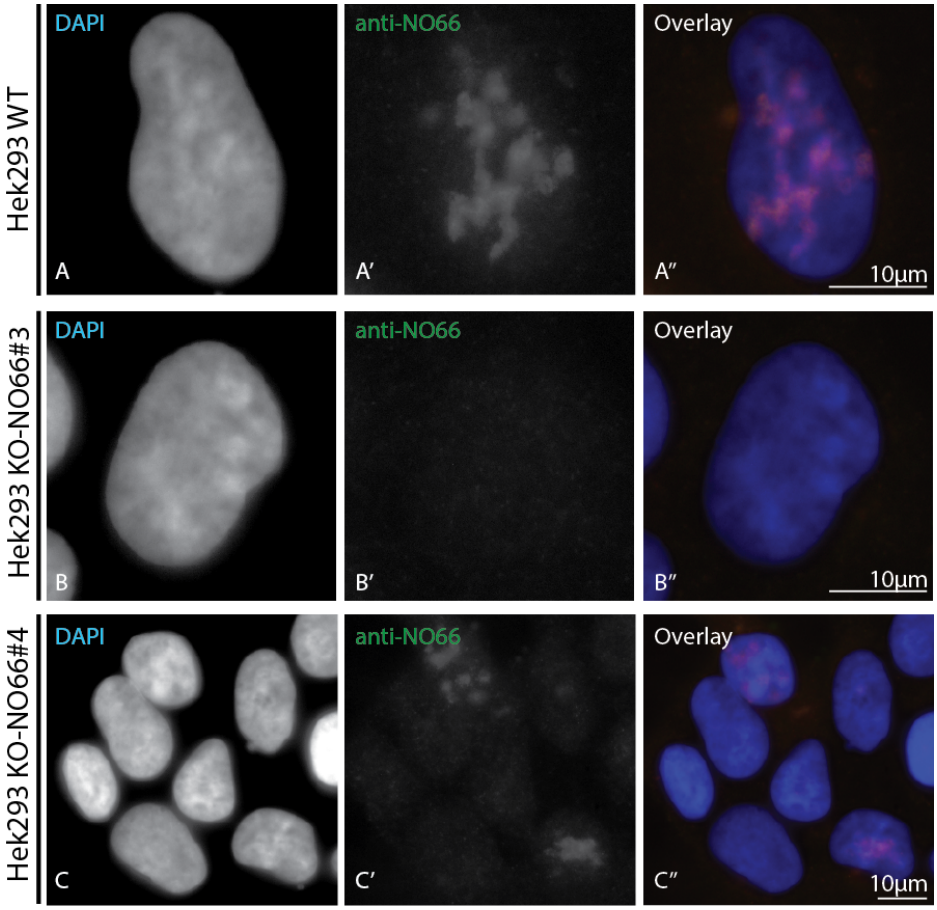

Figure 52: NO66 protein levels in Hek293 and Hek293 KO-NO66 #3 and #4; fixed cells were stained with anti-NO66 antibody and Alexa-488 coupled secondary antibody, DNA was counterstained with DAPI.

MINA53 protein distribution in Hek293 KO-NO66#3 was not changed in comparison to wild type cells (Figure 53 A' and B').

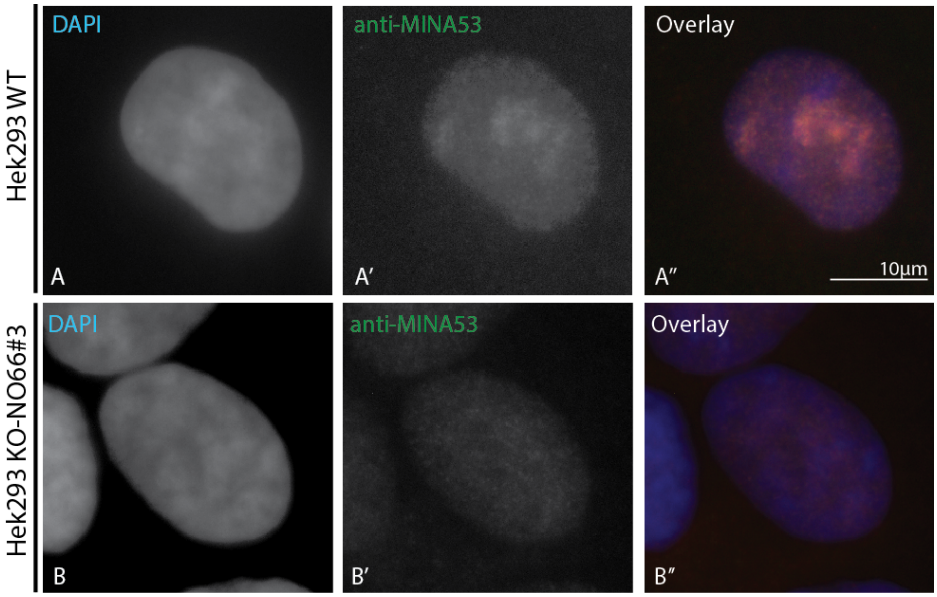

Figure 53: MINA53 protein levels in Hek293 and Hek293 KO-NO66 #3; fixed cells were stained with anti-MINA53 antibody and Alexa-488 coupled secondary antibody, DNA was counterstained with DAPI.

Analysis of MINA53 and NO66 knockout strains in growth assays

The different knockout strains and wild type Hek293 cells were grown under normoxia and hypoxia (Figure 54). MINA53 knockout strain #3 (MinA_3) and MINA53 knockout strain #4 (MinA_4) grew slower compared to wild type in normoxic as well as in hypoxic conditions. MinA_4 showed a significant slower growth in normoxia and hypoxia. MinA_3 grew significantly slower in normoxia, in hypoxia no significant difference could be observed (Figure 54 A and B).

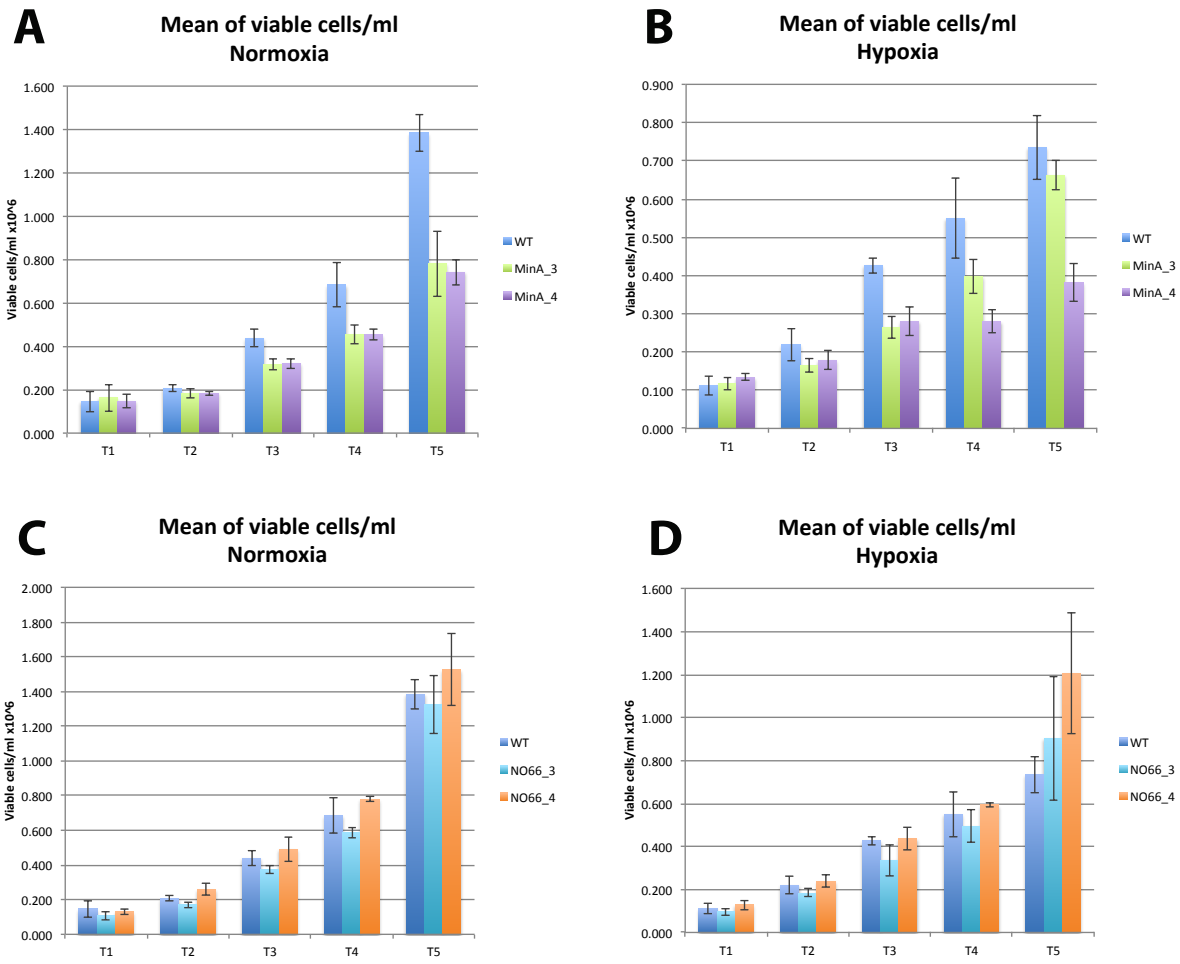

Figure 54: Growth assay for MINA53 and NO66 knockout cell lines; growth was performed in three independent experiments, values and standard error bars represent the mean of three replicates of one experiment; knockout cell lines MINA53#3 and #4, NO66#3 and #4, and wild type Hek293 were seeded at approximatly the same amounts and harvested and counted for 5 days; A) and C) cells were kept under normal oxygen conditions (approx. 21 %); B) and D) cells were kept under hypoxic conditions (0.1 %)

NO66 knockout cells proliferate like wild type in normoxic conditions (Figure 54 C). Knockout cell proliferation in hypoxia seemed to be elevated, but not in a significant range (Figure 54 D).

Analysis of ribosomes isolated from MINA53 and NO66 knockout strains

Ribosomes of knockout cell lines Hek293 KO-MINA53#4 and Hek293 KO-NO66#3 were isolated and analyzed in two different assays. Firstly, ribosome profiles after sucrose gradients were determined. Secondly, isolated ribosomes were subjected to LC-MS/MS and analyzed for altered modifications on ribosomal proteins.

Isolated ribosomes were analyzed by analytical sucrose gradients (Appendix 6.1.2, Figure 74 C and D). MINA53-KO#4 and NO66-KO#3 ribosomes showed no obvious differences compared to wild type (Appendix 6.1.2, Figure 74 A). Major ribosome assembly defects can be excluded (personal communication with Dr. Sarah Matheisl, Prof. Dr. Roland Beckmanns Laboratory, Gene Center Munich, LMU).

To analyze the ribosomes with regard to differences in protein modifications, 2 pmol of crude ribosomes were analyzed by label-free LC MS/MS (Ignasi Forné, Axel Imhof laboratory, Biomedical Center Munich, LMU). Three biological replicates of Hek293 (WT) ribosomes, and two replicates of MINA53-KO, NO66-KO and OGFOD1-D2 ribosomes were analyzed by LC-MS/MS.
The proteins identified in all samples were analyzed by GO term analysis (Figure 55). Most proteins were related to translation and peptide biosynthesis. In fact, all human ribosomal proteins were found in the samples confirming isolation of ribosomes and the ribo-interactome. Further analyses of alterations in protein contents in individual samples will be undertaken.

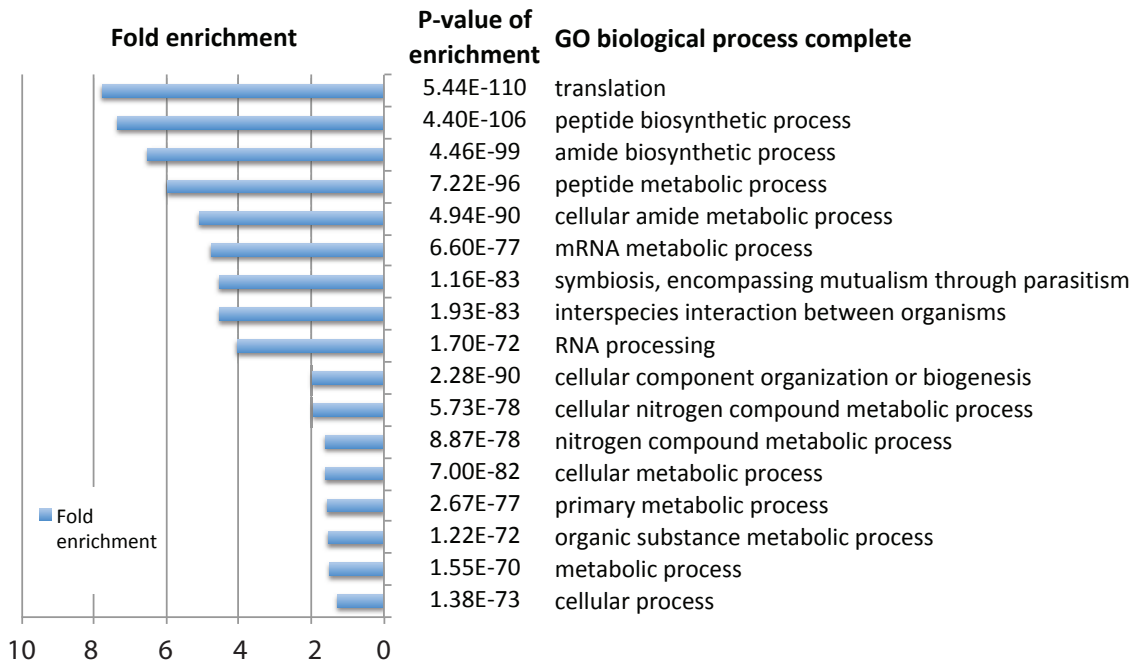

Figure 55: Panther gene ontology (GO) term analysis for proteins of isolated ribosomes identified by LC-MS/MS, displayed are the fold enrichment of certain GO terms and P-values of the enrichment

MINA53, NO66, and OGFOD1 are reported to modify certain amino acids in different ribosomal proteins. MINA53 hydroxylates His39 in RPL27a, NO66 His216 in RPL8 and OGFOD1 Pro62 in RPS23[5,6]. Having a deeper look into those proteins and corresponding peptides revealed that those peptides of interest could be detected in LC-MS/MS (Table 3). RPL27a peptides were identified with hydroxylated His (His OH) in all samples but not in MINA53-KO replicates (Table 3), here only unmodified RPL27a peptide was found. Also for RPL8 and NO66 in the knockout sample, only unmodified peptide could be detected, in all other samples hydroxylation of His216 takes place. In OGFOD1 D2 ribosomes, only RPS23 peptides with hydroxylated Pro62 were found, in accordance with OGFOD1 D2 cell line still exhibiting comparable OGFOD1 protein levels as wild type cells (see Chapter 2.2.4.3).

	RPL27a peptide		RPL8 peptide		RPS23 peptide	
	GNAGGL HHHR	_GNAGGL **H(ox)**HHR_	_GVAMN PVEHPFGGGN HQHIGKPSTIRR_	_GVAMN **P(ox)**VEHPFGGGN **H(ox)**QHIGKPSTIRR_	_VGVEAKQ PNSAIR_	_VGVEAKQ **P(ox)**NSAIR_
	- H(ox)	+ H(ox)	- H/P(ox)	+ H/P(ox)	- P(ox)	+ P(ox)
Experiment	Intensity	Intensity	Intensity	Intensity	Intensity	Intensity
WT_1	0	771490	0	2436787	0	1655721
WT_2	0	2958200	0	4396868	0	1470175
WT_3	0	637970	0	5565551	0	2598005
MINA53KO_1	1735200	0	0	3276900	0	429275
MINA53KO_2	3081800	0	0	1768712	0	77292
NO66KO_1	0	190520	6106797	0	0	1045812
NO66KO_2	0	22365000	16539008	0	0	3034149
O1D2pm_1	0	2259800	0	7609789	0	1702980
O1D2pm_2	0	260170	0	517795	0	462882

Table 3: Peptides of interest in ribosome preparations from different knockout cell lines, identified by LC-MS/MS and described by intensities

With the fragmentation spectra, the 16 Dalton mass shift corresponding most likely to an oxidation can be pinpointed to one particular amino acid (Figure 56 E). For MINA53 substrate RPL27a as example, the fragmented ion spectra assigned His39 to be hydroxylated in wild type and NO66 KO (Figure 56 A and B), but not in both MINA53 KO samples (Figure 56 C and D).

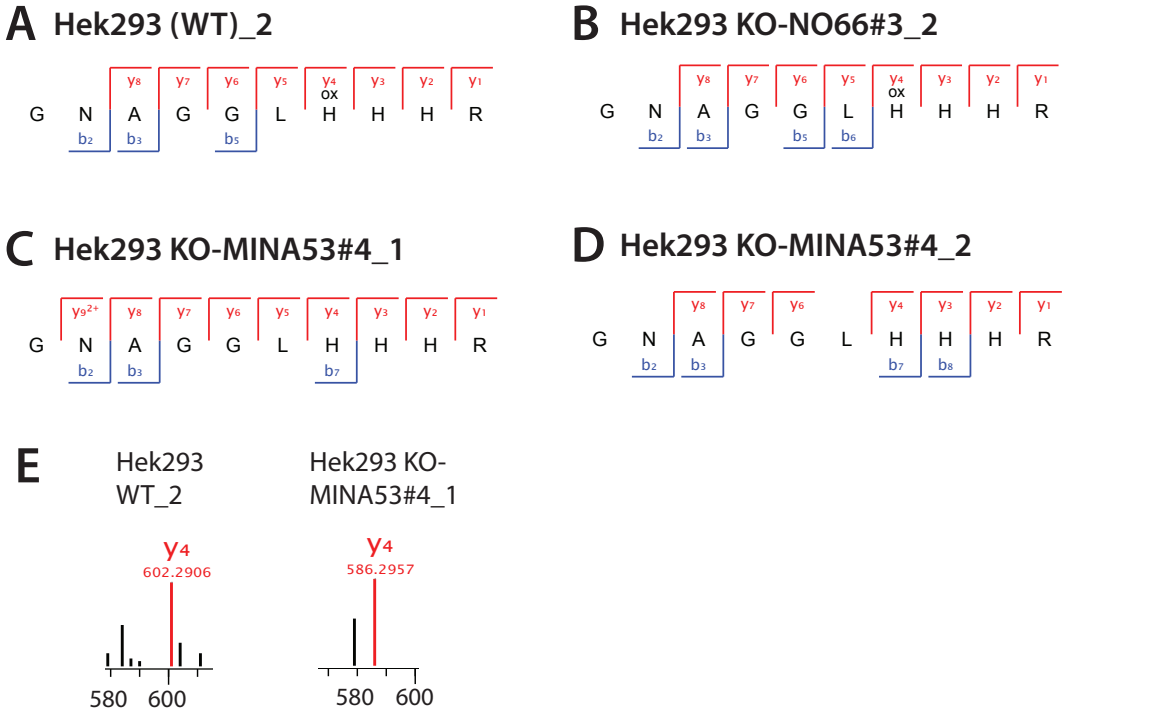

Figure 56: Fragmentation assignments for RPL27a peptide in different samples; hydroxylated peptide in A) Hek293 (WT) sample 2 and B) Hek293 KO-NO66#3 sample 2, unmodified peptide in C) Hek293 KO-MINA53#4 sample 1 and D) sample 2, E) y4- ion corresponding to modified H with 16 Da shift in Hek293 WT_2 and unmodified in Hek293 KO-MINA53#4_1

With this data set, novel PTMs on ribosomal proteins could also be identified. For example, another so far not reported modification was found in the RPL8 peptide. Pro206 is suggested to be hydroxylated (Table 3).

The analysis of ribosomes isolated from the different generated cell lines showed no intriguing differences in the ribosome profiles. Mass spectrometry based experiments confirmed Hek293 KO-MINA53#4 and Hek293 KO-NO66#3 being knockout cell lines. Also the reported substrates could be identified and were dependent on MINA53 or NO66. OGFOD1 D2 cell line on the other hand showed no detectable differences to wild type cells with regards to ribosome assembly or hydroxylated RPS23 Pro62.

2.3.2.3 Generation of reconstituted cell lines for MINA53 and NO66

To characterize MINA53 and NO66 in regards to their enyzmatic activity and the dimerization ability, knockout strains were reconstituted by viral transduction with different variants of MINA53 or NO66.

MINA53/NO66 wild type protein, the iron binding AxA (MINA53 H179A, D181A and NO66 H340A, D342A) mutant or the Triple mutant (MINA53 W264A, F267A, L308A and NO66 W428A, F431A, L436A) disrupted in dimerization were brought back into MINA53/NO66 knockout cell lines.

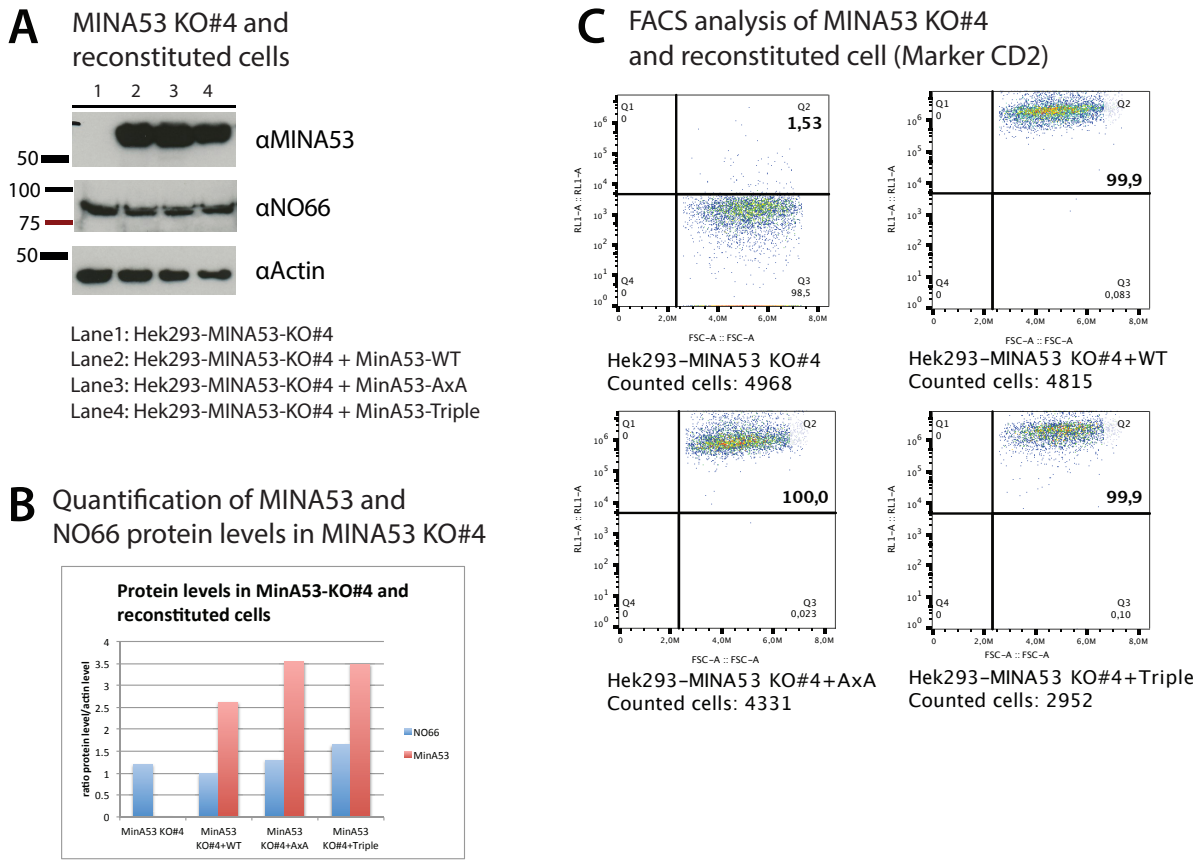

Figure 57: Lentiviral transduction to reconstitute MINA53 knockout cell line #4; A) MINA53, NO66, and Actin protein amounts determined by Western blot with indicated antibodies; B) Quantification of Western blot signals; C) flow cytometric analysis of CD2 positive cells (in the right upper quarter) after viral transduction.

Successful stable expression of proteins was tested in western blot (Figure 57 A and Figure 58 A) and by flow cytometry. The MINA53/NO66 variants were cloned into a vector that encodes the CD2 marker. Cloned insert and CD2 marker sequence are separated by the „self-cleaving“ 2A peptide (T2A site) which causes the ribosome to skip at this sequence and to start translation again at the next C-terminal start codon[125]. In case of reconstitution, marker protein CD2 gets coexpressed but is not fused to the different MINA53/NO66 variants.
CD2 could be detected in the virus transduced cells with percentages ranging from 99.3 to 100% of cells being positive (Figure 57 C and Figure 58 C).

Quantification of western blot signals for MINA53 and NO66 in the different cell lines revealed a high level of reconstituted protein expressed in each cell line. Endogenous MINA53/NO66 levels seemed to be unchanged (Figure 57 B and Figure 58 B).

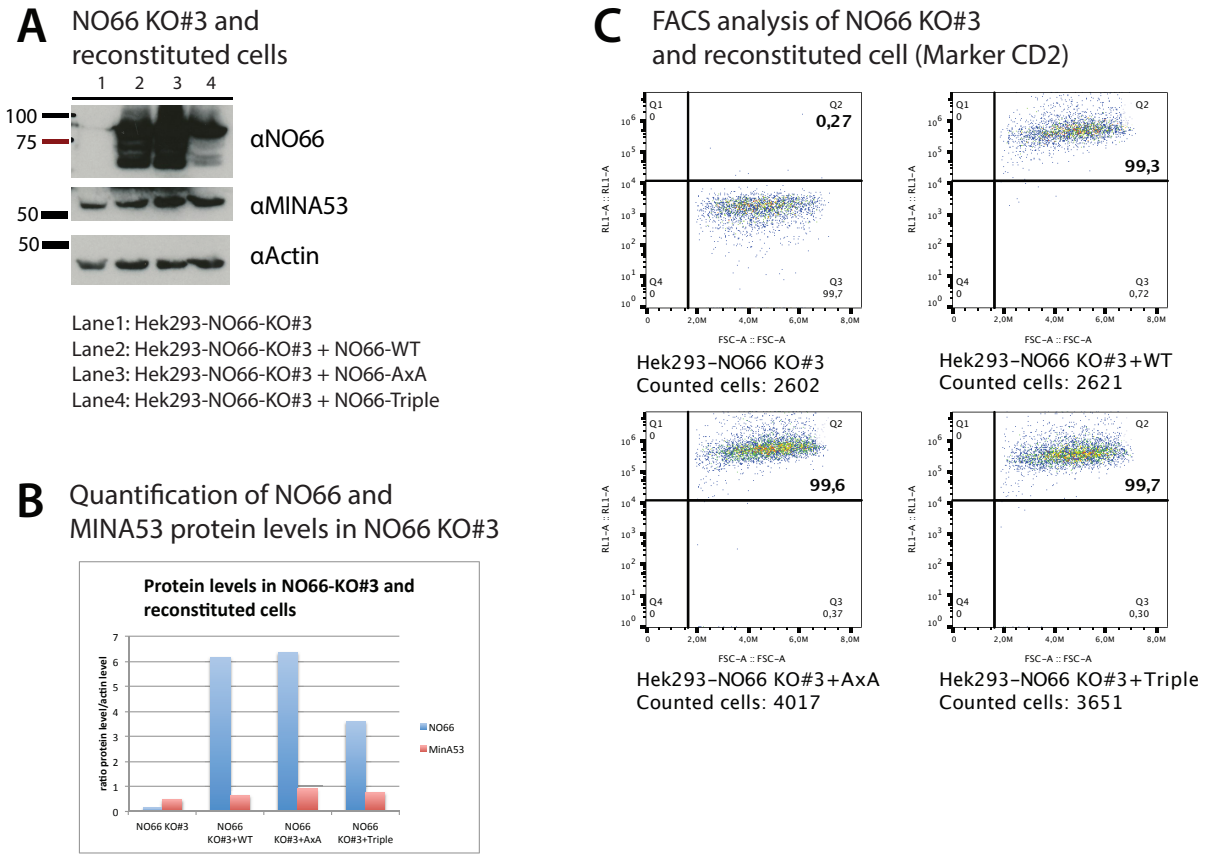

Figure 58: Lentiviral transduction to reconstitute NO66 knockout cell line #3; A) NO66, MINA53, and Actin protein amounts determined by Western blot with indicated antibodies; B) Quantification of Western blot signals; C) flow cytometric analysis of CD2 positive cells (in the right upper quarter) after viral transduction.

The reconstituted cell lines were further tested in a proliferation assay to determine growth phenotypes. In addition to reconstituted knockout cell lines, Hek293 wild type cells have been transduced to generate MINA53 or NO66 overexpression cell lines (MINA53 WT OE or NO66 WT OE).

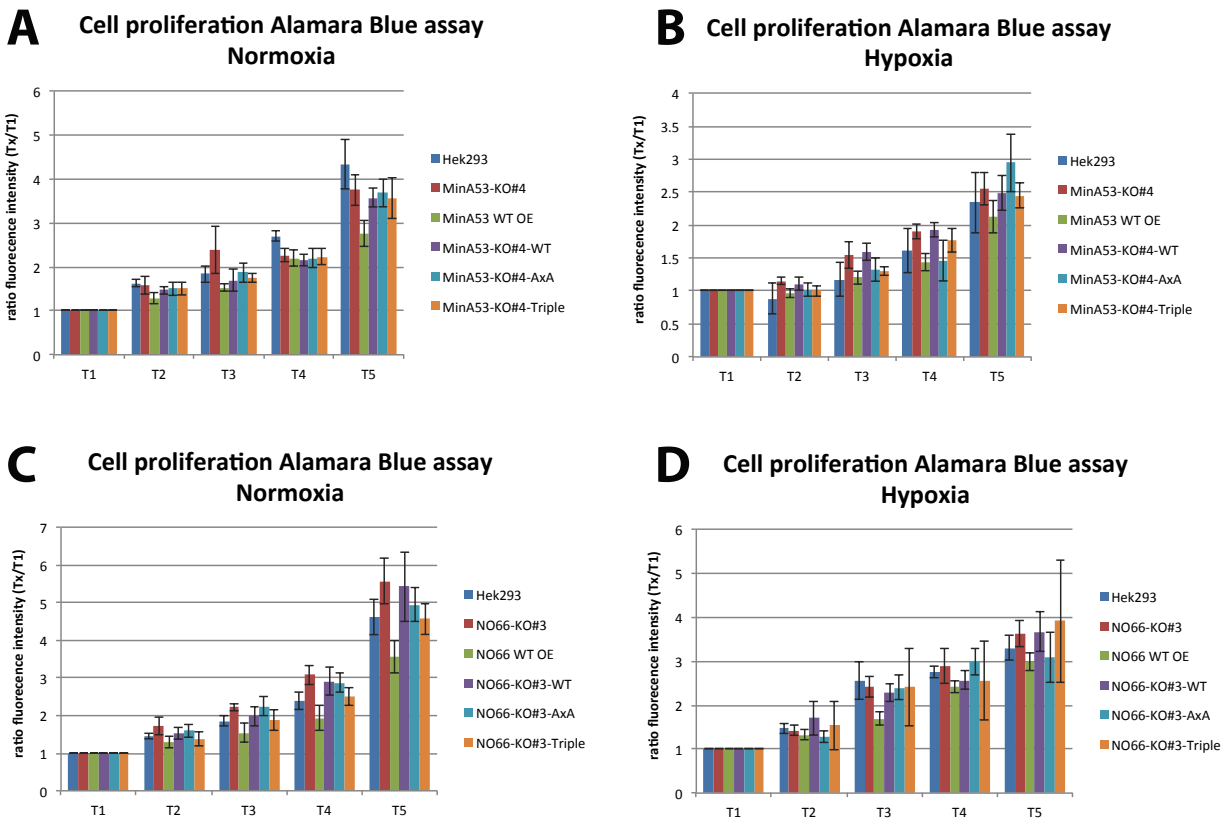

Figure 59: Growth assay for MINA53 and NO66 knockout cell lines and lentiviral transduced rescue cell lines; $1.1*10^3$ cells were seeded in six biological replicates and measured for 5 days for cell viability using AquaBluer (alamar blue); mean values of the six replicates are shown, error bars represent the standard deviations A) MINA53 KO, MINA53 overexpressing (OE), and „rescue" cells were kept under normal oxygen conditions (approx. 21 %) and B) under hypoxic conditions (0.1 %); NO66 KO, NO66 overexpressing (OE), and „rescue" cells were kept in normoxia (C) and hypoxia (D).

The different MINA53 cell lines were tested under normoxic and hypoxic conditions (Figure 59). In normoxia, MINA53-KO#4 displayed a reduced growth in comparison to Hek293 (wild type) cells, the MINA53 overexpressing cell line (MINA53 WT OE) showed an even more reduced growth (Figure 59 A). In hypoxia, those effects could not be detected in a significant range (Figure 59 B). Reconstitution of the knockout cell line with wild type MINA53 (MINA53-KO#4-WT), iron binding defective mutant MINA53-AxA (MINA53-KO#4-AxA) or dimerization triple mutant ((MINA53-KO#4-Triple) resulted in no major differences compared to the knockout or wild type in normoxic or hypoxic conditions (Figure 59 A, B).

Growth of NO66 cell lines showed a quite similar picture as MINA53 cell lines. Overexpression of NO66 in normoxic conditions seemed to slow down growth significantly (Figure 59, C, NO66 WT OE) (Figure 59 C). NO66 knockout cells (NO66-KO#3) grew slightly better than wild type. Reconstitution of the knockout with NO66 wild type (NO66-KO#3-WT), AxA cell line (NO66-KO#3-AxA), and triple mutant (NO66-KO#3-Triple) resulted in no significant differences compared to the knockout or wild type in normoxic conditions (Figure 59 C). However, again the high error bars allow no significant conclusions. In hypoxic conditions, all cell lines behave comparable (Figure 59 D).

2.3.3 Phylogenetic and genomic studies of MINA53 and NO66

Hydroxylation of ribosomal proteins is conserved from bacteria to human. Ribosomal hydroxylases MINA53 and NO66 as well as bacterial ancestor ycfD have a conserved domain structure and dimerize via proposed dimerization domains[6] (Figure 6 in Introduction).

2.3.3.1 Conservation of MINA53 and NO66 proteins

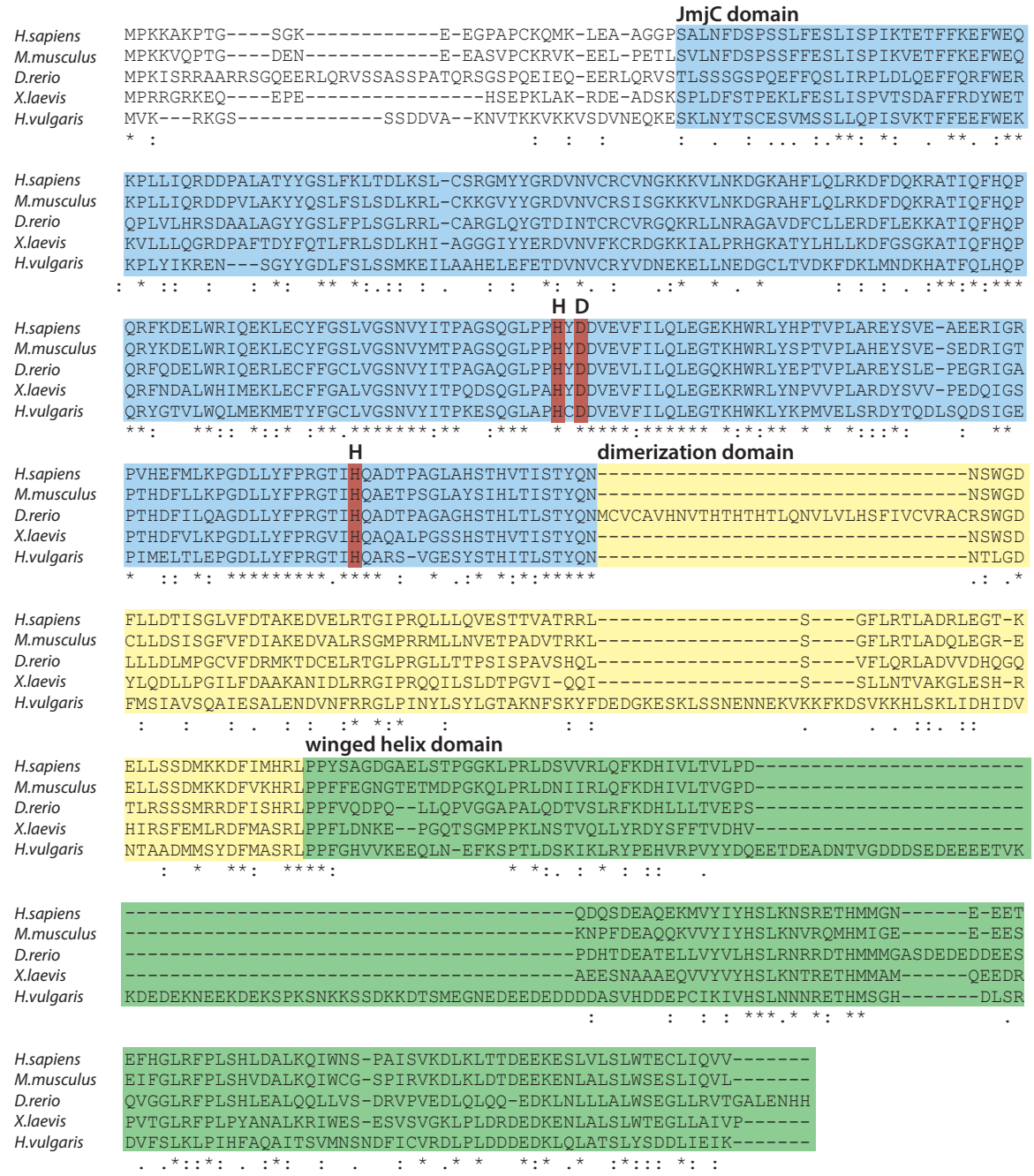

Figure 60: Clustal omega alignment of MINA53 protein sequences from *H.sapiens* (Uniprot : Q8IUF8), *M.musculus* (Q8CD15), *D.rerio* (F1R7K2), *X.*laevis (A0A1L8HCP3), and *H.vulgaris*. The protein domains JmjC (blue), dimerization (yellow), winged-helix (green) as well as the prospective iron-binding motif HxD…H (red) are indicated based on the human sequence[6].

To investigate the evolution of MinA53 and NO66, multiple protein sequence alignments were conducted. Both proteins have a conserved domain structure consisting of a JmjC domain, followed by a dimerization and a winged helix domain (Figure 60 and for NO66 in Appendix 6.1.3 Figure 75).

However, several amino acid insertions longer than 10 amino acids can be observed in the MINA53 protein alignment (Figure 60), like in *D.rerio* in the N-terminus of the dimerization domain or in *H.vulgaris* in the winged helix domain (Figure 60). The iron binding HxD... H motif is conserved in all species (in red, Figure 60).

2.3.3.2 Characterization of *Hydra vulgaris* MINA53 and NO66

Database searches in the basal pre-bilaterian cnidarian *Hydra vulgaris* genome[126,127] predicted two sequences encoding for *Hydra* MINA53 (HvMINA53) and *Hydra* NO66 (HvNO66). Based on those sequences, both genes could be amplified and cloned from *Hydra vulgaris* cDNA. The sequences were thereby confirmed.
Alignment of Hydra proteins with the human homologues revealed that the sequences are conserved and exhibited of the same domain architecture. The Fe(II) binding motif HxD/E…H as well as the 2OG coordinating amino acid were conserved for both hvMINA53 and hvNO66. However, whereas NO66 protein sequence is quite conserved, several amino acid insertions with more than 10 aa in MINA53 were detected (Figure 60 and for NO66 in Appendix 6.1.3 Figure 75).

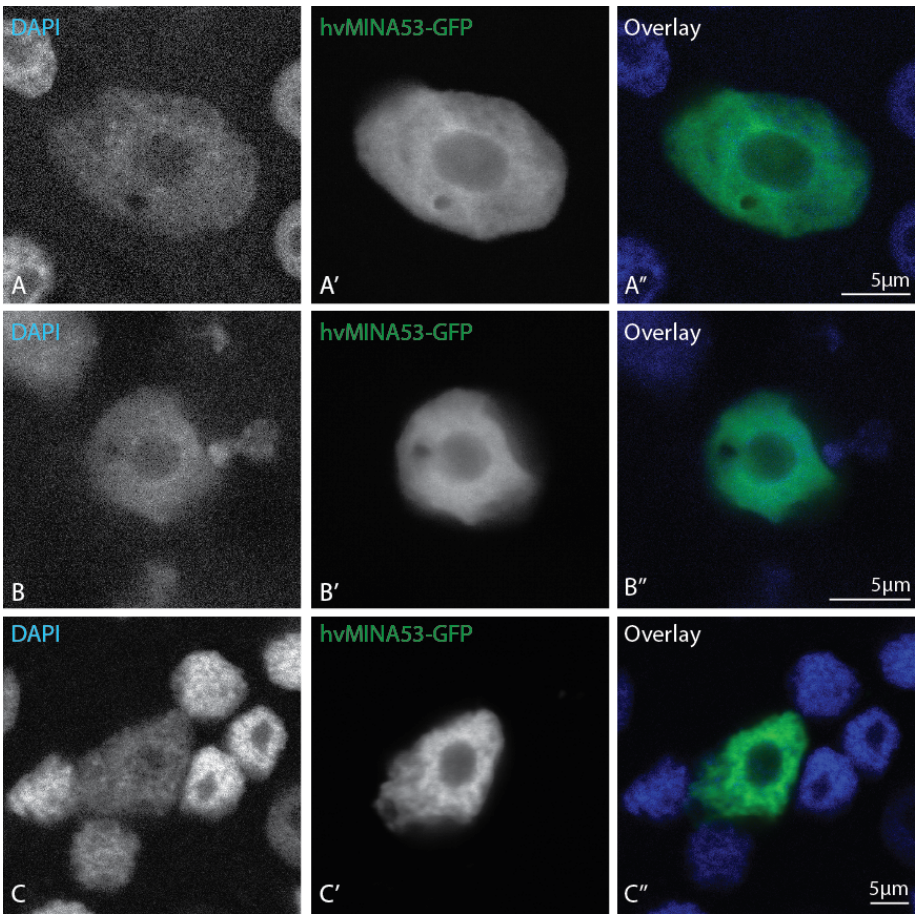

Figure 61: Expression of *Hydra vulgaris* (hv) GFP-tagged MINA53 in Hydra animals; A-C''' shows hvMINA53-GFP positive cells in fixed Hydra vulgaris animals, DNA was counterstained with DAPI

To examine conservation of both proteins, subcellular localization of HvMINA53 and HvNO66 was analyzed. Expression of GFP-tagged proteins in *Hydra* animals was analyzed upon transfection with a particle gun[128]. Confocal imaging of ectopically expressed GFP-tagged HvMINA53 revealed nuclear localization, but in contrast to the human MINA53, HvMINA53 lacks accumulation in the nucleoli (Figure 61).

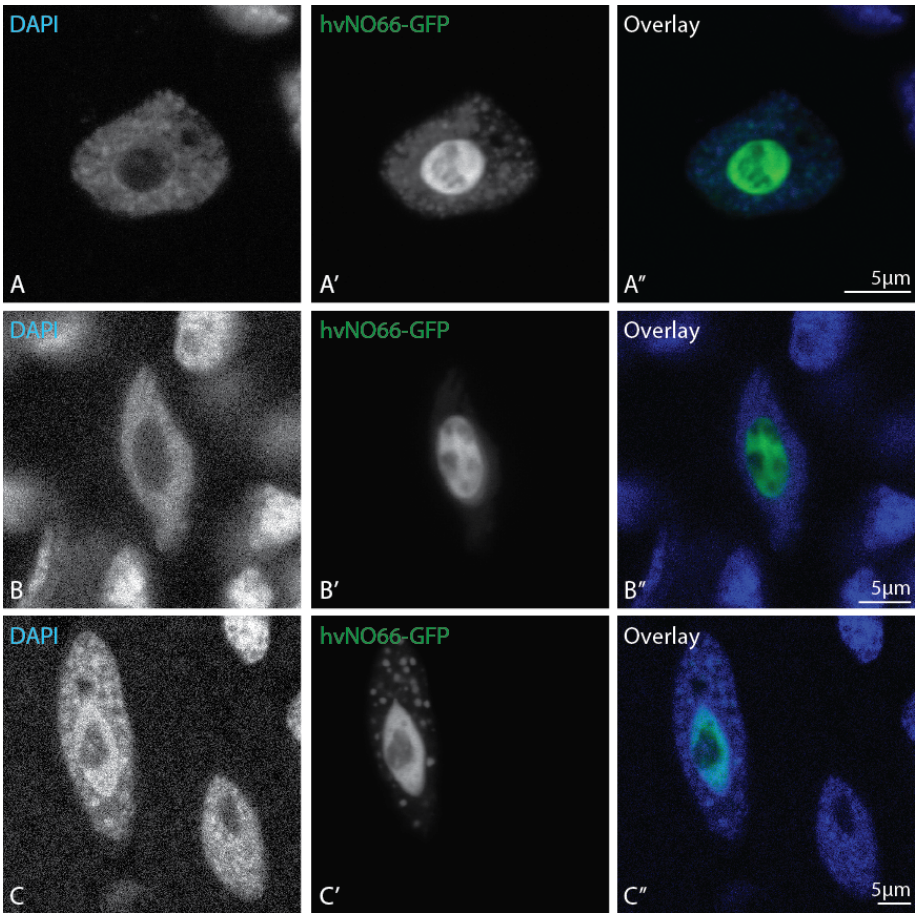

Figure 62: Expression of *Hydra vulgaris* (hv) GFP-tagged NO66 in Hydra animals; A-C''' shows hvNO66-GFP positive cells in fixed Hydra vulgaris animals, DNA was counterstained with DAPI.

HvNO66 showed nuclear localization with a prominent accumulation in nucleoli for the *Hydra* protein (Figure 62) as described for human NO66.

2.3.3.3 Genomic analysis of MINA53 and NO66 across the animal kingdom

Despite high conservation of protein sequences, MINA53 and NO66 genes show differences on genomic level. Whereas human MINA53 consists of 9 exons separated by introns, human NO66 is a so-called single exon gene (SEG), lacking introns. To investigate evolution of MINA53 and NO66 genes and transcripts, phylogenetic studies were conducted.

In 2017, MINA53 and NO66 were renamed to RIOX2 (MINA53) and RIOX1 (NO66). For the following section, RIOX1 and RIOX2 were used for the transcript names.
Analyses of the human MINA53 and NO66 genes using the Ensembl genome browser portal revealed 10 exons for human MINA53 (RIOX2). The gene encodes 9 different transcripts and comprises 9 coding exons and alternatively used non-coding 5'-UTR and 3'-UTR exons. The largest transcript, RIOX2-002 (ENST00000333396.11), encodes a protein of 465 aa and

encompasses a locus of 30639 base pairs (bp) on the human chromosome 3. Surprisingly, in contrast the human NO66 (RIOX1) gene encodes one transcript RIOX1-003 (ENST00000304061.7) and is an intronless gene, spanning 2428 bp with 5'- and 3'-UTRs on chromosome 14.
Initial analyses of MINA53 and NO66 in different organisms revealed, that not all encode both proteins (Figure 63). In Protostomia, like *Drosophila melanogaster* and *C.elegans*, only NO66 could be found.

		Phylum	Class	NO66	MINA53	
Homo sapiens (hs)		Chordata	Mammalia	+	+	
Mus musculus (mm)	(*mouse*)	Chordata	Mammalia	+	+	
Rattus norvegicus (rn)	(*brown rat*)	Chordata	Mammalia	+	+	
Monodelphis domestica (md)	(*gray short-tailed opposum*)	Chordata	Mammalia	+	+	
Gallus gallus (gg)	(*chicken*)	Chordata	Aves	+	+	
Xenopus laevis (xl)	(*african clawed frog*)	Chordata	Amphibia	+	+	
Danio rerio (dr)	(*zebra fish*)	Chordata	Actinopterygii	+	+	
Latimeria chalumnae (lc)	(*west indian ocean coelacanth*)	Chordata	Sarcopterygii	+	+	
Ciona intestinalis (ci)	(*sea squirt*)	Chordata	Tunicata	+	+	
Strongylocentrotus purpuratus (sp)	(*purple sea urchin*)	Echinodermata	Echinoidea	+	+	
Drosophila melanogaster (dm)	(*fruit fly*)	Arthropoda	Insecta	+	-	Protostomia
Tribolium castaneum (tc)	(*red flour beetle*)	Arthropoda	Insecta	+	-	
Caenorhabditis elegans (ce)		Nematoda	Chromadorea	+	-	
Capitella teleta (ct)		Annelida	Polychaeta	+	-	
Clonorchis sinensis (cs)	(*chinese liver fluke*)	Platyhelminthes	Trematoda	+	-	
Biomphalaria glabrata (bg)	(*freshwater snail*)	Mollusca	Gastropoda	+	-	
Hydra vulgaris (hv)	(*freshwater polyp*)	Cnidaria	Hydrozoa	+	+	

Figure 63: Genomic encoded MINA53 and NO66 in different organisms

To gain further insights into the evolution of MINA53 and NO66 genes, more species from the animal kingdom were included. Amino acid sequences of MINA53 and NO66 orthologues were identified in the Ensembl and EnsemblMetazoa genomic resources using the human MINA53 and NO66 protein reference sequences in Protein BLAST (blastp) search (in collaboration with Andreas Lengeling, The Roslin Institute, University of Edinburgh).
In *Trichoplax adhaerens* as very basic metazoan organism, same JmjC protein sequence was found using MINA53 or NO66 sequences. This sequence consists - probably due to low quality of the published genome - of only the JmjC domain, lacking C- and N-termini. Therefore the sequence could not be cleary classified for MINA53 or NO66. However, this sequence was used and acts as outgroup to root the phylogenetic tree (Figure 64).
Comprehensive searches for MINA53 and NO66 sequence revealed for some of those species no MINA53 (Figure 64, in gray boxes). Model organisms *Caenorhabditis elegans* (*C.elegans*) and *Drosophila melanogaster* (*D.melanogaster*) only encode NO66 (Figure 63), the same is true for additional invertebrate species from arthropoda, mullosca, nematoda, and annelida. Whereas *Clonorchis sinensis* and the two organisms of the Caenorhabditis genus have only NO66, two other organisms of the platyhelminthes phylum *Ciona intestinales* and *Ciona savingyi* contain MINA53 and NO66. The fresh-water polyp *Hydra* as

early metazoan animal of the phylum Cnidaria also posseses both MINA53 and NO66 sequences (Figure 63 and Figure 64).

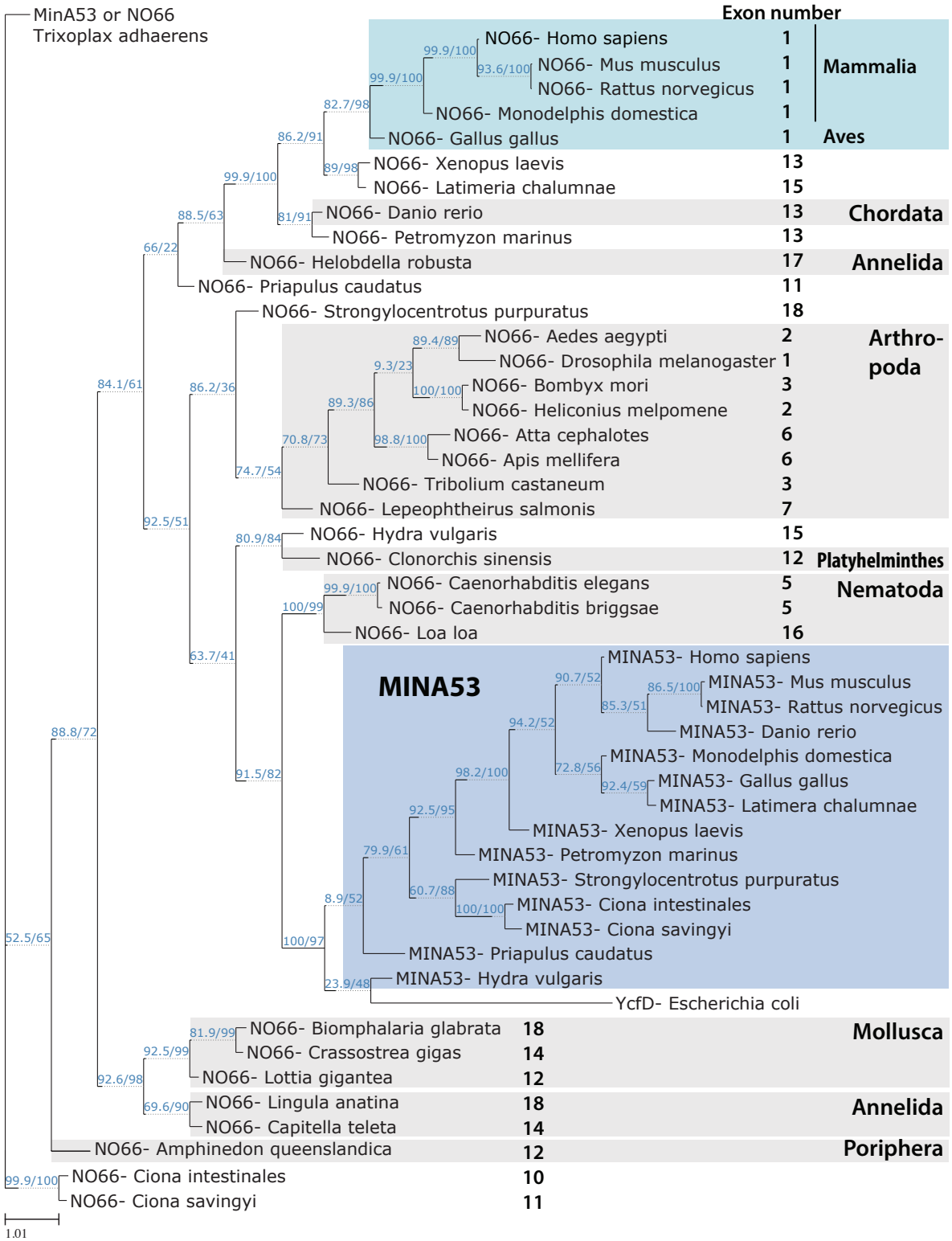

Figure 64: Phylogenetic tree for MINA53 and NO66 JmjC domains in different organisms; maximum likelihood tree was generated using ClustalW-MAFFT-Alignment, ML-IQTree by Evi Lengeling-Wollscheid (The Roslin Institute, University of Edinburgh), support values are written on the branches and are reliable from 80% for the first and 95% of the second value; highlighted in blue MINA53 containing organisms, in light green single exon genes in mammalia and aves, in gray organisms encoding only NO66.

In addition to the observation, that MINA53 is not present in some species, further genomic analysis revealed, that NO66 exists as single exon gene (intron-less gene) in some, but not all species (Figure 64). In the phylogenetic tree of the JmjC domains of MINA53, NO66, and YcfD also exon numbers are provided for NO66. In the examinated Chordata, the mammals with *Homo sapiens*, *Mus musculus*, *Rattus norvegicus*, and *Monodephis domestica* as well as *Gallus gallus* as member of the avian lineage, NO66 consists as single exon gene. The insecta have NO66 encoded as a gene with one to six exons. Other clades like for example the mollusca - represented here by *Biomphalaria glabrata*, *Crassostrea gigas*, and *Lottia gigantea* - exhibit NO66 as multi-exon gene (more than 10 exons). Fish, amphibians and other chordates all possess NO66 genes with up to 15 exons (*Latimeria chalumnae*).
MINA53 JmjC domains cluster in one branch and can be clearly separated from NO66 (Figure 64). JmjC domain from the bacterial ancestor YcfD being in one branching node with HvMINA53 suggests an early invention of MINA53.

Strong support for NO66 Jmjc domains relatedness is given for closely related taxa (*D.rerio* + *O.latipes*, *B.mori* + *H.melpomene*) or higher taxa ranks (e.g. Mammalia, Chordata, Mollusca). Low node support (e.g. *H.robusta* + Chordata, *S.purpuratus* + *L.salmonis*/Insecta) indicates that additional research is needed to fully understand the evolution of this gene and its functional diversification.

These analyses rise the question of the advantage of human NO66 to be a single exon gene. If MINA53 or NO66 is the evolutionary more conserved protein, can not be cleary determined and needs further examination.

3 Discussion

3.1 Ribosomal oxygenase OGFOD1

CCNA2 as novel interactor of OGFOD1

With different assays, interaction of CCNA2 and OGFOD1 could be confirmed. The N-terminal DSBH of OGFOD1 was found to be crucial for binding. The N-terminal domain harbours the motif for iron binding and displays the catalytically active domain. However, as also the iron binding defective AxA mutant was able to bind, the catalytic activity of OGFOD1 is not determining interaction capability. In CCNA2 the interacting domain could not be determined, *in vivo* and *in vitro* assays led to contrary results.

Cyclin A is one of the major regulators of the cell cycle. The mainly nuclear cyclin A (CCNA2) protein can be detected from S-phase until mitosis, where it is rapidly degraded in prometaphase[109,129,130]. In S phase, CCNA2 is bound to cyclin dependent kinase 2 (CDK2) and involved in initiation and termination of DNA replication. During G2/M transition CCNA2 is associated with CDK1 and needed for the activation of the other main cell cycle regulator Cyclin B, probably by regulating its translocation to the nucleus[131,132]. In prometaphase the sudden degradation of CCNA2 is crucial for the stabilization of kinetochore-microtubuli for the correct chromosome segregation[133], ectopical overexpression can even lead to chromosomal double strand breaks[134]. Missregulated CCNA2 causes major defects in cell cycle progression[133-136].

The exact functions of CCNA2 and the regulation by and throughout the cell cycle are still ongoing research. Mechanisms regulating CCNA2 were identified, like post-translational modifications of CCNA2. Acetylations of CCNA2 affect its stability, as acetylated CCNA2 gets ubiquitinylated by the anaphase-promoting complex (APC/C) and subsequently degraded[137,138].

In mass spectromtry (MS), several prolines in CCNA2 with potential hydroxylation were identified. However, in three different experiments with recombinant, endogenous, and Flag-tagged CCNA2, each time different prolines were suggested to be hydroxylated. A limiting factor was also protein coverage of CCNA2. In the best case, 62 % of CCNA2 protein sequence was detected, therefore several prolines could not be analyzed (Figure 65 A). Still, three candidate peptides were chosen based on mass spectrometry (Figure 65 B and C) for a peptide hydroxylation assay.

High conservation scores of P114 in peptide 2 (Figure 65 D) and P137 in peptide 3 made them good candidates for hydroxylation by OGFOD1 which might even be conserved through evolution. Due to high conservation, P402 would also be interesting for further analysis.

Attempts to identify hydroxylation of those peptides by OGFOD1 were performed by cooperation partner Cyrille Thinnes (C. Schofield laboratory, Chemistry Research Laboratory, Oxford) using a MALDI-TOF based assay. Whereas the established positive control with a RPS23 peptide[5] proved the activity of recombinant OGFOD1 in such an assay, the CCNA2 20-mer peptides did not show any hydroxylation associated mass shift.

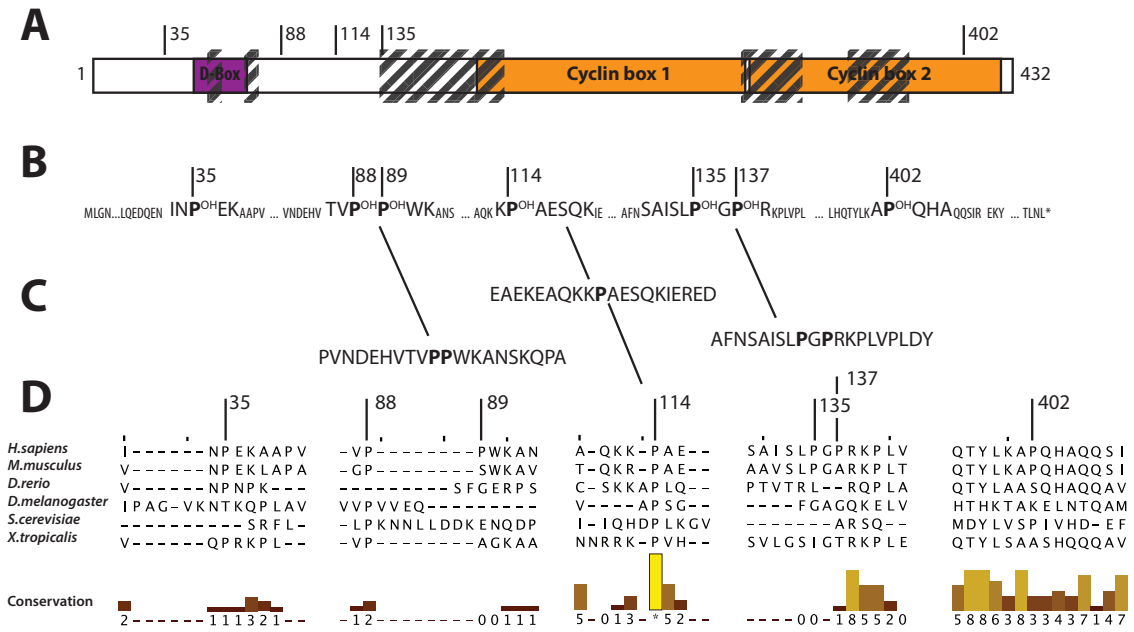

Figure 65: Schematic overview of domains of CCNA2; A) coverage of CCNA2, dashed boxes indicate not covered sequences; B) identified potential hydroxy prolines by LC-MS/MS; C) selected peptides being tested using petide hydroxylation assay based on MALDI-TOF, D) conservation of potential hydroxy prolines; alignments were generated with ClustalOmega, conservation graphes by JalView.

Different peptide lengths or additional protein domains of CCNA2 might be needed for this *in vitro* approach. Limitations of this assay were already reported in 2009[139]. Lysine hydroxylation in U2AF65 by JMJD6 could be detected with LC-MS/MS, but testing the corresponding peptides with MALDI-TOF showed no enzyme activity of JMJD6 towards the distinct lysines[139]. Therefore, in addition to the local hydroxylation site, other domains in CCNA2 may be important for the binding and the catalytic activity of OGFOD1. Further, structural factors supporting the interaction might be needed. Using full length CCNA2 from cell extracts in the *in vivo* CCNA2 IPs analyzed by LC-MS/MS, instead of pure peptide and recombinant OGFOD1 could supply the reaction with potential helping factors.
To define CCNA2 as substrate of OGFOD1 and identify hydroxylated prolines, other methods should be used like a more sensitive mass spectrometry approach or MALDI-TOF with peptides of variable length or full length CCNA2.

OGFOD1 influencing the cell cycle?

OGFOD1 expression did not change throughout the cell cycle, also the interaction with CCNA2 showed no cell cycle dependency. Direct binding of OGFOD1 to CCNA2, which was not in complex with CDK2, could point towards a CDK-independent function of CCNA2 beyond the cell cycle. A recent report assigned CCNA2 a CDK-independent role as RNA binding protein specifically binding Mre11 mRNA and thereby promoting its translation[140]. More experiments concerning the nature of CCNA2-OGFOD1 with regards to potential additional interaction factors or to cell cycle timing should be conducted.

However, OGFOD1 was found to directly influence the cell cycle. IP of CCNA2 with concurrent overexpression of OGFOD1 led to a change of the CCNA2 interactome. Proteins like Replication protein A 70 kDa DNA-binding subunit (RPA1) and Replication protein A 32 kDa subunit (RPA2) were enriched in OGFOD1 overexpressing samples. RPA1 and RPA2 are

components of the heterotrimeric replication protein A complex (RPA). The complex is the major single-stranded DNA binding protein in eukaryotic cells. It binds and thereby stabilizes single-stranded DNA intermediates that occur during DNA replication or as response to DNA damage[141,142]. Additionally, the complex binds proteins involved in DNA replication, DNA repair, and recombination[143]. In 1996, the interaction of CCNA2 and RPA2 and RPA2 phosphorylation mediated by the CDK2-CCNA2 complex was shown by *in vitro* data[144]. In order to confirm interaction of CCNA2 with RPA1 and RPA2 in cells we immunoprecipitated endogenous CCNA2 from 293T cells and identified CCNA2 binding proteins with LC-MS. We were able to co-precipitate well-known CCNA2 interactors like CDC20[145], CDK1 and CDK2[146], but also RPA1 and RPA2 specifically when compared with control IP experiment. In an overexpression system with Flag-CCNA2 and untagged OGFOD1 and OGFOD1 AxA, RPA2 was highly enriched in the Flag-CCNA2 IP sample in comparison to a control. This would imply that enzymatic activity of OGFOD1 is not involved in the regulation of the CCNA2 interactome. Initial experiments determining the progression of synchronized cells through the cell cycle revealed some delay for GFP-OGFOD1 expressing cells. Cell overexpressing NLS-GFP proceeded with no observable time lag, indicating an effect of OGOFD1 overexpression on the cell cycle.

In a recent report, a role of OGFOD1 in cell proliferation was shown in breast cancer cells and chronic lymphocytic leukemia, where OGFOD1 displayed a high expression[91,92]. On the other hand, knockdown in breast cancer cells led to the accumulation of cells in G1- and G2/M phase. Following this, the authors assigned OGFOD1 a role in cell proliferation and tumorigenesis and propose a translation-independent role for OGFOD1 in cell cycle regulation[92]. Recently, using a whole cell proteomics approach these findings were corroborated. In this setting, siRNA induced OGFOD1 knockdown led to a strong reduction of cells in S-phase[93].

Interaction of OGFOD1 with the translation regulator eEF2K

Recently, proline 98 of eukaryotic elongation factor-2 kinase (eEF2K) was found to be hydroxylated. This post-translational modification (PTM) of eEF2K restrained its activity and might in turn regulate translation via eukaryotic elongation factor 2 (eEF2)[118]. As not many proline hydroxylases were identified yet, we were interested if OGFOD1 is the so far unknown enzyme modifying eEF2K. In intitial IP experiments, eEF2K could be co-precipitated with OGFOD1.

Translation is regulated and repressed during distinct phases of the cell cycle and during stress[119,147]. eEF2K seems to provide one mechanisms to stall translation by phosphorylating eEF2. This inhibiting phosphorylation of eEF2 threonin 56 (T56) prevents its binding to the ribosome and thereby impairs translation elongation[148]. EEF2K is regulated by different pathways like mTOR signaling, nutrient starvation, or oxidative stress via phosphorylation by the AMP kinase[149]. Recently, a serine phosphorylation (S595) of eEF2 carried out by the CCNA2-CDK2 complex was identified and contributes to eEF2's regulation[149]. This cell cycle dependent phosphorylation seems to facilitate the following inhibitory phosphorylation by eEF2K. In mitosis, S595 and T56 phosphorylations are increased, probably resulting in repressed translation as it is known for M phase[14] (Figure 66).

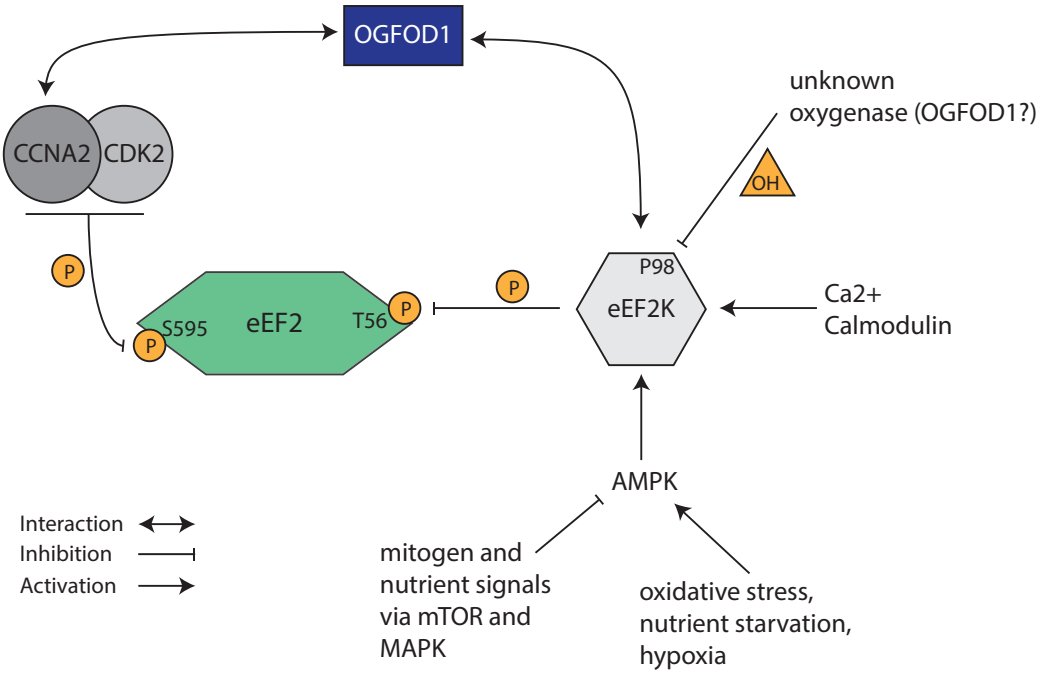

Figure 66: Schematic overview of eEF2K and eEF2 regulation

The CCNA2-CDK2 dependent modificiation might be one mechanism to couple cell cycle progression with translation[149]. This cell cycle regulated translation inhibition might be mediated by OGFOD1-catalyzed eEF2K hydroxylation. With the F2H assay this interaction could not be confirmed. In this experiment, Flag-tagged eEF2K was used. This tag might not be ideal for this assay, therefore, the experimental set-up could be further adjusted to confirm this interaction. Following, mass spectrometry based experiments and MALDI-TOF peptide screening with the reported hydroxylated proline could be performed to determine OGFOD1 as responsible prolyl hydroxylase.

OGFOD1 correlation with stress granules (SGs)

To unravel the function of OGFOD1 in SGs, first the formation of SGs was monitored over time. SGs could be detected by TIA-1 recruitment 15 min after stress induction. Endogenous OGFOD1 was recruited to SGs after 30 min. Overexpressed OGFOD1 independently of size and location of the tag was not recruited to stress granules, even though TIA-1 role in SGs could be studied with GFP-tag[150]. Tagged OGFOD1 might be disturbed in interaction with proteins needed for its recruitment towards SGs.

Translocation of the nuclear protein OGFOD1 towards cytoplasmic stress granules (SGs) was already reported[5,89]. Interacting proteins comprised some stress granule proteins, the eIF2alpha kinase heme-regualted inhibitor (HRI), and eIF2alpha itself. Overexpression of OGFOD1 resulted in decreased polysome levels and increased amounts of phosphorylated eIF2alpha during recovery from stress[89]. Knockdown on the other hand led to enhanced recovery of translation by enhanced polysome formation during the recovery from stress[89].

To further explore function and relevance of OGFOD1 in stress granules, isolation of SGs and analysis of the composition could be performed. To study OGFOD1 domains needed for the translocation, reported interactors related with stress granules could be further examined.

Attempts to generate OGFOD1 knockout cell lines

Generation of OGFOD1 knockout cell lines in Hek293 cells was not possible, only one heterozygous knockout clone could be generated. In contrast, generation of MINA53 and NO66 knockouts in Hek293 cells was successful. Judging from protein levels of wild type and OGFOD1 D2 +/- cells, protein levels seemed even to be compensated by the remaining OGFOD1 gene copy. Considering the unchanged protein amount and a growth behaviour comparable to wild type cells, also the ribosomal profile of the heterozygous OGFOD1 D2 cells did not differ from wild type. Analysis of the ribosomes by MS confirmed the compensation of OGFOD1 protein levels, as the RPS23 P62 was only identified in the hydroxylated status in OGFOD1 D2 cells.

A second attempt to generate homozygous knockout cells starting with the heterozygous clone did not succeed and resulted in no surviving cells. This led us to the conclusion, that OGFOD1 knockout in Hek293 cell is lethal. These findings support a role of OGFOD1 in cell cycle progression.

However, OGFOD1 does not seem to be essential in all cell lines or organisms. In *S.cerevisiae* knockout of the homologue Tpa1 did cause only minor defects[20]. On the contrary, depletion of OGFOD1 homologue Sud-1 in *D. melanogaster* caused lethality in early embryonic development[44]. In mammalian cell culture , siRNAs targeting OGFOD1 caused marked effects on proliferation in HCT116, Hek293, and other cell lines. In HeLa, despite efficient knock down, no effect was observable[5]. Saito and colleagues were even able to generate OGFOD1 knockouts in Nalm-6 cells, a human pre-B acute lymphoblastic leukemia cell line[90].

With regard to this dependency on the cellular background, another cell line could be used for generation of knockout cell lines. Rescue of the knockout with different OGFOD1 variants could then be used for the characterization of OGFDO1's function with regards to ribosome regulation, cell cycle involvment, and the function in stress granules.

3.2 Bacterial oxygenase ycfD

Whereas knockout of OGFOD1 was not possible, generation of bacterial knockout strains lacking ycfD seemed to have no negative effect on bacteria. Earlier studies showed that overexpression of His-tagged ycfD led to tremendous growth defects, the comercially available Keio ycfD knockout strain JW1114-2[103] was viable[4,46]. However, under stress conditions like growth in minimal medium, growth defects of the knockout strain were observed[4].

YcfD knockout strains generated in this work are slightly different, as Keio collection knockouts are full genomic knockouts. In this work, the first and last 50 basepairs of ycfD were used for the recombination event, therefore the knockout strain might still express the first amino acids of ycfD followed by the counter selection cassette. However, the enzymatic JmjC domain is completely lost, leading us to the assumption of the loss of catalytic activity of ycfD.

With the strains generated in this work, the observed growth defects could not be recapitulated. Also the ycfD-AxA strain lacking catalytic activity displayed normal growth behaviour. Consistently, ribosome profiles of knockout and AxA mutant strain obtained in this work did not display obvious effects, suggesting normal ribosomal assembly and translation activity. However, the reported growth phenotype with JW1114 could also not be resumed, ribosome profiles of this strain were comparable to wild type profiles. For

future experiments, the genomic surrounding of ycfD in JW1114 should be further evaluated to exclude residual ycfD expression.

YcfD catalyzed hydroxylation of arginine 81 in RPL16 occurs at a prominent localization in the ribosome, in closest proximity to the peptidyl transferase center (PTC) in the ribosome. L16 itself is needed for formation of the 70S initiation complex[47], for the peptidyl transferase activity[48], and to coordinate and stabilize the binding of A-site tRNAs[49]. Despite the important functions of RPL16 in the ribosomal context, the hydroxylation by ycfD seems not to be essential in bacteria.
Also monooxygenase yfcM knockout in Salmonella grows phenotypically normal[151]. YfcM hydroxylates lysinylated Lys 34 of the conserved translation elongation factor P (EF-P), this modification is the final step in maturation of EF-P[152]. EF-P is needed for translation elongation and stimulates peptide bond formation at the P site[151]. EF-P is also reported to be critial for rapid translation of polyproline stretches, which cause translational pausing. Still, knockout of EF-P causes only a minor growth rate reduction[153,154]. Loss of hydroxylation in EF-P seems to be as harmless to bacteria as loss of hydroxylation of R81 in RPL16. This might suggest, that even if universal, certain modifications only fine-tune translation but are not essential.

3.3 Histidine hydroxylases MINA53 and NO66

Characterization of knockout strains

Knockout of human MINA53 and NO66 in Hek293 using CRISPR/Cas9 showed only minor growth defects and ribosome profiles also revealed no differences compared to wild type. The reconstituted cell lines did also not show drastic effects on the proliferation, even though reconstituted protein expression was much higher than endogenous MINA53 or NO66 expression. Despite these observations, both proteins are described to be involved in cancer cell growth. MINA53[55-70] was reported to be upregulated in different cancer types, NO66 plays a role in osteoblast differentiation[79] and bone formation in mice[81,82].
Their similarities concerning protein domain structure and crystal structure, ribosomal substrates, and subcellular localization might suggest a redundancy of both proteins. Therefore, a double knockout of MINA53 and NO66 could be an option to examine this hypothesis.

Phylogenetic and genomic studies for MINA53 and NO66

The special genomic situation of NO66 and the question of redundancy of MINA53 and NO66 led us to a genomic and phylogenetic approach.
Searching for MINA53 and NO66 sequences in different organisms revealed, that some of those species did not exhibit MINA53 sequences. Model organisms *Caenorhabditis elegans* (*C.elegans*) and *Drosophila melanogaster* (*D.melanogaster*) only encode NO66, the same is true for other invertebrate species from arthropoda, mullosca, nematoda, and annelida. Suprisingly, the fresh-water polyp *Hydra* as early metazoan animal of the phylum Cnidaria posseses both MINA53 and NO66 sequences.
Expression of both *Hydra* NO66 with GFP-tag in *Hydra vulgaris* showed a comparable subcellular distribution for NO66. Human as well as HvNO66 are localized in the nucleoli.

Hydra MINA53 in contrast to human protein, is localized to the nucleus, but not the nucleoli in *Hydra vulgaris*. This might be a hint towards an adapted or slighly changed function of MINA53 through out the evolution, whereas NO66 might have kept the same function. However, this hypothesis needs further experiments. NO66 function in *C.elegans* or *D.melanogaster* could be examined, also organisms harboring both proteins sequences could be analyzed for MINA53 and NO66 protein functions.

Whereas MINA53 – as 91% of eukaryotic genes[155] - consists of introns and exons, NO66 consists of only one exon and is therefore intronless (single exon gene, SEG). Whereas the mammalia and chicken as representative of the aves possess NO66 with only one exon, in protostomia NO66 gene consists of a high exon number up to 18 exons separated by introns. The arthropoda harbour one exon (*D.melanogaster*) up to seven exons. Neither did the exon number decrease consistently over evolution, nor consists NO66 as single exon gene only in organisms harboring both MINA53 and NO66 gene.
Intronless genes are a characteristic feature of prokaryotes, but still ca. 9% of the human encoding genes consist of only one exon[155]. All histons, around 50% of the G-protein coupled receptors (GPCRs) and several proteins involved in transcription and translation, are encoded by intronless genes[156]. Advantages of SEGs might be of economical nature. Generating mRNAs with introns would need more time and energy, splicing requires additional factors. On the other hand, intron containing genes would allow diversity in protein products by alternative splicing[155-157].
NO66 might be a single exon gene to allow the cell to react quickly to changing environmental or stress conditions. This might change the hydroxylation status of ribosomal protein RPL8, which could fine-tune translation in response to different stimuli. Nevertheless, the research about SEGs is just at the beginning to unravel the function and the importance of being intronless. However, NO66 is the only human 2OG oxygenase with no introns.

In addition, the phylogenetic analysis implies that MINA53 could be the earlier invented protein due to the branching of ycfD and MINA53. The consistency of NO66 being present in all studied organisms might contradict this. Others suggest ycfD to be evolved into NO66[6]. However, they used not only MINA53 and NO66 but also other 2OG oxygenases for their phylogenetic analyses.

Studies concerning the connection of dimerization and catalytic activity

A few 2OG oxygenases are reported to form homo-dimers or -multimers, but not much is known about the function of oligomerization.
MINA53 and NO66 as well as bacterial ancestor ycfD have a very conserved domain structure and dimerize via proposed dimerization domains[6]. For MINA53 and NO66, three amino acids in the dimerization domain could be identified which – if mutated - led to disruption of the homo-oligomerization. For NO66 and substrate RPL8, inhibition of NO66 dimerization also disrupted substrate binding. MINA53 triple mutant could not be examined in substrate binding, but the cellular localization changed from nucleolar to an evenly distribution over the cell nucleus (data not shown). Therefore, for MINA53 and NO66, dimerization seems to be essential for substrate binding, localization, and maybe for enzymatic activity. A change in localization controlled by homo-oligomerization has been described for another 2OG oxygenase. JMJD6 has been shown to shuttle between

nucleoplasm and nucleoli upon homo-oligomerization[158]. Another example describing homo-oligomerization as factor determining activity is the oxygenase FIH, is reported to be only catalytically active in the form of a dimer[159]. Also in the hypoxic pathway, prolyl hydroxylase domain protein 2 (PHD2) displays the opposite catalytic function of dimerization. Dimerization in response to oxidative stress leads to the inactivation of the protein and thereby the hypoxic response pathway is activated[160].

OGFOD1 as third human oxygenase modifying the ribosome directly is not reported to dimerize. The crystal structure and the domain architecture is different from MINA53 and NO66. However, not forming homo-oligomers, OGFOD1 protein itself consists of two DSBH folds[88]. This might mimic a dimerization and could play a role in substrate recognition and protein activity. Another ROX, the tRNA modifying TYW5 seems to dimerize via C-terminal α-helices[2].

In view of the involvment of MINA53 and NO66 in cell proliferation and cancer, disruption of the dimerization might offer a new therapeutic approach. General 2OG oxygenase inhibitors are dimethyloxalglycine (DMOG) or N-oxalylglycine (NOG)[161]. Both are unreactive 2OG analogues, which are not released from the catalytic side of 2OG oxygenases after the reaction and thereby inhibiting further catalytic activity. This way of inhibition is very unspecific as it targets nearly all 2OG oxygenases, specific inhibitiors for single 2OG oxygenase are rare[161]. As some 2OG oxygenases form homo-oligomers with a functional significance, it might be promising to search for specific inhibitors targeting oligomerization.

4 Material

4.1 Chemicals and consumables

Chemical	Producer/Manufacturer
4',6-Diamidino-2-phenylindole dihydrochloride (DAPI)	Sigma
Acetic acid	VWR
Agarose	Biozym
Albumin from bovine serum/BSA	Sigma
Ammonium persulfate (APS)	Sigma
Ampicillin sodium salt	Roth
AquaBluer™	MultiTarget Pharmaceuticals, LLC
Bacto Agar	Th. Geyer
Calcium chloride	Sigma
Cell extraction buffer	Life Technologies
Chloramphenicol	Roth
D-(+)-Glucose	Roth
Direct PCR lysis reagent	Peqlab
Dithiothreitol (DTT)	Life Technologies
DNA Loading Dye (6x)	Thermo Fisher Scientific
Dulbecco's Modified Eagle Medium (DMEM) (1x), liquid (High Glucose)	Life Technologies
ECL Western blotting detection reagents and analysis system kit	GE Healthcare
Ethanol	Merk
3X FLAG® Peptide	Sigma
FCS (fetal calf serum)	Biochrom
Glycerol	Roth
Glycine	Roth
HD Green plus	Intas
HEPES Buffer salt	Roth
Hoechst33342	Molecular Probes
Hydrochloric acid 32% (Hcl)	Roth
Isopropanol	Th. Geyer
Isopropyl β-D-1-thiogalactopyranoside (IPTG)	Roth
Kanamycin sulphate	Roth
L-Arabinose	Sigma
Laemmli Sample Buffer (4x)	Biorad
LB Broth	Roth
Lipofectamine 2000 Reagent	Life Technologies
Magnesium chloride	Roth
Magnesium sulfate heptahydrate	Sigma
2-Mercaptoethanol	Sigma
Nitrocellulose membran (Amersham Protran Premium 0.45 NC)	GE Healthcare
Nonidet P40 substitute	Sigma

NUCLEAR-ID® Red DNA stain	Enzo Life Sciences
Paraformaldehyde solution 4%	Santa Cruz
PBS Dulbeco's phophate buffered saline	Life Technologies
PEI Polyethylenimine, branched	Sigma
Penicillin-Streptomycin (10,000 U/mL)	Life Technologies
Phosphatase inhibitor cocktail 2	Sigma
Phosphatase inhibitor cocktail 2	Sigma
Ponceau S Solution 0,1 % Ponceau S	Sigma
Potassium chloride (KOH)	Roth
Powdered milk	Roth
Protease inhibitor cocktail	Sigma
Protease inhibitor cocktail, Complete mini, EDTA-free	Roche
Proteinase K, 20 mg/ml	Peqlab
Rotiphorese® Gel 30 (37.5:1 Acrylamide/Bisacrylamide)	Roth
Sodium acetate	AppliChem
Sodium arsenite	Sigma
Sodium chloride	Roth
Sodium dodecyl sulfate (SDS)	Roth
Sodium hydroxide	Sigma
Sucrose	Roth
Tetracyclin hydrochloride	Roth
Tetramethylethylendiamine (TEMED)	Roth
Thymidine (cell culture grade)	Sigma
Tris base	Roth
Triton X-100	AppliChem
Trypsin/EDTA	Biochrom
Tween-20	Roth
Ultrapure water	Biochrom
Vectashield	Biozol
Vitamin B1 (Thiamine)	Roth

4.2 Instruments and Equipment

Name	**Company**
LRSII flow cytometer	BD Biosiences
Attune acoustic Focusing Cytometer	AB, applied biosystems
Vi-CELL XR 2.04	Beckman Coulter
2104 EnVision® Multilabel Plate Readers	PerkinElmer
Invivo 300 Hypoxic Workstation	Baker Ruskinn

Microscope type	**Microscope name**
Confocal laser-scanning	Leica TCS SP5 II
Fluorescence	Carl Zeiss LSM 510 META

4.3 Cell lines

Cell line	Description	Source
HeLa	Human cervix carcinoma cells	ATCC
Hek293	Human embryonic kidney cells	ATCC
Hek293T	Derivative of human embryonic kidney 293 cells containing the SV40 T-antigen	ATCC
BHK	Baby Hamster Kidney cells	AG Leonhardt, LMU München
HeLa-Cell Cycle Chromobody®-TagRFP	HeLa cell line stably expressing Cell Cycle Chromobody® fused to the red fluorescent protein TagRFP	ChromoTek GmbH
Hek293_KO-MINA53 cell line #1 -#4	CRISPR/Cas9 generated MINA53 knockout cell lines	This work
Hek293_KO-NO66 cell line #3, 4, 6, and 7	CRISPR/Cas9 generated NO66 knockout cell lines	This work
Hek293_+/-_O1D2	CRISPR/Cas9 generated cell line with heterozygous knock of OGFOD1	This work
Hek293_NO66KO#3+NO66-WT	NO66 knockout cell line #3 lentiviral stable reconstituted with NO66 wild type protein	This work
Hek293_NO66KO#3+NO66-AxA (H340A,D342A)	NO66 knockout cell line #3 lentiviral stable reconstituted with NO66 active site mutated protein	This work
Hek293_NO66KO#3+NO66-Triple (W428A,F431A,L436A)	NO66 knockout cell line #3 lentiviral stable reconstituted with NO66 protein mutated in three residues in the dimerization domain	This work
Hek293_MINA53KO#4 +MINA53-WT	MINA53 knockout cell line #4 lentiviral stable reconstituted with MINA53 wild type protein	This work
Hek293_MINA53KO#4 +MINA53-AxA (H179A, D181A)	MINA53 knockout cell line #4 lentiviral stable reconstituted with MINA53 active site mutated protein	This work
Hek293_MINA53KO#4 +MINA53-Triple (W264A, F267A, L308A)	MINA53 knockout cell line #4 lentiviral stable reconstituted with MINA53 protein mutated in three residues in the dimerization domain	This work

4.4 Bacterial strains

Bacterial strain	Description	Source
BL21	Sex: F- Chromosomal Markers: lon-11, Δ(ompT-nfrA)885, Δ(galM-ybhJ)884, λDE3 [lacI, lacUV5-T7 gene 1, ind1, sam7, nin5], Δ46, $[mal^+]_{K-12}(\lambda^S)$, hsdS10	AG Hadian, HelmholtzZentrum München
TOP10	Sex: F-, Chromosomal Markers: *mcrA* Δ(*mrr-hsd*RMS-*mcr*BC) Φ80*lac*ZΔM15 Δ *lac*X74 *rec*A1 *ara*D139 Δ(*araleu*)7697 *gal*U *gal*K *rps*L (StrR) *end*A1 *nup*G	AG Hadian, HelmholtzZentrum München
BW25113	parent strain for the Keio Collection of single gene	CGSC Strain#:

	knockouts, Sex: F-, Chromosomal Markers: *Δ(araD-araB)567*, *ΔlacZ4787*(::rrnB-3), *λ*$^-$, *rph-1*, *Δ(rhaD-rhaB)568*, *hsdR514*	7636
JW1114	Keio Collection of single-gene knockout for ycfD, Sex: F- Chromosomal Markers: *Δ(araD-araB)567*, *ΔlacZ4787*(::rrnB-3), *λ*$^-$, *ΔycfD788::kan*, *rph-1*, *Δ(rhaD-rhaB)568*, *hsdR514*	CGSC Strain#: 9045
BW25113 (rpsL150)	BW25113 modified, rpsL was exchanged by rpsL150, Sex: F-, Chromosomal Markers: *Δ(araD-araB)567*, *ΔlacZ4787*(::rrnB-3), *λ*$^-$, *rph-1*, *Δ(rhaD-rhaB)568*, *hsdR514, rps*L (StrR)	This work
BW25113 (rpsL150, ycfD-rpsL-neo-cassette)	BW25113 (rpsL150) modified, nucleotides 51-1071 of ycfD were exchanged by counter selection cassette, Sex: F-, Chromosomal Markers: *Δ(araD-araB)567*, *ΔlacZ4787*(::rrnB-3), *λ*$^-$, *rph-1*, *Δ(rhaD-rhaB)568*, *hsdR514*	This work
BW25113 (rpsL150, ycfD-neo/kan-cassette)	BW25113 (rpsL150) modified, nucleotides 51-1071 of ycfD were exchanged by counter selection cassette, Sex: F-, Chromosomal Markers: *Δ(araD-araB)567*, *ΔlacZ4787*(::rrnB-3), *λ*$^-$, *rph-1*, *Δ(rhaD-rhaB)568*, *hsdR514, rps*L (StrR)	This work
BW25113 (rpsL150, ycfD-AxA)	BW25113 (rpsL150) modified, ycfD wild type gene is replaced by ycfD sequence encoding base pair excange resulting in H125A and D127A, Sex: F-, Chromosomal Markers: *Δ(araD-araB)567*, *ΔlacZ4787*(::rrnB-3), *λ*$^-$, *rph-1*, *Δ(rhaD-rhaB)568*, *hsdR514, rps*L (StrR)	This work

4.5 Primary and secondary antibodies

Antibody target	Catalog number	Source	Species	Dilution IF	Dilution WB
actin-HRP	sc-1616 HRP	Santa Cruz	goat		1:500
CCNA2 (Cyclin A), clone CY-A1	C4710-.2ML	Sigma	mouse	1:200	1:500
Cyclin A (H-432)	sc-751	Santa Cruz	rabbit	1:100, 1:200	1:100, 1:200
Cyclin B1 (H-433)	sc-752	Santa Cruz	rabbit	1:100, 1:200	1:100, 1:200
CDK1/Cdc2 p34 (17)	sc-54	Santa Cruz	mouse		1:100
Cdk2 (D-12)	sc-6248	Santa Cruz	mouse	1:100, 1:200	1:100
GFP	11 814 460 001	Roche	mouse		1:500
HA Tag	sc-Y11	Santa Cruz	rabbit	1:100	
M2 anti-FLAG	F1804-200ul	Sigma	mouse		1:500
MINA53	ab169154	Abcam	mouse		1:300
NO66/C14orf169	ab113975	Abcam	rabbit		1:1000

NO66/C14orf169	ab192861-10ul	Abcam	rabbit		1:1200
OGFOD1	HPA003215	Sigma	rabbit	1:500	1:500
RPS23	ab57644	Abcam	mouse		1:50
TIA1	sc-1751	Santa Cruz	goat	1:50, 1:100	
UBF (H-300)	sc-9131	Santa Cruz	rabbit	1:200	
Isotype control for Cyclin A (H-432)	sc-2027 x	Santa Cruz	rabbit		

Table 4: Primary antibodies

Antibody target	Catalog number	Source	Species	Coupled to	Dilution
Peroxidase-conjugated Donkey anti-Rabbit IgG	711-035-152	Dianova	Donkey	Peroxidase	1:1000
Peroxidase-conjugated Donkey anti-Goat IgG	705-035-147	Dianova	Donkey	Peroxidase	1:1000
Peroxidase-conjugated Donkey anti-Mouse IgG	715-035-150	Dianova	Donkey	Peroxidase	1:1000
Maus IgG anti-Kaninchen IgG (L)	211-032-171	Dianova	Mouse	Peroxidase	1:1000
Anti-Maus IgG (L)-HRPO	115-035-174	Dianova	Goat	Peroxidase	1:1000
Alexa Fluor(R) 488 donkey anti-goat IgG	A11055	Life Technologies	Donkey	Alexa Fluor 488	1:1000
Alexa Fluor ® 594 rabbit anti-mouse IgG	A11062	Life Technologies	Chicken	Alexa Fluor 594	1:1000
Alexa Fluor ® 594 chicken anti-goat IgG	A21468	Life Technologies	Rabbit	Alexa Fluor 594	1:1000
Alexa Fluor ® 488 donkey anti-rabbit IgG	A21206	Life Technologies	Donkey	Alexa Fluor 488	1:1000
Alexa Fluor ® 594 donkey anti-rabbit IgG	A21207	Life Technologies	Donkey	Alexa Fluor 594	1:1000
Alexa Fluor(R) 488 chicken anti-mouse IgG	A21200	Life Technologies	Chicken	Alexa Fluor 488	1:1000

Table 5: Secondary antibodies

4.6 Plasmid/Clones

Insert	Plasmid	Restriction sites	Established by	Expression in	Information
CCNA2 (human)	pmCherry-N1	KpnI/ BamHI	This work	Mammalian cell culture	Full length CCNA2 with a C-terminal mCherry-tag
CCNA2 (human)	pRSet5D-GFP	BstEII/ EcoRI	This work	Bacteria	Full-length CCNA2 with N-terminal GFP-tag
CCNA2 (human)	pGex-4T-2	BamHI/ XhoI	This work	Bacteria	CCNA2 full length in with N-terminal GST-tag
CCNA2 (human)	p3xFlag-CMV-9-10	KpnI/ BamHI	Alex Wolf	Mammalian cell culture	full length CyclinA2 with N-terminal 3xFLAG-tag
CCNA2 (human) aa1-180	p3xFlag-CMV-9-10	KpnI/ BamHI	This work	Mammalian cell culture	aa1-180 of CyclinA2 with N-terminal 3xFLAG-tag
CCNA2 (human) aa1-180	pRSet5D-GFP	BstEII/ EcoRI	Olga Swolski	Bacteria	aa1-180 of CyclinA2 with N-terminal GFP-tag
CCNA2 (human) aa1-46 + 181-432	p3xFlag-CMV-9-10	KpnI/ BamHI	This work	Mammalian cell culture	aa1-46 und 181-342 of CyclinA2 with N-terminal 3xFLAG-tag
CCNA2 (human) aa1-46 + 181-432	pRSet5D-GFP	BstEII/ EcoRI	Olga Swolski	Bacteria	aa1-46 und 181-342 of CyclinA2 with N-terminal GFP-tag
CCNA2 (human) aa181-432	p3xFlag-CMV-9-10	KpnI/ BamHI	This work	Mammalian cell culture	aa181-432 of CyclinA2 with N-terminal 3xFLAG-tag
CCNA2 (human) aa181-432	pRSet5D-GFP	BstEII/ EcoRI	Olga Swolski	Bacteria	aa181-432 of CyclinA2 with N-terminal GFP-tag
CDK2 (human) isoform1	pET28a	BamHI/ HindIII	This work	Bacteria	Full length CDK2 isoform1 with N-terminal His-tag.
eEF2K (human)	p3xFlag-CMV-9-10	KpnI/ BamHI	This work	Mammalian cell culture	Full length eEF2K with N-terminal 3xFLAG-tag
hSpCas9-2A-Puro	PX459		Addgene	Mammalian cell culture	Addgene #48139
MINA53 (human)	pEGFP-C1	XhoI/ KpnI	Kevin Brockers	Mammalian cell culture	Full length MINA53 with N-terminal GFP-tag
MINA53 (human)	pEGFP-N1	XhoI/ AgeI	Kevin Brockers	Mammalian cell culture	Full length MINA53 with C-terminal GFP-tag
MINA53	pLVTHM-	PmeI/	This work	Lentiviral	Full length MINA53

(human)	T2A-CD2	SpeI		vector	with with T2A-CD2-tag
MINA53 (human) H179A, D181A	pEGFP-C1	XhoI/ KpnI	Kevin Brockers	Mammalian cell culture	Full length MINA53 H179A, D181A with N-terminal GFP-tag
MINA53 (human) H179A, D181A	pLVTHM-T2A-CD2	PmeI/ SpeI	This work	Lentiviral vector	Full length MINA53 H179A, D181A with T2A-CD2-tag
MINA53 (human) W264A, F267A, L308A	pEGFP-C1	XhoI/ KpnI	Kevin Brockers	Mammalian cell culture	Full length MINA53 W264A & F267A & L308A with N-terminal GFP-tag
MINA53 (human) W264A, F267A, L308A	pLVTHM-T2A-CD2	PmeI/ SpeI	This work	Lentiviral vector	Full length MINA53 W264A & F267A & L308A with with T2A-CD2-tag
MINA53 (*Hydra vulgaris*)	pHotG	NheI/ XmaI	This work	Hydra vulgaris	Full length MINA53 with C-terminal GFP-tag
NLS	pEGFP-C1	-	Leonhardt group	Mammalian cell culture	GFP fused to a NLS sequence
NO66 (human)	pEGFP-C1	EcoRI/ KpnI	Kevin Brockers	Mammalian cell culture	Full length NO66 with N-terminal GFP-tag
NO66 (human)	pLVTHM-T2A-CD2	PmeI/ SpeI	This work	Lentiviral vector	Full length NO66 with N-terminal GFP-tag
NO66 (human) H340A, D342A	pEGFP-C1	EcoRI/ KpnI	This work	Mammalian cell culture	Full length NO66 H340A & D342A with N-terminal GFP-tag
NO66 (human) H340A, D342A	pLVTHM-T2A-CD2	PmeI/ SpeI	This work	Lentiviral vector	Full length NO66 H340A & D342A with T2A-CD2-tag
NO66 (human) W428A, F431A, L436A	pEGFP-C1	EcoRI/ KpnI	Kevin Brockers	Mammalian cell culture	Full length NO66 W428A & F431A & L436A with N-terminal GFP-tag
NO66 (human) W428A, F431A, L436A	pLVTHM-T2A-CD2	PmeI/ SpeI	This work	Lentiviral vector	Full length NO66 W428A & F431A & L436A with T2A-CD2-tag
NO66 (*Hydra vulgaris*)	pHotG	NheI/ XmaI	This work	Hydra vulgaris	Full length NO66 with C-terminal GFP-tag
OGFOD1 (human)	pET24		Emily Flashman	Bacteria	Untagged full-length OGFOD1
OGFOD1 (human)	pET28a	NheI/ XhoI	Alex Wolf	Bacteria	Full-length OGFOD1 with N-terminal His-tag
OGFOD1 (human)	pEGFP-N1	XhoI/ BamHI	Alex Wolf	Mammalian cell culture	Full length OGFOD1 with C-terminal GFP-tag

OGFOD1 (human)	pEGFP-C1	XhoI/ BamHI	Alex Wolf	Mammalian cell culture	Full length OGFOD1 with N-terminal GFP-tag
OGFOD1 (human)	pHA	Not1/ Not1	Alex Wolf	Mammalian cell culture	Full length OGFOD1 with C-terminal HA-tag
OGFOD1 (human)	pcDNA3	BamHI/ XhoI	Alex Wolf	Mammalian cell culture	Untagged full length OGFOD1
OGFOD1 (human) aa1-238	pEGFP-N1	Xho1/ BamH1	Olga Swolski	Mammalian cell culture	aa1-238 of OGFOD1 with C-terminal GFP-tag
OGFOD1 (human) aa1-260	pEGFP-N1	XhoI/ BamHI	Alex Wolf	Mammalian cell culture	aa1-260 of human Ogfod with C-terminal GFP-tag
OGFOD1 (human) aa1-30 + aa261-542	pEGFP-N1	XhoI/ BamHI	Alex Wolf	Mammalian cell culture	aa1-30 and aa261-542 of OGFOD1 ORF in frame separated by 4 aminoacids (PRAM) with C-terminal GFP-tag
OGFOD1 (human) aa21-542	pEGFP-N1	XhoI/ BamHI	Alex Wolf	Mammalian cell culture	OGFOD1 lacking aa1-20 with C-terminal GFP-tag
OGFOD1 (human) aa31-542	pEGFP-N1	XhoI/ BamHI	This work	Mammalian cell culture	OGFOD1 lacking aa1-30 with C-terminal GFP-tag.
OGFOD1 (human) H155A+D157A	pEGFP-N1	XhoI/ BamHI	Alex Wolf	Mammalian cell culture	Full length OGFOD1 H155A+D157A with C-terminal GFP-tag
OGFOD1 (human) H155A+D157A	pET28a	NheI/ XhoI	This work	Bacteria	Full-length OGFOD1 H155A+ D157A with N-terminal His-Tag
OGFOD1 (human) H155A+D157A	pcDNA3	BamHI/ XhoI	This work	Mammalian cell culture	Untagged full length OGFOD1 H155A&D157A
OGFOD1 (human) R519A+L521A	pEGFP-N1	Xho1/ BamH1	Olga Swolski	Mammalian cell culture	Full length OGFOD1 R519A + L521A with C-terminal GFP-tag
OGFOD1 internal HA	pCDNA3	BamHI/ XhoI	This work	Mammalian cell culture	OGFOD1 linker (nucleotides 745-769) replaced by HA-tag
OGFOD2 Iso1 (human)	pCDNA3	KpnI/ XbaI	Justė Wesche	Mammalian cell culture	Untagged full length OGFOD2I1
RPL27A (human)	pcDNA5-FRT-TO-3xFLAG 5´	HindIII/ XhoI	Kevin Brockers	Mammalian cell culture	Full length Rpl27a with N-terminal Flag-tag, additional 6 amino acids (LESRGPV*) at C-terminus

RPL8 (human)	pcDNA5-FRT-TO-3xFLAG 5´	HindIII/ XhoI	Kevin Brockers	Mammalian cell culture	Full length RPL8 with N-terminal Flag-tag
RPS23 (human)	pmCherry-N1	KpnI/ BamHI	This work	Mammalian cell culture	Full length RPS23 with C-terminal mCherry-tag
--	pRSet5D-GFP		Leonhardt group	Bacteria	Empty vector expressing GFP-His
--	pMD2.G		Krappmann group		Lentiviral envelope plasmid (Addgene ID 12259)
--	psPAX2		Krappmann group		Lentiviral packaging plasmid (Addgene ID 12260)

4.7 Primer

Primer	Sequence (5'-3')	Used for
rpsL_up1	CTTGACACCTTTTCGGCATCGC	Amplification of rpsL150 (StrR)
rpsL_down1	CGTTGTTAATTCAGGATTGTCC	
rpsL-neo-ycfD_F	ATGGAATACCAACTCACTCTTAACTGGCCCGATTTTCTTGAACGTCACTGGGCCTGGTGATGATGGCGGGATCG	Generation of bacterial ycfD mutant
rpsL-neo-ycfD_R	TTACCCTTCGAAGAACCAATACCCGCTATTGACCAGCGCCGCGAGCATCGTCAGAAGAACTCGTCAAGAAGGCG	
ycfD_F1	ATGGAATACCAACTCACTCTTAACTGGCCCGATTTTCTTGAACGTCACTG	
ycfD_R1	TTACCCTTCGAAGAACCAATACCCGCTATTGACCAGCGCCGCGAGCATCG	
O1-AxAmuta_F	GCCCTGCTGTGCGCTGATGCTGAGCTGGAAGGGC	Mutagenesis of OGFOD1 to H155A and D157A, iron binding motif
O1-AxAmuta_R	GCCCTTCCAGCTCAGCATCAGCGCACAGCAGGGC	
O1R519AL521AmutF	GCATATTAACCACGCAAGCGCGGAACAAAAGAAAACC	Mutagenesis of OGFOD1 to R519A and L521A, potential cyclin binding motif
O1R519AL521AmutR	GGTTTTCTTTTGTTCCGCGCTTGCGTGGTTAATATGC	
intHA-O1_intF	CAGATTACGCTCACATCCCACAAGATCATGAG	Generation of OGFOD1 with internal HA-tag
intHA-O1_intR	GAACATCGTATGGGTAGTTGGGAGGCCG	
intHA-O1_overlapF	CTACCCATACGATGTTCCAGATTACGCTCAC	
CCNA2insR	GGTATGTGTGAATATCGGTCCGCGGTTGTTGG	Generation of CCNA2 deletion mutants
CCNA2insF	CCAACAACCGCGGACCGATATTCACACATACC	
CCNA2outBamHIR	CGGGATCCTTACAGATTTAGTGTCTCTGGTGGG	
CCNA2outKpnIF2	CGGGTACCAATGTTGGGCAACTCTGCG	

CCNA2aa1-180BamHR2	GCGGATCCCTACTCATGGTAGTCTGGTACTTCATTAAC	
CCNA2aa181-432KpnIF	CGGGTACCGATATTCACACATACCTTAGGGAAATGG	
O1_31-end_XhoIF	GCCTCGAGATGACGGAAGAAACCTTGAAAAAGC	Generation of OGFOD1 lacking aa 1-30
O1_31-end_BamHIR	CGGGATCCCGTTCATAATAGATGAATGAAAAGTCCCAG	
O1-AA1_XhoIF	GGCTCGAGATGAATGGGAAGCGGCC	Generation of OGFOD1 lacking aa 238-542
O1-AA1-238_BamHR	CCGGATCCCCATGAAACCAGCCACTTATAG	
CDK2_CBPN1Hind3F	CCAAGCTTTTATGGAGAACTTCCAAAAGGTGG	Amplification of CDK2 from cDNA and cloning
CDK2_CBPN1BamHIR	GTGGATCCAAGAGTCGAAGATGGGGTACTGG	
CDK2_CBPC1BamHIR	GTGGATCCTCAGAGTCGAAGATGGGG	
hydraNO66_NheF	CAGGCTAGCATGAATAACAACAAAGTATCAGC	Amplification of *Hydra vulgaris* NO66 from cDNA and cloning
hydraNO66_XmaR	GACCCGGGTGTATGGACCAATGGAACC	
hydraMinA_NheF	CAGGCTAGCATGGTGAAACGCAAAGGTTC	Amplification of *Hydra vulgaris* NO66 from cDNA and cloning
hydraMinA_XmaR	GGCCCGGGTTTGATTTCAATCAAATCATCAC	

Table 6: Cloning primers for different projects

Targeted gene	Name of primer	Sequence of primer (5'-3')
OGFOD1	O1KO_guide1upF	CACCG ATTAGCTCTGCTATGTTACT
	O1KO_guide1upR	AAAC AGTAACATAGCAGAGCTAATC
	O1KO_guide2backF	CACC GCCACATTAACTCTTCCAGC
	O1KO_guide2backR	AAAC GCTGGAAGAGTTAATGTGGC
MINA53	MinAEx1_upGuideF	CACC CTGCACTGGCCACATACTAT
	MinAEx1_upGuideR	AAAC ATAGTATGTGGCCAGTGCAG
	MinAEx1_downGuideF	CACCG AATGTCTGCCGGTGTGTCAA
	MinAEx1_downGuideR	AAAC TTGACACACCGGCAGACATT C
NO66	NO66_upGuide22F	CACC CGTATCTTCCTGGACCTCAA
	NO66_upGuide22R	AAAC TTGAGGTCCAGGAAGATACG
	NO66_downGuide15F	CACC CACCGGGTAGCGCGTCCCCC
	NO66_downGuide15R	AAAC GGGGGACGCGCTACCCGGTG

Table 7: Designed primers for guideRNAs

Primer/ Oligonucleotide	Sequence (5'-3')	Used for
Screen_O1ex2F	GTGCTACCCAAAGTTTGAGGG	Amplification of CRISPR/Cas9 targeted OGFOD1 locus
Screen_O1ex2R	GGAAGACATTATCACTCTCTCCATCC	
ScreenMinAEx1F	GGTAGGTTTGCATTTCCTTACTGC	Amplification of CRISPR/Cas9 targeted MINA53 locus
ScreenMinAEx1R	CACCCTTGAGCTGATATGTGGC	
NO66_screen2F	CTCCAGGCCAGTGCAGG	Amplification of CRISPR/Cas9 targeted NO66 locus
NO66_screen2R	GGTAAAAGTGATCTGGCGGC	

Table 8: Primers for screening of potential CRISPR/Cas9 knockout cell lines

4.8 Beads for immunoprecipitation

Name	Source
GFP-Trap® covalently coupled to the surface of agarose beads	Chromotek
Anti-Flag M2 Affinity Agarose Gel	Sigma-Aldrich
Protein G Sepharose 4 Fast Flow	GE Healthcare
Glutathione Sepharose 4B	GE Healthcare

4.9 Marker and enzymes

Marker	Source
Precision Plus Protein Dual color standard	Biorad
GeneRuler DNA ladder mix 1kb	Thermo Fisher Scientific
GeneRuler 100 bp Plus DNA ladder	Thermo Fisher Scientific

Enzyme	Source
Restriction enzymes	New England Biolabs
MyTaq™ DNA Polymerase	Bioline
Phusion Flash High-Fidelity PCR Master Mix	Biozym
MyTaq™ DNA Polymerase	Bioline
T4 DNA ligase	New England Biolabs
Calf intestinal alkaline phosphatase	New England Biolabs
Lysozym	AppliChem
DNAse	ThermoFisher

4.10 Transfection reagents

Transfection reagent	Source
Polyethylenimine pH 7, branched (PEI)	Sigma
X-tremeGENE HP DNA Transf. Reag. 1.0 ml	Roche
LIPOFECTAMINE 2000 REAGENT 1,5ml	Thermo Fisher Scientific

4.11 Kits

Kit	Company
NucleoSpin Gel and PCR Clean-up	Macherey-Nagel
QIAprep Spin Miniprep Kit	Qiagen
QiaFilter Plasmid Maxi Kit	Qiagen
QuikChange Site-directed mutagenesis kit	Agilent
Counter-Selection BAC Modification Kit	Gene Bridges

4.12 Buffers and Solutions

4.12.1 Cell lysis buffer

Mammalian cell lysis buffer	
NaCl	150 mM
Tris-HCl pH 8	10 mM
NP40	0.5 %
Phosphatase inhibitor cocktail 2	10 µl/ml
Phosphatase inhibitor cocktail 3	10 µl/ml
Protease inhibitor	10 µl/ml

Bacteria lysis buffer	
Tris-HCl pH 7.5	50 mM
Lysozym	0.5 mg/ml
Protease inhibitor EDTA free (Roche)	10 pill/ 10 ml
DNAse	1 U/ml

4.12.2 Gel electrophoresis (DNA)

TAE Buffer	
Tris	40 mM (pH 7.6)
Acetic acid	0.57 % (V/V)
EDTA solution (pH 8,0)	1 mM

1% Agarose gel	
Agarose	1% (W/V)
HDGreen® Plus Safe DNA Dye	0.3% (V/V)
TAE Buffer	

4.12.3 SDS-PAGE and Western blot

0.5 M Tris- buffer pH 6,8	
Tris-HCl	0.5 M
SDS	0.4% (W/V)
adjust pH 6,8	

1.5 M Tris- buffer pH 8,8	
Tris-HCl	1.5 M
SDS	0.4% (W/V)
Adjust pH 8,8	

3 % Stacking gel	
30 % Acrylamide/Bisacrylamide	3% (V/V)
0.5 M Tris-HCl-buffer pH 6.8	0.125 M
SDS	0.1% (W/V)
APS	0.1% (W/V)
Temed	0.01% (V/V)

12.5 % Separating gel	
30 % Acrylamide/Bisacrylamide	12.5% (V/V)
1.5 M Tris-HCl-buffer pH 8.8	0.375 M
SDS	0.1% (W/V)
APS	0.1% (W/V)
Temed	0.01% (V/V)

Electrophoresis buffer (SDS-PAGE)	
Tris	25 mM
Glycin	190 mM
SDS	0.1% (W/V)
check and adjust to pH 8.3	

Blot Buffer	
Tris	25 mM
Glycin	190 mM
check and adjust to pH 8.3	

4.12.4 Immunological protein detection

TBS	
Tris	20 mM
NaCl	140 mM
KCl	2.7 mM
adjust pH 7.4	

TBST	
Tris	20 mM
NaCl	140 mM
Tween 20	0.1% (V/V)
adjust pH 7.4	

4.12.5 Immunofluorescence experiments

Permeabilization solution	
Triton X-100	1 % (V/V)
	In PBS

Blocking solution	
FCS	10 % (V/V)
Tween-20	0.2 % (V/V)
	In PBS

Wash solution	
BSA	1 % (W/V)
Tween-20	0.2 % (V/V)
	In PBS

4.12.6 Immunoprecipitation experiments

Wash buffer 1	
NaCl	150 mM
Tris-HCl pH 8	10 mM

Wash buffer 2	
NaCl	300 mM
Tris-HCl pH 8	10 mM

4.12.7 Cloning

Annealing buffer	
KAc	100 mM
HEPES (pH 7.4)	30 mM
$Mg(Ac)_2$	2 mM

4.12.8 Hydra medium

Hydra culture medium	
KCl	0.1 mM
NaCl	1 mM
$MgSO_4$	0.1 mM
Tris	1 mM
$CaCl_2$	1 mM

4.12.9 Bacterial growth

LB medium	
LB Broth, Powder (Lennox)	20 mg/L

LB agar	
LB Broth, Powder (Lennox)	20 mg/L
Agar	15 mg/L

Minimal medium (M9)	
Na_2HPO_4	42 mM
KH_2PO_4	22 mM
NH_4Cl	18 mM
NaCl	8 mM
$CaCl_2$	2 µM
$MgSO_4$	0.05 mM
Glucose	0.2 % (W/V)
Thiamine	2.5 µM

4.12.10 Ribosome isolation

4.12.10.1 Isolation of bacterial ribosomes

Bacterial ribosome lysis buffer	
Hepes pH 7.8	10 mM
$MgCl_2$	30 mM
NH_4Cl	150 mM
β-mercaptoethanol	6 mM
Lysozym	0.5 mg/ml

Sucrose buffer for sucrose gradients	
Hepes pH 7.8	10 mM
$MgCl_2$	30 mM
NH_4Cl	150 mM
β-mercaptoethanol	6 mM
Sucrose	10 or 40 % (W/V)

4.12.10.2 Isolation of human ribosomes for LC-MS/MS analysis

Mammalian ribosome lysis buffer	
Hepes/KOH pH 7.0	50 mM
KOAc	100 mM
NP40	0.5 %
$Mg(OAc)_2$	25 mM
DTT	1 mM
Protease inhibitor EDTA free (Roche)	1 pill/ 10 ml

Sucrose buffer for sucrose cushion	
Hepes/KOH pH 7.0	50 mM
KOAc	500 mM
$Mg(OAc)_2$	25 mM
β-mercaptoethanol	5 mM
Nikkol	0.1 %
Protease inhibitor EDTA free (Roche)	10 pill/ 10 ml
Sucrose	750 mM

Mammalian ribosome storage buffer	
Hepes/KOH pH 7.0	50 mM
KOAc	500 mM
$Mg(OAc)_2$	6 mM
DTT	1 mM
RNasin Plus RNase Inhibitor	0.2 U/µl

4.12.10.3 Isolation for ribosome profiles for mammalian cells

Mammalian ribosome lysis buffer	
Hepes/KOH pH 7.0	50 mM
NaCl	300 mM
NP40	0.5 %
$MgCl_2$	6 mM
RNasin Plus RNase Inhibitor	0.2 U/µl

Sucrose buffer for sucrose cushion	
Hepes/KOH pH 7.6	50 mM
NaCl	300 mM
$MgCl_2$	6 mM
RNasin Plus RNase Inhibitor	0.2 U/µl
Sucrose	30 % (W/V)

Mammalian ribosome storage buffer	
Hepes/KOH pH 7.6	20 mM
KCl	150 mM
$Mg(OAc)_2$	6 mM
DTT	1 mM
Sucrose	6.8 % (W/V)
RNasin Plus RNase Inhibitor	0.2 U/µl

Sucrose buffer for sucrose gradients	
Hepes pH 7.0	50 mM
KOAc	150 mM
$Mg(OAc)_2$	6 mM
DTT	1 mM
Protease inhibitor EDTA free (Roche)	10 pill/ 10 ml
Sucrose	10 or 40 % (W/V)

5 Methods

5.1 Bacteria

5.1.1 Transformation

Chemically competent cells were transformed by a 45 sec heatshock at 42 °C after 30 min incubation of the bacteria with the plasmid DNA. Following the heatshock, bacteria were incubated for 2 min on ice.
Competent cells for electroporation were transformed following the instructor manual (BioRad).
Independet of transformation methode, bacteria were allowed to recover at 37 °C in LB medium (see 4.12.9) and spread onto LB-Agar plates (see 4.12.9) with the appropriate antibiotic.
Bacteria transformed with a plasmid were stored in 20 % glycerol stocks at -80 °C.

5.1.2 Bacterial growth

Bacteria were grown in LB medium with the appropriate antibiotics at 37 °C or temperatures examined to be the best for following application.

5.1.2.1 Expression trail

To find the best conditions for expression of the protein, several growth conditions were tested. A culture of bacteria carrying the plasmid of interest were inoculated and incubated at 37°C over night (O/N). Per condition, 100 ml cultures are inoculated from the O/N culture and incubated at 37 °C until they reach OD_{600} from 0.6-0.8. Subsequently, cultures were shifted to temperatures of 37 °C, 30 °C and 18-20 °C and if needed bacterial expression was induced with 1 mM IPTG. Cultures at 37 °C and 30 °C were incubated for 4 h, 18 °C cultures over night (O/N).

5.1.2.2 Harvesting and lysis of bacteria

Bacteria were harvested by centrifugation for 30 min at 4000 rpm at room temperature (RT). 1 g bacterial pellet was resuspended in 5 ml 50 mM Tris-HCl pH 7.5 and lysed by three repeated freeze- (-80 °C) and thaw- (37 °C) cycles. Lysates were centrifuged at 13.000 rpm for 20 min at 4 °C to obtain soluble protein. The resulting pellet was resuspend in 50 mM Tris-HCl (pH 7.5). 20 µg of protein were analyzed with the soluble protein on an SDS PAGE by Coomassie staining.
For immunoprecipitation experiments, bacteria pellets were lysed in bacteria lysis buffer (4.12.1).

5.1.2.3 Growth assay for bacteria

Bacterial growth assay was performed in the 2104 EnVision® Multilabel Plate Reader (Perkin Elmer). Per strain, 150 µl of bacteria with same starting OD_{600} of 0.05 were seeded into 96 well flat bottom plates in triplicates. Cultures were grown using 2 mm orbital shaking at 250

rounds per minute (RPM) at 37 °C. OD_{600} was determined by the plate reader every 15 min for at least 20 h.

5.1.3 Generation of bacterial knockout strains

Bacterial knockout strains were generated using the „Counter-Selection BAC Modification Kit“ from Gene Bridges which is based on Red/ET recombination.
The kit provides the pRed/ET plasmid, which carries the λ phage red gba operon expressed under the control of the arabinose-inducible pBAD promoter conferring tetracycline resistance (tet). The origin of replication is temperature sensitive and restricts replication at 37 °C. Therefore, bacteria carrying the plasmid were kept at 30 °C, expression of the red gba genes is induced by addition of L-Arabinose at 37 °C.
Streptomycin resistance is a prerequisite, therefore in BW25113, wild type *rpsL* gene was replaced by the *rpsL150* gene which leads to a streptomycin resistance due to a K43R amino acid substitution. *RpsL150* gene was PCR amplified from TOP10 bacteria and recombined into BW25113 carrying the plasmid pRED/ET (tet). Following the kit instructions, BW25113 strain was transformed with the pRed/ET plamid carrying a ampicillin (amp^R) resistance. After selection for ampicillin, bacteria were transformed with the linear PCR-amplified *rpsL150* flanked by 50 nucleotides (nts) homology arms to target the *rpsL* locus. Subsequent activation of Red/ET recombination led to insertion of the *rpsL150* gene. Schematic procedure for strain generation is depicted for ycfD catalytically inactive mutant strain (BW25113 (rpsL150, ycfD-H125A, D127A) (Figure 67). BW25113 (*rpsL150*) was transformed with pRed/ET and used for generation of different bacterial genomic modifyed strains following the manufacturers instruction.
Electroporation was performed with MicroPulser Electroporator from Biorad. PCR amplification was achived by Phusion High-Fidelity PCR master mix (Thermo Fisher).

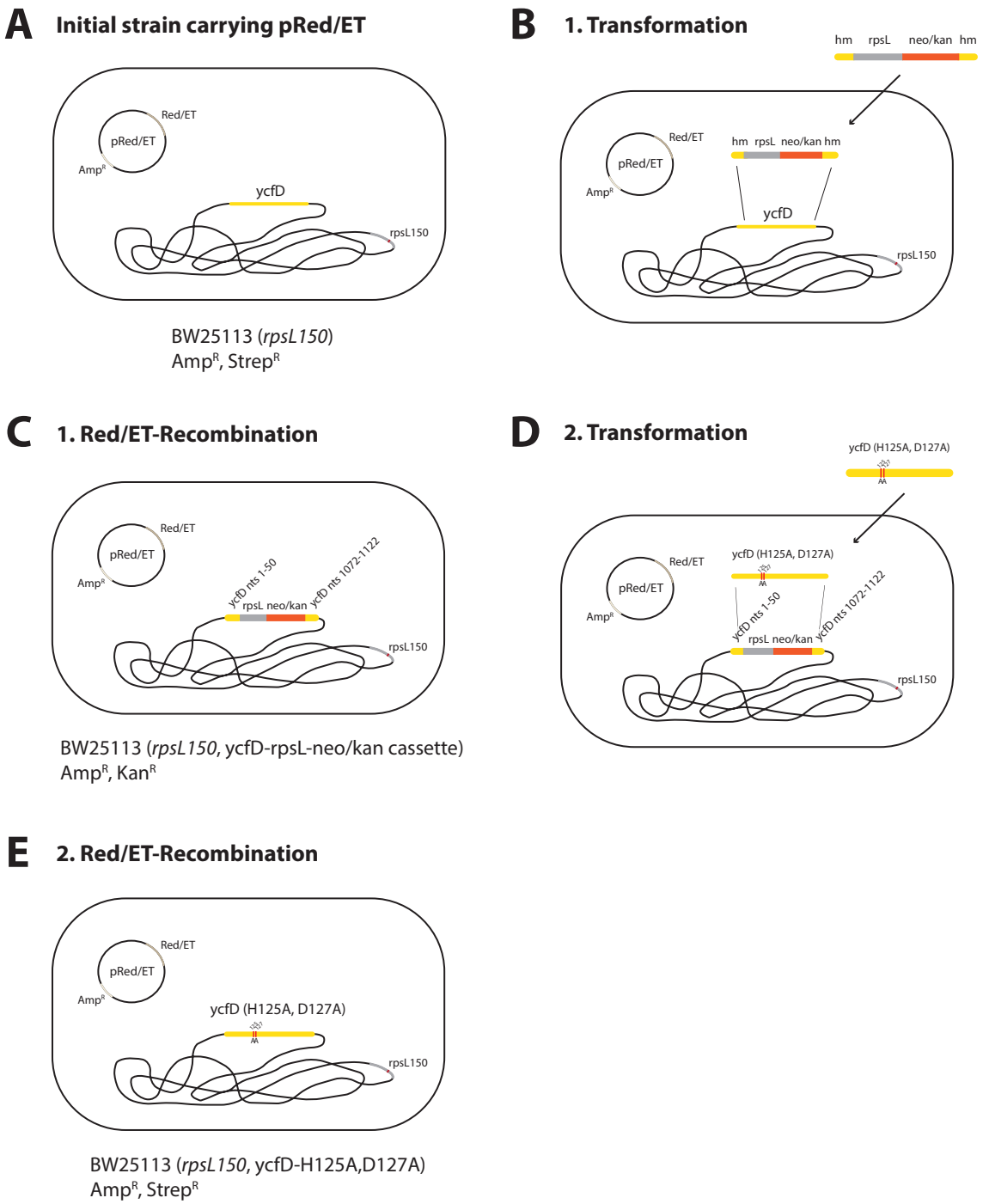

Figure 67: Principle of introducing ycfD mutations into the bacterial chromosome using Red/ET mediated recombination and rpsL-based counter-selection (Gene Bridges "Counter-Selection BAC Modification Kit"); A) Engineered streptomycin-resistant strain is transformed with the pRed/ET plamid carrying a ampicillin (amp^R) resistance, B) Bacteria are transformed with a linear, PCR-amplified rpsL-neo/kan cassette flanked by 50 nucleotides (nts) homology arms, in this case first and last 50 nts of ycfD, C) Activation of Red/ET recombination leads to insertion of the cassette replacing ycfD gene leading to a neomycin(neo^R) and kanamycin (kan^R) resistance, the additional copy of the dominant wild type rpsL gene leads to strep sensitivity, D) With a second transformation, PCR amplified linear DNA of ycfD with the desired mutation, in this case the iron binding sites H125 and D127 are mutated to Ala, is inserted into the bacteria, E) Red/ET directed recombination exchanges the rpsL-neo/kan counter selection cassette with mutated ycfD resulting in BW25113 (rpsL150, ycfD AxA) strain, which is resistant to streptomycin (strep^R).

5.2 Human Cell culture

5.2.1 General culturing conditions

BHK, HeLa, HEK293 and HEK293T cells were cultured in DMEM (Dulbecco's modified Eagle's medium) supplemented with 10% FBS, penicillin (100 units/ml) and streptomycin (100 µg/ml) at 37 °C with 5% CO_2.
HeLa-Cell Cycle Chromobody®-TagRFP were cultured additionally with 50 µg/ml Gentamycin.

5.2.2 Cell treatment methods

Hypoxic culture growth was performed in an Invivo 300 Hypoxic Workstation (Baker Ruskinn) at 37 °C, attached to the Ruskinn gas mixer module Q. Conditions of 0.1 % oxygen and 5 % CO_2 were used.

For stress inductions, cells were incubated with 1 mM sodium arsenite added directly to the medium for 1 h or as indicated.

5.2.3 Transfection

Cells were transfected with expression plasmids using Lipofectamine® 2000 according to the manufacturer´s instructions or PEI pH 7. Cell medium was changed 3 h post-transfection.
Transfection reagent PEI pH 7 was prepared as described in Ehrhardt et al[162].
Amounts used for both transfection reagents are listed in Table 9.

Flask size	Transfection mix for Lipofectamine® 2000	Transfection mix for PEI pH 7
12well	1 µg DNA + 50 µl DMEM; 2µl Lipofectamine® 2000 + 50 µl DMEM	
6well	2.5 µg DNA + 62.5 µl DMEM; 2.5 µl Lipofectamine® 2000 + 62.5 µl DMEM	2.5 µg DNA + 5 µl PEI pH 7 + 50 µl DMEM
T25	10 µg DNA + 250 µl DMEM; 10µl Lipofectamine® 2000 + 250 µl DMEM	10 µg DNA + 20µl PEI pH 7 + 200 µl DMEM
T75		20 µg DNA + 40µl PEI pH7 + 400 µl DMEM
p100	22 µg DNA + 750 µl DMEM; 22 µl Lipofectamine® 2000 + 250 µl DMEM	22 µg DNA + 44 µl PEI pH 7 + 440 µl DMEM

Table 9: Amounts of transfection reagents used for transfections

5.2.4 Harvesting of cells

Cells were harvested by scraping in an appropiate amount of 1x PBS or by trypsinizing and following centrifugation at 800 g for 5 min at room temperature.

5.2.5 Cell lysis

Harvested cells were lysed in Lysis buffer (see 4.12.1 or cell extraction buffer (Life technologies). Both buffers were supplemented with 10 µl/ml protease inhibitor and each 10

µl/ml phosphatase inhibitor cocktail 2 and 3. Lysis was carried out for 10-30 min rocking at 8 °C. Supernatant achieved from centrifugation at 14000 g for 10 min at 4 °C was used for further experiments.

5.2.6 Growth assay

Two methods were used to monitor cell proliferation.
1) 0.1x 10^6 cells were seeded in the appropriate amount of 6 well plates. To monitor growth, every day cells from one 6 well plate were trypsinated and counted by the cell viability analyzer Vi-CELL XR 2.04. Each cell line was seeded and counted in triplicates.
2) On day 0 (T0), 10^3 cells were seeded into 96 well plates in 6 replicates. To monitor growth, media was removed and AquaBluer™ diluted 1:100 in growth medium was added to each well and incubated at 37 °C, 5 % CO_2 for 5 h. Fluorecence intensity at 540 nm extinction and 590 nm emmission was read in the 2104 EnVision® Multilabel Plate Reader (Perkin Elmer).

5.2.7 Synchronization

For synchronization, cells at 30-50 % confluency were grown with growth medium containing 2 mM thymidine. After 17/18 h incubation at 37 °C and 5 % CO_2, cells were released from the first thymidine block by removing the thymidine-containing medium and rinsing the cells two times with growth medium. Subsequently, cells were trypsinized and seeded to appropriate cell culture dishes.
6 h after seeding, cells could be transfected using the appropriate amount of DNA and Lipofectamine® 2000. The second thymidine block was applied after 10/9 h by addition of 2 mM thymidine to the growth medium. In case of transfection, cell growth medium was exchanged with medium containing 2 mM thymidine. Release of the second block after 15/17 h was initiated as mentioned above.

Progression through cell cycle was monitored by flow cytomerty. For living cells, 5 µg/ml Hoechst33342 DNA stain (Gift from W. Beisker, HelmholtzZentrum München) was added to the cells in growth medium and incubated for at least 30 min. For longer storage, cells were fixed in 70 % EtOH at 4 °C for at least 30 min. After two times washing with 1x PBS, DNA was stained with NUCLEAR-ID® Red DNA stain diluted 1:500 in 1x PBS.
Subsequently, cells were analyzed using flow cytometry. At least 1x10^4 cells were analyzed using LRSII flow cytometer (BD Biosiences), data was collected using FACSDiva software (BD Biosciences) and analyzed using FlowJo software.

Samples for Western blot were harvested by trypsination (see 5.2.4). Protein levels were analyzed directly by SDS PAGE with subsequent Western blot or after immunoprecipitation of OGFOD1 and/or CCNA2.

5.2.8 Immunofluorecence

5.2.8.1 Preparation of samples

HeLa cells grown to 50–70 % confluence on 18 mm diameter glass coverslips were transfected with expression constructs using Lipofectamin® 2000 according to the manufacturer's instructions. 24 h post-transfection, cells were fixed with 4%

paraformaldehyde for 10 min at RT. If no antibody staining was needed, the cells slides were directly stained with 1 µg/ml DAPI, mounted in Vectashield and sealed with nail polish.
For immunostaining with antibodies, the cells were permeabilized with 1 % Triton X-100 in PBS. After blocking in blocking solution for 1 h, primary antibodies were diluted in blocking solution and applied to the slides for 1 hour at RT. Subsequently, same procedure was used with the secondary antibodies, incubation was carried out in the dark. Between and after antibody incubations, slides were washed three times for 10 min with wash solution. After staining with 1 µg/ml DAPI, slides were mounted in Vectashield and sealed with nail polish. Buffers and solutions are listed in 4.12.5.
Slides were stored at 4 °C in the dark and analyzed by fluorescence microscopy.

5.2.8.2 Imaging using confocal microscopy

Light optical sections were acquired with a Leica TCS SP5-2 confocal laser-scanning microscope (Böttger Lab, Biocenter LMU). Fluorochromes were visualised with the 405 laser with an excitation wavelength of 405nm and emission filters 413 to 443nm for DAPI. The argon laser with excitation wavelength of 488nm and emission filters 496 to 537nm was used for GFP. To obtain an improved signal-to-noise ratio, each section image was averaged from three successive scans.

5.2.8.3 Imaging using fluorescence microscopy

Classic fluorescence microscopy was carried out using Carl Zeiss LSM 510 META (Dr. Annette Feuchtinger, Andreas Voss, Abteilung Analytische Pathologie, Helmholtz Zentrum Neuherberg).

5.3 Immunoprecipitation assays (IP)

5.3.1 Immunoprecipitation with overexpressed proteins

All steps of the procedure were carried out on ice. Transfected cells were harvested and lysed in lysis buffer (see 4.12.1). Lysed cells were centrifuged at 14000 g for 10 min at 4 °C and the resulting supernatant diluted with wash buffer 1 (see 4.12.6). For subsequent analysis, around 10 % of the input were spared (Input fraction, „I“). Proteins not bound to beads were saved for subsequent analysis („Flow through fraction“ or „F“). Elution of protein complexes („Beads fraction“, „B“ or „Elution fraction“, „E“) was achieved dependent on precipitation methode, see following subitems. Samples were analyzed by SDS PAGE and Western blot.

5.3.1.1 GFP IP

GFP immunoprecipitation in mammalian cells was performed using GFP-Trap® following manufacture’s instructions. Protein complexes were eluted from the beads by incubation of beads with 1x Laemmli buffer at 95 °C for 5 min.

For recombinant IP, bacteria were transformed with appropriate plasmids and grown. For GFP-immunoprecipitation, in total 2500 µg crude bacterial lysate was mixed and incubated for 2h before GFP-IP was performed following GFP-Trap® instructions.

5.3.1.2 Flag IP

For IP of Flag-tagged protein, ANTI-FLAG® M2 Affinity Gel was used following the instructions. Elution of protein complexes was achived by incubation of the beads with 100 µg/ml 3X FLAG® Peptide for 30 min at 4 °C.

5.3.1.3 GST IP

For recombinant IP, bacteria were transformed with appropriate plasmids and grown. For GST-immunoprecipitation, in total 2500 µg crude bacterial lysate was mixed and incubated for 2h before GST-IP was performed using Glutathione Sepharose 4B (GE Healthcare) following manufacture's instructions.

5.3.2 Immunoprecipitation with endogenous proteins

1.5x 10^8 cells were harvested and lysed (5.2.4 and 5.2.5). To capture endogenous proteins with the appropriate antibody, 3 µg antibody was coupled to Protein G Sepharose 4 Fast Flow (GE Healthcare) for 2 h. For immunoprecipitations after synchronization, 1.5 µg antibody was used for 8x 10^6 cells. Subsequently, immunoprecipitation was carried out following manufacture's instructions. Protein complexes were eluted by incubation of the beads with 1x Laemmli buffer at 95 °C for 5 min. Samples were analyzed by SDS PAGE and Western blot.

5.4 Analysis of samples by LC-MS/MS

5.4.1 Analysis of IP samples

IP samples were analyzed by label-free LC–MS/MS (Juliane Merl-Pham, Stephanie Hauck, HelmholtzZentrum München).

5.4.2 Analysis of isolated ribosomes

Isolated ribosomal fractions (see 5.10.2) were analyzed by label-free LC MS/MS (Axel Imhof laboratory, Ignasi Forné, Biomedical Center Munich, LMU).

5.5 F2H® Assay (ChromoTek)

Fluorescence-2-hydrid assay (Chromotek) experiments were carried out following the manufacture's protocol. Differing from the protocol, 1.2 µg GFP-bait and 1.2 µg mCherry-prey DNA with 1.6 µg platform reagent were co-transfected using Lipofectime 2000. Cells were fixed with 4 % paraformaldehyde (10 min at room temperature) and stained with 1 µg/ml DAPI. Slides were mounted in Vectashield, sealed with nail polish, and stored at 4 °C in the dark until analysis by fluorescence microscopy.

5.6 Molecular cloning

5.6.1 Classic cloning

For classic cloning, the insert was amplified by PCR using primer which introduced the required restriction sites. The PCR product was seperated by size in gel electrophoresis. PCR products or DNA were mixed with 6x DNA gel loading dye and loaded for analysis on a 1 % agarose gel in 1x TAE buffer (see 4.12.2) supplemented with 3 µl HDGreen (Intas) for 50 ml of gel. Electrophoresis was carried out at 90 V. Gel elution of the corresponding DNA band was carried out with the Macherey-Nagel „NucleoSpin Gel and PCR Clean-up“ kit. PCR product and 1 µg of the cloning vector were digested. Afterwards, the vector was dephosphorylated using Calf intestine alkine phosphatase (New England Biolabs). Ligation of around 50 ng gel-eluted insert and 10 ng vector was carried out with T4 ligase (New England Biolabs) for 10 min-1 h at RT. Ligated product was transformed to heat shock competent TOP10 (see 5.1.1). Positive clones were identified by colony PCR. DNA from positive clones was isolated from bacteria culture using „QIAprep Spin Miniprep kit“ (Qiagen) and verified by sequencing.

5.6.2 Cloning by alignment

For cloning of gRNAs to the Cas9 containing vector, sense and antisense gRNAs were purchased from Eurofins. Aligned gRNAs (in buffer 4.12.7) formed overhangs mimiking BbsI restriction. The vector was digested with BbsI. Subsequent procedure as described in 5.6.1.

5.6.3 Mutagenesis

Mutagenesis was carried out following the manufacture’s instructions (QuikChange Site-directed mutagenesis kit, Agilent).

5.7 Generation of knockout cell using CRISPR/Cas9 system

Based on the protocol of Ran and colleagues[121], knockout cell lines were generated using the genome editing method CRISPR/Cas9.

5.7.1 Generation of knockout constructs

Using the online CRISPR Design tool (http://crispr.mit.edu/), guide RNAs were designed for OGFOD1, NO66 and MINA53 (see Table 7) according to the nature protocol of Ran et al[121].
Guide RNAs (gRNAs) were cloned into the pSpCas9(BB)-2A-Puro (Addgene plasmid ID: PX459; gift from Krappmann Lab, Helmholtz Zentrum München) plasmid as described in 5.6.2.

5.7.2 Transfection

pSpCas9(BB)-2A-Puro plasmids with inserted gRNAs were transfected into Hek293 cells using Lipofectamine 2000. 24 h post transfection, cells carrying the plasmids were selected by 3 µg/ml puromycin for 72 h.

5.7.3 Validation of knockout on genomic level

Isolation of clonal cell lines was achieved by serial dilution into 96 well plates. Single cell clones were allowed to expand and later screened for successful genome editing by PCR amplification of the corresponding DNA loci.
For isolation of genomic DNA, 0.1x 10^6 cells were used. Cell were harvested by trypsination and following centrifugation at 1000 g at room temperature for 4 min. The cell pellet was washed twice with 1x PBS and resuspended in 100 µl Peqlab DirectPCR lysis reagent, 1 µl of proteinase K and incubated over night at 56°C. Inactivation of Proteinase K was achieved by incubation at 95 °C for 30 min. Supernatant after centrifugation at 16000 g at 4 °C for 20 min was transfered to a new tube and 1-2 µl used for PCR.
Primers used for amplification of engineered genomic loci see in 4.7, Table 8. PCR program consisted of a initial denaturation of 5 min of 95 °C, 50 cycles of 95 °C for 30 sec, 57 °C for 30 sec and elongation at 72 °C for 1 min. Additional elongation was allowed after the cycles for 1 min at 72 °C. PCR products were analyzed on a 1 % agarose gel.

5.7.4 Confirmation of knockout on protein level

Validation of knock-out on protein level was achieved by SDS PAGE with subsequent Western Blot analysis and immuno-staining with appropriate antibodies (see 5.9).

5.8 Reconstitution of cells by lentiviral infection

To insert DNA randomly into the genome, cells were infected with lentivirus carrying the construct of interest in the pLVTHM-T2A-CD2 vector (gift from Krappmann Lab, Helmholtz Zentrum München). Lentivirus was produced by transfecting 2x 10^6 Hek293T cells with 1 µg pMD2.G, 1.5 µg pPAX (gift from Krappmann Lab, Helmholtz Zentrum München), and 2 µg pLVTHM-T2A-CD2 with insert using XtremeGene. After 72 h, virus was collected, filtered and target Hek293 cells were infected in the presence of 10 µg/ml polybrene by spin infection for 1.5 h. Following centrifugation, the virus containing medium was removed and cells expanded.
Positive reconsitution was validated by SDS PAGE with subsequent Western Blot analysis and immuno-staining with appropriate antibodies. Additionally, cells were analyzed for CD2-positive cells by flow cytometry using Attune Acoustic Focusing Cytometer (AB, applied biosystems) and FlowJo software.

5.9 SDS PAGE and Western blot

Polyacrylamid gels were casted following manufacture's instructions (Biorad). Buffers are listed in 4.12.3. Samples were mixed with 4x Laemmli buffer and incubated for 5 min at 95 °C. SDS gels were run at 80 V for 20 min, then at 160 V in electrophoresis buffer.
Following SDS PAGE, protein are blotted onto a nitrocellulose membran at 200 mA for 2 h in blot buffer. Ponceau S Solution was used to visualize the protein loading. Membrans were block in 5 % milk powder in TBST for 1 h at RT or O/N in 8 °C.
After blotting proteins on a nitrocellulose membran, the membran was incubated in 5 % milk powder in TBST for at least one hour to reduce unspecific antibody binding.
Immunodetection was carried out by incubation of the membrane with antibodies diluted in 5 % milk powder in TBST. After incubation with the primary antibody and the appropriate

secondary HRP-coupled antibody for 1h at room temperature, protein detection was carried out with chemiluminescent solution ECL western blotting detection reagents.

5.10 Ribosome isolation

5.10.1 Isolation of ribosomes for bacteria

Bacteria were harvested in late log phase of growth by centrifugation for 10 min at 3500 rpm at 4 °C. The pellets were lysed in bacteria cell lysis buffer and frozen immediately with DNaseI in liquid nitrogen and transferred to -80 °C for at least 30 min. Following, the lysates were incubated for 10 min on ice and centrifugated at 13200 rpm for 30 min at 4 °C. Around 4 mg of the supernatant was loaded on top of a 10-40 % (w/v) linear gradient prepared with BioComp PGFip (Piston Gradient Fractionator). The gradient was ultracentrifugated for 3 h, 35000 rpm at 4 °C (SW41 rotor, Beckman Coulter).
Fractions were collected from top to bottom (Gradient Station ip, BioComp) while continuously recording the absorption profile at λ = 254 nm (Econo UV Monitor, BIO-RAD).
Buffers are listed in 4.12.10.1
This experiment was performed in Dr. Daniel Wilson's Laboratory, Gene Center Munich, with the help of Dr. Agata Starosta.

5.10.2 Isolation of ribosomes for LC-MS/MS analysis

1.4x 10^7 cells were lysed in 300 µl freshly prepared lysis buffer. After 30 min lysis by inverting at 4 °C, the lysate was centrifuged at 14.000 rpm for 15 min at 4 °C to remove debris, nuclei and mitochondria. The supernatant was loaded onto 650 µl of sucrose cushion solution and centrifuged for 45 min at 100000 rpm (TLA120.2 rotor, Beckman Coulter). After centrifugation, supernatant was removed immediately. The ribosomal pellet was carefully resuspended in storage buffer on ice to homogeneity. Buffers are listed in 4.12.10.2.
The resulting supernatant are the solved ribosomes and was measured for OD_{260} absorption. 1 unit OD_{260} corresponds to 20 pmol/ml ribosomes. 2 pmol ribosomes were used for LC-MS/MS analysis.

5.10.3 Isolation for ribosome profiles for mammalian cells

6x 10^8 cells were lysed in 600 µl freshly prepared lysis buffer. After 1 h 10 min incubation on ice, the lysate was centrifuged at 12.000 g for 10 min for 4 °C to remove debris. The supernatant was loaded onto 500 µl of 30 % sucrose cushion solution and centrifuged for 16 h at 26000 rpm (TLA120.2 rotor, Beckman Coulter). After centrifugation, supernatant was removed immediately. The ribosomal pellet was carefully resuspended on ice in storage buffer until homogeneity. To remove non-suspended particles, the solution was centrifuged for 1 min at 12000 g at 4 °C. The resulting supernatant contained the solved ribosomes and was measured for A_{260} absorption and frozen in liquid nitrogen.
To analyze the mono- and polysome fractions in the ribosome preparation of different cell lines, 2.6 units OD_{260} were directly loaded onto a 10 - 40 % sucrose gradient. Gradients were generated with BioComp PGFip (Piston Gradient Fractionator) with 10 % and 40 % sucrose buffer. Gradients were centrifuged for 19 h at 16500 rpm at 4 °C (SW40 rotor, Beckman Coulter). Buffers are listed in 4.12.10.3. Procedure is depicted in Figure 68.

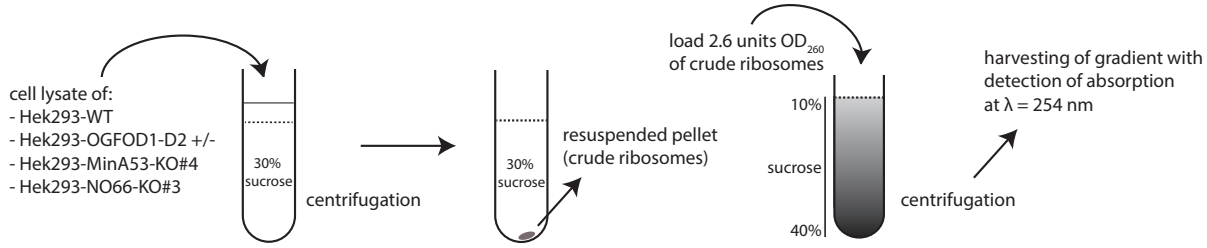

Figure 68: Sucrose gradient A260 absorbance ribosome profiles. Cell lysates were layered onto a 30% sucrose cushion. Crude ribosome pellets achieved from centrifugation were resuspended and loaded onto a 10-40% sucrose gradient. Following ultracentrifugation, the gradients were fractionated from top to bottom while continuously recording the absorption profile at λ = 254 nm.

Fractions were collected from top to bottom (Gradient Station ip, BioComp) while continuously recording the absorption profile at λ = 254 nm (Econo UV Monitor, BIO-RAD).
The protocol was adapted by Sarah Matheisl from Khatter and colleagues [163]. This experiment was performed in Prof. Dr. Roland Beckmanns Laboratory, Gene Center Munich, LMU, with the help of Dr. Sarah Matheisl.

5.11 Hydra culture

Hydra experiments were carried out with the help of Jasmin Moneer in the Böttger Lab, Biocenter LMU. *Hydra vulgaris* strain Basel was held in mass culture in hydra medium at a constant temperature of 18 °C and were fed regularly with freshly hatched *Artemia nauplii*.

5.11.1 Transfection of Hydra cells

2.4 mg Gold particles (1.0 μm diameter, BioRad) were coated with 10 μg plasmid DNA according to instructions of manufacturer. DNA was introduced into the hydra cells with a Helios gene gun system (BioRad) as described before [128].

5.11.2 Fixation and mounting of Hydra

Animals were relaxed in 2 % urethane in hydra medium and fixed with 4 % paraformaldehyde at room temperature for 1 hour. After three washes with PBS, animals were counterstained with 1 μg/ml DAPI and mounted on slides in Vectashield.

5.12 Phylogenetic analyses

5.12.1 Ensemble database searches

Sequences were obtained in collaboration with Andreas Lengeling (The Roslin Institute, University of Edinburgh). Orthologes of NO66 (RIOX1) and MINA53 (RIOX2) genes were identified using Ensembl (http://www.ensembl.org/info/about/species.html) and EnsemblMetazoa (http://metazoa.ensembl.org/species.html) portals by employing pblast searches. The genome of each selected species was queried with the human or *Hydra vulgaris* RIOX1/Riox1 (Q9H6W3 and XP_002157896.3) and ROX2/Riox2 (Q8IUF8 and XP_002167270) protein reference sequences. For phylogenetic analyses of orthologues

proteins only sequences were included in which both, the human and hydra pblast queries, matched to a single locus of the selected species and the identified protein displayed the characteristic domain architecture of Riox1 and Riox2 proteins. Species were selected throughout the animal kingdom to represent main taxonomic classes, where available with at least to species per class depending on genome sequence coverage and quality of gene structure annotations. *Hydra vulgaris* protein sequences and gene annotations for Riox1 and Riox2 were obtained from https://metazome.jgi.doe.gov/pz/portal.html.

5.12.2 Multiple-sequence alignments and construction of phylogenetic trees

Dr. Evi Lengeling-Wollscheid (The Roslin Institute, University of Edinburgh) performed the sequence alignments and generated the phylogenetic tree. Therefore, JmjC domain sequences of MINA53 and NO66 from 49 species and of YcfD (ecycfD), the ROX protein from *Escherichia coli* were subjected to a maximum likelihood analysis using the online phylogenetic tool W-IQ-TREE (Version 1.5.4 at http://iqtree.cibiv.univie.ac.at, Trifinopoulos et al., NAR 2016; PMID: 27084950). In the IQ-Tree webserver the 'Substitution model' and the default 'Auto' settings were selected to determine the best-fit substitution model followed by tree construction. Within the 'Branch Support Analysis' the default settings of an ultrafast bootstrap analysis with 1000 replicates was used, with maximum number of iterations set at 1000 and a minimum correlation coefficient of 0.99 and for the 'Single branch tests' the SH-aLRT branch test with 1000 replicates was selected[164].

6 Appendix

6.1 Additional data

6.1.1 CCNA2 and OGFOD1 interaction

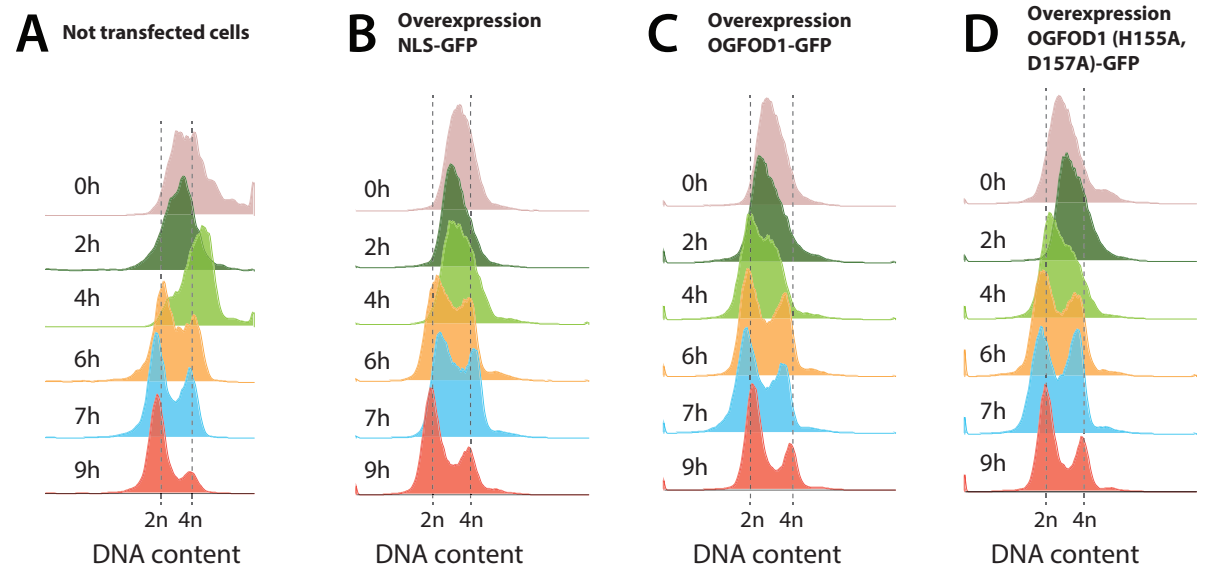

Sample Name	Subset Name	Count
Specimen 0h.fcs	GFP-negative	2895
Specimen 2h.fcs	GFP-negative	2580
Specimen 4h.fcs	GFP-negative	13352
Specimen 6h.fcs	GFP-negative	12851
Specimen 7h.fcs	GFP-negative	22288
Specimen 9h.fcs	GFP-negative	15874

Sample Name	Subset Name	Count
Specimen 0h nls.fcs	GFP-positive	27857
Specimen 2h nls.fcs	GFP-positive	15670
Specimen 4h nls.fcs	GFP-positive	19868
Specimen 6h nls.fcs	GFP-positive	35312
Specimen 7h nls.fcs	GFP-positive	37452
Specimen 9h nls.fcs	GFP-positive	70167

Sample Name	Subset Name	Count
Specimen 0h O1.fcs	GFP-positive	41771
Specimen 2h o1.fcs	GFP-positive	29504
Specimen 4h o1.fcs	GFP-positive	41997
Specimen 6h o1.fcs	GFP-positive	41716
Specimen 7h o1.fcs	GFP-positive	54308
Specimen 9h o1.fcs	GFP-positive	62084

Sample Name	Subset Name	Count
Specimen 0h O1axa.fcs	GFP-positive	48525
Specimen 2h O1axa.fcs	GFP-positive	31005
Specimen 4h o1axa.fcs	GFP-positive	50568
Specimen 6h o1 axa.fcs	GFP-positive	27852
Specimen 7h o1axa.fcs	GFP-positive	53982
Specimen 9h o1axa.fcs	GFP-positive	50248

Figure 69: Influence of GFP-tagged OGFOD1 on cell cycle progression; Hek293T cells were synchronized with a double thymidine block. Between the first and second block, cells were transfected with indicated GFP-tagged proteins using Lipofectamine. Samples were taken after indicated hours after release. Cell cycle profiles were obtained by flow cytometry after NUCLEAR-ID® Red DNA stain (ENZO life sicence, ENZ-52406) staining of DNA. In A) untransfected cells B)-D) overexpression of GFP-tagged proteins as indicated, cell numbers are listed under the graphs.

Accession	Unique peptides	Confidence score	Name	Description	ratio CCNA2-IP/control
P67870	2	54	CSNK2B	Casein kinase II subunit beta	Infinity
Q9HD26	2	55	GOPC	Golgi-associated PDZ and coiled-coil motif-containing protein	Infinity
Q12834	2	67	CDC20	Cell division cycle protein 20 homolog	Infinity
P33552	3	82	CKS2	Cyclin-dependent kinases regulatory subunit 2	1104.3
P01857	2	32	IGHG1	Ig gamma-1 chain C region	407.7
Q13309	6	199	SKP2	S-phase kinase-associated protein 2	168.7
P20248	**14**	**649**	**CCNA2**	**Cyclin-A2**	**106.2**
P61024	3	101	CKS1B	Cyclin-dependent kinases regulatory subunit 1	76.7
A5YKK6	6	159	CNOT1	CCR4-NOT transcription complex subunit 1	72.8
Q15369	2	32	TCEB1	Transcription elongation factor B polypeptide 1	63.7
O60343	5	159	TBC1D4	TBC1 domain family member 4	58.5
P61962	2	60	DCAF7	DDB1- and CUL4-associated factor 7	42.7
P28749	12	440	RBL1	Retinoblastoma-like protein 1	37.8
P63208	5	168	SKP1	S-phase kinase-associated protein 1	36.9
P30291	9	304	WEE1	Wee1-like protein kinase	35.1
Q9H211	3	94	CDT1	DNA replication factor Cdt1	33.7
Q9BY12	6	174	SCAPER	S phase cyclin A-associated protein in the endoplasmic reticulum	26.3
P24941	9	363	CDK2	Cyclin-dependent kinase 2	26.0
Q92793	8	254	CREBBP	CREB-binding protein	23.4
P19474	7	211	TRIM21	E3 ubiquitin-protein ligase TRIM21	17.6
O75496	3	86	GMNN	Geminin	15.5
P55209	2	46	NAP1L1	Nucleosome assembly protein 1-like 1	15.2
Q9H0U4	2	89	RAB1B	Ras-related protein Rab-1B	14.6
Q09472	2	79	EP300	Histone acetyltransferase p300	14.4
P46782	3	125	RPS5	40S ribosomal protein S5	13.7
Q6PJG2	5	170	ELMSAN1	ELM2 and SANT domain-containing protein 1	12.7
P06493	7	310	CDK1	Cyclin-dependent kinase 1	10.4
P61254	2	39	RPL26	60S ribosomal protein L26	8.4
Q9Y3Z3	13	423	SAMHD1	Deoxynucleoside triphosphate triphosphohydrolase SAMHD1	8.4
Q7Z2Z1	7	195	TICRR	Treslin	8.2
Q04917	2	70	YWHAH	14-3-3 protein eta	7.6
P13674	2	47	P4HA1	Prolyl 4-hydroxylase subunit alpha-1	5.8
P12268	4	130	IMPDH2	Inosine-5'-monophosphate dehydrogenase 2	5.7
Q4VCS5	7	251	AMOT	Angiomotin	5.6
Q15459	2	55	SF3A1	Splicing factor 3A subunit 1	4.7
Q14974	3	108	KPNB1	Importin subunit beta-1	4.4
P15927	2	72	RPA2	Replication protein A 32 kDa subunit	4.2
P31946	2	47	YWHAB	14-3-3 protein beta/alpha	4.0
Q9UJZ1	2	65	STOML2	Stomatin-like protein 2, mitochondrial	3.9
P05141	2	40	SLC25A5	ADP/ATP translocase 2	3.9
Q71U36	10	408	TUBA1A	Tubulin alpha-1A chain	3.7
P27694	6	154	RPA1	Replication protein A 70 kDa DNA-binding subunit	3.6
P48735	2	53	IDH2	Isocitrate dehydrogenase [NADP], mitochondrial	3.6
P31939	2	57	ATIC	Bifunctional purine biosynthesis protein PURH	3.5
P07437	2	459	TUBB	Tubulin beta chain	3.5
P78527	10	266	PRKDC	DNA-dependent protein kinase catalytic subunit	3.4
P61247	2	46	RPS3A	40S ribosomal protein S3a	3.4
P13489	2	87	RNH1	Ribonuclease inhibitor	3.2
P62081	2	36	RPS7	40S ribosomal protein S7	3.1
P55060	2	86	CSE1L	Exportin-2	2.9
Q04837	3	74	SSBP1	Single-stranded DNA-binding protein, mitochondrial	2.6
P62258	9	374	YWHAE	14-3-3 protein epsilon	2.5
P60174	7	203	TPI1	Triosephosphate isomerase	2.5
O00571	3	82	DDX3X	ATP-dependent RNA helicase DDX3X	2.5
P31930	2	62	UQCRC1	Cytochrome b-c1 complex subunit 1, mitochondrial	2.3
P07954	2	56	FH	Fumarate hydratase, mitochondrial	2.2
Q13162	2	75	PRDX4	Peroxiredoxin-4	2.2
P63104	6	194	YWHAZ	14-3-3 protein zeta/delta	2.1
Q92499	2	44	DDX1	ATP-dependent RNA helicase DDX1	2.1
P60660	3	64	MYL6	Myosin light polypeptide 6	2.1
Q16576	2	79	RBBP7	Histone-binding protein RBBP7	2.0

Figure 70: Proteins identified in CCNA2 IP sample using LC-MS/MS with enrichment higher than two fold.

Accession	Unique peptides	Confidence score	Name	Description	Ogfod1 WT/ control	Ogfod1 MUT/ control
P55795	2	353	HNRNPH2	Heterogeneous nuclear ribonucleoprotein H2	77.98	88.12
Q7L014	6	189	DDX46	Probable ATP-dependent RNA helicase DDX46	68.95	2.76
Q9BYN8	2	64	MRPS26	28S ribosomal protein S26, mitochondrial	47.59	63.52
O00299	2	49	CLIC1	Chloride intracellular channel protein 1	46.40	67.65
P49591	2	55	SARS	Serine--tRNA ligase, cytoplasmic	31.58	38.92
Q15637	2	41	SF1	Splicing factor 1	30.96	57.78
P20674	2	59	COX5A	Cytochrome c oxidase subunit 5A, mitochondrial	30.67	42.04
Q86VP6	3	61	CAND1	Cullin-associated NEDD8-dissociated protein 1	22.18	18.08
P30520	2	58	ADSS	Adenylosuccinate synthetase isozyme 2	18.87	25.95
Q8N543	9	224	OGFOD1	Prolyl 3-hydroxylase OGFOD1	18.10	16.01
P49755	2	72	TMED10	Transmembrane emp24 domain-containing protein 10	16.82	20.95
Q15181	3	86	PPA1	Inorganic pyrophosphatase	14.69	19.46
Q99497	3	75	PARK7	Protein deglycase DJ-1	12.45	15.62
P30048	2	68	PRDX3	Thioredoxin-dependent peroxide reductase, mitochondrial	11.73	10.62
P62937	3	90	PPIA	Peptidyl-prolyl cis-trans isomerase A	11.18	12.62
P62273	2	56	RPS29	40S ribosomal protein S29	11.02	12.37
P35080	2	60	PFN2	Profilin-2	10.35	18.36
P15927	2	46	RPA2	Replication protein A 32 kDa subunit	10.05	9.10
P27797	8	222	CALR	Calreticulin	10.00	11.56
O43663	2	50	PRC1	Protein regulator of cytokinesis 1	9.53	7.95
O95983	2	53	MBD3	Methyl-CpG-binding domain protein 3	8.84	7.32
P51858	2	52	HDGF	Hepatoma-derived growth factor	8.71	10.18
P60174	8	273	TPI1	Triosephosphate isomerase	8.71	10.28
P67775	3	100	PPP2CA	Serine/threonine-protein phosphatase 2A catalytic subunit alpha isoform	8.70	9.20
P54819	2	43	AK2	Adenylate kinase 2, mitochondrial	8.69	11.52
P22234	5	126	PAICS	Multifunctional protein ADE2	8.66	8.65
P22695	2	42	UQCRC2	Cytochrome b-c1 complex subunit 2, mitochondrial	8.27	9.23
P61204	4	119	ARF3	ADP-ribosylation factor 3	8.19	9.98
P33316	3	89	DUT	Deoxyuridine 5'-triphosphate nucleotidohydrolase, mitochondrial	8.18	9.97
P19623	2	39	SRM	Spermidine synthase	8.16	9.07
P62736	2	329	ACTA2	Actin, aortic smooth muscle	7.94	6.44
O15347	2	73	HMGB3	High mobility group protein B3	7.60	8.29
P52565	2	44	ARHGDIA	Rho GDP-dissociation inhibitor 1	7.25	7.86
O14929	4	127	HAT1	Histone acetyltransferase type B catalytic subunit	7.16	8.84
Q92688	2	71	ANP32B	Acidic leucine-rich nuclear phosphoprotein 32 family member B	7.07	7.46
O15355	2	44	PPM1G	Protein phosphatase 1G	6.35	6.91
P13797	6	202	PLS3	Plastin-3	6.10	6.92
P00505	2	68	GOT2	Aspartate aminotransferase, mitochondrial	6.06	7.30
P51148	2	62	RAB5C	Ras-related protein Rab-5C	6.06	5.85
O76003	2	45	GLRX3	Glutaredoxin-3	6.03	7.34
P30086	2	65	PEBP1	Phosphatidylethanolamine-binding protein 1	6.03	7.25
P07737	5	144	PFN1	Profilin-1	5.53	6.82
Q9NQT5	2	56	EXOSC3	Exosome complex component RRP40	5.52	6.11
P13667	9	277	PDIA4	Protein disulfide-isomerase A4	5.43	6.61
Q92973	2	50	TNPO1	Transportin-1	5.40	11.07
Q52LJ0	2	93	FAM98B	Protein FAM98B	5.32	7.23
Q8WUM4	3	97	PDCD6IP	Programmed cell death 6-interacting protein	5.24	6.16
Q16630	4	83	CPSF6	Cleavage and polyadenylation specificity factor subunit 6	5.19	6.02
P20618	2	57	PSMB1	Proteasome subunit beta type-1	5.03	5.76
Q15185	3	82	PTGES3	Prostaglandin E synthase 3	5.03	5.54
O14980	4	119	XPO1	Exportin-1	4.86	4.93
P00918	2	39	CA2	Carbonic anhydrase 2	4.84	5.45
P27694	3	95	RPA1	Replication protein A 70 kDa DNA-binding subunit	4.74	3.72
Q9BRJ2	2	36	MRPL45	39S ribosomal protein L45, mitochondrial	4.56	5.42
P13693	2	70	TPT1	Translationally-controlled tumor protein	4.55	4.91
Q9UBS4	3	92	DNAJB11	DnaJ homolog subfamily B member 11	4.54	6.26
P31150	2	43	GDI1	Rab GDP dissociation inhibitor alpha	4.53	5.06
Q9NY27	2	57	PPP4R2	Serine/threonine-protein phosphatase 4 regulatory subunit 2	4.53	5.74
Q9UNZ2	2	41	NSFL1C	NSFL1 cofactor p47	4.49	5.39
Q13405	2	67	MRPL49	39S ribosomal protein L49, mitochondrial	4.49	4.56
O95684	2	44	FGFR1OP	FGFR1 oncogene partner	4.46	5.00
P24666	3	68	ACP1	Low molecular weight phosphotyrosine protein phosphatase	4.45	5.05
P15531	4	87	NME1	Nucleoside diphosphate kinase A	4.41	4.84
O14737	2	73	PDCD5	Programmed cell death protein 5	4.39	4.34
Q9Y5L4	2	63	TIMM13	Mitochondrial import inner membrane translocase subunit Tim13	4.39	5.01
P40925	2	38	MDH1	Malate dehydrogenase, cytoplasmic	4.34	4.05
P55209	6	227	NAP1L1	Nucleosome assembly protein 1-like 1	4.26	4.32
P07237	4	131	P4HB	Protein disulfide-isomerase	4.17	5.00
Q15365	3	180	PCBP1	Poly(rC)-binding protein 1	4.13	4.02
Q9Y2L1	2	38	DIS3	Exosome complex exonuclease RRP44	4.10	4.28
				...		
P63208	4	121	SKP1	S-phase kinase-associated protein 1	0.50	0.42
Q9Y4P3	2	58	TBL2	Transducin beta-like protein 2	0.50	0.46
Q96HS1	9	257	PGAM5	Serine/threonine-protein phosphatase PGAM5, mitochondrial	0.50	0.47
Q15208	12	418	STK38	Serine/threonine-protein kinase 38	0.49	0.49
Q9Y2W1	25	861	THRAP3	Thyroid hormone receptor-associated protein 3	0.48	0.55
O14744	26	868	PRMT5	Protein arginine N-methyltransferase 5	0.47	0.46
P62314	3	74	SNRPD1	Small nuclear ribonucleoprotein Sm D1	0.47	0.48

Figure 71: Selection of proteins with enrichment higher than 4 or lower than 0.5 identified in Flag-CCNA2 IP, part I.

Q16875	12	439	PFKFB3	6-phosphofructo-2-kinase/fructose-2,6-bisphosphatase 3	0.46	0.47
Q8TDN6	2	48	BRIX1	Ribosome biogenesis protein BRX1 homolog	0.45	0.48
Q9Y3Z3	24	778	SAMHD1	Deoxynucleoside triphosphate triphosphohydrolase SAMHD1	0.45	0.38
P35527	43	1377	KRT9	Keratin, type I cytoskeletal 9	0.45	0.29
Q9BRP8	3	95	PYM1	Partner of Y14 and mago	0.44	0.42
P62857	3	99	RPS28	40S ribosomal protein S28	0.44	0.35
P16989	8	366	YBX3	Y-box-binding protein 3	0.44	0.55
P98179	2	60	RBM3	RNA-binding protein 3	0.44	0.44
Q9H211	5	149	CDT1	DNA replication factor Cdt1	0.43	0.43
Q9UPP1	8	195	PHF8	Histone lysine demethylase PHF8	0.42	0.35
P24941	7	291	CDK2	Cyclin-dependent kinase 2	0.42	0.34
P67809	9	472	YBX1	Nuclease-sensitive element-binding protein 1	0.41	0.47
P04264	31	1183	KRT1	Keratin, type II cytoskeletal 1	0.40	0.31
Q14681	7	265	KCTD2	BTB/POZ domain-containing protein KCTD2	0.39	0.43
P35908	21	934	KRT2	Keratin, type II cytoskeletal 2 epidermal	0.38	0.29
P13645	20	876	KRT10	Keratin, type I cytoskeletal 10	0.37	0.32
Q9NXV2	7	323	KCTD5	BTB/POZ domain-containing protein KCTD5	0.36	0.41
P23588	12	431	EIF4B	Eukaryotic translation initiation factor 4B	0.36	0.43
Q7RTV0	2	86	PHF5A	PHD finger-like domain-containing protein 5A	0.36	0.39
P02768	8	221	ALB	Serum albumin	0.35	0.29
P02647	2	70	APOA1	Apolipoprotein A-I	0.34	0.27
P63220	5	169	RPS21	40S ribosomal protein S21	0.34	0.31
Q02413	4	121	DSG1	Desmoglein-1	0.33	0.36
P46778	4	69	RPL21	60S ribosomal protein L21	0.32	0.30
P09234	2	44	SNRPC	U1 small nuclear ribonucleoprotein C	0.32	0.18
P05109	3	62	S100A8	Protein S100-A8	0.31	0.37
Q7Z353	2	39	HDX	Highly divergent homeobox	0.31	0.51
Q8N5Z5	10	344	KCTD17	BTB/POZ domain-containing protein KCTD17	0.29	0.33
Q96DR8	2	34	MUCL1	Mucin-like protein 1	0.26	0.27
P07477	3	84	PRSS1	Trypsin-1	0.22	0.20
Q86YZ3	7	325	HRNR	Hornerin	0.22	0.16
P31944	3	87	CASP14	Caspase-14	0.22	0.24
P06702	3	100	S100A9	Protein S100-A9	0.18	0.26
P31025	2	51	LCN1	Lipocalin-1	0.16	0.07
Q9NZT1	2	102	CALML5	Calmodulin-like protein 5	0.14	0.14
P81605	3	96	DCD	Dermcidin	0.14	0.13
P25311	2	50	AZGP1	Zinc-alpha-2-glycoprotein	0.14	0.20
P29508	2	57	SERPINB3	Serpin B3	0.12	0.22
Q6UWP8	2	94	SBSN	Suprabasin	0.08	0.14
Q6N063	2	66	OGFOD2	2-oxoglutarate and iron-dependent oxygenase domain-containing protein 2	0.06	0.04

Figure 72: (Continued list from Figure 71) Selection of proteins with enrichment higher than 4 or lower than 0.5 identified in Flag-CCNA2 IP, part II.

Accession	Unique peptides	Confidence score	Name	Description	Ogfod1 WT/ control	Ogfod1 AxA/ control
P15927	2	46	RPA2	Replication protein A 32 kDa subunit	10.05	9.10
P60174	8	273	TPI1	Triosephosphate isomerase	8.71	10.28
P27694	3	95	RPA1	Replication protein A 70 kDa DNA-binding subunit	4.74	3.72
P55209	6	227	NAP1L1	Nucleosome assembly protein 1-like 1	4.26	4.32
Q9H0U4	2	57	RAB1B	Ras-related protein Rab-1B	3.65	3.34
Q14974	7	184	KPNB1	Importin subunit beta-1	2.79	3.15
P31930	2	68	UQCRC1	Cytochrome b-c1 complex subunit 1, mitochondrial	2.78	2.95
Q04837	2	70	SSBP1	Single-stranded DNA-binding protein, mitochondrial	2.68	2.66
P78527	23	628	PRKDC	DNA-dependent protein kinase catalytic subunit	2.20	2.15
P55060	8	231	CSE1L	Exportin-2	2.14	2.68
P12268	10	309	IMPDH2	Inosine-5'-monophosphate dehydrogenase 2	2.00	1.90
P31946	6	251	YWHAB	14-3-3 protein beta/alpha	1.96	2.20
P07437	2	557	TUBB	Tubulin beta chain	1.75	1.89
P63104	6	278	YWHAZ	14-3-3 protein zeta/delta	1.66	1.90
P62258	10	409	YWHAE	14-3-3 protein epsilon	1.51	1.62
P31939	4	107	ATIC	Bifunctional purine biosynthesis protein PURH	1.49	1.91
P05141	2	134	SLC25A5	ADP/ATP translocase 2	1.19	1.04
Q16576	4	179	RBBP7	Histone-binding protein RBBP7	1.17	1.26
Q71U36	2	289	TUBA1A	Tubulin alpha-1A chain	1.09	1.03
Q92499	14	438	DDX1	ATP-dependent RNA helicase DDX1	0.99	0.97
P67870	3	87	CSNK2B	Casein kinase II subunit beta	0.97	0.98
A5YKK6	4	118	CNOT1	CCR4-NOT transcription complex subunit 1	0.95	0.90
Q15369	2	48	TCEB1	Transcription elongation factor B polypeptide 1	0.93	1.22
P60660	5	143	MYL6	Myosin light polypeptide 6	0.90	0.76
Q13162	2	67	PRDX4	Peroxiredoxin-4	0.86	0.96
P20248	**21**	**784**	**CCNA2**	**Cyclin-A2**	**0.82**	**0.60**
Q15459	9	247	SF3A1	Splicing factor 3A subunit 1	0.81	0.78
P33552	3	88	CKS2	Cyclin-dependent kinases regulatory subunit 2	0.80	0.56
O60343	10	314	TBC1D4	TBC1 domain family member 4	0.77	0.63
P62081	6	132	RPS7	40S ribosomal protein S7	0.75	0.74
P61254	3	220	RPL26	60S ribosomal protein L26	0.74	0.66
O00571	16	552	DDX3X	ATP-dependent RNA helicase DDX3X	0.71	0.64
P61247	14	427	RPS3A	40S ribosomal protein S3a	0.71	0.71
P13489	7	236	RNH1	Ribonuclease inhibitor	0.69	0.68
P06493	19	724	CDK1	Cyclin-dependent kinase 1	0.68	0.52
Q04917	3	121	YWHAH	14-3-3 protein eta	0.68	0.76
P61024	4	116	CKS1B	Cyclin-dependent kinases regulatory subunit 1	0.66	0.60
P46782	6	186	RPS5	40S ribosomal protein S5	0.64	0.58
Q13309	7	212	SKP2	S-phase kinase-associated protein 2	0.64	0.55
Q9BY12	15	475	SCAPER	S phase cyclin A-associated protein in the endoplasmic reticulum	0.64	0.59
Q7Z2Z1	10	340	TICRR	Treslin	0.62	0.60
P28749	16	477	RBL1	Retinoblastoma-like protein 1	0.56	0.55
Q12834	16	599	CDC20	Cell division cycle protein 20 homolog	0.55	0.48
Q92793	4	107	CREBBP	CREB-binding protein	0.54	0.55
O75496	5	104	GMNN	Geminin	0.52	0.44
P63208	4	121	SKP1	S-phase kinase-associated protein 1	0.50	0.42
Q9Y3Z3	24	778	SAMHD1	Deoxynucleoside triphosphate triphosphohydrolase SAMHD1	0.45	0.38
Q9H211	5	149	CDT1	DNA replication factor Cdt1	0.43	0.43
P24941	7	291	CDK2	Cyclin-dependent kinase 2	0.42	0.34

Figure 73: Proteins with altered CCNA2 binding behaviour identified in Flag-CCNA2 IP with additional overexpression of OGFOD1 wild type (WT), OGOFD1 H155A, D157A (MUT), and OGFOD2 Isoform 1 (OGFOD2I1, „control“) using LC-MS/MS.

6.1.2 Ribosomal profiles for knockout cell lines

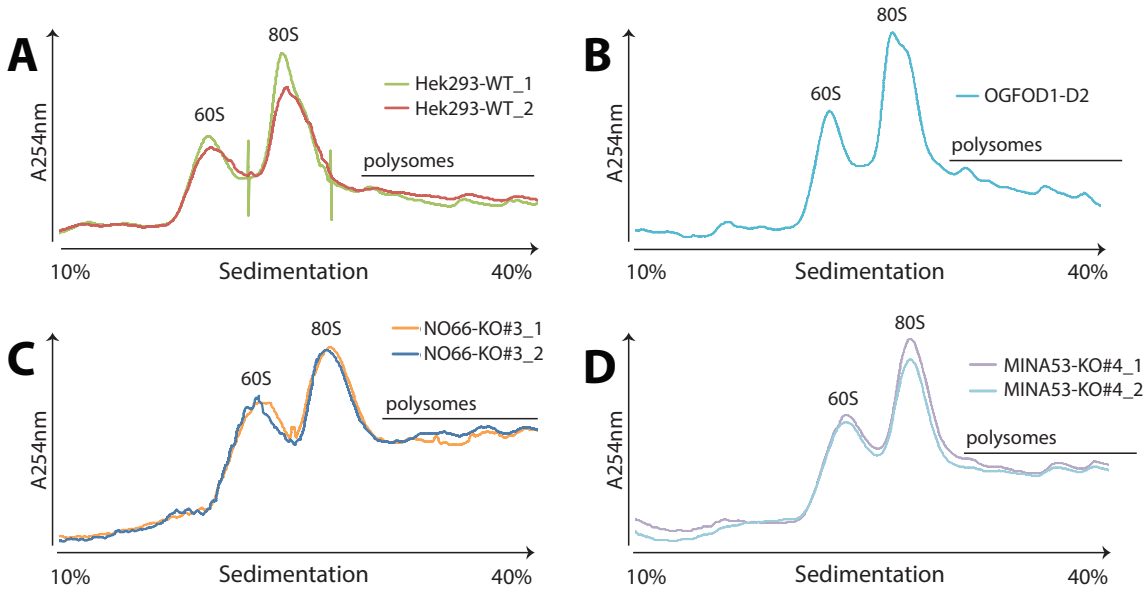

Figure 74: Sucrose gradient A260 absorbance ribosome profiles of Hek293, Hek293-OGFOD1 D2 +/-, Hek293 MINA53-KO#4, and Hek293 NO66-KO#3 ribosomes; two technical replicates of ribosome profiles from A) Hek293 wild type (WT) cells, B) Hek293-OGFOD1-D2 +/- cells, C) Hek293 NO66-KO#3, and D) Hek293 MINA53-KO#4; the positions of different ribosomal species are indicated.

The wild type profiles display a typical polysome profile (Figure 74 A). The first peak detectable with this experimental setting was the 60S peak corresponding to the large (60S) subunit, followed by the monosome peak (80S) and several smaller polysomal peaks.

6.1.3 MINA53 and NO66

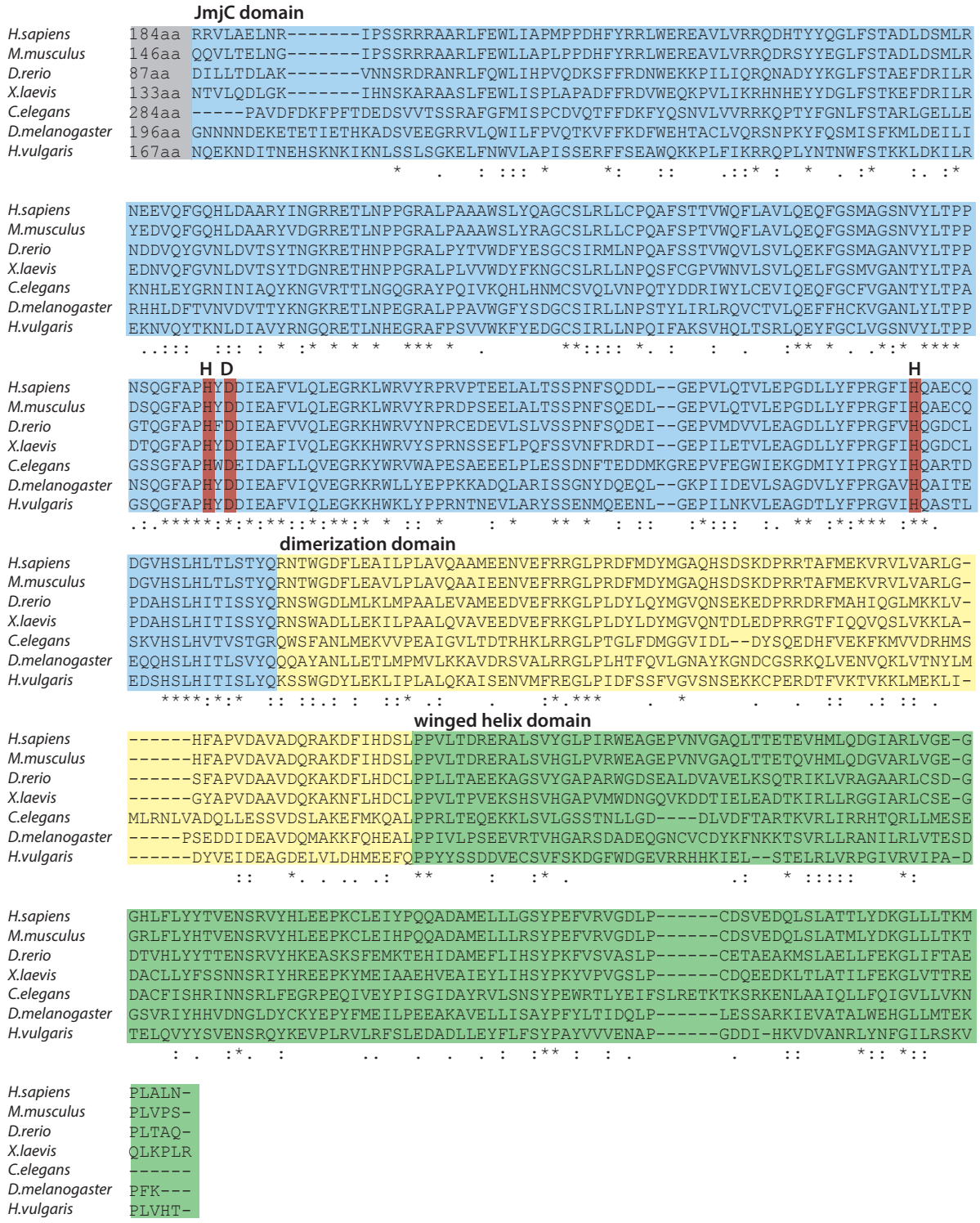

Figure 75: Clustal omega alignment of NO66 protein sequences from *H.sapiens* (Uniprot: Q9H6W3), *M.musculus* (Q9JJF3), *D.rerio* (A3KP59), *X.laevis* (A0A1L8G801), *C.elegans* (O01658), *D.melanogaster* (E2QD64) and *H.vulgaris*. The protein domains JmjC (blue), dimerization (yellow), winged-helix (green) as well as the prospective iron-binding motif HxD…H (red) are indicated based on the human sequence[6]. Lengths of the individual N-terminal extension domains are indicated (grey).

6.2 Manuscripts in progress

„The ribosomal oxygenase Ogfod1 binds Cyclin A2 (CCNA2) directly and alters the CCNA2 interactome"

by Katharina E Bräuer, Olga Swolski, Juliane Merl-Pham, Annette Feuchtinger, Stefanie Hauck, Mukram Mackeen, Alexander Wolf (submitted)

„Phylogenetic and genomic analyses of the ribosomal oxygenases Riox1 (NO66) and Riox2 (MINA53) provide new insights into their evolution“

by Katharina E Bräuer, Kevin Brockers, Jasmin Moneer, Annette Feuchtinger, Evi Wollscheid-Lengeling, Andreas Lengeling, Alexander Wolf (submitted)

6.3 List of abbrevations

A	Alanine
2OG	2-oxoglutarate
aa	Amino acid
AxA	Iron binding motif HxD mutated to Alanine
bp	Base pair
CRISPR	Clustered Regularly Interspaced Short Palindromic Repeats
D	Aspartic acid
DNA	Deoxyribonucleic acid
DSBH	Double-stranded β-helix
FCS	Fetal calf serum
FeII	Iron II
g	Gramm
GFP	Green fluorescent protein
H	Histidine
h	Hour
IP	Immunoprecipitation
KO	Knockout
L	Leucine
LC-MS/MS	Liquid chromatography- Mass spectrometry/Mass spectrometry
M	Mol
MALDI-TOF-MS	Laser desorption/ionization - time of flight mass spectrometry
min	Minute
NLS	Nuclear localization sequence
O/N	Over night
P	Proline
PBS	Phosphate buffered saline
PCR	Polymerase chain reaction
PTM	Post-translational modification
R	Arginine
RNA	Ribonucleic acid
ROX	Ribosomal oxygenase
RPM	Rounds per minute
RT	Room temperature
S	Serine
SDS	Sodium dodecyl sulfate
sec	Second
SEG	Single exon gene
SG	Stress granule
T	Threonine
WT	Wild type

7 References

1 Feng, T. *et al.* Optimal translational termination requires C4 lysyl hydroxylation of eRF1. *Molecular cell* **53**, 645-654, doi:10.1016/j.molcel.2013.12.028 (2014).

2 Kato, M. *et al.* Crystal structure of a novel JmjC-domain-containing protein, TYW5, involved in tRNA modification. *Nucleic acids research* **39**, 1576-1585, doi:10.1093/nar/gkq919 (2011).

3 van den Born, E. *et al.* ALKBH8-mediated formation of a novel diastereomeric pair of wobble nucleosides in mammalian tRNA. *Nat Commun* **2**, 172, doi:10.1038/ncomms1173 (2011).

4 Ge, W. *et al.* Oxygenase-catalyzed ribosome hydroxylation occurs in prokaryotes and humans. *Nature chemical biology* **8**, 960-962, doi:10.1038/nchembio.1093 (2012).

5 Singleton, R. S. *et al.* OGFOD1 catalyzes prolyl hydroxylation of RPS23 and is involved in translation control and stress granule formation. *Proceedings of the National Academy of Sciences of the United States of America* **111**, 4031-4036, doi:10.1073/pnas.1314482111 (2014).

6 Chowdhury, R. *et al.* Ribosomal oxygenases are structurally conserved from prokaryotes to humans. *Nature* **510**, 422-426, doi:10.1038/nature13263 (2014).

7 Alberts, B. *Molecular biology of the cell*. 5th edn, (Garland Science, 2008).

8 Clancy, S., Brown, W. Translation: DNA to mRNA to Protein. *Nature Education* **1**, 101 (2008).

9 Xue, S. & Barna, M. Specialized ribosomes: a new frontier in gene regulation and organismal biology. *Nature reviews. Molecular cell biology* **13**, 355-369, doi:10.1038/nrm3359 (2012).

10 Shi, Z. & Barna, M. Translating the genome in time and space: specialized ribosomes, RNA regulons, and RNA-binding proteins. *Annu Rev Cell Dev Biol* **31**, 31-54, doi:10.1146/annurev-cellbio-100814-125346 (2015).

11 Byrgazov, K., Vesper, O. & Moll, I. Ribosome heterogeneity: another level of complexity in bacterial translation regulation. *Curr Opin Microbiol* **16**, 133-139, doi:10.1016/j.mib.2013.01.009 (2013).

12 Filipovska, A. & Rackham, O. Specialization from synthesis: how ribosome diversity can customize protein function. *FEBS letters* **587**, 1189-1197, doi:10.1016/j.febslet.2013.02.032 (2013).

13 Nesterchuk, M. V., Sergiev, P. V. & Dontsova, O. A. Posttranslational Modifications of Ribosomal Proteins in Escherichia coli. *Acta naturae* **3**, 22-33 (2011).

14 Al-Hadid, Q. *et al.* Histidine methylation of yeast ribosomal protein Rpl3p is required for proper 60S subunit assembly. *Molecular and cellular biology*, doi:10.1128/MCB.01634-13 (2014).

15 Ladror, D. T. *et al.* Methylation of yeast ribosomal protein S2 is elevated during stationary phase growth conditions. *Biochemical and biophysical research communications* **445**, 535-541, doi:10.1016/j.bbrc.2014.01.040 (2014).

16 Odintsova, T. I. *et al.* Characterization and analysis of posttranslational modifications of the human large cytoplasmic ribosomal subunit proteins by mass spectrometry and Edman sequencing. *J Protein Chem* **22**, 249-258 (2003).

17 Ban, N. *et al.* A new system for naming ribosomal proteins. *Current opinion in structural biology* **24**, 165-169, doi:10.1016/j.sbi.2014.01.002 (2014).

18 Lhoest, J. & Colson, C. Cold-sensitive ribosome assembly in an Escherichia coli mutant lacking a single methyl group in ribosomal protein L3. *European journal of biochemistry / FEBS* **121**, 33-37 (1981).

19 Sharma, D., Cukras, A. R., Rogers, E. J., Southworth, D. R. & Green, R. Mutational analysis of S12 protein and implications for the accuracy of decoding by the ribosome. *Journal of molecular biology* **374**, 1065-1076, doi:10.1016/j.jmb.2007.10.003 (2007).

20 Loenarz, C. *et al.* Hydroxylation of the eukaryotic ribosomal decoding center affects translational accuracy. *Proceedings of the National Academy of Sciences of the United States of America* **111**, 4019-4024, doi:10.1073/pnas.1311750111 (2014).

21 McDonough, M. A., Loenarz, C., Chowdhury, R., Clifton, I. J. & Schofield, C. J. Structural studies on human 2-oxoglutarate dependent oxygenases. *Current opinion in structural biology* **20**, 659-672, doi:10.1016/j.sbi.2010.08.006 (2010).

22 Loenarz, C. & Schofield, C. J. Physiological and biochemical aspects of hydroxylations and demethylations catalyzed by human 2-oxoglutarate oxygenases. *Trends in biochemical sciences* **36**, 7-18, doi:10.1016/j.tibs.2010.07.002 (2011).

23 Klose, R. J., Kallin, E. M. & Zhang, Y. JmjC-domain-containing proteins and histone demethylation. *Nature reviews. Genetics* **7**, 715-727, doi:10.1038/nrg1945 (2006).

24 Markolovic, S., Wilkins, S. E. & Schofield, C. J. Protein Hydroxylation Catalyzed by 2-Oxoglutarate-dependent Oxygenases. *The Journal of biological chemistry* **290**, 20712-20722, doi:10.1074/jbc.R115.662627 (2015).

25 Hausinger, R. P. FeII/alpha-ketoglutarate-dependent hydroxylases and related enzymes. *Crit Rev Biochem Mol Biol* **39**, 21-68, doi:10.1080/10409230490440541 (2004).

26 Markolovic, S. *et al.* Structure-function relationships of human JmjC oxygenases-demethylases versus hydroxylases. *Current opinion in structural biology* **41**, 62-72, doi:10.1016/j.sbi.2016.05.013 (2016).

27 Hutton, J. J., Jr., Trappel, A. L. & Udenfriend, S. Requirements for alpha-ketoglutarate, ferrous ion and ascorbate by collagen proline hydroxylase. *Biochemical and biophysical research communications* **24**, 179-184 (1966).

28 Hutton, J. J., Jr., Kaplan, A. & Udenfriend, S. Conversion of the amino acid sequence gly-pro-pro in protein to gly-pro-hyp by collagen proline hydroxylase. *Archives of biochemistry and biophysics* **121**, 384-391 (1967).

29 Bruick, R. K. & McKnight, S. L. Transcription. Oxygen sensing gets a second wind. *Science* **295**, 807-808, doi:10.1126/science.1069825 (2002).

30 Kooistra, S. M. & Helin, K. Molecular mechanisms and potential functions of histone demethylases. *Nature reviews. Molecular cell biology* **13**, 297-311, doi:10.1038/nrm3327 (2012).

31 He, Y. F. *et al.* Tet-mediated formation of 5-carboxylcytosine and its excision by TDG in mammalian DNA. *Science* **333**, 1303-1307, doi:10.1126/science.1210944 (2011).

32 Ito, S. *et al.* Tet proteins can convert 5-methylcytosine to 5-formylcytosine and 5-carboxylcytosine. *Science* **333**, 1300-1303, doi:10.1126/science.1210597 (2011).

33 Hill, P. W., Amouroux, R. & Hajkova, P. DNA demethylation, Tet proteins and 5-hydroxymethylcytosine in epigenetic reprogramming: an emerging complex story. *Genomics* **104**, 324-333, doi:10.1016/j.ygeno.2014.08.012 (2014).

34 Jia, G. *et al.* N6-methyladenosine in nuclear RNA is a major substrate of the obesity-associated FTO. *Nature chemical biology* **7**, 885-887, doi:10.1038/nchembio.687 (2011).

35 Bleijlevens, B. *et al.* Changes in Protein Dynamics of the DNA Repair Dioxygenase AlkB upon Binding of Fe(2+) and 2-Oxoglutarate. *Biochemistry* **51**, 3334-3341, doi:10.1021/bi201699e (2012).

36 Fu, D. *et al.* Human AlkB homolog ABH8 Is a tRNA methyltransferase required for wobble uridine modification and DNA damage survival. *Molecular and cellular biology* **30**, 2449-2459, doi:10.1128/MCB.01604-09 (2010).

37 Songe-Moller, L. *et al.* Mammalian ALKBH8 possesses tRNA methyltransferase activity required for the biogenesis of multiple wobble uridine modifications implicated in translational decoding. *Molecular and cellular biology* **30**, 1814-1827, doi:10.1128/MCB.01602-09 (2010).

38 Katz, M. J., Gandara, L., De Lella Ezcurra, A. L. & Wappner, P. Hydroxylation and translational adaptation to stress: some answers lie beyond the STOP codon. *Cellular and molecular life sciences : CMLS* **73**, 1881-1893, doi:10.1007/s00018-016-2160-y (2016).

39 Zhuang, Q., Feng, T. & Coleman, M. L. Modifying the maker: Oxygenases target ribosome biology. *Translation* **3**, e1009331, doi:10.1080/21690731.2015.1009331 (2015).

40 Aik, W., McDonough, M. A., Thalhammer, A., Chowdhury, R. & Schofield, C. J. Role of the jelly-roll fold in substrate binding by 2-oxoglutarate oxygenases. *Current opinion in structural biology* **22**, 691-700, doi:10.1016/j.sbi.2012.10.001 (2012).

41 Fu, Y. *et al.* The AlkB domain of mammalian ABH8 catalyzes hydroxylation of 5-methoxycarbonylmethyluridine at the wobble position of tRNA. *Angew Chem Int Ed Engl* **49**, 8885-8888, doi:10.1002/anie.201001242 (2010).

42 Pastore, C. *et al.* Crystal structure and RNA binding properties of the RNA recognition motif (RRM) and AlkB domains in human AlkB homolog 8 (ABH8), an enzyme catalyzing tRNA hypermodification. *The Journal of biological chemistry* **287**, 2130-2143, doi:10.1074/jbc.M111.286187 (2012).

43 Ploumakis, A. & Coleman, M. L. OH, the Places You'll Go! Hydroxylation, Gene Expression, and Cancer. *Molecular cell* **58**, 729-741, doi:10.1016/j.molcel.2015.05.026 (2015).

44 Katz, M. J. *et al.* Sudestada1, a Drosophila ribosomal prolyl-hydroxylase required for mRNA translation, cell homeostasis, and organ growth. *Proceedings of the National Academy of Sciences of the United States of America* **111**, 4025-4030, doi:10.1073/pnas.1314485111 (2014).

45 Arnold, R. J. & Reilly, J. P. Observation of Escherichia coli ribosomal proteins and their posttranslational modifications by mass spectrometry. *Anal Biochem* **269**, 105-112, doi:10.1006/abio.1998.3077 (1999).

46 van Staalduinen, L. M., Novakowski, S. K. & Jia, Z. Structure and functional analysis of YcfD, a novel 2-oxoglutarate/Fe(2)(+)-dependent oxygenase involved in translational regulation in Escherichia coli. *Journal of molecular biology* **426**, 1898-1910, doi:10.1016/j.jmb.2014.02.008 (2014).

47 Kazemie, M. The importance of Escherichia coli ribosomal proteins L1, L11 and L16 for the association of ribosomal subunits and the formation of the 70-S initiation complex. *European journal of biochemistry / FEBS* **58**, 501-510 (1975).

48 Moore, V. G., Atchison, R. E., Thomas, G., Moran, M. & Noller, H. F. Identification of a ribosomal protein essential for peptidyl transferase activity. *Proceedings of the National Academy of Sciences of the United States of America* **72**, 844-848 (1975).

49 Voorhees, R. M., Weixlbaumer, A., Loakes, D., Kelley, A. C. & Ramakrishnan, V. Insights into substrate stabilization from snapshots of the peptidyl transferase center of the intact 70S ribosome. *Nature structural & molecular biology* **16**, 528-533, doi:10.1038/nsmb.1577 (2009).

50 Nishimura, M. *et al.* Solution structure of ribosomal protein L16 from Thermus thermophilus HB8. *Journal of molecular biology* **344**, 1369-1383, doi:10.1016/j.jmb.2004.10.011 (2004).

51 Eilbracht, J. *et al.* NO66, a highly conserved dual location protein in the nucleolus and in a special type of synchronously replicating chromatin. *Molecular biology of the cell* **15**, 1816-1832, doi:10.1091/mbc.E03-08-0623 (2004).

52 Eilbracht, J., Kneissel, S., Hofmann, A. & Schmidt-Zachmann, M. S. Protein NO52--a constitutive nucleolar component sharing high sequence homologies to protein NO66. *Eur J Cell Biol* **84**, 279-294, doi:10.1016/j.ejcb.2004.12.022 (2005).

53 Brockers, K. *Analysis of the 2OG dependent oxygenases NO66 and MinA53*, Fachhochschule Aachen, Campus Jülich, (2015).

54 Tsuneoka, M., Koda, Y., Soejima, M., Teye, K. & Kimura, H. A novel myc target gene, mina53, that is involved in cell proliferation. *The Journal of biological chemistry* **277**, 35450-35459, doi:10.1074/jbc.M204458200 (2002).

55 Zhang, Y. *et al.* The Human mineral dust-induced gene, mdig, is a cell growth regulating gene associated with lung cancer. *Oncogene* **24**, 4873-4882, doi:10.1038/sj.onc.1208668 (2005).

56 Tsuneoka, M. *et al.* Mina53 as a potential prognostic factor for esophageal squamous cell carcinoma. *Clinical cancer research : an official journal of the American Association for Cancer Research* **10**, 7347-7356, doi:10.1158/1078-0432.CCR-03-0543 (2004).

57 Ishizaki, H. *et al.* Overexpression of the myc target gene Mina53 in advanced renal cell carcinoma. *Pathology international* **57**, 672-680, doi:10.1111/j.1440-1827.2007.02156.x (2007).

58 Teye, K. *et al.* Expression of Myc target gene mina53 in subtypes of human lymphoma. *Oncology reports* **18**, 841-848 (2007).

59 Zhang, Q. *et al.* Expression of Mina53 and its significance in gastric carcinoma. *The International journal of biological markers* **23**, 83-88 (2008).

60 Komiya, K. *et al.* Mina53, a novel c-Myc target gene, is frequently expressed in lung cancers and exerts oncogenic property in NIH/3T3 cells. *Journal of cancer research and clinical oncology* **136**, 465-473, doi:10.1007/s00432-009-0679-0 (2010).

61 Ogasawara, S. *et al.* Accelerated expression of a Myc target gene Mina53 in aggressive hepatocellular carcinoma. *Hepatology research : the official journal of the Japan Society of Hepatology* **40**, 330-336, doi:10.1111/j.1872-034X.2009.00604.x (2010).

62 Tan, X. P., Zhang, Q., Dong, W. G., Lei, X. W. & Yang, Z. R. Upregulated expression of Mina53 in cholangiocarcinoma and its clinical significance. *Oncology letters* **3**, 1037-1041, doi:10.3892/ol.2012.620 (2012).

63 Tan, X. P. *et al.* Potential effects of Mina53 on tumor growth in human pancreatic cancer. *Cell biochemistry and biophysics* **69**, 619-625, doi:10.1007/s12013-014-9841-7 (2014).

64 Thakur, C. *et al.* Increased expression of mdig predicts poorer survival of the breast cancer patients. *Gene* **535**, 218-224, doi:10.1016/j.gene.2013.11.031 (2014).

65 Xing, J., Wang, K., Liu, P. W., Miao, Q. & Chen, X. Y. Mina53, a novel molecular marker for the diagnosis and prognosis of gastric adenocarcinoma. *Oncology reports* **31**, 634-640, doi:10.3892/or.2013.2918 (2014).

66 Teye, K. *et al.* Increased expression of a Myc target gene Mina53 in human colon cancer. *The American journal of pathology* **164**, 205-216, doi:10.1016/S0002-9440(10)63111-2 (2004).

67 Kuratomi, K. *et al.* Immunohistochemical expression of Mina53 and Ki67 proteins in human primary gingival squamous cell carcinoma. *The Kurume medical journal* **53**, 71-78 (2006).

68 Komiya, K. *et al.* Expression of Mina53, a novel c-Myc target gene, is a favorable prognostic marker in early stage lung cancer. *Lung cancer* **69**, 232-238, doi:10.1016/j.lungcan.2009.10.010 (2010).

69 Thakur, C. & Chen, F. Current understanding of mdig/MINA in human cancers. *Genes Cancer* **6**, 288-302, doi:10.18632/genesandcancer.73 (2015).

70 Wu, K. *et al.* Proteomic Characterization of the World Trade Center dust-activated mdig and c-myc signaling circuit linked to multiple myeloma. *Sci Rep* **6**, 36305, doi:10.1038/srep36305 (2016).

71 Pelengaris, S., Khan, M. & Evan, G. c-MYC: more than just a matter of life and death. *Nature reviews. Cancer* **2**, 764-776, doi:10.1038/nrc904 (2002).

72 Okamoto, M. *et al.* Mina, an Il4 repressor, controls T helper type 2 bias. *Nature immunology* **10**, 872-879, doi:10.1038/ni.1747 (2009).

73 Mori, T. *et al.* Ablation of Mina53 in mice reduces allergic response in the airways. *Cell structure and function* **38**, 155-167 (2013).

74 Yosef, N. *et al.* Dynamic regulatory network controlling TH17 cell differentiation. *Nature* **496**, 461-468, doi:10.1038/nature11981 (2013).

75 Thakur, C. *et al.* Oncoprotein mdig contributes to silica-induced pulmonary fibrosis by altering balance between Th17 and Treg T cells. *Oncotarget* **6**, 3722-3736, doi:10.18632/oncotarget.2914 (2015).

76 Lu, Y. *et al.* Lung cancer-associated JmjC domain protein mdig suppresses formation of tri-methyl lysine 9 of histone H3. *Cell cycle* **8**, 2101-2109, doi:10.4161/cc.8.13.8927 (2009).

77 Williams, S. T. *et al.* Studies on the catalytic domains of multiple JmjC oxygenases using peptide substrates. *Epigenetics* **9**, 1596-1603, doi:10.4161/15592294.2014.983381 (2014).

78 Wang, W. *et al.* The proteomic investigation reveals interaction of mdig protein with the machinery of DNA double-strand break repair. *Oncotarget* **6**, 28269-28281, doi:10.18632/oncotarget.4961 (2015).

79 Sinha, K. M., Yasuda, H., Coombes, M. M., Dent, S. Y. & de Crombrugghe, B. Regulation of the osteoblast-specific transcription factor Osterix by NO66, a Jumonji family histone demethylase. *The EMBO journal* **29**, 68-79, doi:10.1038/emboj.2009.332 (2010).

80 Sinha, K. M. & Zhou, X. Genetic and molecular control of osterix in skeletal formation. *Journal of cellular biochemistry* **114**, 975-984, doi:10.1002/jcb.24439 (2013).

81 Chen, Q. *et al.* Mesenchymal Deletion of Histone Demethylase NO66 in Mice Promotes Bone Formation. *J Bone Miner Res* **30**, 1608-1617, doi:10.1002/jbmr.2494 (2015).

82 Chen, Q., Zhang, L., de Crombrugghe, B. & Krahe, R. Mesenchyme-specific overexpression of nucleolar protein 66 in mice inhibits skeletal growth and bone formation. *FASEB J* **29**, 2555-2565, doi:10.1096/fj.14-258970 (2015).

83 Sinha, K. M., Yasuda, H., Zhou, X. & deCrombrugghe, B. Osterix and NO66 histone demethylase control the chromatin of Osterix target genes during osteoblast differentiation. *J Bone Miner Res* **29**, 855-865, doi:10.1002/jbmr.2103 (2014).

84 Brien, G. L. *et al.* Polycomb PHF19 binds H3K36me3 and recruits PRC2 and demethylase NO66 to embryonic stem cell genes during differentiation. *Nature structural & molecular biology* **19**, 1273-1281, doi:10.1038/nsmb.2449 (2012).

85 Rojas, A. *et al.* Epigenetic Control of the Bone-master Runx2 Gene during Osteoblast-lineage Commitment by the Histone Demethylase JARID1B/KDM5B. *The Journal of biological chemistry* **290**, 28329-28342, doi:10.1074/jbc.M115.657825 (2015).

86 Kim, H. S. *et al.* Crystal structure of Tpa1 from Saccharomyces cerevisiae, a component of the messenger ribonucleoprotein complex. *Nucleic acids research* **38**, 2099-2110, doi:10.1093/nar/gkp1151 (2010).

87 Henri, J. *et al.* Structural and functional insights into Saccharomyces cerevisiae Tpa1, a putative prolylhydroxylase influencing translation termination and transcription. *The Journal of biological chemistry* **285**, 30767-30778, doi:10.1074/jbc.M110.106864 (2010).

88 Horita, S. *et al.* Structure of the Ribosomal Oxygenase OGFOD1 Provides Insights into the Regio- and Stereoselectivity of Prolyl Hydroxylases. *Structure*, doi:10.1016/j.str.2015.01.014 (2015).

89 Wehner, K. A., Schutz, S. & Sarnow, P. OGFOD1, a novel modulator of eukaryotic translation initiation factor 2alpha phosphorylation and the cellular response to stress. *Molecular and cellular biology* **30**, 2006-2016, doi:10.1128/MCB.01350-09 (2010).

90 Saito, K., Adachi, N., Koyama, H. & Matsushita, M. OGFOD1, a member of the 2-oxoglutarate and iron dependent dioxygenase family, functions in ischemic signaling. *FEBS letters* **584**, 3340-3347, doi:10.1016/j.febslet.2010.06.015 (2010).

91 Marina, O. *et al.* Serologic markers of effective tumor immunity against chronic lymphocytic leukemia include nonmutated B-cell antigens. *Cancer research* **70**, 1344-1355, doi:10.1158/0008-5472.CAN-09-3143 (2010).

92 Kim, J. H. *et al.* OGFOD1 is required for breast cancer cell proliferation and is associated with poor prognosis in breast cancer. *Oncotarget* **6**, 19528-19541, doi:10.18632/oncotarget.3683 (2015).

93 Kustatscher, G. *et al.* Proteomics of a fuzzy organelle: interphase chromatin. *The EMBO journal* **33**, 648-664, doi:10.1002/embj.201387614 (2014).

94 Katz, M. J., Acevedo, J. M. & Wappner, P. Growing with the wind. Ribosomal protein hydroxylation and cell growth. *Fly (Austin)* **8**, 153-156, doi:10.4161/fly.29943 (2014).

95 Paolini, N. A. *et al.* A Ribosomopathy Reveals Decoding Defective Ribosomes Driving Human Dysmorphism. *American journal of human genetics* **100**, 506-522, doi:10.1016/j.ajhg.2017.01.034 (2017).

96 Keeling, K. M., Salas-Marco, J., Osherovich, L. Z. & Bedwell, D. M. Tpa1p is part of an mRNP complex that influences translation termination, mRNA deadenylation, and mRNA turnover in Saccharomyces cerevisiae. *Molecular and cellular biology* **26**, 5237-5248, doi:10.1128/MCB.02448-05 (2006).

97 Shivange, G., Kodipelli, N., Monisha, M. & Anindya, R. A role for Saccharomyces cerevisiae Tpa1 protein in direct alkylation repair. *The Journal of biological chemistry*, doi:10.1074/jbc.M114.590216 (2014).

98 Hughes, B. T. & Espenshade, P. J. Oxygen-regulated degradation of fission yeast SREBP by Ofd1, a prolyl hydroxylase family member. *The EMBO journal* **27**, 1491-1501, doi:10.1038/emboj.2008.83 (2008).

99 Lee, C. Y., Stewart, E. V., Hughes, B. T. & Espenshade, P. J. Oxygen-dependent binding of Nro1 to the prolyl hydroxylase Ofd1 regulates SREBP degradation in yeast. *The EMBO journal* **28**, 135-143, doi:10.1038/emboj.2008.271 (2009).

100 Lee, C. Y., Yeh, T. L., Hughes, B. T. & Espenshade, P. J. Regulation of the Sre1 hypoxic transcription factor by oxygen-dependent control of DNA binding. *Molecular cell* **44**, 225-234, doi:10.1016/j.molcel.2011.08.031 (2011).

101 Yeh, T. L., Lee, C. Y., Amzel, L. M., Espenshade, P. J. & Bianchet, M. A. The hypoxic regulator of sterol synthesis nro1 is a nuclear import adaptor. *Structure* **19**, 503-514, doi:10.1016/j.str.2011.01.017 (2011).

102 Porter, J. R., Lee, C. Y., Espenshade, P. J. & Iglesias, P. A. Regulation of SREBP during hypoxia requires Ofd1-mediated control of both DNA binding and degradation. *Molecular biology of the cell* **23**, 3764-3774, doi:10.1091/mbc.E12-06-0451 (2012).

103 Baba, T. *et al.* Construction of Escherichia coli K-12 in-frame, single-gene knockout mutants: the Keio collection. *Molecular systems biology* **2**, 2006 0008, doi:10.1038/msb4100050 (2006).

104 Chasse, H., Boulben, S., Costache, V., Cormier, P. & Morales, J. Analysis of translation using polysome profiling. *Nucleic acids research* **45**, e15, doi:10.1093/nar/gkw907 (2017).

105 Zolghadr, K. *et al.* A fluorescent two-hybrid assay for direct visualization of protein interactions in living cells. *Mol Cell Proteomics* **7**, 2279-2287, doi:10.1074/mcp.M700548-MCP200 (2008).

106 Schulman, B. A., Lindstrom, D. L. & Harlow, E. Substrate recruitment to cyclin-dependent kinase 2 by a multipurpose docking site on cyclin A. *Proceedings of the National Academy of Sciences of the United States of America* **95**, 10453-10458 (1998).

107 Bogdanow, B. *et al.* Human cytomegalovirus tegument protein pp150 acts as a cyclin A2-CDK-dependent sensor of the host cell cycle and differentiation state. *Proceedings of the National Academy of Sciences of the United States of America* **110**, 17510-17515, doi:10.1073/pnas.1312235110 (2013).

108 Fung, T. K., Yam, C. H. & Poon, R. Y. The N-terminal regulatory domain of cyclin A contains redundant ubiquitination targeting sequences and acceptor sites. *Cell cycle* **4**, 1411-1420, doi:10.4161/cc.4.10.2046 (2005).

109 Pines, J. Mitosis: a matter of getting rid of the right protein at the right time. *Trends Cell Biol* **16**, 55-63, doi:10.1016/j.tcb.2005.11.006 (2006).

110 Bendris, N., Lemmers, B., Blanchard, J. M. & Arsic, N. Cyclin A2 mutagenesis analysis: a new insight into CDK activation and cellular localization requirements. *PloS one* **6**, e22879, doi:10.1371/journal.pone.0022879 (2011).

111 Brown, N. R. *et al.* Cyclin B and cyclin A confer different substrate recognition properties on CDK2. *Cell cycle* **6**, 1350-1359, doi:10.4161/cc.6.11.4278 (2007).

112 Xu, Y., Wen, X., Shao, X. J., Deng, N. Y. & Chou, K. C. iHyd-PseAAC: predicting hydroxyproline and hydroxylysine in proteins by incorporating dipeptide position-

specific propensity into pseudo amino acid composition. *International journal of molecular sciences* **15**, 7594-7610, doi:10.3390/ijms15057594 (2014).

113 Shi, S. P., Chen, X., Xu, H. D. & Qiu, J. D. PredHydroxy: computational prediction of protein hydroxylation site locations based on the primary structure. *Molecular bioSystems* **11**, 819-825, doi:10.1039/c4mb00646a (2015).

114 Ismail, H. D., Newman, R. H. & Kc, D. B. RF-Hydroxysite: a random forest based predictor for hydroxylation sites. *Molecular bioSystems* **12**, 2427-2435, doi:10.1039/c6mb00179c (2016).

115 Rothbauer, U. *et al.* Targeting and tracing antigens in live cells with fluorescent nanobodies. *Nat Methods* **3**, 887-889, doi:10.1038/nmeth953 (2006).

116 Burgess, A., Lorca, T. & Castro, A. Quantitative live imaging of endogenous DNA replication in mammalian cells. *PloS one* **7**, e45726, doi:10.1371/journal.pone.0045726 (2012).

117 Sivakumar, S. & Gorbsky, G. J. Spatiotemporal regulation of the anaphase-promoting complex in mitosis. *Nature reviews. Molecular cell biology* **16**, 82-94, doi:10.1038/nrm3934 (2015).

118 Moore, C. E. *et al.* Elongation Factor 2 Kinase Is Regulated by Proline Hydroxylation and Protects Cells during Hypoxia. *Molecular and cellular biology* **35**, 1788-1804, doi:10.1128/MCB.01457-14 (2015).

119 Buchan, J. R. & Parker, R. Eukaryotic stress granules: the ins and outs of translation. *Molecular cell* **36**, 932-941, doi:10.1016/j.molcel.2009.11.020 (2009).

120 Kedersha, N., Ivanov, P. & Anderson, P. Stress granules and cell signaling: more than just a passing phase? *Trends in biochemical sciences* **38**, 494-506, doi:10.1016/j.tibs.2013.07.004 (2013).

121 Ran, F. A. *et al.* Genome engineering using the CRISPR-Cas9 system. *Nature protocols* **8**, 2281-2308, doi:10.1038/nprot.2013.143 (2013).

122 Tao, Y. *et al.* Structural insights into histone demethylase NO66 in interaction with osteoblast-specific transcription factor osterix and gene repression. *The Journal of biological chemistry* **288**, 16430-16437, doi:10.1074/jbc.M112.446849 (2013).

123 Wang, C. *et al.* Structure of the JmjC domain-containing protein NO66 complexed with ribosomal protein Rpl8. *Acta Crystallogr D Biol Crystallogr* **71**, 1955-1964, doi:10.1107/S1399004715012948 (2015).

124 Russell, J. & Zomerdijk, J. C. The RNA polymerase I transcription machinery. *Biochem Soc Symp*, 203-216 (2006).

125 Donnelly, M. L. *et al.* Analysis of the aphthovirus 2A/2B polyprotein 'cleavage' mechanism indicates not a proteolytic reaction, but a novel translational effect: a putative ribosomal 'skip'. *J Gen Virol* **82**, 1013-1025, doi:10.1099/0022-1317-82-5-1013 (2001).

126 Leclere, L., Copley, R. R., Momose, T. & Houliston, E. Hydrozoan insights in animal development and evolution. *Current opinion in genetics & development* **39**, 157-167, doi:10.1016/j.gde.2016.07.006 (2016).

127 Chapman, J. A. *et al.* The dynamic genome of Hydra. *Nature* **464**, 592-596, doi:10.1038/nature08830 (2010).

128 Bottger, A. *et al.* GFP expression in Hydra: lessons from the particle gun. *Dev Genes Evol* **212**, 302-305 (2002).

129 Bertoli, C., Skotheim, J. M. & de Bruin, R. A. Control of cell cycle transcription during G1 and S phases. *Nature reviews. Molecular cell biology* **14**, 518-528, doi:10.1038/nrm3629 (2013).

130 Musacchio, A. & Salmon, E. D. The spindle-assembly checkpoint in space and time. *Nature reviews. Molecular cell biology* **8**, 379-393, doi:10.1038/nrm2163 (2007).

131 Gong, D. & Ferrell, J. E., Jr. The roles of cyclin A2, B1, and B2 in early and late mitotic events. *Molecular biology of the cell* **21**, 3149-3161, doi:10.1091/mbc.E10-05-0393 (2010).

132 Gong, D. *et al.* Cyclin A2 regulates nuclear-envelope breakdown and the nuclear accumulation of cyclin B1. *Curr Biol* **17**, 85-91, doi:10.1016/j.cub.2006.11.066 (2007).

133 Kabeche, L. & Compton, D. A. Cyclin A regulates kinetochore microtubules to promote faithful chromosome segregation. *Nature* **502**, 110-113, doi:10.1038/nature12507 (2013).

134 Tane, S. & Chibazakura, T. Cyclin A overexpression induces chromosomal double-strand breaks in mammalian cells. *Cell cycle* **8**, 3900-3903, doi:10.4161/cc.8.23.10071 (2009).

135 den Elzen, N. & Pines, J. Cyclin A is destroyed in prometaphase and can delay chromosome alignment and anaphase. *The Journal of cell biology* **153**, 121-136 (2001).

136 Murphy, M. Delayed early embryonic lethality following disruption of the murine cyclin A2 gene. *Nat Genet* **23**, 481, doi:10.1038/70612 (1999).

137 Mateo, F. *et al.* Degradation of cyclin A is regulated by acetylation. *Oncogene* **28**, 2654-2666, doi:10.1038/onc.2009.127 (2009).

138 Vidal-Laliena, M. *et al.* Histone deacetylase 3 regulates cyclin A stability. *The Journal of biological chemistry* **288**, 21096-21104, doi:10.1074/jbc.M113.458323 (2013).

139 Webby, C. J. *et al.* Jmjd6 catalyses lysyl-hydroxylation of U2AF65, a protein associated with RNA splicing. *Science* **325**, 90-93, doi:10.1126/science.1175865 (2009).

140 Kanakkanthara, A. *et al.* Cyclin A2 is an RNA binding protein that controls Mre11 mRNA translation. *Science* **353**, 1549-1552, doi:10.1126/science.aaf7463 (2016).

141 Chen, R. & Wold, M. S. Replication protein A: single-stranded DNA's first responder: dynamic DNA-interactions allow replication protein A to direct single-strand DNA intermediates into different pathways for synthesis or repair. *Bioessays* **36**, 1156-1161, doi:10.1002/bies.201400107 (2014).

142 Liu, T. & Huang, J. Replication protein A and more: single-stranded DNA-binding proteins in eukaryotic cells. *Acta Biochimica et Biophysica Sinica* **48**, 665-670, doi:10.1093/abbs/gmw041 (2016).

143 Treuner, K., Findeisen, M., Strausfeld, U. & Knippers, R. Phosphorylation of replication protein A middle subunit (RPA32) leads to a disassembly of the RPA heterotrimer. *The Journal of biological chemistry* **274**, 15556-15561 (1999).

144 Gibbs, E., Pan, Z. Q., Niu, H. & Hurwitz, J. Studies on the in vitro phosphorylation of HSSB-p34 and -p107 by cyclin-dependent kinases. Cyclin-substrate interactions dictate the efficiency of phosphorylation. *The Journal of biological chemistry* **271**, 22847-22854 (1996).

145 Hein, J. B. & Nilsson, J. Interphase APC/C-Cdc20 inhibition by cyclin A2-Cdk2 ensures efficient mitotic entry. *Nat Commun* **7**, 10975, doi:10.1038/ncomms10975 (2016).

146 Otto, T. & Sicinski, P. Cell cycle proteins as promising targets in cancer therapy. *Nat Rev Cancer* **17**, 93-115, doi:10.1038/nrc.2016.138 (2017).

147 Pyronnet, S. & Sonenberg, N. Cell-cycle-dependent translational control. *Curr Opin Genet Dev* **11**, 13-18 (2001).

148 Ryazanov, A. G. & Davydova, E. K. Mechanism of elongation factor 2 (EF-2) inactivation upon phosphorylation. Phosphorylated EF-2 is unable to catalyze translocation. *FEBS letters* **251**, 187-190 (1989).

149 Hizli, A. A. *et al.* Phosphorylation of eukaryotic elongation factor 2 (eEF2) by cyclin A-cyclin-dependent kinase 2 regulates its inhibition by eEF2 kinase. *Molecular and cellular biology* **33**, 596-604, doi:10.1128/MCB.01270-12 (2013).

150 Kedersha, N. *et al.* Dynamic shuttling of TIA-1 accompanies the recruitment of mRNA to mammalian stress granules. *The Journal of cell biology* **151**, 1257-1268 (2000).

151 Bullwinkle, T. J. *et al.* (R)-beta-lysine-modified elongation factor P functions in translation elongation. *The Journal of biological chemistry* **288**, 4416-4423, doi:10.1074/jbc.M112.438879 (2013).

152 Peil, L. *et al.* Lys34 of translation elongation factor EF-P is hydroxylated by YfcM. *Nature chemical biology* **8**, 695-697, doi:10.1038/nchembio.1001 (2012).

153 Ude, S. *et al.* Translation elongation factor EF-P alleviates ribosome stalling at polyproline stretches. *Science* **339**, 82-85, doi:10.1126/science.1228985 (2013).

154 Woolstenhulme, C. J. *et al.* Nascent peptides that block protein synthesis in bacteria. *Proceedings of the National Academy of Sciences of the United States of America* **110**, E878-887, doi:10.1073/pnas.1219536110 (2013).

155 Jorquera, R. *et al.* SinEx DB: a database for single exon coding sequences in mammalian genomes. *Database (Oxford)* **2016**, doi:10.1093/database/baw095 (2016).

156 Grzybowska, E. A. Human intronless genes: functional groups, associated diseases, evolution, and mRNA processing in absence of splicing. *Biochemical and biophysical research communications* **424**, 1-6, doi:10.1016/j.bbrc.2012.06.092 (2012).

157 Shabalina, S. A. *et al.* Distinct patterns of expression and evolution of intronless and intron-containing mammalian genes. *Mol Biol Evol* **27**, 1745-1749, doi:10.1093/molbev/msq086 (2010).

158 Wolf, A. *et al.* The polyserine domain of the lysyl-5 hydroxylase Jmjd6 mediates subnuclear localization. *The Biochemical journal* **453**, 357-370, doi:10.1042/BJ20130529 (2013).

159 Lancaster, D. E. *et al.* Disruption of dimerization and substrate phosphorylation inhibit factor inhibiting hypoxia-inducible factor (FIH) activity. *The Biochemical journal* **383**, 429-437, doi:10.1042/BJ20040735 (2004).

160 Lee, G. *et al.* Oxidative Dimerization of PHD2 is Responsible for its Inactivation and Contributes to Metabolic Reprogramming via HIF-1alpha Activation. *Sci Rep* **6**, 18928, doi:10.1038/srep18928 (2016).

161 Rose, N. R., McDonough, M. A., King, O. N., Kawamura, A. & Schofield, C. J. Inhibition of 2-oxoglutarate dependent oxygenases. *Chem Soc Rev* **40**, 4364-4397, doi:10.1039/c0cs00203h (2011).

162 Ehrhardt, C. *et al.* Polyethylenimine, a cost-effective transfection reagent. *Signal Transduction* **6**, 179-184, doi:10.1002/sita.200500073 (2006).

163 Khatter, H. *et al.* Purification, characterization and crystallization of the human 80S ribosome. *Nucleic acids research* **42**, e49, doi:10.1093/nar/gkt1404 (2014).

164 Guindon, S. *et al.* New algorithms and methods to estimate maximum-likelihood phylogenies: assessing the performance of PhyML 3.0. *Syst Biol* **59**, 307-321, doi:10.1093/sysbio/syq010 (2010).

8 Acknowledgments

Many people helped and supported me in the last years.

First, I thank Alex Wolf for offering me this project and giving me the freedom to follow my own ideas. His door was always open for questions, discussions and help.
Dirk Eick supervised my thesis and gave me advice and helpful suggestions.
Also Daniel Wilson contributed to this work as member of my HELENA thesis committee. He brought me in contact with the ribosomal field with Agata Starosta from his own lab and Sarah Matheisl from the Beckmann lab. Ignasi Forné from the Imhof lab analyzed my ribosomal preparations. Jasmin Moneer from the Böttger Lab helped me with the Hydra experiments. Those collaborations made this work more profound.

Current and previous members of the Wolf Lab made work enjoyable and easy. Thank you Kevin Brockers, Gitta Heinz, Chia-Hua Maggie Ho, Olga Swolski, Anita Wagner, Justė Wesche. Also several students contributed a lot to this work, I am very grateful for their participations.

Last but not least, I want to thank my family, my very good friends (the second family), and a special man (and little girl) for supporting me and enjoying with me a great life outside of work!

9 Erklärungen

Eidesstattliche Erklärung

Ich versichere hiermit an Eides statt, dass die vorgelegte Dissertation mit dem Titel "Activity and substrate specificity of bacterial and human ribosomal oxygenases " von mir selbständig und ohne unerlaubte Hilfe angefertigt wurde.

München, den 22.02.2018

Katharina Bräuer

Erklärung über frühere Promotionsversuche

Hiermit erkläre ich,

☐ dass die Dissertation nicht ganz oder in wesentlichen Teilen einer anderen Prüfungskommission vorgelegt worden ist.

☐ dass ich mich anderweitig einer Doktorprüfung ohne Erfolg nicht unterzogen habe.

München, den 22.02.2018

Katharina Bräuer